NORTH ATLANTIC TREATY ORGANIZATION

ADVISORY GROUP FOR AEROSPACE RESEARCH AND DEVELOPMENT

(ORGANISATION DU TRAITE DE L'ATLANTIQUE NORD)

NONREACTING AND CHEMICALLY REACTING VISCOUS FLOWS OVER A HYPERBOLOID AT HYPERSONIC CONDITION

edited by

Clark H. Lewis

This AGARDograph is sponsored by the Fluid Dynamics Panel
of AGARD-NATO

The papers in this AGARDograph have been reproduced directly from copy supplied and set by each author.

Published September 1970

532.516:533.6.011.55:533.6.011.8

Printed by Technical Editing and Reproduction Ltd
Harford House, 7-9 Charlotte St, London. W1P 1HD

FOREWORD

An AGARD Seminar was held at the National Physical Laboratory, Teddington, England, in September 1967. The seminar on Numerical Methods in Viscous Flows considered (I) solutions to the complete Navier-Stokes equations and (II) solutions to the boundary-layer equations. A portion of Part II was devoted to a section on Engineering Applications in which various investigators were invited to make and present calculations for specific sets of conditions so that comparisons could be made to assess the results of various numerical methods.

The body chosen for the numerical experiments was a 10-degree half-angle hyperboloid at two altitude-velocity conditions and one perfect gas condition. Inviscid pressure distributions and boundary-layer edge conditions were given to all investigators. Each participant was asked to compute wall skin friction and heat-transfer coefficients and provide velocity, temperature, species, etc. profiles across the viscous layer at various locations along the body.

Preliminary results were presented and discussed at the AGARD seminar in 1967. Since that time considerable developments and extensions have been made in many of the numerical methods, and it is now possible to make some direct comparisons and draw some conclusions regarding the chemical models, numerical methods and the applicability of boundary-layer theory under low Reynolds number conditions.

At the opening of Part II of the seminar, Professor Milton Van Dyke gave a survey paper on higher-order boundary-layer theory. That paper has been revised and is included in this AGARDograph. A survey of numerical methods for laminar boundary-layer flows has recently been prepared by Dr. F. G. Blottner and is also included here. A paper on chemically reacting boundary-layer flows was given by A. M. O. Smith. The stagnation point viscous shock layer is treated by F. G. Blottner and J. C. Adams. Higher-order boundary-layer effects were considered by C. H. Lewis, J. C. Adams, and R. T. Davis. Results are shown from W. Schönauer, University of Karlshrue, Germany; however, a complete paper describing in detail his method is not available.

The purpose of the seminar and this AGARDograph was to provide a means for presenting and comparing various methods for predicting laminar viscous flows. Although the range of conditions specified for the test cases was not large, the results should be useful to those seeking reliable numerical methods to use in engineering studies and to provide extensive numerical results which can be used to test and compare with other numerical methods.

Clark H. Lewis
Blacksburg, Virginia

June 1, 1970

CONTENTS

	Page
FOREWORD	iii
A SURVEY OF HIGHER-ORDER BOUNDARY-LAYER THEORY by Milton Van Dyke	1
FINITE DIFFERENCE SOLUTION OF THE FIRST-ORDER BOUNDARY-LAYER EQUATIONS by F.G.Blottner	13
LAMINAR BOUNDARY-LAYER CALCULATIONS ON BODIES OF REVOLUTION IN HYPERSONIC FLOW by G.L.Keltner and A.M.O.Smith	37
SOLUTION OF THE VISCOUS SHOCK-LAYER EQUATIONS FOR A BINARY MIXTURE by R.T.Davis	55
VISCOUS SHOCK-LAYER PROBLEM FOR THE STAGNATION POINT OF A BLUNT BODY by F.G.Blottner	71
CHEMICALLY REACTING BOUNDARY LAYER EFFECTS FOR THE AGARD ENGINEERING APPLICATIONS BODY AND FLOW CONDITIONS by J.C.Adams	89
COMPUTATION OF HIGHER-ORDER BOUNDARY-LAYER EFFECTS WITH A FIRST-ORDER TREATMENT AND COMPARISON WITH EXPERIMENTAL DATA by C.H.Lewis	105
HIGHER-ORDER BOUNDARY-LAYER EFFECTS FOR THE AGARD ENGINEERING APPLICATIONS BODY AND FLOW CONDITIONS by J.C.Adams	121
THE HYPERSONIC VISCOUS SHOCK-LAYER PROBLEM by R.T.Davis	135
NUMERICAL METHODS FOR NONREACTING AND CHEMICALLY REACTING LAMINAR FLOWS - TESTS AND COMPARISONS by C.H.Lewis	155

A SURVEY OF HIGHER-ORDER BOUNDARY-LAYER THEORY

by

Milton Van Dyke

Professor of Aeronautics and Astronautics,
Stanford University, Stanford, California

A SURVEY OF HIGHER-ORDER BOUNDARY-LAYER THEORY*

by Milton Van Dyke**

INTRODUCTION

If I undertake a survey of higher-order boundary-layer theory, at the present time it almost goes without saying that I am going to discuss only steady, plane or axisymmetric, laminar flows, and at most second-order theory. Laminar, because my knowledgeable colleagues assure me that turbulent boundary layers are not yet well enough understood that a sensible person would trouble himself with higher-order refinements. Second-order, because for gases on the one hand the Navier-Stokes equations are not valid to any higher order, and for liquids on the other hand the law of diminishing returns probably sets in after the second approximation - which itself extends the utility of Prandtl's theory down to Reynolds numbers of the order of ten. And steady and two-dimensional, because none of us has yet ventured further.

When we set out to improve upon boundary-layer theory in a systematic way, we naturally ask first what approximations were adopted by Prandtl in the classical theory. Consider first the simplest case of plane, steady, incompressible flow. The continuity equation and surface boundary conditions are left intact. Streamwise diffusion is neglected compared with transverse diffusion in the longitudinal momentum equation, the transverse pressure gradient is disregarded, and the distant boundary condition is replaced by the requirement that far out in the boundary layer the tangential velocity component approach the inviscid surface speed.

These three approximations introduce errors of relative order $R^{-1/2}$, where R is a representative Reynolds number. Hence if we count Prandtl's theory as the first approximation (some writers call it the "zeroth"!), second-order theory will add corrections of order $R^{-1/2}$, third-order theory terms of order R^{-1}, and so on.

DISPLACEMENT EFFECT

The neglect of streamwise diffusion actually causes only a third-order error. Likewise, for flat surfaces - plates and wedges - the normal pressure gradient exerts only a third-order effect. Hence for flat shapes the only second-order effect is the change in the outer tangential speed induced by the boundary layer itself. This is called the displacement effect.

This effect appears in the first discussion of higher-order boundary-layer theory that I know of, due to Prandtl himself. In volume three of Durand's "Aerodynamic Theory" he wrote, in discussing the flat plate

> The displacement of the stream-lines by the amount δ^* produces a slight alteration in the potential flow which was made the basis of the calculations. Instead of a simple parallel flow, the flow around a parabolic cylinder of thickness $2\delta^*$ should be introduced, which would slightly alter the pressure distribution. The above calculation would have to be repeated for this new pressure distribution and if necessary the process repeated on the basis of the new measure of displacement so obtained. Such calculations have so far not been performed; they would, in any case, make little difference in the regions where the calculations are usually applied in practice. They would however become necessary if the transition to smaller Reynolds number $u_o\ell/\nu$ were attempted.

To this we need only add that - according to thin-airfoil theory - it happens that a thin parabola induces no pressure change upon itself. Thus we see that there are no second-order corrections at all to the boundary layer on a semi-infinite plate.

For a finite flat plate, however, the displacement thickness is parabolic only back to the trailing edge, and then nearly constant in the wake. Consequently there is a small favorable pressure gradient induced upon the boundary layer. On this basis Kuo (1953) calculated the second-order effect, finding that the local skin friction is slightly increased everywhere. However, he made the mistake of integrating to find the total drag. This is not proper, because the boundary-layer approximation breaks down altogether in a small neighborhood of the leading edge; and, as I shall discuss later in more detail, this local deviation affects the drag to second order.

"ONE-AND-A-HALF-ORDER" THEORY

The displacement effect is often more difficult to calculate than any of the other second-order effects, because it alone is global in nature - the correction at any point depending upon the entire course of the boundary layer. Nevertheless, I have discussed it first because it is invariably present. (The only exception might arise if we contrived to apply suction to a porous wall, or to cool the wall in a compressible fluid, in just such a way that the displacement thickness was everywhere zero.)

Before discussing other second-order effects, I want to express the opinion that displacement effects deserve more attention than they have received. Indeed, very useful results can be obtained by stopping short of second-order boundary-layer theory, at what we might call "one-and-a-half-order theory" - that is, the classical boundary layer plus its flow due to displacement.

---

*This paper was presented at the AGARD seminar in September 1967, and at the same time issued as Stanford University Department of Aeronautics and Astronautics report SUDAAR No. 326, AFOSR No. 67-2291. A considerably revised and extended version of most of this material was published in June 1969 (Van Dyke 1969). Several points have been elaborated in other papers (Conti and Van Dyke 1969a, 1969b; Van Dyke 1970), whereas a few matters have not been reconsidered elsewhere at all. Accordingly, the paper is presented here in its original form; but a series of notes has been inserted throughout to bring it up to date, and the papers cited therein have been added to the list of references.

**Professor of Aeronautics and Astronautics, Stanford University, Stanford, California.

For example, chemical engineers have in the last few years disputed the old problem of viscous entry into a channel. This problem was first treated in 1934 by Schlichting, who applied boundary-layer theory to the walls, and assumed in between a uniform core that accelerates downstream. Obviously this assumption fails near the entry. Recently Wang and Longwell (1964) solved the full Navier-Stokes equations numerically for a cascade of plates at a Reynolds number of 150, based on channel width and upstream conditions. However, at such a large Reynolds number it is scarcely necessary to appeal to the full equations, or even to second-order boundary-layer theory. One need only calculate properly the flow due to displacement thickness.

Near the entry, the displacement thickness is a parabola for each plate, as indicated in Fig. 1. Hence the flow due to displacement thickness is just the potential flow past a cascade of parabolas, which can be found by elementary means (with due attention to indeterminate forms). Fig. 2 shows how well the result for the velocity profile across the entry plane agrees with the numerical solution of the full equations. The details of this analysis of channel entry are to be published soon (Van Dyke 1970). It is found that Schlichting's solution is a "downstream approximation" discussed above in the sense of the method of matched asymptotic expansions.

I have recently calculated also the flow induced by a variety of jets and plumes - results that have apparently never appeared in print, but are useful in understanding the flow pattern. For example, the well-known boundary-layer solution for an axisymmetric laminar jet yields, in cylindrical coordinates, the pattern of streamlines shown in Fig. 3, which appears in Prandtl's (1938) article. The flow far outside the jet happens, with this choice of coordinates, to be that appropriate to a jet issuing from an infinite plane wall. Suppose, however, that we are interested rather in a jet issuing from a long slender nozzle. Calculating the flow due to displacement shows that the outer stream surfaces are paraboloids of revolution. The composite solution shown in Fig. 4 is indistinguishable from the exact solution of the full Navier-Stokes equations sketched by Whitham on page 153 of Rosenhead's "Laminar Boundary Layers". Some of these flows were calculated earlier for turbulent jets by Stewart (1956). Recently, Rubin & Falco (1968) have carried out the corresponding calculations for a plane laminar jet.

Let me add one last remark on "one-and-a-half-order" theory. This is the province of Kaplun's (1954) optimal coordinates; and it seems to me imperative that we extend that remarkable idea - first to axisymmetric flows, and then if possible to three-dimensional and unsteady motions as well as to higher approximations.

LONGITUDINAL CURVATURE

If the surface of a body is curved, rather than flat, centrifugal forces yield pressure changes across the boundary layer that exert a second-order effect. This effect of longitudinal curvature was first investigated by Tani in 1949. He studied the special case of a plate with curvature varying as the inverse square root of distance from the leading edge, because this admits a self-similar solution. He found a reduction of local skin friction due to convex curvature (in contrast to earlier Japanese work, based on a momentum integral, that suggested an increase).

The same problem was solved independently by Murphy in 1953, who found the same trend but a smaller coefficient. Tani thereupon realized that his treatment had been inconsistent, and in 1954 published a revised version with yet another value of the coefficient. Fig. 5 shows the subsequent history of this ridiculous comedy of errors, which seems to have been resolved only within the last year.

Further details of this prolonged controversy, including the various second-order equations of motion adopted by different writers, are given in Van Dyke (1969).

Of the investigators whose names appear here, Murphy, Cooke, Massey and Clayton, and Narasimha and Ojha have calculated the effects of longitudinal curvature for a more general class of flows. These are what I will call completely self-similar solutions, in the sense that the second-order correction is similar not only to itself but also to the first-order solution - which is a member of the Falkner-Skan family. With equal ease I have calculated several cases of what I may call separately self-similar solutions: the first- and second-order solutions are similar to themselves, but not to each other. These have the advantage that the curvature may be taken to be everywhere finite. It might be worthwhile to calculate a few more of these; whereas I believe the subject of completely self-similar flows is closed with the appearance of the definitive papers of Cooke and Narasimha and Ojha. (That of Murphy is invalidated by certain inconsistencies that have been pointed out by Massey and Clayton (1966), and the work of the latter is also open to some objection.)

Werle (1968) recently made an admirably detailed analysis and comprehensive calculation of the "separately self-similar" solutions for each second-order effect; see also Werle and Davis (1970). That study has disclosed some singularities in the second-order terms whose physical significance is not yet understood.

Let me now make a possibly controversial comment on the range of applicability of these results. Murphy, Massey and Clayton, and Schultz-Grunow and Breuer assume - either explicitly or tacitly - that their solutions remain valid even when the wall curvature is so great that the radius is of the order of the boundary-layer thickness. I am sure that this is not true, and that - as I will discuss later - quite a different approximation must be adopted in that range. They therefore spend an unnecessary amount of labor in solving equations that are not split into first- and second-order components, and in presenting results for a range of curvature parameter. As Narasimha and Ojha point out, there is no justification for attaching any significance to the departure of their curves from the initial tangents.

TRANSVERSE CURVATURE

A second curvature effect arises when we extend our considerations to bodies of revolution. In the classical theory the boundary layer is negligibly thin compared with the local radius of the body; and this permits it to be related to an equivalent plane boundary layer by the Mangler transformation. However, on a very long slender body - a needle - the boundary layer may grow much thicker than the body even at high Reynolds number. We exclude this situation - which requires a fresh approach initiated by Glauert and

Lighthill (1955) and Stewartson (1955) - and consider the effects of transverse curvature over a short body or the forward portions of a long one.*

Transverse curvature appears in its most nearly pure form in the boundary layer on a circular pipe. The internal flow was studied by Atkinson and Goldstein (cf. Goldstein 1938, p. 304), and the external flow by Seban and Bond (1959), with important corrections by Kelly (1954). The latter find the local skin friction to be increased over the flat-plate value by the factor

$$1 + 2.10\sqrt{\frac{\nu}{Ua}}\sqrt{\frac{x}{a}} - 0.48\,\frac{\nu}{Ua}\,\frac{x}{a} + \cdots$$

where a is the radius of the pipe. In this form we recognize the second term as a second-order boundary-layer effect - proportional to the inverse square root of the Reynolds number - and the third term as a third-order effect. Whereas convex longitudinal curvature usually reduces the skin friction, convex transverse curvature appears to always increase it, as in this case.

Although longitudinal curvature is absent in this problem, the second-order displacement effect does not vanish for a tube as it does for a plate. Hence a correction for displacement must be added to the above result. For the internal flow, Atkinson and Goldstein adopted Schlichting's idea of a uniform accelerated core; and this alters the coefficient of the second term. I intend to calculate properly the flow due to displacement thickness, in order to assess the error in these theories.**

EXTERNAL VORTICITY

The next second-order effect I want to mention was first recognized in supersonic problems, but can occur also in incompressible flows. Ferri and Libby (1954) pointed out that the boundary layer must be affected to some extent by the external vorticity generated by a curved bow shock wave. Li (1955) then proposed a simple incompressible model of this phenomenon that displays its essential features - a semi-infinite flat plate in a uniform shear flow. He at first omitted the pressure gradient that is induced by interaction of the external shear flow with the displacement thickness of the boundary layer, but corrected himself the following year (Li 1956). However, that correction was challenged by Glauert (1957) and others; and a lively and extended controversy arose. Finally, however, thanks to the careful analysis of Murray (1961) and the diplomatic intercession of Toomre and Rott (1964), the dispute has been resolved in a consensus of nearly all the participants. Further details of this controversy are given in Van Dyke (1969).

THE METHOD OF MATCHED ASYMPTOTIC EXPANSIONS

We see that even in the simplest case of steady, plane, laminar incompressible flow the development of higher-order boundary-layer theory has been marred by an unfortunate series of errors, misunderstandings, and controversies. The reason is simply that the insight of even Prandtl begins to fail at about the second approximation. What one then wants is a rote procedure that can be applied automatically, without undue mental effort.

The required technique is the method of matched asymptotic (or "inner and outer") expansions. This useful method is in fact an outgrowth of Prandtl's boundary-layer idea, as developed by Friedrichs (1953), Kaplun and Lagerstrom (1957), and others. I believe that this method can no longer be dismissed as an esoteric special technique, but should be part of the working equipment of every applied mathematician and theoretical engineer.

In the present subject, it is fair to assert that all the many errors and disputes have arisen from relying upon physical insight; and that not a single false step has been made by any of us who trusted rather to systematic application of the method of matched asymptotic expansions.

COMPRESSIBLE FLOW

Even though the emphasis of this meeting is on compressible flow, I have spoken so far only of incompressible motion, because it is simpler and exemplifies most of the essential features. Just as in the classical theory, dramatic compressibility effects are limited to the outer inviscid flow, and the boundary layer itself suffers changes only of detail, even into the hypersonic range. This point of view has recently been challenged by Weinbaum and Garvine (1966); but I think it would be charitable to say that they have misunderstood the asymptotic nature of boundary-layer theory, confusing it with the so-called "strong-interaction" theory, which is based upon quite a different double limit process.

The four second-order effects that I have discussed so far - displacement, longitudinal curvature, transverse curvature, and external vorticity - persist for compressible motion. In my own work, I found it convenient to subdivide the effect of external vorticity into that of entropy gradient and of stagnation enthalpy gradient, the latter being absent for the usual isoenergetic flows of aerodynamics. To these are added two new phenomena associated with the boundary conditions at the surface: the effects of slip and temperature jump. It should be emphasized, however, as pointed out by Rott and Lenard (1962), that this classification is not unique, and a considerable part of the controversy in this subject has arisen only because of different ways of dividing among displacement, curvature, and external vorticity.

*We think of bodies that grow more slowly than a paraboloid. The situation is reversed for those that grow more rapidly, such as a cone, for which the ratio of boundary-layer thicknes to body radius decreases downstream.

**This analysis has not yet been prepared for publication.

In contrast to the incompressible theory, the more complicated compressible second-order boundary-layer theory has been developed with a minimum of error. In particular, the comprehensive analyses of myself (Van Dyke 1961), Maslen (1962), and Lenard (1962) - developed independently in about the same year - seem to have withstood the test of time.

APPLICATIONS IN COMPRESSIBLE FLOW

The first applications of the theory for compressible flow were again to stagnation points and leading edges, for which self-similar solutions exist (Van Dyke 1961, Maslen 1962, Fannelöp and Flügge-Lotz 1965, Davis and Flügge-Lotz 1961a). Later, numerical integration of the first- and second-order equations was undertaken (Devan 1964), the most comprehensive results - until this meeting - being those of Fannelöp and Flügge-Lotz (1966) for plane flow past a circular cylinder and a plate with semi-circular leading edge, and of Davis and Flügge-Lotz (1964b) for axisymmetric flow past a paraboloid, sphere, and hyperboloid.

The most troublesome component of these calculations is the flow due to displacement thickness. In principle, we should perturb the basic inviscid blunt-body solution. However, we have all resorted to the strategem of approximating the body plus the displacement thickness by a magnified and shifted replica of itself; and this does not seem to have introduced serious errors.

These results show that the various second-order contributions may vary widely in sign and magnitude, depending upon body shape, surface temperature, and other parameters in the problem. The same is true of the resultant, which is often smaller than any of its components. Consequently it is important to calculate all second-order effects if any significance is to be attached to the result.

Experimental confirmation is perhaps still not conclusive. A few years ago the situation seemed to be that experiments carried out in New York agreed with the rather large effects predicted by several partial theories developed in the same state, and experiments in California tended to agree with the smaller effects predicted by theories developed there. I am not sure how much this situation has been clarified; but I hope to learn more about it at this meeting.

SEPARATION

One point of special interest at this meeting is the light that second-order theory can shed on laminar separation. Until recently, most of us believed that the classical boundary-layer theory breaks down shortly before the skin friction vanishes - as in Howarth's (1938) solution for a linearly decreasing surface speed. As usual in perturbation theories, we might expect this failure of the first approximation to be confirmed by compounded singularities in higher approximations.

Two bits of evidence suggest that this does happen. In their completely self-similar solutions for incompressible flow, Narasimha and Ojha have observed that the second-order coefficient of skin friction due to longitudinal curvature seems to be rising rapidly as the critical value of the Falkner-Skan parameter is approached. Again, in their full second-order solution for a sphere at Mach number 10, Davis and Flügge-Lotz (1964b) found the effects of longitudinal curvature becoming large as the skin friction fell.

Our ideas on separation have, however, been overturned by the recent discovery of Catherall and Mangler (1966) that the classical boundary-layer solution will proceed smoothly through zero skin friction if it is permitted the slightest freedom to choose the local pressure distribution so as to avoid catastrophe. It would be interesting to re-examine the second-order theory in the light of this remarkable turn of events.

CORNERS AND EDGES

I have already expressed the opinion that higher-order boundary-layer theory will break down long before the surface curvature becomes so great that the radius of curvature is comparable with the boundary-layer thickness - and this would be true of transverse as well as longitudinal curvature. I believe that the proper way of treating such problems has been pointed out by Brailovskaya (1965) and Neiland and Sychev (1966). They consider plane flow past a corner that is slightly rounded, with a radius of the order of the local boundary-layer thickness. Classical boundary-layer theory holds as a first approximation ahead of the corner, and again behind it. In the immediate neighborhood of the corner, however, the small viscous forces are insignificant compared with the pressure and inertial forces, so the flow is governed locally by the Euler equations of rotational inviscid flow. This local solution matches the boundary layers upstream and downstream in the sense of the method of matched asymptotic expansions. Finally, because the local inviscid solution violates the no-slip condition, a thin sub-boundary layer must be added close to the wall.

Neiland and Sychev consider only rounded corners in order to avoid having to deal with the full Navier-Stokes equations. For if the corner is sharp, a local solution of the full equations is evidently required. However, it will have a certain simple and universal character, and may therefore be worth working out numerically.

One case that seems to be well in hand is incompressible flow near a cusped leading edge. The local problem is the standard one of viscous flow past a semi-infinite flat plate. Thirteen years ago Imai (1957) showed, by ingenious use of global momentum balance, that although the Prandtl-Blasius boundary-layer solution breaks down near the leading edge, it can be used to find the second term in the integrated skin friction (which from the crude point of view of the boundary-layer approximation appears as a concentrated force at the leading edge). More recently, Davis (1967) has solved the problem in detail using the semi-numerical method of series truncation; and his solution agrees so well with both the global result of Imai and a much-neglected analysis of Dean (1954) that we can accept it with confidence. This local correction can be applied to Kuo's solution for the finite flat plate, to the cascade of flat plates, to the solutions of Atkinson and Goldstein and Seban and Bond for the circular pipe, and so on. In supersonic and hypersonic flow the problem is more difficult, and has not yet been satisfactorily solved.

Perhaps the simplest case of flow over a sharp corner is a cusped trailing edge in an incompressible stream, because there is no question of separation. If we consider, for example, the standard problem of the finite flat plate, we see that the Prandtl-Blasius solution applies over most of the surface, and the wake solution of Goldstein (1930) and Tollmien (1931) almost everywhere behind it. The boundary-layer solution fails in a circular neighborhood of the leading edge whose radius is of the order of R^{-1} times the length of the plate, R being the Reynolds number based on length; and here we can use the results of Imai, Dean, and Davis. At the trailing edge the thickness of the boundary layer is of order $R^{-1/2}$, and the theory of Neiland and Sychev would suggest that a local Euler solution is required in a neighborhood of that size. However, in this simple case that correction vanishes. I have convinced myself that a correction is then required only in a smaller neighborhood of the trailing edge, whose radius is of the order of $R^{-3/4}$ times the length of the plate. (This corresponds to Neiland and Sychev's sub-boundary layer.) The full Navier-Stokes equations must be solved there; and we hope to carry this out by series truncation.

Without making the detailed calculations, we can see that this trailing-edge correction will contribute to the integrated skin friction a term of order $R^{-5/4}$. Thus for cusp-ended shapes we must reconsider our numbering scheme. What we have heretofore called second-order theory adds a correction of relative order $R^{-1/2}$, and third-order theory a term of order R^{-1}; but now we see that the trailing-edge correction supplies a "two-and-one-half-order" term in $R^{-3/4}$, and so on (whatever that may mean!).

That the structure of the flow near the trailing edge is more complicated than that suggested above has recently been shown independently by Stewartson (1969) and Messiter (1970). In addition to the region of order $R^{-3/4}$ in size mentioned above, there is a "triple deck" consisting of nested regions with transverse dimensions of orders $R^{-5/8}$, $R^{-1/2}$, and $R^{-3/8}$, and streamwise dimensions of orders $R^{-1/2}$ and $R^{-3/8}$. As a consequence, the first correction to the integrated skin friction is of order $R^{-7/8}$.

The situation is different again when we encounter large or infinite transverse curvature. The simplest example is perhaps the incompressible flow along a corner, which has been re-examined recently by Rubin (1966) from the point of view of matched asymptotic expansions. In this case the crucial problem to be solved in the immediate vicinity of the corner involves equations simpler than the full Navier-Stokes equations, but more complicated than the conventional boundary-layer equations. The only attempt at solving this problem numerically was made by Pearson (1957) thirteen years ago in his unpublished Cambridge University thesis. If this correction is applied to the flow inside a rectangular channel, we see that it contributes a term of relative order $R^{-1/2}$ to the drag - and is therefore to be included with the second-order displacement effect discussed earlier.

The flow near the outside corner on such a channel is more complicated, as is indicated by Stewartson's (1961) study of the quarter-infinite plate. And again the corresponding supersonic problems are still more difficult.

SINGULAR OUTER FLOWS

Finally, I want to discuss an intriguing new field of application for higher-order boundary-layer theory. This is motion in which the basic inviscid flow is singular at the surface of the body. This situation has arisen recently in various branches of high-speed aerodynamics, of which I will mention four: (1) Perhaps the simplest case to understand is the inviscid stagnation region of a blunt body in hypersonic flight through a completely transparent radiating gas. A particle of fluid on the stagnation streamline requires an infinite time to reach the stagnation point, and so - because there is no re-absorption - radiates away all its energy. Hence the inviscid surface streamline is at absolute zero temperature. In a model of this phenomenon studied by Burggraf (1966) the velocity and enthalpy both vanish as negative fractional powers of the logarithm of the distance from the wall. (2) Similarly, for an inviscid stagnation point in a chemically-reacting gas, the temperature and degree of dissociation (as well as the other thermodynamic properties) approach some equilibrium values at the stagnation point; and the normal gradients are zero for sufficiently fast reactions, finite for a particular intermediate rate, and infinite for slower reactions (Fig. 6). This behavior has been discussed by Conti and myself. (3) Hayes (1964) has studied the rotational inviscid flow near a three-dimensional stagnation point. He finds that in all but very special cases the solution is non-analytic and the vorticity infinite at the wall, the stagnation streamline being tangent to the surface. (4) In hypersonic small-disturbance theory the self-similar solutions associated with strong power-law bow shock waves are singular at the surface of the body. This case is the subject of a paper to be presented at this meeting by Lee and Cheng, entitled "Higher-order approximation in the theory of hypersonic boundary layers on slender bodies."

If we now consider applying boundary-layer theory to any of these problems, questions arise that force us to re-examine the basis of Prandtl's classical theory. Should we still use the inviscid surface speed as the tangential velocity at the outer edge of the boundary layer, even though the gradient is infinite? Is the boundary-layer thickness still of order $R^{-1/2}$? Do higher approximations proceed in the usual way? Is a single boundary layer sufficient, or are intermediate transition layers required?

Conti and I have concluded that - at least in the first two cases, of stagnation points in radiating or reacting flows - the situation is in general as follows: Classical boundary-layer theory remains valid even though the inviscid surface gradients are infinite. That is, the boundary-layer thickness is still of order $R^{-1/2}$, and the inviscid surface speed is approached at the outer edge. However, important differences appear in higher approximations. Rather than being smaller by a full inverse half power of Reynolds number, the second-order correction follows close on the heels of the classical solution. In the case of slow chemical reactions, it may differ by only a very small negative power of Reynolds number, so that several or even a great many higher-order terms intervene before the conventional second-order correction. And in the case of radiation, successive terms differ from one another only by fractional powers of the logarithm of the Reynolds number, so that an infinite number of terms intervene.

These conclusions differ somewhat from those of Burggraf. The reason is that he considers only the degenerate case of vanishing surface temperature. Then the surface boundary conditions on both velocity and temperature are satisfied by the inviscid solution, so that no conventional boundary layer is required. The

first correction is what would ordinarily be the second-order term; and it is a consequence of the non-linearity of the governing equations that the boundary layer then has a thickness that is slightly greater than usual, by an amount smaller than any power of the Reynolds number.

Our conclusions appear also to differ from those reached by Lee and Cheng in their study of power-law bodies in hypersonic flow, for they invoke a third region that serves to join the inviscid flow to the boundary layer. From my point of view, this meeting will be a success if we can clarify our thoughts on this fascinating new branch of the subject.

The study of an inviscid stagnation point in a chemically-reacting gas has now been published (Conti and Van Dyke 1969a), as has the corresponding boundary-layer analysis (Conti and Van Dyke 1969b). Lee and Cheng's analysis of hypersonic small-disturbance theory has also appeared elsewhere (Lee and Cheng 1969). A still simpler example of a boundary layer under singular external conditions is that on an ogive of revolution in supersonic flow. This was pointed out several years ago by Cheng (1966), and the details have now been worked out by Stahara (1969).

Convincing confirmation of higher-order boundary-layer theory by experiment has not yet been achieved. However, as outlined briefly in Van Dyke (1969), most experiments seem to show at least qualitative agreement with the predictions of second-order boundary-layer theory.

ACKNOWLEDGEMENT

This paper was prepared for the Air Force Office of Scientific Research under Contract No. AF49(638) - 1274, Project No. 9781-01.

REFERENCES

Brailovskaya, I. Yu. 1965 "A Method for Calculating Flows with Strong Viscous Interaction (Russian). Doklady Akad. Nauk SSSR, Vol. 162, pp. 36-40.

Burggraf, O.R. 1966 "Asymptotic Solution for the Viscous Radiating Shock Layer." AIAA Journal, Vol. 4, pp. 1725-1734.

Catherall, D. and Mangler, K.W. 1966 "The Integration of the Two-Dimensional Laminar Boundary-Layer Equations Past the Point of Vanishing Skin Friction." J. Fluid Mech., Vol. 26, pp. 163-182.

Cheng, H.K. 1966 "Viscous Hypersonic Blunt-Body Problems and the Newtonian Theory." Fundamental Phenomena in Hypersonic Flow, pp. 90-132. Cornell University Press.

Conti, R. and Van Dyke, M. 1969a "Inviscid Reacting Flow Near a Stagnation Point." J. Fluid Mech., Vol. 35, pp. 799-813.

Conti, R. and Van Dyke, M. 1969b "Reacting Flow as an Example of a Boundary Layer under Singular External Conditions." J. Fluid Mech., Vol. 38, pp. 513-535.

Davis, R.T. 1967 "Laminar Incompressible Flow Past a Semi-Infinite Flat Plate." J. Fluid Mech., Vol. 27, pp. 691-704.

Davis, R.T. and Flügge-Lotz, I. 1964a "The Laminar Compressible Boundary-Layer in the Stagnation-Point Region of an Axisymmetric Blunt Body Including the Second-Order Effect of Vorticity Interaction." Int. J. Heat Mass. Transf., Vol. 7, pp. 341-370.

Davis, R.T. and Flügge-Lotz, I. 1964b "Second-Order Boundary-Layer Effects in Hypersonic Flow Past Axi-Blunt Bodies." J. Fluid Mech., Vol. 20, pp. 593-623.

Dean, W.R. 1954 "On the Steady Motion of Viscous Liquid Past a Flat Plate." Mathematika, Vol. 1, pp. 143-156.

Cooke, J.C. 1966 "Similar Second-Order Incompressible Laminar Boundary Layers." RAE Tech. Rept. No. 66044.

Devan, L. 1964 "Second-Order Incompressible Laminar Boundary Layer Development on a Two-Dimensional Semi-Infinite Body." Ph.D. Dissertation, University of California at Los Angeles.

Fannelöp, T.K. and Flügge-Lotz, I. 1965 "Two-Dimensional Hypersonic Stagnation Flow at Low Reynolds Numbers." Z. Flugwiss, Vol. 13, pp. 282-296.

Fannelöp, T.K. and Flügge-Lotz, I. 1966 "Viscous Hypersonic Flow Over Simple Blunt Bodies; Comparison of a Second-Order Theory with Experimental Results." J. Mecanique, Vol. 5, pp. 69-100.

Ferri, A. and Libby, P.A. 1954 "Note on an Interaction Between the Boundary Layer and the Inviscid Flow." J. Aero. Sci., Vol. 21, p. 130.

Friedrichs, K.O. 1953 "Special Topics in Fluid Dynamics, pp. 120-130, New York Univ.; Gordon and Breach, New York, 1966, pp. 153-162.

Glauert, M.B. 1957 "The Boundary Layer in Simple Shear Flow Past a Flat Plate." J. Aero. Sci., Vol. 24, pp. 848-849.

Glauert, M.B. and Lighthill, M.J. 1955 "The Axisymmetric Boundary Layer on a Long Thin Cylinder." Proc. Roy. Soc. A, Vol. 230, pp. 188-203.

Goldstein, S. 1930 "Concerning Some Solutions of the Boundary-Layer Equations in Hydrodynamics." Proc. Camb. Phil. Soc., Vol. 26, pp. 1-30.

Goldstein, S. 1938 "Modern Developments in Fluid Dynamics." Clarendon Press, Oxford.

Hayashi, N. 1963 "Effects of Surface Curvature on Laminar Boundary Layer Flows." AIAA Journal, Vol. 1, pp. 914-915.

Hayes, W.D. 1964 "Rotational Stagnation Point Flow." J. Fluid Mech., Vol. 19, pp. 366-374.

Howarth, L. 1938 "On the Solution of the Laminar Boundary Layer Equations." Proc. Roy. Soc. A, Vol. 164, pp. 547-579.

Imai, I. 1957 "Second Approximation to the Laminar Boundary-Layer Flow Over a Flat Plate." J. Aero. Sci., Vol. 24, pp. 155-156.

Kaplun, S. 1954 "The Role of Coordinate Systems in Boundary-Layer Theory." ZAMP, Vol. 5, pp. 111-135.

Kaplun, S. and Lagerstrom, P.A. 1957 "Asymptotic Expansions of Navier-Stokes Solutions for Small Reynolds Numbers." J. Math. Mech., Vol. 6, pp. 585-593.

Kelly, H.R. 1954 "A Note on the Laminar Boundary Layer on a Circular Cylinder in Axial Incompressible Flow. J. Aero. Sci., Vol. 21, p. 634.

Kuo, Y.H. 1953 "On the Flow of an Incompressible Viscous Fluid Past a Flat Plate at Moderate Reynolds Numbers." J. Math. and Phys., Vol. 32, pp. 83-101.

Lee, R.S. and Cheng, H.K. 1969 "On the Outer-Edge Problem of a Hypersonic Boundary Layer." J. Fluid Mech., Vol. 38, pp. 161-179.

Li, T.Y. 1955 "Simple Shear Flow Past a Flat Plate in an Incompressible Fluid of Small Viscosity." J. Aero Sci., Vol. 22, pp. 651-652.

Li, T.Y. 1956 "Effects of Free Stream Vorticity on the Behavior of a Viscous Boundary Layer." J. Aero. Sci Vol. 23, pp. 1128-1129.

Maslen, S.H. 1963 "Second Order Effects in Laminar Boundary Layers." AIAA Journal, Vol. 1, pp. 33-40.

Massey, B.S. and Clayton, B.R. 1965 "Laminar Boundary Layers and Their Separation from Curved Surfaces." Trans. ASME, J. Basic Engr., Vol. 87D, p. 483.

Massey, B.S. and Clayton, B.R. 1966 "Comment on 'Extensions of the Falkner-Skan Similar Solutions to Flows with Surface Curvature.'" AIAA Journal, Vol. 4, p. 1149.

Messiter, A.F. 1970 "Boundary-Layer Flow Near the Trailing Edge of a Flat Plate." SIAM J. Appl. Math., to appear.

Murphy, J.S. 1953 "Some Effects of Surface Curvature on Laminar Boundary-Layer Flow." J. Aero. Sci., Vol. 2 pp. 338-344.

Murphy, J.S. 1961 "Extensions of the Falkner-Skan Similar Solutions of the Boundary-Layer Equations to Flow With Surface Curvature." Douglas Aircraft Co. Rept. ES 40487.

Murphy, J.S. 1965 "Extensions of the Falkner-Skan Similar Solutions to Flows with Surface Curvature." AIAA Journal, Vol. 3, pp. 2043-2049.

Narasimha, R. and Ojha, S.K. 1967 "Effects of Longitudinal Surface Curvature on Boundary Layers." J. Fluid Mech., Vol. 29, pp. 187-199.

Neiland, V. Ya. and Sychev, V.V. 1966 "Asymptotic Solutions of the Navier-Stokes Equations in Regions with Large Local Perturbations." Fluid Dynamics, Vol. 1, No. 4, pp. 25-28.

Rott, N. and Lenard, M. 1962 "The Effect of Slip, Particularly for Highly Cooled Walls." J. Aero. Sci., Vol. 29, pp. 591-595.

Rubin, S.G. 1966 "Incompressible Flow Along a Corner." J. Fluid Mech., Vol. 26, pp. 97-110.

Rubin, S.G. and Falco, R. 1968 "Plane Laminar Jet." AIAA Journal, Vol. 6, pp. 186-187.

Schlichting, H. 1934 "Laminare Kanaleinlaufströmung." ZAMM, Vol. 14, pp. 368-373.

Schultz-Grunow, F. and Breuer, W. 1965 "Laminar Boundary Layers on Cambered Walls." Basic Developments in Fluid Dynamics, pp. 377-436, Academic Press.

Seban, R.A. and Bond, R. 1951 "Skin-Friction and Heat-Transfer Characteristics of a Laminar Boundary Layer on a Cylinder in Axial Incompressible Flow." J. Aero. Sci., Vol. 18, pp. 671-675.

Stahara, S.J. 1969 "Supersonic Flow over an Ogive of Revolution - An Example of a Boundary Layer under Singular Outer Conditions." Ph.D. Dissertation, Stanford University.

Stewart, R.W. 1956 "Irrotational Motion Associated with Free Turbulent Flows." J. Fluid Mech., Vol. 1, pp. 593-606.

Stewartson, K. 1955 "The Asymptotic Boundary Layer on a Circular Cylinder in Axial Incompressible Flow." Quart. Appl. Math., Vol. 13, pp. 113-122.

Stewartson, K. 1969 "On the Flow Near the Trailing Edge of a Flat Plate II." Mathematika, Vol. 16, pp. 106-121.

Tani, I. 1949 "Effect of Curvature on the Velocity Distribution in the Boundary Layer." (Japanese) J. Japan. Soc. Mech. Engrs., Vol. 52, pp. 476-477.

Tani, I. 1954 "Effect of Curvature on the Velocity Distribution in the Boundary Layer." (revised)(Japanese). J. Japan. Soc. Mech. Engrs., Vol. 57, pp. 596-598.

Toomre, A. and Rott, N. 1964 "On the Pressure Induced by the Boundary Layer on a Flat Plate in Shear Flow." J. Fluid Mech., Vol. 19, pp. 1-10.

Van Dyke, M. 1961 "Second-Order Compressible Boundary-Layer Theory with Application to Blunt Bodies in Hypersonic Flow." Stanford University, SUDAER Rept. No. 112; Hypersonic Flow Research, pp. 37-76, Academic Press, New York.

Van Dyke, M. 1969 "Higher-Order Boundary-Layer Theory." Annual Review of Fluid Mechanics, Vol. 1, pp. 265-292. Annual Reviews, Inc., Palo Alto, California.

Van Dyke, M. 1970 "Channel Entry as a Boundary-Layer Problem." J. Fluid Mech., to appear.

Wang, Y.L. and Longwell, P.A. 1964 "Laminar Flow in the Inlet Section of Parallel Plates." AIChE Journal, Vol. 10, pp. 323-329.

Weinbaum, S. and Garvine, R.W. 1966 "The Pressure Field in Compressible Boundary Layer Theory - A Critical Re-Examination and Treatment." General Electric Space Sci. Lab. Rept. No. R66SD13.

Werle, M.J. 1968 "Solutions of the Second-Order Boundary-Layer Equation for Laminar Incompressible Flow." Naval Ordnance Lab. Rept. No. NOLTR-68-19.

Werle, M.J. and Davis, R.T. 1970 "Self-Similar Solutions to the Second-Order Incompressible Boundary Layer Equations." J. Fluid Mech., Vol. 40, pp. 343-360.

Yen, K.T. and Toba, K. 1961 "A Theory of the Two-Dimensional Boundary Layer over a Curved Surface." J. Aero. Sci., Vol. 28, pp. 877-884.

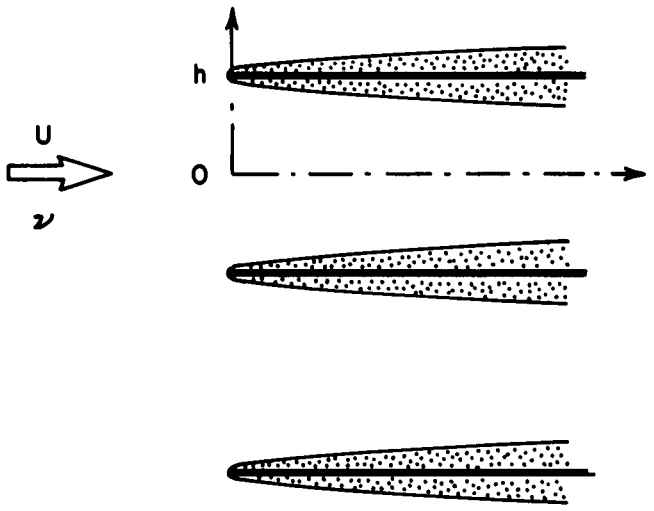

Fig.1 Boundary layers on cascade

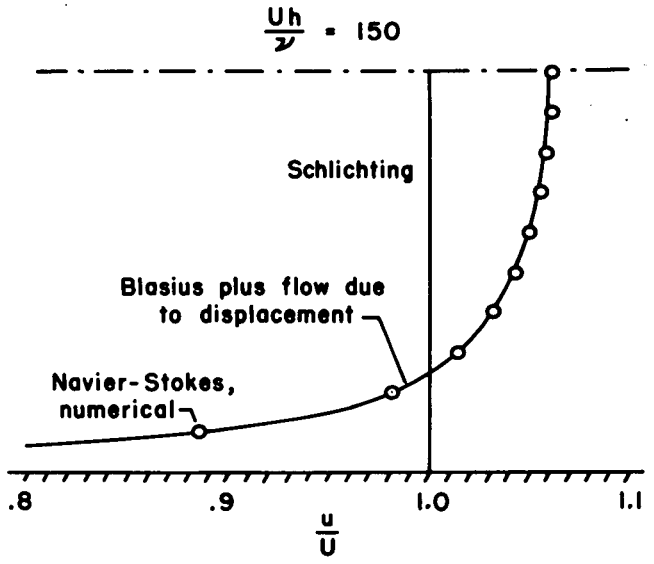

Fig.2 Entry profile

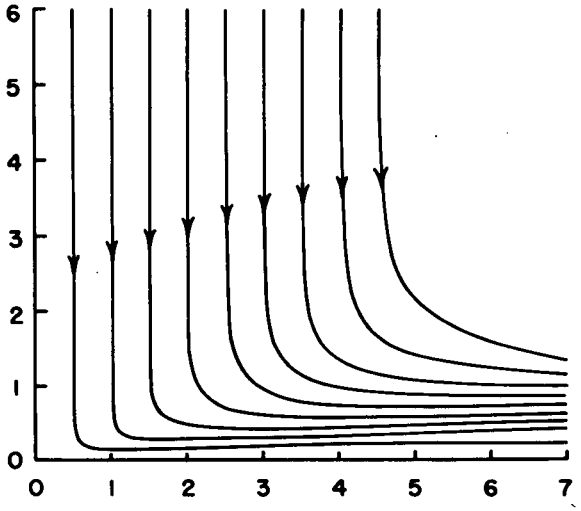

Fig.3 Boundary-layer solution for axisymmetric laminar jet in cylindrical coordinates

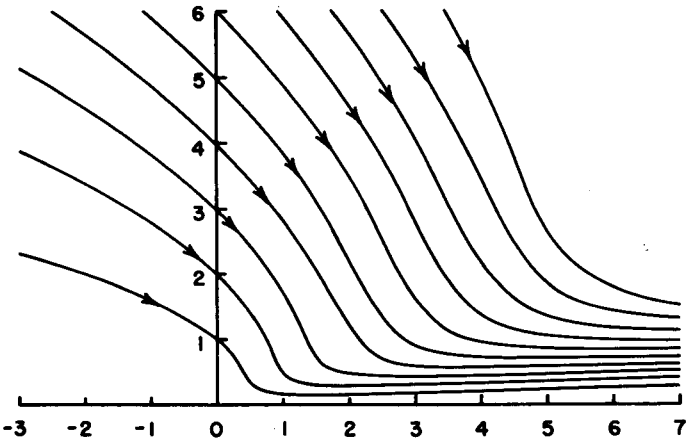

Fig.4 Boundary layer plus displacement flow for axisymmetric laminar jet from nozzle

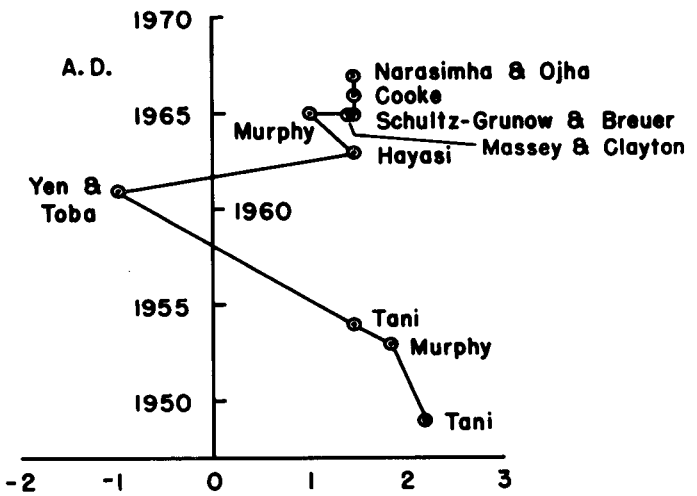

Fig.5 Coefficient of second-order skin friction due to curvature

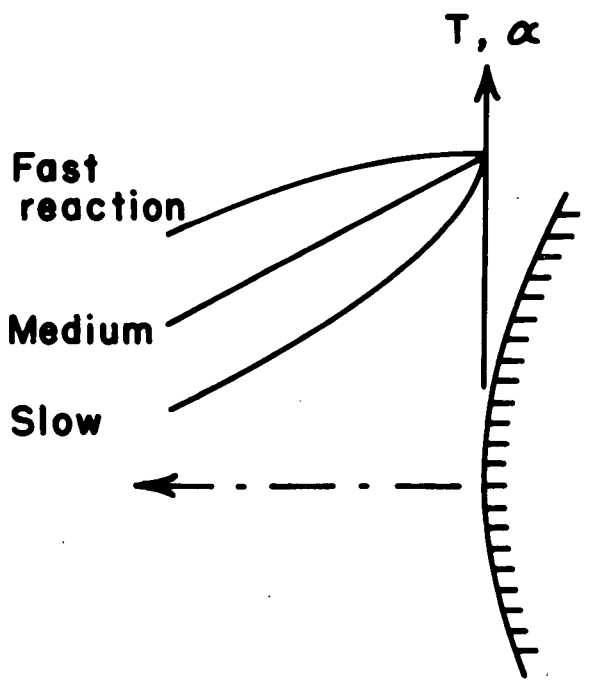

Fig.6 Nonanalytic outer flow near stagnation point

FINITE DIFFERENCE SOLUTION OF THE FIRST-ORDER BOUNDARY LAYER EQUATIONS

by

F.G.Blottner

Staff Member, Aero and Thermodynamics Department,
Sandia Corporation, Albuquerque, New Mexico

FINITE DIFFERENCE SOLUTION OF THE FIRST-ORDER BOUNDARY LAYER EQUATIONS

by F. G. Blottner*

SUMMARY

A review of various methods for solving the laminar-boundary-layer equations by numerical techniques is given. The emphasis is on the finite-difference schemes that have been employed recently and how the presently employed techniques have evolved.

The governing equations are presented in the similarity coordinate system for a multi-component gas with finite reaction rates. An implicit finite-difference technique is presented which is appropriate for solving flows with a large number of chemical species, as occurs with ablation contaminants. This method does not require iterations at each step, and solutions can be obtained when the gas is near chemical equilibrium. Two test cases are presented for the boundary-layer flow on a sharp cone and hyperboloid at reentry conditions.

REVIEW OF NUMERICAL TECHNIQUES

The step-by-step solution of the first-order boundary-layer equations was considered by Prandtl [1] as early as 1938. A review of the early work (up to 1955) on numerical solutions of the boundary-layer equations is given in [2], while a more recent review of the Russian literature is given in [3,4]. There has been a rapid development of numerical techniques in recent years, and these can be divided into the following categories: (i) difference-differential procedure, (ii) method of integral relations, (iii) finite-difference schemes.

The difference-differential procedure was originally developed by Hartree and Womersley [5] and has been applied by Leight [6] and Manohar [7] to the boundary-layer equations. Smith and colleagues [8-13] have exploited and developed this procedure even further, and have applied it to a variety of problems. In this scheme the derivatives in the direction along the surface are usually replaced with finite-difference relations, the partial differential equations reduce to ordinary differential equations with two-point boundary conditions. The ordinary differential equations are solved as an initial-value problem which requires an iteration procedure to satisfy the boundary conditions at the outer edge. The difference-differential approach has been used by Zamurayev [14] and Le Maréchal and Ronat [15], but these authors linearize the ordinary differential equations and obtain the solution in an iterative manner with finite-difference method. Steiger and Sepri [16] have investigated the solution of the boundary layer with the difference-differential procedure where the normal derivatives are replaced by finite-difference relations. This results in a system of first-order ordinary differential equations of the initial-value type, and these equations are of the "stiff" type also. This approach has been developed further by Lubard and Schetz [17].

The method of integral relations is a special case of the method of weighted residuals, as has been discussed by Finlayson and Scriven [18]. This method is due to Dorodnitsyn [19] and has been employed in a number of Russian papers [19-22]. The procedure has also been employed by Pallone and colleagues [23,24], and investigated further by Bethel [25,26]. This technique reduces the partial differential equations to a system of ordinary differential equations of the initial-value type.

Recently Kendall and Bartlett [27] have used the integral method to replace the normal derivatives, while the differential-difference procedure of replacing the tangential derivatives has also been employed. The partial differential equations are thus reduced to a system of nonlinear algebraic equations which must be solved at each step along the body.

After the early finite-difference techniques [28-36], which have been reviewed in [2], the emphasis was on the solution of the boundary-layer equations in the Crocco form, as exemplified by [37-41]. The approach was partially used by Eichelbrenner; the procedure was developed further, and preliminary examples were computed by Flügge-Lotz using a desk calculation. This work was extended by Baxter and Flügge-Lotz, and a digital computer was utilized for the finite-difference solution. In this work an explicit finite-difference scheme was employed in which the step size along the wall is restricted by stability considerations.

In order to avoid the stability restrictions required in explicit schemes, Kramer and Lieberstein [42] employed an implicit scheme with the Crocco form of the equations.†

Another difference scheme that has been used by Raetz [43] for solving the three-dimensional boundary-layer equations is that of Dufort-Frankel. This scheme is stable, but care must be taken to insure that the truncation error is sufficiently small. In differencing the partial differential equation, a term has been added to the equations, and this term will only be small if the appropriate ratio of the step sizes are taken.

Besides employing various finite-difference procedures, the form of the boundary-layer equation can be changed. The von Mises transformed boundary-layer equations have been solved with an explicit finite-difference scheme by Mitchell and Thomson [44,45]. The advantage of this form of the boundary-layer equations is that the continuity equation has been eliminated. There is a singularity at the wall which introduces difficulties, but these have been overcome in the papers by Mitchell and Thomson.

*Staff Member, Aero and Thermodynamics Department, Sandia Corporation, Albuquerque, New Mexico.

†The Crocco form of the equations is attractive because the continuity equation has been eliminated and the independent variable u/u_e, which is related to the thickness of the boundary layer, goes from zero to one. If the velocity within the boundary layer exceeds the edge velocity, the Crocco form of the equations is difficult to apply.

The solution of the boundary-layer equations in untransformed or physical coordinates appears to be the next development in the numerical schemes. In the paper by Flügge-Lotz and Yu [46], an explicit finite-difference procedure was applied to the compressible equations. This proved rather unsuccessful, as the stability requirements are very stringent and the replacement of the continuity equation caused many problems. In the paper by Wu [47], the treatment of the continuity was such that more stable solutions were obtained with an explicit difference scheme. Also, by transforming the compressible equations into incompressible form, with the Howarth-Dorodnitsyn relation, the stability requirements are not as restrictive when a constant step size across the boundary layer is used and when the step size is the same for both coordinate systems. For these conditions, the physical distance for the first grid point away from the wall is much larger in the Howarth-Dorodnitsyn variables. In Russia, Chudov and Brailovskaya [48,49] also studied the solution of the boundary-layer equation in physical coordinates; however, an implicit six-point finite-difference scheme was used. The governing equations are replaced with finite differences such that the coupling between equations is initially neglected. Then an iteration process is employed to obtain the desired accuracy of the dependent variables with coupling and nonlinear effects included. This type of procedure has been developed into a standard program for equations of the boundary-layer type by Paskonov [50]. In this program a procedure is described which allows the step size across the boundary layer to vary. At about the same time, in the United States a similar implicit technique was developed independently for the boundary-layer equations in physical coordinates by Flügge-Lotz and Blottner [51]. The main difference between this work and that of Chudov and Brailovskaya is that coupling between the equations is allowed. This results in a tridiagonal matrix with matrix elements, which is somewhat more complicated to solve than the uncoupled equations. The boundary-layer equations transformed with the Howarth-Dorodnitsyn relations was also investigated by Flügge-Lotz and Blottner, and both a four-point and six-point (Crank-Nicolson) difference scheme were considered. For hypersonic boundary-layer flows, using the transformed equations with the six-point implicit scheme is the better procedure.

One of the problems with all the previous methods is the starting of the solutions of the equations. Initial profiles of the dependent variables are required across the boundary layer at some point, and the solution then proceeds downstream. For sharp bodies one would want to start the solution at the tip, while for a blunt body the solution should start at the stagnation point. At the tip of a sharp body, the boundary layer thickness goes to zero and the finite-difference scheme is inappropriate in the physical coordinates.* If the boundary-layer equations are transformed into similarity variables (relations developed by Mangler, Görtler, Howarth-Dorodnitsyn, Levy, and Lees), then in the transformed plane the boundary layer is nearly of uniform thickness for many flow situations. Also the partial differential equations reduce to ordinary differential equations at the tip of a body or at a stagnation point. The solution of these ordinary differential equations provides initial conditions for a finite-difference solution which can start at the beginning of the body. This type of procedure was applied to a binary gas mixture with finite chemical reaction rate by Blottner [52]. The transformed boundary-layer equations were replaced with an implicit six-point finite-difference scheme, and coupling between the equations was included. This procedure was extended to the air boundary layer with seven chemical species and finite reaction rates by Blottner [53]. The chemically reacting boundary layer has been solved with an explicit finite-difference scheme by Galowin and Gould [54]. The boundary-layer equations are transformed into von Mises coordinates before the derivatives are replaced with difference quotients. In this study for flow on blunt bodies, the swallowing of the inviscid flow by the boundary layer is taken into account.

The application of the finite-difference technique to second-order boundary-layer theory has been made by Davis and Flügge-Lotz [55] and Fannelop and Flügge-Lotz [56] for axisymmetric and two-dimensional bodies, respectively. An implicit finite-difference technique similar to that developed by Flügge-Lotz and Blottner [51] was employed. In linearizing the finite-difference equation, certain terms are evaluated at the known grid point rather than at the point halfway between the known and the unknown points. For stagnation-point flows, Davis and Flügge-Lotz found it advantageous to use linear extrapolation to approximate the unknown quantities at the halfway point. This procedure requires that two profiles of the dependent variable be known.

In a paper by Fussell and Hellums [57], an implicit finite-difference procedure is applied to the similarity form of the boundary-layer equation. The momentum equation has a third-order derivative and results in a pentadiagonal matrix, while the energy equation becomes a tridiagonal matrix. The procedure recommended in this paper is to use a 10-point symmetric implicit finite-difference scheme, with the equations replaced initially by a linear difference equation. An iteration procedure is used until the nonlinear difference equations corresponding to the grid points employed have been solved.

An explicit finite-difference scheme has been used by Kleinstein [58] to solve the boundary-layer equations in von Mises variables. This work is for a compressible perfect gas, and the approach is similar to that of Mitchell and Thomson [42] and Galowin and Gould [54], where an incompressible gas and a reacting gas are employed, respectively. Later a revision of this work was reported by Kleinstein [59], and a description and operation instructions for the program were given by Nabi [60].

For boundary-layer programs at General Applied Science Laboratories, Lane [61] initially recommended that an explicit finite-difference technique be used. Later Lane, Lieberman, and Fox [62] used an implicit finite-difference scheme to solve the compressible boundary-layer equations in physical coordinates. The momentum and energy equations are uncoupled, and iterations are performed until a solution of the nonlinear coupled equations is obtained. This method is that of Brailovskaya and Chudov [48,49]. Lieberman, Lane, and Fox [63] have also investigated boundary-layer flow of air in chemical equilibrium and finite rate chemistry. In this work an implicit finite-difference scheme is used near the initial station to start the solution, and then reverts to an explicit scheme downstream.

The numerical solution of reacting boundary layers has also been investigated by Gruenich and Pindroh [64]. The difference-differential method of Smith [8-13] is used for the momentum and energy equations, while

*The boundary-layer equations at the tip of a body are also physically inappropriate, as continuum theory is not valid; and when it is, more complete equations are required. However, from a mathematical point of view, one can still consider the boundary-layer solution.

an implicit scheme is used for the species equations. In this method an iteration procedure is required to solve the momentum equation, and two trial solutions are required for the energy equation.

In the implicit finite-difference procedure developed by Flügge-Lotz and Blottner [51], it was assumed that both the normal and tangential velocity components and the temperature distribution are known from similarity solutions across the boundary layer. In a recent paper by Ting [65], the compatibility conditions for the velocity components have been investigated further than in the original work of Prandtl. The proper formulation is to specify the tangential velocity component and then to determine the normal velocity component from the compatibility conditions. This approach has been incorporated into the implicit finite-difference scheme originally developed by Flügge-Lotz and Blottner, and this technique has been examined further by Krause [66]. The normal velocity component is obtained in an iterative manner by requiring that the continuity, momentum, and energy equations are satisfied at each step. The finite-difference procedure is the same as that of Flügge-Lotz and Blottner, except the normal velocity component is assumed initially in order to solve the momentum and energy equations. Then the continuity equation is solved to obtain a better value of the normal velocity component which is averaged with the initially assumed value to obtain a new estimate of the normal velocity component. This type of procedure is repeated until convergence is obtained.

To avoid third-order derivatives in the governing equations, when the boundary-layer equations are transformed into similarity form, a transformed normal velocity is introduced by Blottner [52] and the continuity equation is retained. Fannelop [67] has applied the same type of transformation but has introduced the stream function such that the continuity equation is satisfied. However, in introducing the stream function, the momentum equation is still written as a second-order equation. The new partial differential equation for momentum involves f and $\partial f/\partial \xi$. The value of f can be readily obtained from an integration once the value of the tangential velocity component across the boundary layer is known. The value of f and $\partial f/\partial \xi$ are required for the solution of the momentum equation, and the solution of this equation gives the tangential velocity component. The value of the quantities f and $\partial f/\partial \xi$ for the difference equation are evaluated by employing a linear extrapolation of the values of these quantities at two previous profiles.

A multicomponent reacting gas with thermal diffusion effects included has been investigated by Moore [68], where the implicit finite-difference scheme was provided by Farrington [69]. The similarity coordinates are used with a stretching of the normal coordinate near the surface. A Crank-Nicolson implicit finite-difference scheme is used with the equation uncoupled. The final solution is obtained after an iteration procedure is performed that corrects the linearized terms and approximations made to uncouple the governing equations. In this work it was observed that stability problems occurred for the Crank-Nicolson scheme with boundary condition involving derivatives. This problem was eliminated by using a four-point implicit scheme at the first grid point away from the wall.

An implicit finite-difference scheme of the boundary-layer equations in nearly the Crocco form has been studied by Schönauer [70]. Rather than using the shearing stress as a dependent variable, a quantity proportional to the square of the velocity gradient is used. The independent variable for the coordinate normal to the surface is the tangential velocity which is nondimensionalized with the velocity at the edge of the boundary layer, and the independent variable therefore varies from 0 to 1.

A method has been given by Shchennikov [71] for constructing finite-difference schemes for the boundary layer on the basis of the laws of conservation. The governing equations are written as the divergence of a vector as two integrals. The integrals are then expanded with the trapezoidal formula and normal derivatives are replaced with central differences. The result of these operations is a system of nonlinear finite-difference equations with coupling between the equations involving the dependent variables.

An implicit finite difference has been developed by Patanker and Spalding [72] for solving boundary-layer equations. The governing equations are transformed with a von Mises-type coordinate system, where the stream function is an independent variable across the layer. A nondimensional stream function is defined such that it varies from 0 to 1 from the wall to the outer edge. A parameter in the nondimensional stream function is determined as the calculation proceeds such that the grid adjusts its width so as to conform to the thickness of the layer. The finite difference scheme is the Crank-Nicolson implicit scheme, except the convection terms are based on an integrated average over a small control volume. This results in the streamwise derivative being approximated as a weighted average of the derivatives at the point of interest and those on both sides of this point. This method of differencing the equations is similar to that used by Shchennikov [71].

The boundary-layer flow on a rotating cone has been obtained with a finite-difference method by Koh and Price [73]. The governing equations are transformed with similarity-type variables, and the stream function is introduced in the manner employed by Fannelop [67] as previously described. An implicit finite-difference scheme of the Crank-Nicolson type is employed, and linear difference equations are written such that the coupling between equations is neglected initially. The linear difference equations are solved in an iterative manner which gives the solution of the coupled nonlinear difference equations.

The finite-difference procedure has also been employed for the Rayleigh problem and a flat-plate boundary-layer flow, with radiation effects included by Solan and Cohen [74] and Sibulkin and Dispaux [75], respectively. The boundary-layer equations are transformed with the von Mises transformation initially, and then new independent variables are introduced which transform the equations to the similarity-type form. In the absence of radiation or at the leading edge of the flat plate, the governing equations become ordinary differential equations, or similarity solutions are obtained. The partial differential equations are solved with a Crank-Nicolson six-point finite-difference scheme. The resulting difference equations are nonlinear algebraic equations and are solved by an iteration scheme given by Douglas [76]. A finite-difference method proposed by Douglas [76] was also investigated for the Rayleigh problem, but stability restriction required a relatively small step along the body. In this method nine points at three time levels are employed and the resulting difference equations are linear and are readily solved.

The boundary-layer equations for real equilibrium gases has been solved with an implicit finite difference method by Levine [77]. This method is that employed by Blottner [52], where the difference equations are coupled.

A transformation that maps the infinite region of the boundary-layer flow into a finite interval has been used by Sills [78]. The transformed governing equations are then solved with an implicit finite difference scheme similar to that employed by Paskonov [50].

In this paper a technique for solving the boundary-layer equations for a multicomponent flow with finite chemical reactions is presented. This procedure has evolved over a number of years, and an earlier version was reported in [79]. The motivation for the present finite-difference scheme is the desire for a method for solving the governing equations where there are many chemical species in the flow (for example, 25). The technique is described in the following sections, and typical results are presented for the boundary-layer flow on a hyperboloid.

GOVERNING EQUATIONS

The general equations for a multicomponent nonequilibrium gas are given in [80], and the resulting equations for the boundary layer have been given in [53]. The boundary-layer equations are transformed into similarity form in order to obtain them in a form more appropriate for numerical solution. The new independent variables are

$$\xi(x) = \int_0^x (\rho\mu)_r u_e r_b^{2j}\, dx \tag{1a}$$

$$\eta(x,y) = \frac{u_e r_b^j}{(2\xi)^{1/2}} \int_0^y \rho\, dy \tag{1b}$$

and the derivatives become

$$\frac{\partial}{\partial x} = (\rho\mu)_r u_e r_b^{2j} \frac{\partial}{\partial \xi} + \frac{\partial \eta}{\partial x}\frac{\partial}{\partial \eta} \tag{2a}$$

$$\frac{\partial}{\partial y} = \frac{\rho u_e r_b^j}{(2\xi)^{1/2}} \frac{\partial}{\partial \eta} \quad . \tag{2b}$$

When the new dependent variables

$$V = \frac{2\xi}{(\rho\mu)_r u_e r_b^{2j}} \left(f' \frac{\partial \eta}{\partial x} + \frac{\rho v r_b^j}{(2\xi)^{1/2}} \right) \tag{3a}$$

$$f' = u/u_e \tag{3b}$$

$$\theta = T/T_e \tag{3c}$$

are introduced and the transformations are applied, the boundary-layer equations become the following in the transformed plane.

Continuity Equation

$$2\xi \frac{\partial f'}{\partial \xi} + \frac{\partial V}{\partial \eta} + f' = 0 \tag{4a}$$

Momentum Equation

$$2\xi \frac{\partial f'}{\partial \xi} + \left(\frac{V - \ell'}{f'} \right) \frac{\partial f'}{\partial \eta} + \beta \left[f' + \frac{\bar{M}_e}{\bar{e}\bar{M}} \frac{\theta}{f'} \right] - \frac{\ell}{f'} \frac{\partial^2 f'}{\partial \eta^2} = 0 \tag{4b}$$

Energy Equation

$$2\xi f' \frac{\partial \theta}{\partial \xi} + \left(V - \frac{\bar{c}'}{\bar{c}_p} + d + b \right) \frac{\partial \theta}{\partial \eta} - \alpha\ell \left(\frac{\partial f'}{\partial \eta} \right)^2 + \left(- \alpha\beta \frac{\bar{M}_e}{\bar{M}\bar{e}} + \bar{e} \right) \theta f' - \frac{\bar{c}}{\bar{c}_p} \frac{\partial^2 \theta}{\partial \eta^2} - \frac{\bar{a}}{\theta} \left(\frac{\partial \theta}{\partial \eta} \right)^2 + \frac{e}{\bar{c}_p T_e} \sum_{i=1}^{NI} h_i \left(\frac{w_i}{\rho} \right) = 0 \tag{4c}$$

Species Equations

$$2\xi f' \frac{\partial c_i}{\partial \xi} + (V - b_i') \frac{\partial c_i}{\partial \eta} - b_i \frac{\partial^2 c_i}{\partial \eta^2} - \frac{\bar{a}_i}{\theta} \frac{\partial^2 \theta}{\partial \eta^2} - \frac{\bar{a}_i}{\theta} \frac{\partial \theta}{\partial \eta} + \left(\frac{\bar{a}_i}{\theta^2} \right) \left(\frac{\partial \theta}{\partial \eta} \right)^2 - \bar{b}_i' - e \left(\frac{w_i}{\rho} \right) = 0 \tag{4d}$$

where

$$\bar{a}_i = \frac{\ell L_i^T}{Pr} \quad , \qquad a = \frac{1}{\bar{c}_p} \sum_{i=1}^{NI} \bar{a}_i c_{p_i} \qquad b_i = \frac{\ell Le_i}{Pr} \quad , \qquad \bar{b}_i = \frac{\ell}{Pr} \sum_{\substack{k=1 \\ k \neq 1}}^{NI} \Delta\bar{\bar{b}}_{i,k} \frac{\partial c_k}{\partial \eta}$$

$$b = - \sum_{i=1}^{NI} \frac{c_{p_i} \bar{b}_i}{\bar{c}_p} \quad , \quad \bar{c} = \frac{\ell \bar{c}_p}{Pr} \qquad e = \frac{2\xi}{u_e \frac{d\xi}{dx}} \quad , \quad \bar{e} = \frac{2\xi}{T_e} \frac{dT_e}{d\xi} \quad ,$$

$$\bar{\bar{e}} = \rho_e u_e \frac{du_e/dx}{dp_e/dx} \qquad d = -\sum_{i=1}^{NI} \frac{c_{p_i}}{\bar{c}_p} b_i \frac{\partial c_i}{\partial \eta}$$

$$\alpha = \frac{u_e^2}{\bar{c}_p T_e} , \qquad \beta = \frac{2\xi}{u_e}\frac{du_e}{d\xi} = e\frac{du_e}{dx}$$

$$\ell' = \frac{\partial \ell}{\partial \eta} \qquad \bar{a}_i = \frac{\partial \bar{a}_i}{\partial \eta} \qquad b_i' = \frac{\partial b_i}{\partial \eta} \qquad \bar{b}_i' = \frac{\partial \bar{b}_i}{\partial \eta}$$

The above equations differ from those given in [53] by the quantity $\bar{\bar{e}}$ which has been set equal to -1 in that reference. For the classical boundary-layer approach, the inviscid flow body streamline results are used as the conditions at the edge of the boundary layer. For this case, $\bar{\bar{e}} = -1$. For the more general case where swallowing of the inviscid flow into the boundary layer is taken into account, the value of $\bar{\bar{e}}$ must be determined from the expression given above.

In the above relations, the mass flux relative to the mass-average velocity, j_i has been used and was written as

$$j_i = -\frac{\mu}{Pr}\left\{\sum_{k=1}^{NI} \bar{\bar{b}}_{ik}\frac{\partial c_k}{\partial y} + \frac{L_i^T}{T}\frac{\partial T}{\partial y}\right\} \tag{5}$$

where

$$\bar{\bar{b}}_{ik} = \begin{cases} Le_i & i = k \\ \Delta\bar{\bar{b}}_{ik} & i \neq k \end{cases}$$

$$Le_i = \frac{\sum_{\substack{j=1 \\ j\neq l}}^{NI} \frac{c_j}{M_j}}{\sum_{\substack{j=1 \\ j\neq l}}^{NI} \frac{c_j}{M_j L_{ij}}}$$

$$\Delta\bar{\bar{b}}_{ik} = Le_i - \left[\frac{M_i}{\bar{M}} L_{ik} + \left(1 - \frac{M_i}{M_k}\right)\sum_{j=1}^{NI} L_{ij} c_j\right]$$

If the Lewis-Semenov numbers, L_{ij}, are constant for all the species or if a trace species is being considered, the term $\Delta\bar{\bar{b}}_{ik}$ is zero. In Eq. (5), the pressure diffusion term is neglected due to the boundary-layer assumption, and the forced diffusion term is assumed zero.

The equation of state is also required and is written as

$$\rho = \frac{p_e}{RT\sum_{i=1}^{NI}(c_i/M_i)} = \frac{p_e \bar{M}}{RT} \tag{6}$$

where it is assumed the gas consists of a mixture of chemically reacting perfect gases with the pressure change across the boundary layer neglected.

The chemical mass rate of production of species i per unit volume, w_i, is obtained from the Law of Mass Action, and the desired form is given in [53]. The gas model for air and the chemical kinetics employed are the same as described in [81]. Also the thermodynamic and transport properties of the individual species and the mixture are required. These properties are obtained from the same relations and information as was employed in [81]. The multicomponent Lewis-Semenov numbers were obtained from relations given in [82], which are written as

$$L_{ij} = \bar{F}_{ij} - \frac{M_i}{M_j}\bar{F}_{ii} \tag{7}$$

The quantities $\bar{F}_{ij}$ are coefficients in a matrix which is the inverse of the matrix with the following coefficients:

$$F_{ij} = \frac{c_i}{L_{ij}} + M_j \sum_{\substack{\ell=1 \\ \ell\neq l}}^{NI} \frac{c_\ell}{M_\ell L_{i\ell}} \qquad i \neq j \tag{8a}$$

$$F_{ij} = 0 \qquad i = j \tag{8b}$$

The binary Lewis-Semenov numbers are obtained using the definition and binary diffusion coefficients which are expressed as

$$\mathcal{D}_{ij} = (\bar{\mathcal{D}}_{ij}/\bar{p})\ 1.0764 \times 10^{-3} \quad (ft^2/sec) \tag{9}$$

where

$\bar{p}$ = pressure in atmospheres

$$\bar{\mathcal{D}}_{ij} = e^{C_{T_K}^{A \ln T_K + B}} \quad (cm^2 \text{ atm/sec})$$

The above expression for $\bar{\mathcal{D}}_{ij}$ was used to curve-fit tabulated binary diffusion coefficients given by Yos [83]. A revised table of values was used for the NO-NO^+ interaction as given in a later paper by Yos [84]. The collision cross sections for the atomic and molecular interactions in these results were obtained from calculations of Mason et al [85,86]. Some of the interaction cross sections were calculated as averages of the other interaction cross sections, while the cross sections for the interactions N-O_2 and N-NO were assumed the same as N-N_2. Also the interaction cross sections for NO^+ with a neutral species have been taken the same as the N-O^+ and O-N^+ cross sections. The curve-fit coefficients for the various binary diffusion coefficients are given in Table I.

The conditions at the surface and outer edge of the boundary layer determine the necessary boundary conditions for the foregoing equations. At the wall, it is assumed that the tangential velocity is zero and the surface temperature is specified, and these conditions are expressed as

$$u(x,0) = 0; \qquad T(x,0) = T_b(x) \tag{10a,b}$$

In addition, the boundary condition on the mass flux of a species "i" at the surface, $(\rho_i v_i)_b$, is

$$(\rho_i v_i)_b = \dot{m}_i = (c_i \rho v)_b + (j_i)_b \qquad (i = 1, 2, \ldots, NI) \tag{10c}$$

The mass flux of a species at the surface depends on the surface material and what phenomena occur at the gas-surface interface. The surface conditions employed are given with the numerical examples presented.

The total mass flux at the surface can be determined from

$$\rho v = \sum_{i=1}^{NI} (\dot{m}_i)_b \tag{11}$$

and this is the boundary condition employed with the continuity equation.

The flow at the edge of the boundary layer is determined from the inviscid non-equilibrium flow around the body.

The boundary conditions at the outer edge of the boundary layer are

$$u \to u_e \; ; \quad T \to T_e \; ; \quad c_i \to c_{i_e} \qquad (i = 1, 2, \ldots, NI) \tag{12}$$

where u_e, T_e, and the c_{i_e}'s are obtained from the inviscid flow. The technique for matching the inviscid flow with the boundary layer is discussed where the numerical results are presented.

FINITE DIFFERENCE PROCEDURE

The solution of multicomponent chemically reacting boundary layers for pure air, or as many as 11 chemical species, has been solved with a finite-difference procedure by Blottner [53]. When the partial differential equations are replaced with the finite-difference equations, the resulting difference equations are coupled, as more than one of the unknown independent variables appear in each equation. Hence, the equations must be solved simultaneously. Since these equations are of a special form, the procedure requires an inversion of 12 x 12 matrices (number of species plus one), where there will be as many of these matrices as points across the boundary layer (50 in this program). All the coefficients of the matrices must be saved (stored in the computer memory), which requires 7200 storage locations. The storage requirements for these matrices increases rapidly when the number of species is increased. This program, with 11 chemical species and 20 reactions, requires nearly the full capacity of the IBM 7094 computer with 32K memory. The computation time for this method increases rapidly when the number of species becomes large. At best, one would expect the computation time to vary nearly directly with the number of species. For matrix inversions, the computation time is proportional to the number of rows or columns of the matrix cubed. Since many matrix inversions are performed, the computation time must be proportional to the number of species to a power greater than one and less than three. The actual time required per step for the present implicit procedure is shown in Fig. 1. Due to the rapid increase in computation time and storage requirements, the implicit procedure does not seem appropriate when one is interested in boundary-layer flows with ablation contaminants where there can be a large number of chemical species.

The question might be asked, why not use an explicit procedure where the computation time is nearly proportional to the number of species and the storage requirements are probably a minimum? For boundary-layer computations, the explicit method has not proved very successful, as stability requirements demand that the step size be exceedingly small, which will result in an excessive overall computation time. In addition, there are problems in starting the solution at the tip or stagnation point of the body.

A method is described below which has the desirable stability characteristics of the implicit procedure (large step size), with the computing time being nearly proportional to the number of species, as in the explicit scheme. The procedure is similar to the implicit procedure of the Crank-Nicolson type which has been employed previously, except the difference equations are written such that only one dependent variable appears in each equation. Therefore, the resulting implicit difference equations are solved for each dependent variable separately.*

*In Russia, this idea of solving the equations individually has also been developed (see [4]).

Another variation of this procedure has also been investigated and is a "predictor-corrector" procedure similar to the method employed by Douglas and Jones [87]. With this method, the variables are predicted at a half step forward, and then these quantities are used to give the value of the variables a complete step ahead. The truncation error for such a procedure is of the order of the step-size $(\Delta x)^2$. The procedure described below consists of only the corrector part of the above method, with variables required at the half step evaluated at the known step, and has a truncation error of the order of the step-size. While the present method (corrector only) is less accurate for the same step-size as the predictor-corrector procedure, the predictor-corrector method requires approximately twice the amount of computer time as the present method. When the step-size of the present method is reduced to one-half of the predictor-corrector step-size, the computation time of the two methods is nearly the same and the accuracy appears to be about the same. Hence, the two methods appear almost equivalent as far as computer time required, but the present method is easier to program and requires less storage.

The boundary-layer equations, with the exception of the continuity equation, are of the following form:

$$\frac{\partial^2 W}{\partial \eta^2} + \alpha_1 \frac{\partial W}{\partial \eta} + \alpha_2 W + \alpha_3 + \alpha_4 2\xi \frac{\partial W}{\partial \xi} = 0 \tag{13}$$

where W represents any of the dependent variables. The coefficients in the above equation are obtained after the boundary-layer equations (4) have been linearized, with the following relations:

$$\frac{1}{f'} = \frac{1}{f'_{m,n}}\left(2 - \frac{f'}{f'_{m,n}}\right) \qquad \frac{1}{f'}W = \left(\frac{W}{f'}\right)_{m,n} + \frac{W}{f'_{m,n}} - \left(\frac{W}{f'}\right)_{m,n}\frac{f'}{f'_{m,n}} \tag{14a,b}$$

$$e\sum_{i=1}^{NI} h_i(w_i/\rho) = \sum_{i=1}^{NI}\left[\bar{W}_i \Delta h_i^F - e\theta h_i \frac{\partial}{\partial\theta}\left(\frac{w_i}{\rho}\right)\right]_{m,n} + \theta T_e \sum_{i=1}^{NI}\left[\bar{W}_i C_{l_i} + \frac{eh_i}{T_e}\frac{\partial}{\partial\theta}\left(\frac{w_i}{\rho}\right)\right]_{m,n} \tag{14c}$$

$$\frac{w_i}{\rho} = W_i^0 - W_i^1 c_i \tag{14d}$$

In the above relations, the quantities without subscripts are evaluated in the neighborhood of the point (m,n). The coefficients in Eq. (13) become

Momentum Equation

$$\alpha_1^1 = -(V - \ell')/\ell \tag{15a}$$

$$\alpha_2^1 = -2\beta f'/\ell - F/f' \tag{15b}$$

$$\alpha_3^1 = -\frac{\beta}{\ell}\left[-(f')^2 + \frac{\bar{M}_e\theta}{\bar{\bar{e}}\bar{M}}\right] + F \tag{15c}$$

$$\alpha_4^1 = -f'/\ell \tag{15d}$$

where

$$F = \frac{\partial^2 f'}{\partial \eta^2} + \alpha_1^1 \frac{\partial f'}{\partial \eta} - \frac{\beta}{\ell}\left[(f')^2 + \frac{\bar{M}_e\theta}{\bar{\bar{e}}\bar{M}}\right] = \frac{2\xi f'}{\ell}\frac{\partial f'}{\partial \xi}$$

Energy Equation

$$\alpha_1^2 = \left[\bar{c}' - \bar{c}_p(V + d + b)\right]\Big/\bar{c} \tag{15e}$$

$$\alpha_2^2 = \left\{\bar{c}_p f'\left(\alpha\beta\frac{\bar{M}_e}{\bar{\bar{e}}\bar{M}} - \bar{e}\right) - \sum_{i=1}^{NI}\left[\bar{W}_i C_{l_i} + \frac{eh_i}{T_e}\frac{\partial}{\partial\theta}\left(\frac{w_i}{\rho}\right)\right]\right\}\Big/\bar{c} \tag{15f}$$

$$\alpha_3^2 = \left\{\bar{c}_p\,\alpha\ell\left(\frac{\partial f'}{\partial \eta}\right)^2 - \frac{1}{T_e}\sum_{i=1}^{NI}\left[\bar{W}_i \Delta h_i^F - \theta e h_i \frac{\partial}{\partial\theta}\left(\frac{w_i}{\rho}\right)\right]\right\}\Big/\bar{c} \tag{15g}$$

$$\alpha_4^2 = -f'\bar{c}_p/\bar{c} \tag{15h}$$

Species Equation (i = 3, 4 ..., NI + 2)

$$\alpha_1^i = -(V - b_i')/b_i \qquad \alpha_2^i = -eW_i^1/b_i \tag{15i,j}$$

$$\alpha_3^i = \left(eW_i^0 + \bar{b}'_i\right)/b_i \qquad \alpha_4^i = -f'/b_i \tag{15k,l}$$

The boundary layer is divided with a grid of size $\Delta\eta$ and $\Delta\xi$ with $\xi = m \cdot \Delta\xi$ and $\eta = n \cdot \Delta\eta$. It is assumed that f', θ, and the c_i's are known at the grid points in the m^{th} column and unknown in the $(m + 1)^{th}$ column. In the present implicit scheme, the derivatives are replaced with linear difference quotients, and the partial differential equations are evaluated at (m + 1/2, n). However, the equations are written with a parameter θ which will give the various finite-difference schemes as indicated below:

$$\theta = \begin{cases} 0 & \text{Explicit} \\ 1/2 & \text{Crank-Nicholson (present scheme)} \\ 1 & \text{Implicit} \end{cases}$$

With the function $W(\xi, \eta)$ representing the dependent variables, the difference quotients are written as

$$\frac{\partial W}{\partial \xi} = (W_{m+1,n} - W_{m,n})/\Delta\xi \tag{16a}$$

$$\frac{\partial W}{\partial \eta} = \left[\theta(W_{m+1,n+1} - W_{m+1,n-1}) + (1 - \theta)(W_{m,n+1} - W_{m,n-1})\right] \Big/ (2\Delta\eta) \tag{16b}$$

$$\frac{\partial^2 W}{\partial \eta^2} = \left[\theta(W_{m+1,n+1} - 2W_{m+1,n} + W_{m+1,n-1}) + (1 - \theta)(W_{m,n+1} - 2W_{m,n} + W_{m,n-1})\right] \Big/ \Delta\eta^2 \tag{16c}$$

$$W = \theta W_{m+1,n} + (1 - \theta)W_{m,n} \qquad W \cdot Z = (1 - 2\theta)W_{m,n}Z_{m,n} + \theta(W_{m,n}Z_{m+1,n} + Z_{m,n}W_{m+1,n}) \tag{16d,e}$$

When the above difference quotients and expressions are used with the partial differential equations (13), the finite-difference equations become the simultaneous (involving only one dependent variable across the boundary layer) linear algebraic equations

$$A_n^i W_{m+1,n+1}^i + B_n^i W_{m+1,n}^i + C_n^i W_{m+1,n-1}^i = D_n^i \tag{17}$$

where $n = 2, 3, \ldots, n - 1$

$i = 1$	Momentum equation	$W^1 = f'$
$i = 2$	Energy equation	$W^2 = \theta$
$i = 3$	First species equation	$W^3 = c_1$
$i = 4$	Second species equation	$W^4 = c_2$
$\vdots$	$\vdots$	$\vdots$
$i + NI + 1$	NI - 1 species equation	$W^{NI+1} = c_{NI-1}$

The coefficients in the above equations with $L_i^T = 0 (\bar{a}_i = a = 0)$ are

$$A_n^i = \theta P\left(1 + \Delta\eta\alpha_1^i/2\right) \tag{18a}$$

$$B_n^i = \bar{\delta} + \theta P\left(-2 + \alpha_2^i\Delta\eta^2\right) \tag{18b}$$

$$C_n^i = \theta P\left(1 - \Delta\eta\alpha_1^i/2\right) \tag{18c}$$

$$D_n^i = -(1 - \theta)P\left[\left(1 + \Delta\eta\alpha_1^i/2\right)W_{m,n+1} + \left(-2 + \alpha_2^i\Delta\eta^2\right)W_{m,n} + \left(1 - \Delta\eta\alpha_1^i/2\right)W_{m,n-1}\right] + \bar{\delta}W_{m,n} - P\Delta\eta^2\alpha_3^i \tag{18d}$$

where

$$P = \Delta\xi \Big/ \left(2\xi\Delta\eta^2\alpha_4^i\right); \qquad \bar{\delta} = 1$$

In the above coefficients, the α^i's are determined from relations (15), where all quantities are evaluated at the m^{th} column of grid points across the boundary layer. The independent variable ξ is evaluated at (m) for the explicit, (m + 1/2) for the Crank-Nicolson, and (m + 1) for the implicit schemes. In the relation (15g) it was found necessary to express the following derivative in the energy equation as

$$\left(\frac{\partial f'}{\partial \eta}\right)^2 = (f'_{m,n+1} - f'_{m,n-1})(f'_{m+1,n+1} - f'_{m+1,n-1}) \Big/ 4\Delta\eta^2$$

It should be noted that the momentum equation is solved before the energy equation in order that the values of f' at the $(m + 1)^{th}$ column are available for the above expression.

From truncation-error considerations, the mass fraction in relation (14d) would be evaluated as shown; however, such a form can encounter stability problems. Although stability is usually considered to be practically unaffected by lower order terms, as discussed by Richtmyer [88], in actual computations with finite step size, these terms can control the stability. As considered by Richtmyer, stability is concerned with what happens in the limit as the mesh sizes approach zero. Therefore, such stability analyses cannot be completely satisfactory when finite mesh sizes are employed. If W_i^0 and W_i^1 were constants, then it appears that stable solutions are obtained without any restrictions on the step sizes. However, W_i^0 and W_i^1 are not constant, and stability problems can occur if the step size becomes too large, but the formulation below appears to minimize unstable solutions. In relation (14d) the mass fraction is evaluated at (m + 1) for all

difference schemes and the evaluation of relation (15j) must be changed. For the species equation, the value of α_2 becomes

$$\alpha_2^i = \begin{cases} -eW_i^1 \Big/ (\theta b_i) & \text{in } B_n^i \\ 0 & \text{in } D_n^i \end{cases}$$

At a stagnation point or at the tip of a sharp body, $\xi = 0$ and the partial differential equations (13) become ordinary differential equations and provide initial profiles to start the solution along the body. The ordinary differential equations can be solved with the same finite-difference procedure employed for the partial differential equations. The coefficients in Eq. (18) for the ordinary differential equations are the same except the following quantities become $\theta = P = 1$; $\bar{\delta} = 0$ and $F = 0$.

To complete the system of equations (17), the boundary conditions are written in the following form:

$$W_{m+1,1}^i = H^i W_{m+1,2}^i + F^i W_{m+1,3}^i + h^i \tag{19a}$$

$$W_{m+1,n}^i = g^i \tag{19b}$$

The boundary conditions for the momentum and energy equations (conditions (10a), (10b), (12a), and (12b)) are readily written in the above form. The mass flux of species i at the wall is expressed as

$$\dot{m}_i = P_i + Q_i (c_i)_b = c_i \rho v + j_i \tag{20}$$

The relative mass flux with $L_i^T = 0$ is written as

$$j_i = -\frac{1}{\bar{W}} \left\{ Le_i \frac{\partial c_i}{\partial \eta} + \Delta b_i \right\} \tag{21}$$

where

$$\bar{W} = \frac{Pr_b \sqrt{2\xi}}{\ell_b (\rho\mu)_r r_b^j u_e} ; \quad \Delta b_i = \sum_{\substack{k=1 \\ k \neq i}}^{NI} \Delta \bar{b}_{ik} \left(\frac{\partial c_k}{\partial \eta} \right)_m$$

The derivative in the above expression is written as

$$\frac{\partial c_i}{\partial \eta} = \frac{1}{2\Delta\eta} \left(-3c_{i_1} + 4c_{i_2} - c_{i_3} \right)_{m+1} \tag{22}$$

The relations (20) through (22) can now be employed to determine the wall boundary condition coefficients H^i, F^i, and h^i. The remaining boundary-condition coefficients for the momentum and energy equation are given below, while the edge condition for the species equations comes from relation (12c).

Momentum: $H^1 = 0$; $F^1 = 0$; $h^1 = 0$; $g^1 = 1$ (23a)

Energy: $H^2 = 0$; $F^2 = 0$; $h^2 = T_b/T_e$; $g^2 = 1$ (23b)

Species for i = 1, 2, ..., NI:

$$H^{i+2} = 4/D_i ; \quad F^{i+2} = -1/D_1 ; \quad h^{i+2} = \frac{2\Delta\eta}{(Le_i)_b} (P_i \bar{W} + \Delta b_i)/D_i \qquad g^{i+2} = c_{i_e} \tag{23c}$$

where

$$D_i = 3 + \frac{2\Delta\eta}{(Le_i)_b} \bar{W} \left[(\rho v)_b - Q_i \right] \qquad (\rho v)_b = \sum_{i=1}^{NI} \dot{m}_i = \sum_{i=1}^{NI} (P_i + Q_i c_i)$$

The quantities in the above relations are evaluated at the m^{th} step where they can be determined without an iteration process. The values of P_i and Q_i depend on the boundary conditions at the wall and are determined by the mass flux $\dot{m}_i$ of the species, as was discussed in an earlier section. The total mass flux is determined from the sum of the individual species mass flux.

The difference equation (17) and the boundary conditions (19) form a system of linear algebraic equations of the tridiagonal type. These are readily solved with the technique discussed by Richtmyer [88]. Since the equations are uncoupled, a choice of the order for solving the dependent variables must be made. Experience has shown that this order is important. The tangential and normal velocity are solved for first, and the species must be solved for before the temperature. The continuity equation is then used to obtain $V_{m+1/2,n}$ with the finite-difference representation

$$V_{m+1/2,n} = V_{m+1/2,n-1} - \Delta\eta \left(\frac{\xi}{\Delta\xi} + \frac{1}{4} \right) (f'_{m+1,n} + f'_{m+1,n-1}) + \Delta\eta \left(\frac{\xi}{\Delta\xi} - \frac{1}{4} \right) (f'_{m,n} + f'_{m,n-1}) \tag{24}$$

In the above finite-difference procedure, certain quantities should be evaluated at (m + 1/2), but have used the known values at (m). An iteration could be employed such that the values at (m + 1/2) would be used when convergence is obtained. However, the present calculations have shown that this is not necessary.

In solving the boundary-layer equations, the finite-difference procedure is applied in the transformed ξ,η coordinate system. The results must be related back to the physical x,y coordinate system. Also the edge conditions are given as a function of x and are required for the finite-difference solution as a function of ξ. The procedure of specifying $\Delta x (x_{m+1} = x_m + \Delta x)$ and then finding $\Delta\xi$ has been employed. The transformed coordinate ξ is related to x by the ordinary differential equation (see Eq. (1a)).

$$\frac{d\xi}{dx} = (\rho\mu)_r u_e r_b^{2j} \tag{25}$$

The conditions at the edge of the boundary layer as a function of x and the body radius r_b are required to solve the foregoing equation. For a sharp or blunt conical body, the body radius is an algebraic expression while, for a hyperboloid, an ordinary differential equation must be solved to obtain r_b as a function of x.

For the value of ξ as a function of x, the ordinary differential equation (25) has to be solved numerically for most body shapes. When the Runge-Kutta method is applied to this equation, the following is obtained:

$$\xi_{m+1} = \xi_m + \Delta\xi$$

where

$$\Delta\xi = \frac{1}{6}\Delta x\left[\lambda(x_M) + 4\lambda\left(x_M + \frac{1}{2}\Delta x\right) + \lambda(x_M + \Delta x)\right] \qquad \lambda(x_M) = \left[(\rho\mu)_r u_e r_b^{2j}\right]_{x=x_M}$$

The value of ξ at $(m + 1/2)$ can be obtained from

$$\xi_{m+1/2} = \xi_m + \frac{1}{2}\Delta\xi \ .$$

The conditions at the edge of the boundary layer, u_e, T_e, p_e, and c_{i_e}'s (air species only), are required as a function of x. A table of these edge properties as a function of x is employed, with Lagrange interpolation used to obtain the edge conditions and the derivatives of the edge conditions for any value of x.

DISCUSSION OF NUMERICAL RESULTS

The present technique for solving the boundary-layer equations has been used to obtain the flow on a sharp cone and a hyperboloid. These examples are used as test cases to illustrate the present implicit finite-difference scheme when applied to an air gas model with finite reaction rates. The first case is a sharp cone at 150-Kft altitude, 22 Kfps velocity, and a wall temperature of 1000°K with the gas undissociated at the surface. This problem has been investigated by the author [53] previously and also by Galowin and Gould [54], Gruenich and Pindroh [64], and Moore [68]. Although sharp-cone results have been presented in [24], Moore has shown that these results differ significantly from finite-difference solutions. He attributed these differences to the inaccuracies associated with the use of polynomials in [24].

The present results for the peak electron density are given in Fig. 2 and are compared to the results of other authors. The present results employ 28 points across the boundary layer and an initial value of $\Delta x_o = 0.001$, and the step size increases according to the relation $\Delta x = \Delta x_o(2m - 1)$, where $m = 1,2,3,\ldots, M$ as each step is taken. A total of 122 steps are taken to obtain the solution of 14.884 ft. The present method has been employed with all the binary Lewis-Semenov numbers equal to 1.4 and with complete multicomponent diffusion results are slightly higher than the binary diffusion results, but the difference would not be distinguishable if both were plotted in Fig. 2. When the present method employs the reaction rates of [53], the peak electron density is close to the value given in [53]. The difference between the various results is mainly due to reaction rates, transport properties, and thermodynamic properties. When Moore [68] used the rates of [53], his prediction of the peak electron density was in close agreement with [53]. The difference from the present results can be attributed to the reaction rates used. The results of Gruenich and Pindroh [64] employ the same reaction rates of those of [53], but Sutherland's viscosity law is used and electronic excitation is ignored in the thermodynamic properties. The results of Galowin and Gould [54] are different because of the reaction rates and transport properties that are employed.

AGARD CASE A

The boundary-layer flow on a hyperboloid has been investigated at conditions corresponding to an altitude of 100 Kft and a velocity of 20 Kfps, with a wall temperature of 1000°K. This case is a way to verify if a numerical technique will operate properly when the gas is near chemical equilibrium. Also, the blunt body requires the solution from a stagnation point downstream where edge conditions change significantly. The edge conditions were provided by Lewis, and are given in Table II as used in the computer program. These conditions are obtained from the inviscid streamline along the surface of the hyperboloid with finite rate chemistry. The pressure along the streamline or body surface is that obtained from modified Newtonian theory. The conditions at the edge of the boundary layer are used as the reference conditions; for example, as required in Eq. (1a). When the body streamline is used, the classical boundary-layer approach is being followed. For the case of chemically reacting flows, there is considerable error in the prediction of the chemical species at the edge of the boundary layer far downstream on the body. The usual approach of taking into account the swallowing of the inviscid flow is not employed. As this case is intended to be a test example, the introduction of swallowing introduces another variable that can influence the results obtained by any method.

The surface boundary conditions employed in this study are such that the wall is either noncatalytic or fully catalytic. For the case of the noncatalytic wall, the terms $\dot{m}_i$, P_i, and Q_i in Eq. (20) are zero for all of the air species. A fully catalytic recombination surface for air is defined as a wall where every dissociated and ionized species that strikes the surface is converted to a molecular species due to the heterogeneous reactions. For dissociated and ionized species, the P_i's are zero, while

$$Q_i = -\rho_b \sqrt{\frac{RT_b}{2\pi M_i}} \qquad i = O,\ N,\ NO,\ NO^+$$

For the molecular species, the Q_i's are zero and

$$P_i = -\sum_k \frac{\alpha_k^j}{2} \frac{M_i}{M_k} c_{k_b} Q_k \qquad \begin{matrix} k = O,\ N,\ NO,\ NO^+ \\ i = O_2,\ N_2 \end{matrix}$$

where

α_k^j = amount of element j in species k

i = molecular species of element j

The variation of the radius of the hyperboloid is required as a function of the distance along the surface. This is obtained by solving the ordinary differential equation

$$\frac{dr_b}{dx} = \left\{ 1 + (r_b/R_N)^2 \Big/ \left[1 + (r_b/R_N)^2 \tan^2 \theta \right] \right\}^{-1/2}$$

In the results presented, 28 points are employed across the boundary layer, with $\eta = 5.4$ at the outer edge. The step size along the body was increased as the computation proceeded. The step sizes employed were 0.01, 0.025, 0.05, 0.1, 0.25, 0.5, 1.0, and 2.0, where the numbers of steps taken of each were 10, 16, 16, 20, 12, 12, 14, and 12, respectively, for a total of 106 steps. The time required per step along the body is given in Fig. 1 for the case of binary diffusion. For the case of air with multicomponent diffusion, the computation is approximately twice as large. In Fig. 1, the times for the IBM 7094 computer correspond to the computer program employed in [53] and [79]. The times for the CDC 3600 are for the computer program described in this paper.

The boundary-layer flow results for the hyperboloid test case with a catalytic and noncatalytic wall are given in Fig. 3 through 7. Not too much physical significance should be attached to the results, since the swallowing of the inviscid flow has been neglected. The displacement thickness,

$$\delta^*/R_N = \int_0^{y_e/R_N} (1 - \rho u/\rho_e u_e)\, d(y/R_N) \ ;$$

Stanton number,

$$St = \left(k \frac{\partial T}{\partial y} - \sum_{i=1}^{NI} h_i j_i \right)_b \Big/ \rho_\infty V_\infty (H_0 - H_b) \ ;$$

and the local skin friction coefficient,

$$c_{f_\infty} = \mu_b \left(\frac{\partial u}{\partial y} \right)_b \Big/ \left(\frac{1}{2} \rho_\infty V_\infty^2 \right)$$

are given in Fig. 3 and 4. The velocity, temperature, and species distribution across the boundary layer at 50 nose radii downstream for a catalytic and noncatalytic wall are given in Fig. 5, 6, and 7.

For the solution with a noncatalytic wall, unstable results were obtained with the Crank-Nicolson ($\theta = 0.5$) method. To avoid this problem, the implicit method with $\theta = 1.0$ was employed. The results for the sharp-cone test were compared with $\theta = 0.5$ and 1.0, and the results were in close agreement downstream on the cone. Near the tip (first few inches) there was a difference between the predictions of the two methods for the mass fraction of the species, with the implicit method giving more accurate results. This type of stability problem has also been observed by Moore [68] and was corrected by using the implicit scheme for the first grid point away from the wall.

The examples indicate that the present method provides a technique for computing the boundary-layer flow with finite reaction rates when there are a large number of chemical species and when the flow is near local chemical equilibrium. With the equations uncoupled and the technique not requiring iterations at each step, the overall computing time for flows with many chemical species is reasonable.

TABLE I

Diffusion Curve Fit Constants

Interaction	A	B	C
N-O	-0.0043383	1.9119177	-11.891342
$N-N_2$	0.0191055	1.4904448	-10.358828
$N-O_2$	0.0191055	1.4904448	-10.358828
N-NO	0.0191055	1.4904448	-10.358828
$O-O_2$	0.0216586	1.3875747	- 9.7389971
$O-N_2$	0.0168907	1.5276702	-10.629306
N_2-O_2	0.0435927	0.9784219	- 8.3354916
O-NO	0.0183441	1.4750189	-10.265935
O_2-NO	0.0410864	1.0124720	- 8.4455480
N_2-NO	0.0315955	1.2225368	- 9.4862934
$O-NO^+$	0.0003467	1.8941393	-12.978394
$N-NO^+$	0.0003467	1.8941393	-12.978394
O_2-NO^+	0.0003467	1.8941393	-12.978394
N_2-NO^+	0.0003467	1.8941393	-12.978394
$NO-NO^+$	0.0039930	1.5689336	-11.441502

TABLE II

PROPERTIES AT EDGE OF BOUNDARY LAYER

	X(ft.)	P_e(psf)	U_e(fps)	T_e(°R)	C_{O_2}	C_{N_2}	C_O	C_N	C_{NO}	C_{NO^+}
1	0.	1.2772E+04	0.	1.2603E+04	4.6176E-04	5.8273E-01	2.2608E-01	1.7538E-01	1.4884E-02	6.2807E-04
2	3.3333E-03	1.2751E+04	3.1854E+02	1.2597E+04	4.6176E-04	5.8273E-01	2.2608E-01	1.7538E-01	1.4884E-02	6.2807E-04
3	5.0000E-03	1.2726E+04	4.7781E+02	1.2590E+04	4.6176E-04	5.8273E-01	2.2608E-01	1.7538E-01	1.4884E-02	6.2807E-04
4	6.6667E-03	1.2691E+04	6.3709E+02	1.2589E+04	4.6176E-04	5.8273E-01	2.2608E-01	1.7538E-01	1.4884E-02	6.2807E-04
5	7.8943E-03	1.2659E+04	7.3727E+02	1.2589E+04	4.6176E-04	5.8273E-01	2.2608E-01	1.7538E-01	1.4884E-02	6.2807E-04
6	1.0471E-02	1.2575E+04	9.7938E+02	1.2578E+04	4.6080E-04	5.8301E-01	2.2608E-01	1.7510E-01	1.4851E-02	6.2597E-04
7	1.3353E-02	1.2456E+04	1.2516E+03	1.2562E+04	4.5920E-04	5.8329E-01	2.2608E-01	1.7468E-01	1.4803E-02	6.2297E-04
8	1.6382E-02	1.2305E+04	1.5381E+03	1.2541E+04	4.5696E-04	5.8413E-01	2.2624E-01	1.7412E-01	1.4740E-02	6.1876E-04
9	1.7913E-02	1.2214E+04	1.6868E+03	1.2529E+04	4.5568E-04	5.8441E-01	2.2624E-01	1.7370E-01	1.4704E-02	6.1636E-04
10	2.0041E-02	1.2084E+04	1.8921E+03	1.2510E+04	4.5376E-04	5.8497E-01	2.2624E-01	1.7314E-01	1.4644E-02	6.1246E-04
11	2.2564E-02	1.1922E+04	2.1379E+03	1.2484E+04	4.5120E-04	5.8553E-01	2.2624E-01	1.7244E-01	1.4566E-02	6.0766E-04
12	2.4595E-02	1.1779E+04	2.3374E+03	1.2461E+04	4.4896E-04	5.8637E-01	2.2640E-01	1.7188E-01	1.4497E-02	6.0316E-04
13	2.6698E-02	1.1623E+04	2.5471E+03	1.2434E+04	4.4608E-04	5.8694E-01	2.2640E-01	1.7118E-01	1.4416E-02	5.9806E-04
14	3.0447E-02	1.1330E+04	2.9263E+03	1.2380E+04	4.4064E-04	5.8862E-01	2.2632E-01	1.6964E-01	1.4251E-02	5.8756E-04
15	3.3755E-02	1.1059E+04	3.1995E+03	1.2347E+04	4.4128E-04	5.9002E-01	2.2656E-01	1.6824E-01	1.4215E-02	5.8035E-04
16	3.5109E-02	1.0945E+04	3.2929E+03	1.2335E+04	4.4128E-04	5.9058E-01	2.2656E-01	1.6782E-01	1.4200E-02	5.7765E-04
17	3.6774E-02	1.0804E+04	3.4067E+03	1.2319E+04	4.4032E-04	5.9114E-01	2.2656E-01	1.6712E-01	1.4167E-02	5.7435E-04
18	3.9481E-02	1.0572E+04	3.5882E+03	1.2290E+04	4.3808E-04	5.9226E-01	2.2656E-01	1.6613E-01	1.4095E-02	5.6865E-04
19	4.3853E-02	1.0196E+04	3.8714E+03	1.2237E+04	4.3328E-04	5.9394E-01	2.2672E-01	1.6459E-01	1.3948E-02	5.5875E-04
20	4.9474E-02	9.7151E+03	4.2168E+03	1.2165E+04	4.2656E-04	5.9590E-01	2.2672E-01	1.6263E-01	1.3732E-02	5.4555E-04
21	5.6219E-02	9.1516E+03	4.6055E+03	1.2075E+04	4.1728E-04	5.9842E-01	2.2688E-01	1.6011E-01	1.3453E-02	5.2904E-04
22	6.2065E-02	8.6824E+03	4.9202E+03	1.1994E+04	4.0864E-04	6.0066E-01	2.2704E-01	1.5815E-01	1.3198E-02	5.1494E-04
23	6.9260E-02	8.1390E+03	5.2740E+03	1.1895E+04	3.9808E-04	6.0346E-01	2.2736E-01	1.5549E-01	1.2879E-02	4.9783E-04
24	7.8614E-02	7.4937E+03	5.6975E+03	1.1770E+04	3.8464E-04	6.0683E-01	2.2752E-01	1.5241E-01	1.2486E-02	4.7593E-04
25	9.0126E-02	6.7917E+03	6.1538E+03	1.1619E+04	3.6800E-04	6.1075E-01	2.2784E-01	1.4862E-01	1.1988E-02	4.5222E-04
26	1.0509E-01	6.1493E+03	6.6535E+03	1.1440E+04	3.5040E-04	6.1551E-01	2.2816E-01	1.4428E-01	1.1463E-02	4.2101E-04
27	1.2351E-01	5.2555E+03	7.1665E+03	1.1235E+04	3.2640E-04	6.2055E-01	2.2864E-01	1.3955E-01	1.0743E-02	3.9370E-04
28	1.4838E-01	4.4633E+03	7.7179E+03	1.0993E+04	3.0131E-04	6.2644E-01	2.2896E-01	1.3417E-01	1.0014E-02	3.5710E-04
29	1.7969E-01	3.7398E+03	8.2715E+03	1.0717E+04	2.6544E-04	6.3260E-01	2.2976E-01	1.2857E-01	8.9574E-03	3.2169E-04
30	2.2194E-01	3.0667E+03	8.8286E+03	1.0409E+04	2.3469E-04	6.3876E-01	2.3008E-01	1.2282E-01	8.0541E-03	2.7721E-04
31	2.6424E-01	2.6040E+03	9.2646E+03	1.0141E+04	1.9949E-04	6.4409E-01	2.3072E-01	1.1821E-01	6.9979E-03	2.5468E-04
32	3.1120E-01	2.2340E+03	9.6338E+03	9.8955E+03	1.7302E-04	6.4829E-01	2.3120E-01	1.1436E-01	6.1907E-03	2.2923E-04
33	3.8536E-01	1.8412E+03	1.0075E+04	9.5422E+03	1.5184E-04	6.5333E-01	2.3200E-01	1.0964E-01	5.2244E-03	1.9916E-04
34	4.5149E-01	1.6076E+03	1.0363E+04	9.3672E+03	1.2410E-04	6.5670E-01	2.3232E-01	1.0652E-01	4.6302E-03	1.8008E-04
35	5.3165E-01	1.4014E+03	1.0637E+04	9.1536E+03	1.0685E-04	6.6006E-01	2.3264E-01	1.0353E-01	4.0511E-03	1.6222E-04
36	6.3584E-01	1.2151E+03	1.0909E+04	8.9359E+03	9.0080E-05	6.6342E-01	2.3296E-01	1.0049E-01	3.5109E-03	1.4515E-04
37	7.4007E-01	1.0834E+03	1.1116E+04	8.7660E+03	8.0448E-05	6.6594E-01	2.3312E-01	9.8140E-02	3.1238E-03	1.3258E-04
38	8.2023E-01	1.0060E+03	1.1247E+04	8.6599E+03	7.4656E-05	6.6762E-01	2.3312E-01	9.6557E-02	2.9057E-03	1.2498E-04
39	9.2043E-01	9.2915E+02	1.1384E+04	8.5498E+03	6.8768E-05	6.6958E-01	2.3328E-01	9.4834E-02	2.6860E-03	1.1736E-04
40	1.0407E+00	8.5750E+02	1.1518E+04	8.4430E+03	6.3584E-05	6.7126E-01	2.3344E-01	9.3069E-02	2.4847E-03	1.1016E-04
41	1.2812E+00	7.5662E+02	1.1721E+04	8.2876E+03	5.6736E-05	6.7435E-01	2.3360E-01	9.0155E-02	2.2143E-03	9.9927E-05
42	1.4615E+00	7.0394E+02	1.1835E+04	8.2063E+03	5.3600E-05	6.7631E-01	2.3360E-01	8.8362E-02	2.0888E-03	9.4645E-05
43	1.7321E+00	6.4673E+02	1.1965E+04	8.1209E+03	5.0144E-05	6.7855E-01	2.3376E-01	8.6093E-02	1.9892E-03	8.9094E-05
44	1.9124E+00	6.1814E+02	1.2034E+04	8.0814E+03	4.9376E-05	6.7995E-01	2.3376E-01	8.4762E-02	1.9169E-03	8.6393E-05
45	2.0924E+00	5.9492E+02	1.2091E+04	8.0527E+03	4.8704E-05	6.8135E-01	2.3376E-01	8.3530E-02	1.8860E-03	8.4322E-05
46	2.3453E+00	5.6884E+02	1.2158E+04	8.0255E+03	4.9056E-05	6.8275E-01	2.3376E-01	8.1975E-02	1.8641E-03	8.2192E-05
47	2.5978E+00	5.4825E+02	1.2212E+04	8.0097E+03	4.8256E-05	6.8415E-01	2.3376E-01	8.0560E-02	1.8623E-03	8.0662E-05
48	2.9513E+00	5.2589E+02	1.2273E+04	8.0010E+03	4.8800E-05	6.8611E-01	2.3376E-01	7.8767E-02	1.8809E-03	7.9281E-05
49	3.3048E+00	5.0879E+02	1.2321E+04	8.0037E+03	4.9888E-05	6.8751E-01	2.3376E-01	7.7142E-02	1.9196E-03	7.8501E-05
50	3.7997E+00	4.9077E+02	1.2374E+04	8.0198E+03	5.2352E-05	6.8947E-01	2.3376E-01	7.5069E-02	2.0027E-03	7.7991E-05
51	4.2947E+00	4.8040E+02	1.2414E+04	8.0445E+03	5.5136E-05	6.9143E-01	2.3376E-01	7.3192E-02	2.0955E-03	7.8051E-05

ACKNOWLEDGEMENT

This work was supported by the United States Atomic Energy Commission.

REFERENCES

[1] Prandtl, L., "Zur Berechnung der Grenzschichten," Z. angew. Math. Mech., Vol. 18, Vol. 18, 1938, pp. 77-82. (Translated as "Note on the Calculation of Boundary Layers," Tech. Memor. No. 959, Nat. Adv. Comm. Aero., Washington, D.C.)

[2] Rosenhead, L. (Editor), Laminar Boundary Layers, Oxford at the Clarendon Press, 1963, p. 247.

[3] Chudov, L.A., "Review of Boundary-Layer Studies Carried Out at the Computational Center of Moscow State University," Numerical Methods in Gas Dynamics, G. S. Roslyakov and L. A. Chudov, Editors, Moscow University Press, Moscow, 1963.

[4] Belotserkovskii, O.M. and Chushkin, P.I., "The Numerical Solution of Problems in Gas Dynamics," Basic Developments in Fluid Dynamics, Vol. 1, Maurice Holt, Editor, Academic Press, New York, 1965.

[5] Hartree, D.R. and Womersley, J.R., "A Method for the Numerical or Mechanical Solution of Certain Types of Partial Differential Equations," Proceedings, Royal Society, Vol. 161A, Aug. 1937, p. 353.

[6] Leight, D.C.F., "The Laminar Boundary-Layer Equation: A Method of Solution by Means of an Automatic Computer," Proceedings, Comb. Phil. Soc., Vol. 51, 1955, pp. 320-332.

[7] Manohar, R., "A Characteristic Difference Method for the Calculation of Steady Boundary-Layer Flow," Proceedings, 4th Congress Theoret. Applied Mech., Indian Soc. Theoret. Applied Mech., Kharagpur, 1958, pp. 135-144.

[8] Smith, A.M.O. and Clutter, Darwin, W., "Solution of the Incompressible Laminar Boundary-Layer Equations," AIAA Journal, Vol. 1, No. 9, Sept. 1963, pp. 2062-2070.

[9] Smith, A.M.O. and Clutter, D.W., "Solution of the Incompressible Laminar Boundary-Layer Equations," AIAA Journal, Vol. 1, 1963, pp. 2062-2071.

[10] Clutter, D.W. and Smith, A.M.O., "Solution of the General Boundary-Layer Equations for Compressible Laminar Flow, Including Transverse Curvature," LB 31088, Feb. 15, 1963, Douglas Aircraft Co., revised Oct. 10, 1964.

[11] Smith, A.M.O. and Clutter, D.W., "Machine Calculation of Compressible Boundary-Layers," AIAA Journal, Vol. 3, 1965, pp. 639-647.

[12] Clutter, D.W., Smith, A.M.O. and Jaffe, N.A., "General Method for Solving Nonequilibrium Laminar Boundary-Layer Flow of a Binary Gas," LB 31616, Oct. 15, 1964, Douglas Aircraft Co.

[13] Jaffe, N.A., Lind, R.C. and Smith, A.M.O., "Solution to the Binary Diffusion Laminar Boundary-Layer Equations Including the Effects of Second-Order Transverse Curvature," AEDC-TR-66-183, 1967.

[14] Zamurayev, V.P., "The Laminar Boundary Layer in a Radiating-Absorbing Gas Near a Flat Plate," NASA-TT-F-10, 177, May 1966. (Translation from Zhurnal Prikladnoy Mekhaniki i Tekhnicheskoy Fiziki, No. 3, 1964, pp. 73-80).

[15] Le Maréchal, T. and Ronat, J., "On the Numerical Solution of the Equations of a Laminar, Compressible Two-Dimensional Boundary Layer," (in French), Comptes Rendus de l'Academie des Sciences, Series A, 262, Vol. No. 9, Feb. 1966, pp. 512-515.

[16] Steiger, M.H. and Sepri, Paavo, "On the Solution of Initial-Valued Boundary Layer Flows," PIBAL Report No. 872, May 1965, Polytechnic Institute of Brooklyn.

[17] Lubard, S.C. and Schetz, J.A., "The Numerical Solution of Boundary Layer Problems," Proceedings, 1968 Heat Transfer and Fluid Mechanics Institute, A.F. Emery and C.A. Depew, Editors, Stanford University Press, June 1968.

[18] Finlayson, B.A. and Scriven, L.E., "The Method of Weighted Residuals - A Review," Applied Mechanics Review, Vol. 19, No. 9, Sept. 1966.

[19] Dorodnitsyn, A.A., "General Method of Integral Relations and its Application to Boundary Layer Theory," Advances in Aeronautical Sciences, Vol. 3, Macmillan Company, New York, 1960.

[20] Pavlovskii, Yu. N., "The Numerical Calculations of the Laminar Boundary-Layer in a Compressible Gas," Zh. Vych. Mat., Vol. 2, No. 5, 1962, pp. 884-901.

[21] Belotserkovskii, O.M. and Chushkin, P.I., "A Numerical Method of Integral Relations," Zh. Vych. Mat., Vol. 2, No. 5, 1962, pp. 731-759.

[22] Shen'-Tsyuan', Lyu, "Calculation of the Laminar Boundary Layer in a Compressible Gas in the Presence of Suction or Blowing," Zh. Vych. Mat., Vol. 2, No. 5, 1962, pp. 868-883.

[23] Pallone, Adrian, "Nonsimilar Solutions of the Compressible Laminar Boundary-Layer Equations with Applications to the Upstream-Transportation Cooling Problem," Journal of the Aerospace Sciences, Vol. 28, No. 6, June 1961.

[24] Pallone, A.J., Moore, J.A., and Erdos, J.I., "Nonequilibrium Nonsimilar Solutions of the Laminar Boundary Layer Equations," AIAA Journal, Vol. 2, No. 10, Oct. 1964, pp. 1706-1713; also, Tech. Memo RAD-TM-63-58, Nov. 1963, Avco Corporation.

[25] Bethel, Howard, E., "On the Convergence and Exactness of Solutions of the Laminar Boundary-Layer Equations Using the N-Parameter Integral Formulation of Galerkin-Kantorovich-Dorodnitsyn," ARL-66-0090, July 1966, Aerospace Research Laboratories, Wright-Patterson Air Force Base, Ohio.

[26] Bethel, H.E., "Approximate Solution of the Laminar Boundary-Layer Equations with Mass Transfer," AIAA Journal, Vol. 6, No. 2, Feb. 1968, pp. 220-225.

[27] Kendall, R.M. and Bartlett, E.P., "Nonsimilar Solution of the Multicomponent Laminar Boundary Layer by an Integral Matrix Method," AIAA Journal, Vol. 6, No. 6, June 1968, pp. 1089-1097.

[28] Görtler, H., "Weiterentwicklung eines Grenzschichtprofils bei gegebenem Druckverlauf," Z. angew, Math. Mech., Vol. 19, 1939, pp. 129-140.

[29] Görtler, H., "A Method of Differences for the Calculation of Laminar Boundary Layers," unpublished translation Min. Aviation, 1946, London (from "Ein Differenzenverfahren zur Berechnung Laminarer Grenzschichten," Untersuch. Mitt. dtsch. Luftfahrft. No. 6615, 1944).

[30] Görtler, H., "Ein Differenzenverfahren zur Berechnung Laminarer Grenzschichten," Ingen.-Arch., Vol. 16, 1948, pp. 178-187.

[31] Schröder, K., "Ein einfaches numerisches Verfahren zur Berechnung der Laminaren Grenzschicht," ForschBer. Dtsch. Luftfahrft. No. 1741 (Translated as "A Simple Numerical Method for the Calculation of the Laminar Boundary Layer," Tech. Memo No. 1317, 1943, Nat. Adv. Comm. Aero., Washington, D.C.)

[32] Schröder, K., "Verwendung der Differenzenrechnung zur Berechnung der laminaren Grenzschicht," Math. Nachr., Vol. 4, 1951, pp. 439-467.

[33] Gadd, G.E., "The Numerical Integration of the Laminar Compressible Boundary Layer Equations, with Special Reference to the Position of Separation When the Wall is Cooled," Curr. Pap. No. 312, 1952, Aero. Res. Count., Lond.

[34] Witting, H., "Verbesserung des Differenzenverfahrens von H. Görtler zur Berechnung laminarer Grenzschichten," Z. Angew, Math. Phys., Vol. 4, 1953, pp. 376-397.

[35] Terrill, R.M., "Laminar Boundary Layer Flow Near Separation With and Without Suction," Phil. Trans., Vol. A253, 1960, pp. 55-100.

[36] Rouleau, W.T. and Osterle, J.F., "Application of Finite Difference Methods to Boundary Layer Type Flows," Journal of the Aeronautical Sciences, Vol. 22, 1955, p. 249.

[37] Flügge-Lotz, I., "The Computation of the Laminar Compressible Boundary Layer," ARDC Contract AF 18(600)-586, Project No. R-352-30-7, June 1954, Dept. of Mech. Eng., Stanford University, California. (Abbreviated version appeared as: "A Difference Method for the Computation of the Laminar Compressible Boundary Layer," 50 Jahre Grenzschichtforschung, Publ. Fr. Vieweg und Sohn, Braunschweig, 1955, p. 393.)

[38] Flügge-Lotz, I. and Baxter, D.C., "The Solution of Compressible Laminar Boundary Layer Problems by a Finite Difference Method. Part I: Description of the Method," Tech. Rep. No. 103, Sept. 1956, Div. of Engr. Mechanics, Stanford University, California.

[39] Flügge-Lotz, I. and Eichelbrenner, E.A., "La Couche limite laminaire dans l'ecoulement compressible le long d'une surface courbe," Rapport 1/694 A, Aug. 1948, O.N.E.R.A. See also: Eichelbrenner, "Methodes de calcul de la couche limite laminaire bidimensionelle en regime compressible," Publication No. 83, 1956, Office National d'Etudes et de Recherches Aeronautiques, p. 39.

[40] Baxter, D.C. and Flügge-Lotz, I., "The Solution of Compressible Laminar Boundary Layer Problems by a Finite Difference Method, Part II: Further Discussion of the Method and Computation of Examples," Tech. Rep. No. 110, 1957, Div. of Engr. Mech., Stanford University, California. (Abbreviated version published in ZAMP, Vol. IXb, pp. 81-96.)

[41] Howe, J.T., "Some Finite Difference Solutions of the Laminar Compressible Boundary Layer Showing the Effects of Upstream Transpiration Cooling," Memo 2-26-59A, Feb. 1959, National Aeronautics and Space Administration.

[42] Kramer, R.F. and Lieberstein, H.M., "Numerical Solution of the Boundary Layer Equations Without Similarity Assumptions," J. of the Aero-Space Sciences, Vol. 26, No. 8, Aug. 1959, pp. 508-514.

[43] Raetz, G.S., "A Method of Calculating Three-Dimensional Laminar Boundary Layers of Steady Compressible Flows," NAI-58-73, Dec. 1957, Northrop Aircraft, Inc.

[44] Mitchell, A.R. and Thomson, J.Y., "Finite Difference Methods of Solution of the von Mises Boundary Layer Equation with Special Reference to Conditions Near a Singularity," Z. angew Math. Phys., Vol. 9, 1958, pp. 26-37.

[45] Mitchell, A.R., "Solution of the von Mises Boundary Layer Equation Using a High-Speed Computer," Math. of Computation, Vol. 15, No. 75, July 1961, pp. 238-242.

[46] Flügge-Lotz, I. and Yu, E., "Development of a Finite Difference Method for Computing a Compressible Laminar Boundary Layer with Interaction," Tech. Rep. No. 127, Div. Engr. Mech., May 1960, Stanford University, California.

[47] Wu, J.C., "The Solution of Laminar Boundary Layer Equations by the Finite Difference Method," SM-37484, June 1, 1960, Douglas Aircraft Co., Inc.

[48] Brailovskaya, I. Yu, and Chudov, L.A., "Reshenie uravnenii progranichnogo sloya metodom setok," (Solution of Boundary Layer Equations by Difference Methods); 1960, Otchet VTs MGU.

[49] Brailovskaya, I.Y. and Chudov, L.A., "The Solution of Boundary Layer Equations by a Difference Method," Sbornik Computing Methods and Programming, Moscow State University (MGU), Moscow, 1962, pp. 167-182.

[50] Paskonov, V.M., "A Standard Program for the Solution of Boundary Layer Problems," Numerical Methods in Gas Dynamics, G. S. Roslyakov and L. A. Chudov, Editors, Moscow University Press, Moscow, 1963.

[51] Flügge-Lotz, I. and Blottner, F.G., "Computation of the Compressible Laminar Boundary Layer Flow Including Displacement-Thickness Interaction Using Finite-Difference Methods," Tech. Rep. No. 131, Jan. 1962, Div. of Engr. Mech., Stanford University, Stanford, California. (Abbreviated version in J. de Mecanique, Vol. II, No. 4, Dec. 1963).

[52] Blottner, F.G., "Chemical Non-Equilibrium Boundary Layer," AIAA Journal, Vol. 2, 1964, pp. 232-240; also, R63SD17, June 1963, General Electric Space Sciences Lab.

[53] Blottner, F.G., "Nonequilibrium Laminar Boundary Layer Flow of Ionized Air," AIAA Journal, Vol. 2, No. 11, Nov. 1964, pp. 1921-1927; also R64SD56, Nov. 1964, General Electric Space Sciences Lab.

[54] Galowin, L.S. and Gould, H.E., "A Finite Difference Method Solution of Non-Similar, Non-Equilibrium Air, Laminar and Turbulent Boundary Layer Flows," Tech. Rep. No. 422, Mar. 13, 1964, General Applied Science Laboratories.

[55] Davis, R.T. and Flügge-Lotz, I., "Laminar Compressible Flow Past Axisymmetric Blunt Bodies (Results of a Second-Order Theory)," J. Fluid Mech., Vol. 20, Part 4, 1964, pp. 593-623; also, Report No. 143, Dec. 1963, Div. of Engr. Mech. Tech., Stanford University, California.

[56] Fannelop, T.K. and Flügge-Lotz, I., "Two-Dimensional Viscous Hypersonic Flow Over Simple Blunt Bodies Including Second-Order Effects," Tech. Rep. No. 144, June 1964, Div. Engr. Mech., Stanford University, California. (Abbreviated version in J. de Mecanique, Vol. 1, Mar. 1966.)

[57] Fussell, D.D. and Hellums, J.D., "The Numerical Solution of Boundary Layer Problems," AIChE Journal, Vol. 11, No. 4, July 1965, pp. 733-739.

[58] Kleinstein, Gdalia, "A Finite Difference Solution for an Initial Value Problem in a Compressible Laminar Boundary Layer," ARL 65-107, May 1965, USAF, Wright-Patterson Air Force Base, Ohio.

[59] Kleinstein, Gdalia, "Finite Difference Solution of the Laminar Compressible Boundary Layer Equations in the von Mises Variables with Applications," ARL 67-0050, Mar. 1967, USAF, Wright-Patterson Air Force Base, Ohio.

[60] Nabi, Faiza, "Operation Instructions and Description of Computer Program for Finite Difference Solutions of the Laminar Compressible Boundary Layer Equations in the von Mises Variables," ARL 67-0098, May 1967, USAF, Wright-Patterson Air Force Base, Ohio.

[61] Lane, Frank, "Discussion of Problems Relating to the Finite-Difference Solution of Boundary-Layer Flows," TM-145, May 1966, General Applied Science Laboratory.

[62] Lane, F., Lieberman, E. and Fox, H., "Analysis and User's Manual for Implicit Finite-Difference Computer Program for Laminar Compressible Boundary Layer Calculations," TR No. 629, Nov. 1966, GASL.

[63] Lieberman, E., Lane, E. and Fox, H., "Analysis and Computer Program for Calculation of Non-similar Laminar Boundary-Layer Properties: Air in Chemical Equilibrium and Finite Rate Chemistry," AMC-67-22, June 1967, Picatinny Arsenal, Dover, New Jersey.

[64] Gruenich, F.A. and Pindroh, A.L., "An Efficient Generalized Solution for Reacting Laminar Boundary Layers," D2-125228-1, Nov. 1966, Boeing Company.

[65] Ting, L., "On the Initial Conditions for Boundary Layer Equations," J. Math and Phys., Vol. XLIV, No. 4, Dec. 1965.

[66] Krause, Egon, "Numerical Solution of the Boundary Layer Equations," AIAA Journal, Vol. 5, No. 7, July 1967, pp. 1231-1237; also, NYU-AA-66-57, June 1966, New York University, Dept. of Aeronautics and Astronautics.

[67] Fannelop, T.K., "A Method of Solving the Three-Dimensional Laminar Boundary-Layer Equations with Application to a Lifting Reentry Body," Paper 67-159, presented at AIAA Fifth Aerospace Sciences Meeting, New York, Jan. 23-26, 1967; also BSD-TR-66-209, Aug. 1966, Avco Missile System Division.

[68] Moore, J.A., "Chemical Nonequilibrium in Viscous Flows," Ph.D. Dissertation, State University of New York at Buffalo, May 1967.

[69] Farrington, C.C., "Calculation of Non-similar Boundary Layer Flows," Tech. Memo 9851-122, June 1964, TRW Systems Inc.

[70] Schönauer, W., "A Differencing Method for Solving the Boundary Layer Equations for Stationary, Laminar, Incompressible Flow," (in German), Ing. Arch., Vol. 33, 1964, pp. 173-189.

[71] Shchennikov, V.V., "Calculation of the Laminar Boundary Layer Along the Generating Line of a Sublimating Body of Revolution," J. Computer Math. and Math. Phys., Vol. 5, No. 1, 1965, pp. 139-144.

[72] Patankar, S.V. and Spalding, "A Finite-Difference Procedure for Solving the Equations of the Two-Dimensional Boundary-Layer," Int. J. Heat Mass Transfer, Vol. 10, 1967, pp. 1389-1411.

[73] Koh, J.C.Y. and Price, J.F., "Nonsimilar Boundary-Layer Heat Transfer of a Rotating Cone in Forced Flow," Journal of Heat Transfer, Trans. ASME, Series C., Vol. 88, May 1967, pp. 139-145.

[74] Solan, Alexander and Cohen, I.M., "The Rayleigh Problem in a Radiating Compressible Gas. Part 1: Plate Mach Number Finite," Nonr - 562 (35) 10, Mar. 1966, Div. of Engr., Brown University.

[75] Sibulkin, M. and Dispaux, J.C., "Numerical Solutions for Radiating Hypervelocity Boundary Layer Flow on a Flat Plate," AIAA Journal, Vol. 6, No. 6, June 1968, pp. 1098-1104.

[76] Douglas, J. (Jr.), "A Survey of Numerical Methods for Parabolic Differential Equations," Advances in Computers, Vol. 2, F. L. Alt, Editor, Academic Press, New York, 1961.

[77] Levine, J.N., "Finite Difference Solution of the Laminar Boundary Layer Equations Including Second-Order Effects," Paper No. 68-739, June 1968, AIAA Fluid and Plasma Dynamics Conference.

[78] Sills, J.A., "Transformations for Infinite Regions and Their Application to Flow Problems," AIAA Journal, Vol. 7, No. 1, Jan. 1969, pp. 117-123.

[79] Blottner, F.G., "Chemically Reacting Boundary Layer with Ablation Products and Nose Bluntness Effects," TIS R67SD14, April 1967, General Electric.

[80] Bird, R.B., Stewart, W.E. and Lightfoot, E.N., "Transport Phenomena, John Wiley and Sons, 1960.

[81] Blottner, F.G., "Viscous Shock Layer Problem for the Stagnation Point of a Blunt Body," to be published.

[82] Hirschfelder, J.O., Curtiss, C.F. and Bird, R.B., Molecular Theory of Gases and Liquids, John Wiley & Sons, Inc., New York, 1954, p. 486.

[83] Yos, J.M., "Transport Properties of Nitrogen, Hydrogen, Oxygen, and Air to 30000°K," RAD-TM-63-7, March 1963, Avco Corporation.

[84] Yos, J.M., "Revised Transport Properties for High Temperature Air and Its Components," Technical Release, Nov. 28, 1967, Space Systems Division, Avco Corporation.

[85] Yun, K.S. and Mason, E.A., "Collision Integrals for the Transport Properties of Dissociating Air at High Temperature," Physics of Fluids, Vol. 5, No. 4, 1962, pp. 380-386.

[86] Yun, K.S., Weissman, Stanley, and Mason, E.A., "High-Temperature Transport Properties of Dissociating Nitrogen and Dissociating Oxygen," Physics of Fluids, Vol. 5, No. 6, June 1962, pp. 672-678.

[87] Douglas, Jim, Jr. and Jones, B.F., Jr., "On Predictor-Corrector Methods for Nonlinear Parabolic Differential Equation," Journal Soc. Indust. Applied Math., Vol. 11, No. 1, March 1963, pp. 195-204.

[88] Richtmyer, R.D., Difference Methods for Initial-Value Problems, Interscience Publishers, Inc., New York, 1957, Chapter 9.

NOMENCLATURE

c_i mass fraction of species i, ρ_i/ρ

c_{p_i} specific heat at constant pressure of species i, $ft^2/(sec^2\ °R)$

$\bar{c}_p$ frozen specific heat at constant pressure of the mixture $\sum_i c_i c_{p_i}$, $ft^2/(sec^2\ °R)$

D_{ij} multicomponent diffusion coefficient, ft^2/sec

$\mathcal{D}_{ij}$ binary diffusion coefficient, ft^2/sec

D_i^T thermal diffusion coefficient, lb sec/ft

h enthalpy, $\sum_i h_i c_i$, ft^2/sec^2

h_i enthalpy of species i, ft^2/sec^2

k thermal conductivity of mixture, lb/(sec °R)

ℓ density-viscosity product, $\rho\mu/(\rho\mu)_r$

L_{ij} multicomponent Lewis-Semenov number, $\bar{c}_p \rho D_{ij}/k$

$\mathcal{L}_{ij}$ binary Lewis-Seminov number $\bar{c}_p \rho \mathcal{D}_{ij}/k$

L_i^T thermal Lewis-Semenov number $\bar{c}_p D^T{}_i /k$

$\bar{M}$ molecular weight of the mixture, $1/(\sum_i c_i/M_i)$, lb/lb-mole

M_i molecular weight of species i, lb/lb-mole

NI number of chemical species

Pr Prandtl number $\bar{c}_p \mu/k$

p pressure, lb/ft^2

p'_o normal shock stagnation pressure, atm

R universal gas constant, lb $ft^2/(lb\text{-mole}\ sec^2\ °R)$

R_N nose radius, ft

r distance from axis in axisymmetric problems, ft

T temperature, °R

T'_o normal shock stagnation temperature, °K

T_K temperature, °K

u,v velocity components tangential and normal to body surface, ft/sec

V transformed normal velocity (Eq. 3a)

V_∞ freestream velocity, fps

w_i mass rate of formation of species i, lb $sec^2/(ft^4\ sec)$

x distance along surface from leading edge or stagnation point, ft

y distance along normal from surface, ft

μ viscosity, lb sec/ft^2

ρ density, lb sec^2/ft^4

ρ_i density of species i, lb sec^2/ft^4

Subscripts

b,w conditions at body surface

e conditions at outer edge of shock layer or boundary layer

r quantities evaluated at some reference condition

∞ freestream conditions

Superscripts

j = 0 two-dimensional body

j = 1 axisymmetric body

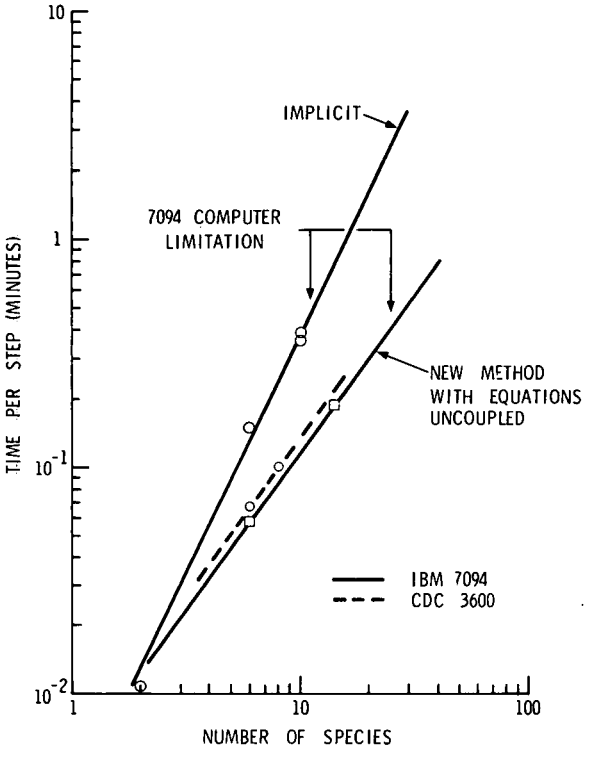

Fig. 1 Computation time for various number of chemical species (binary diffusion)

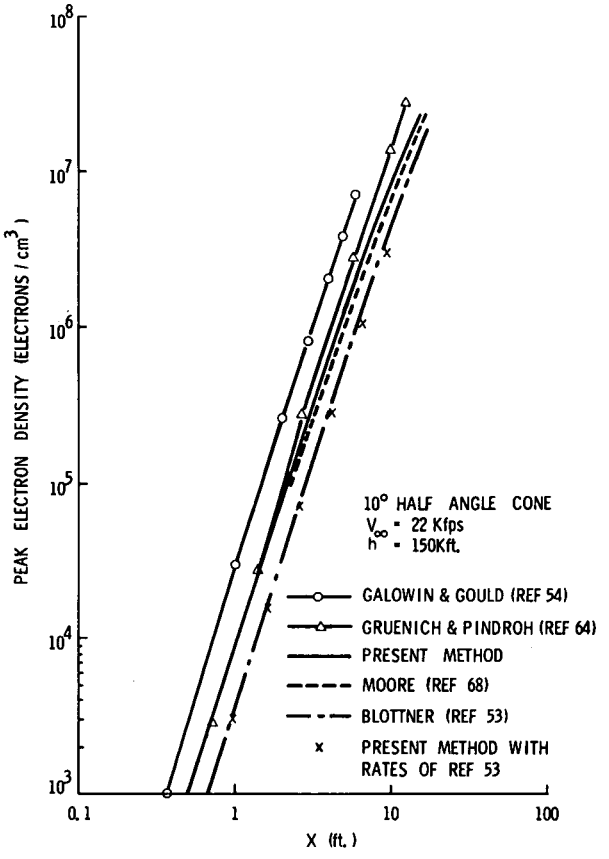

Fig. 2 Peak electron number density on sharp cone

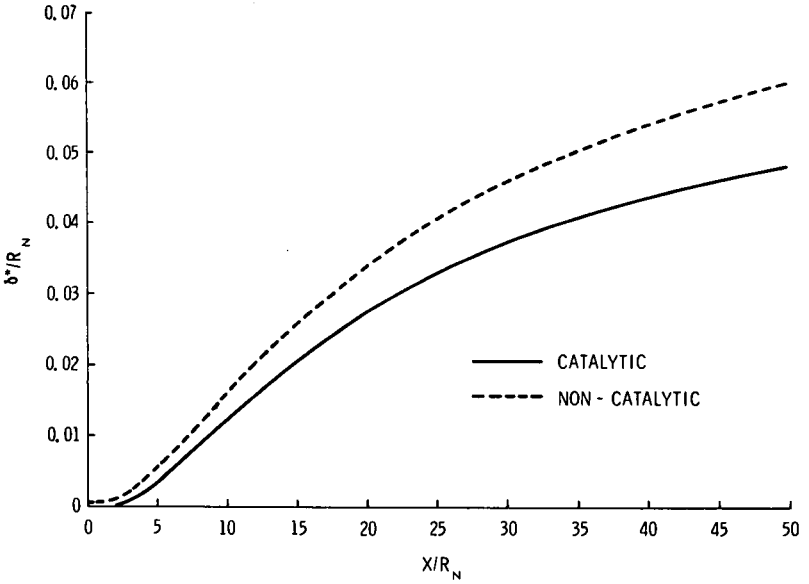

Fig. 3 Displacement thickness along hyperboloid

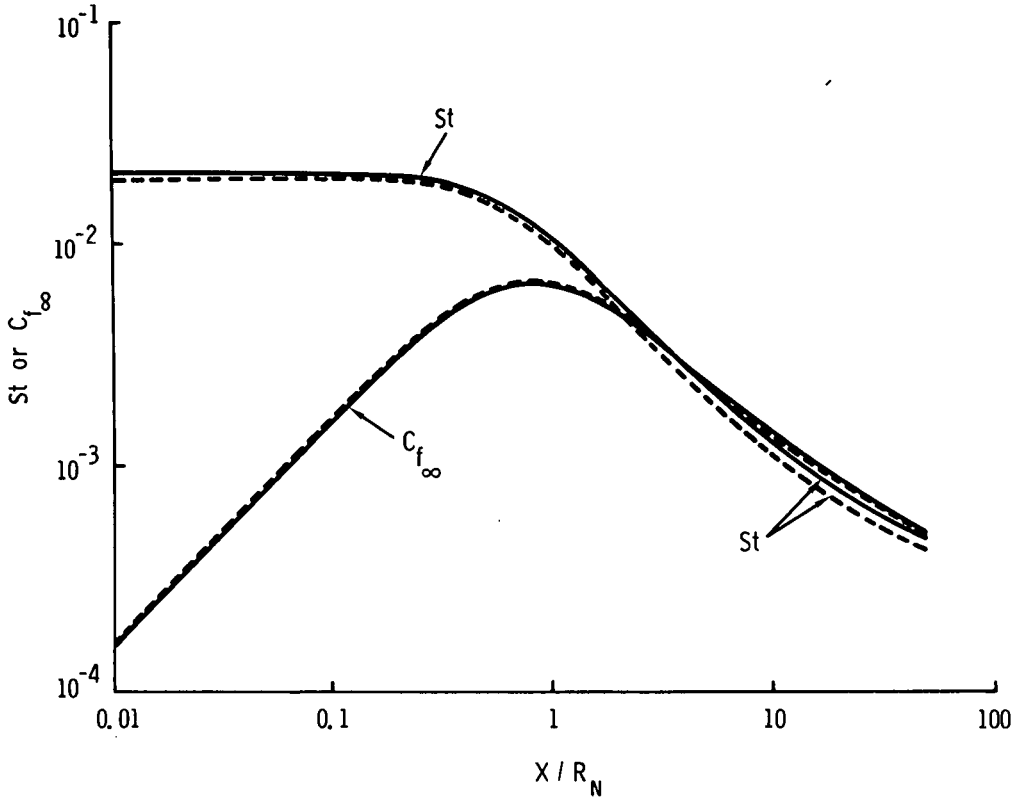

Fig.4 Stanton number and skin friction along hyperboloid

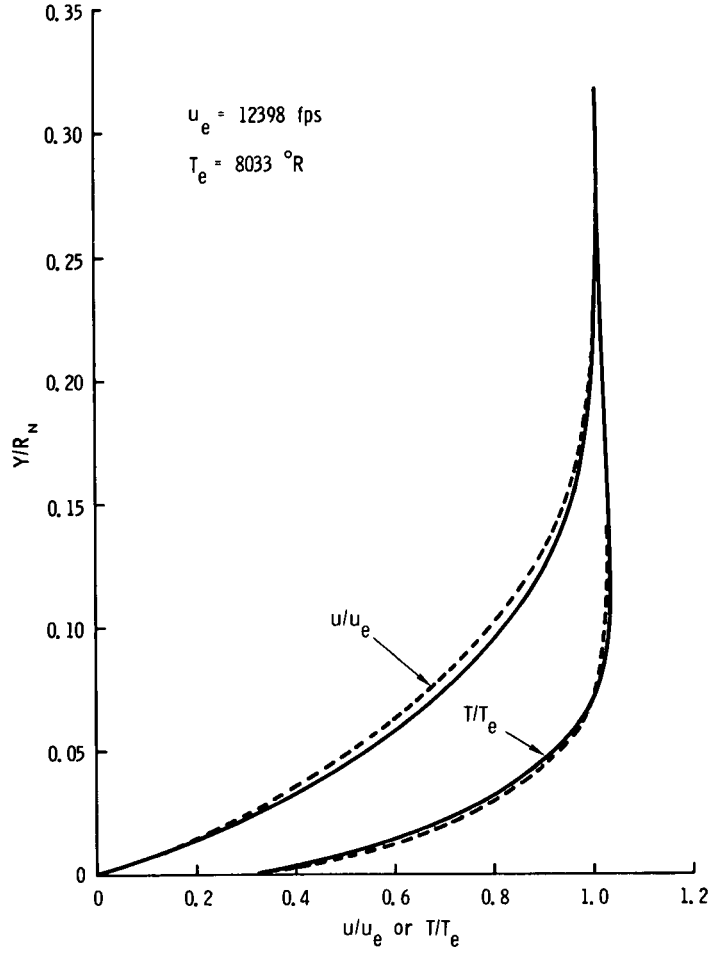

Fig.5 Velocity and temperature across the boundary layer at X/R_N = 50

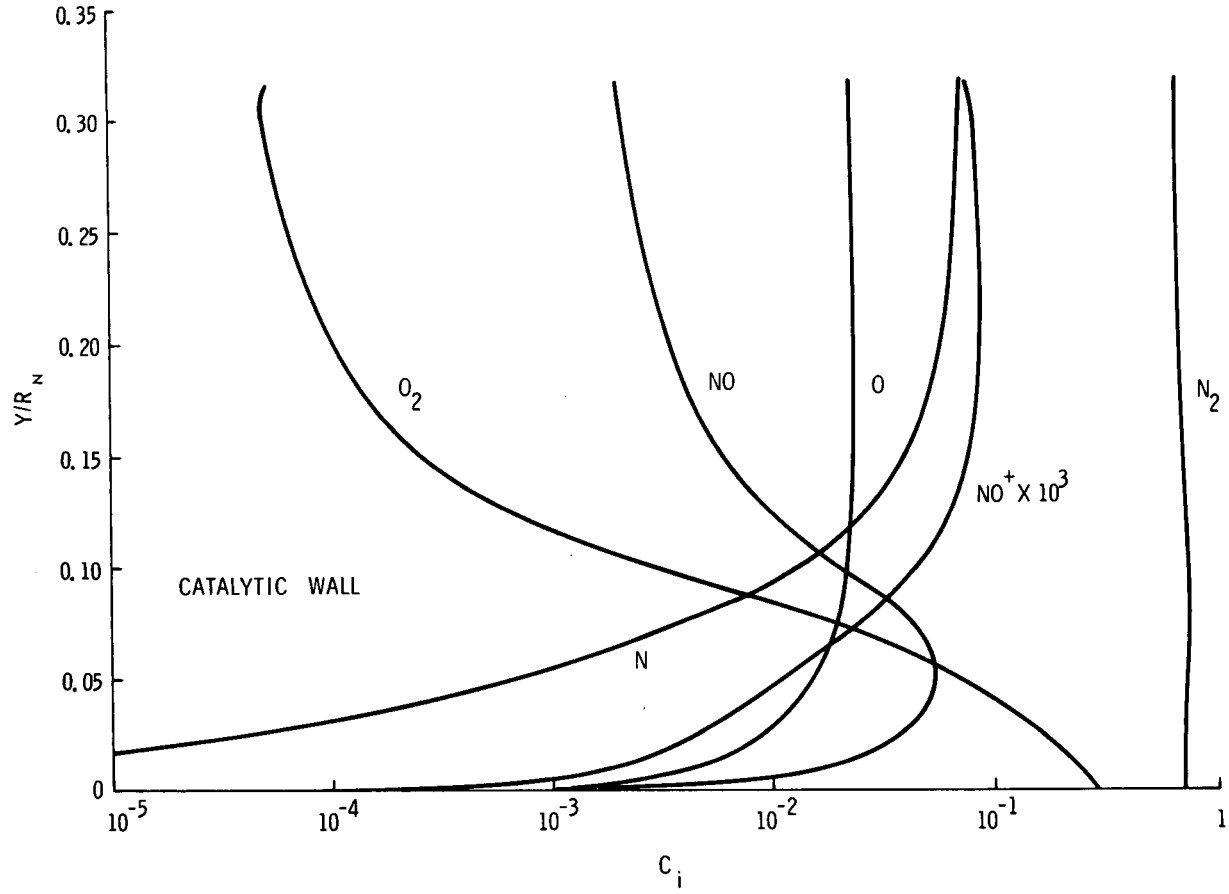

Fig.6 Mass fraction of chemical species across the boundary layer at $X/R_N = 50$

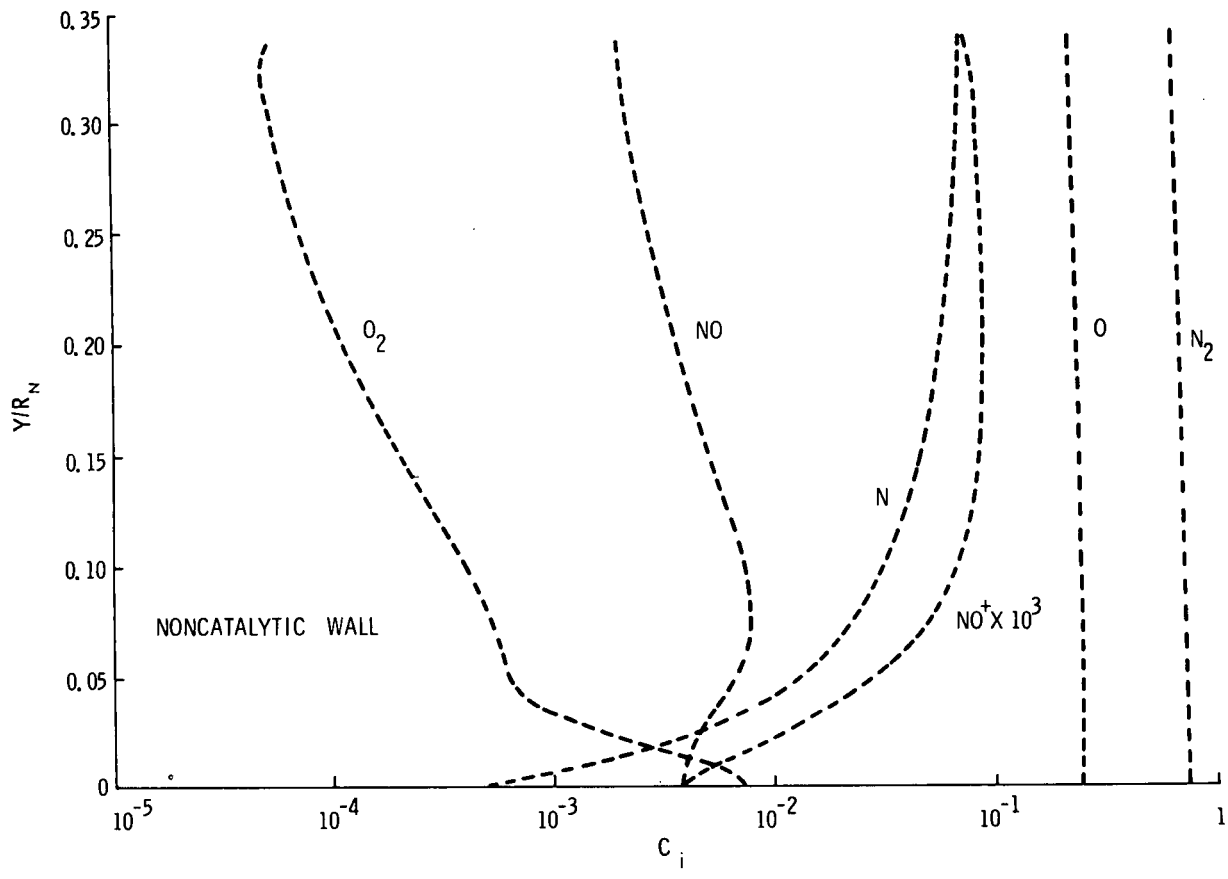

Fig.7 Mass fraction of chemical species across the boundary layer at $S/R_N = 50$

LAMINAR BOUNDARY LAYER CALCULATIONS ON BODIES OF REVOLUTION IN HYPERSONIC FLOW

by

Gerlina L.Keltner and A.M.O.Smith*

*Chief Aerodynamics Engineer,
Douglas Aircraft Company, Long Beach, California

LAMINAR BOUNDARY LAYER CALCULATIONS ON BODIES OF REVOLUTION IN HYPERSONIC FLOW

by Gerlina L. Keltner and A.M.O. Smith*

SUMMARY

Two sets of laminar boundary layer problems in hypersonic flow are presented. One set consists of boundary layer calculations for equilibrium, frozen and nonequilibrium flows on a hyperboloid of revolution for a high Reynolds number at Mach 20 and a low Reynolds number at Mach 22. The results are presented for each Reynolds number showing a comparison between the three types of flows on the body. The other set consists of boundary layer calculations for experimental equilibrium flows on two three-quarter power-law bodies of revolution at Mach 8 and comparisons with experimental boundary layer measurements. The results did not compare well with experiment since this was a case where the conditions assumed when deriving the inviscid flow theory used to obtain additional data from the experimental pressure distributions were violated by the experimental conditions.

The boundary layer calculations were done on the IBM 7094 using two boundary layer programs already in existence, one for the equilibrium boundary layers and the other for the frozen and nonequilibrium boundary layers. Real gas fluid properties were used for the equilibrium cases on the hyperboloid and ideal gas fluid properties were used for the cases on the power-law body. Fluid properties derived for a binary air model were used for the frozen and nonequilibrium cases. The binary model was improved by making modifications to the fluid properties as originally programmed.

INTRODUCTION

Two sets of laminar boundary layer calculations on bodies of revolution in hypersonic flow are presented. One set consists of boundary layer calculations for equilibrium frozen and nonequilibrium flows on a hyperboloid of revolution. The other set consists of boundary layer calculations for equilibrium flow on two three-quarter power-law bodies of revolution. The calculations were done using two computer programs already in existence.

The first set of boundary layer calculations was done in response to the Engineering Applications Section of the AGARD Seminar at M.P.L. on "Numerical Methods for Viscous Flows," September 18-21, 1967, attended by A.M.O. Smith. Calculations were made for each of the three types of flows at two free stream Reynolds numbers, 2.158×10^6/ft at Mach 20 and 5.192×10^3/ft at Mach 22, making six cases in this set. The inviscid flow data was taken from [1] for equilibrium, frozen and nonequilibrium expansions about the body. The equilibrium boundary layer calculations were done on the IBM 7094 under the program number 44KA using the method developed by Smith [2]. Real gas fluid properties as developed by Cohen [3] were used. The frozen and nonequilibrium boundary layer calculations were done on the IBM 7094 under the program number 61RA using the method developed by Smith [4]. Fluid properties developed for a binary air model with modifications to the original method were used. These modifications will be discussed later.

The second set of boundary layer calculations were made for comparison with the experimental results in [5] for equilibrium air at Mach 8. This was done since experimental boundary layer measurements are difficult to find thus enabling the theoretical calculations to be checked out. The inviscid flow data were obtained from surface pressure measurements and theoretical relationships in [5]. The measurements were made at three reservoir stagnation pressures for each of two power-law bodies. The boundary layer calculations were made using the method in [2]. Ideal gas fluid properties were used since these were appropriate for the wind tunnel conditions of the experiments.

The boundary layer equations applicable to the flows described above will be presented. However, the methods of solution will be discussed only briefly since these are adequately covered in the references cited. The calculation results will be presented along with any appropriate comparisons. Details of preparation of the inviscid flow data for use in the boundary layer programs will be discussed in the appendix.

METHOD OF SOLUTION

Boundary-Layer Equations and Fluid Properties

The general coordinate system and notation are shown in Fig. 1. The equilibrium cases were solved by the method described in [2]. The laminar boundary layer equations for equilibrium flow on a body of revolution, neglecting second-order transverse curvature are:

Continuity

$$\frac{\partial(\rho r u)}{\partial x} + \frac{\partial(\rho r v)}{\partial y} = 0 \tag{1}$$

Momentum

$$u \frac{\partial u}{\partial x} + v \frac{\partial u}{\partial y} = -\frac{1}{\rho}\frac{dp}{dx} + \frac{1}{\rho}\frac{\partial}{\partial y}\left(\mu \frac{\partial u}{\partial y}\right) \tag{2}$$

Energy

$$u \frac{\partial H}{\partial x} + v \frac{\partial H}{\partial y} = \frac{1}{\rho}\frac{\partial}{\partial y}\left[\frac{\mu}{Pr}\frac{\partial H}{\partial y} + \mu(1 - 1/Pr)u \frac{\partial u}{\partial y}\right] \tag{3}$$

where

$$H = h + \frac{1}{2}u^2 \qquad (v^2 \text{ neglected})$$

*Chief Aerodynamics Engineer, Douglas Aircraft Company, Long Beach, California.

The coordinates are transformed by

$$\eta = \sqrt{\frac{u_e}{\rho_\infty \mu_\infty x}} \int_0^y \rho \, dy \tag{4a}$$

$$x = x \tag{4b}$$

Using a stream function ψ defined as

$$\rho r u = \frac{\partial(\psi r)}{\partial y} \tag{5a}$$

$$\rho r v = -\frac{\partial(\psi r)}{\partial x} \tag{5b}$$

a dimensionless stream function such that

$$\frac{\partial f}{\partial \eta} = \frac{u}{u_e} \tag{5c}$$

and the coordinate transformations (4), the equations become:

Momentum

$$\frac{1}{C_\infty}(C f'')' = -P\left[\frac{\rho_e}{\rho} - f'^2\right] - \left[\frac{P+1}{2} + R\right] ff'' + x\left[f' \frac{\partial f'}{\partial x} - f'' \frac{\partial f}{\partial x}\right] \tag{6}$$

Energy

$$\frac{1}{C_\infty}\left[\frac{C}{Pr} g' + \frac{u_e^2}{H_e} C\left(1 - \frac{1}{Pr}\right) f'f''\right]' = -\left[\frac{P+1}{2} + R\right] fg' + x\left[f' \frac{\partial g}{\partial x} - g' \frac{\partial f}{\partial x}\right] \tag{7}$$

where $C = \frac{\rho\mu}{\rho_e \mu_e}$, $C_\infty = \frac{\rho_\infty \mu_\infty}{\rho_e \mu_e}$, $f = \psi / \sqrt{\rho_\infty \mu_\infty u_e x}$, $f' = \frac{u}{u_e}$, $P = \frac{x}{u_e}\frac{du_e}{dx}$, $R = \frac{x}{r}\frac{dr}{dx} = \frac{x}{r_o}\frac{dr_o}{dx}$,

$g = \frac{H}{H_e}$, $H_e = h_e + \frac{1}{2}u_e^2 = h_\infty + \frac{1}{2}u_\infty^2 =$ constant outside the boundary layer.

Prime denotes differentiation with respect to η.

The continuity equation (1) is automatically satisfied by the stream function, Eq. (5).

The fluid properties ρ, C and Pr in (6) and (7) are arbitrary functions of local enthalpy h. The method of solution in [2] allows a choice between ideal gas fluid properties and the fluid properties including equilibrium dissociation described in [3].

The nonequilibrium and frozen cases were solved by the method described in [4]. The coordinate system is shown in Fig. 1. The laminar boundary layer equations for nonequilibrium dissociated flow on a body of revolution, neglecting second-order transverse curvature are:

Continuity

$$\frac{\partial(\rho r u)}{\partial x} + \frac{\partial(\rho r v)}{\partial y} = 0 \tag{8}$$

Species

$$u \frac{\partial c_a}{\partial x} + v \frac{\partial c_a}{\partial y} = \frac{1}{\rho}\frac{\partial}{\partial y}\left[\rho D_{am} \frac{\partial c_a}{\partial y} + \frac{D_a^T}{T}\frac{\partial T}{\partial y}\right] + \dot{w}_a \tag{9}$$

Momentum

$$u \frac{\partial u}{\partial x} + v \frac{\partial u}{\partial y} = -\frac{1}{\rho}\frac{dp}{dx} + \frac{1}{\rho}\frac{\partial}{\partial y}\left(\mu \frac{\partial u}{\partial y}\right) \tag{10}$$

Energy

$$u \frac{\partial H}{\partial x} + v \frac{\partial H}{\partial y} = \frac{1}{\rho}\frac{\partial}{\partial y}\left[\frac{\mu}{Pr}\frac{\partial H}{\partial y} + \mu\left(1 - \frac{1}{Pr}\right) u \frac{\partial u}{\partial y}\right] + \frac{1}{\rho}\frac{\partial}{\partial y}\left[\frac{\mu}{Pr}(Le - 1)(h_a - h_m)\frac{\partial c_a}{\partial y} + \frac{D_a^T}{T}(h_a - h_m)\frac{\partial T}{\partial y}\right] \tag{11}$$

Using the coordinate transformations (4) and the stream function (5), the equations become:

Species

$$\frac{1}{C_\infty}\left[\frac{Le}{Pr} C z' + \frac{D_a^T}{c_{a_e} \mu T} C \frac{\partial T}{\partial \eta}\right]' = S z f' - \left[\frac{P+1}{2} + R\right] fz' + x\left[f' \frac{\partial z}{\partial x} - z' \frac{\partial f}{\partial x}\right] - \frac{x}{c_{a_e} \rho u_e} \dot{w}_a \tag{12}$$

Momentum

$$\frac{1}{C_\infty}(Cf'') = -P\left[\frac{\rho_e}{\rho} - f'^2\right] - \left[\frac{P+1}{2} + R\right] ff'' + x\left[f' \frac{\partial f'}{\partial x} - f'' \frac{\partial f}{\partial x}\right] \tag{13}$$

Energy

$$\frac{1}{C_\infty}\left[\frac{C}{Pr} g' + \frac{u_e^2}{H_e} C\left(1 - \frac{1}{Pr}\right) f'f'' + \frac{h_a - h_m}{H_e}\left[\frac{Le - 1}{Pr} C c_{a_e} z' + \frac{D_a^T}{\mu T} C \frac{\partial T}{\partial \eta}\right]\right]' = -\left[\frac{P+1}{2} + R\right] fg' + x\left[f' \frac{\partial g}{\partial x} - g' \frac{\partial f}{\partial x}\right] \tag{14}$$

where

$$z = \frac{c_a}{c_{a_e}} , \qquad S = \frac{x}{c_{a_e}} \frac{dc_{a_e}}{dx}$$

Frozen boundary layer calculations are made by setting the chemical source term in $\dot{w}_a$ in Eq. (12) equal to zero. The chemical source term calculated for nonequilibrium boundary layer is derived in [4] using atomic properties obtained by averaging the values for oxygen and nitrogen. The fluid properties were derived for a binary air model of molecules and atoms as functions of local temperature. The atomic properties used in the binary air model are also averages of the oxygen and nitrogen values.

Modifications to Fluid Properties

It was noticed by the author that the binary air model fluid properties in [4] used for frozen and nonequilibrium cases did not give very accurate values. Therefore, modifications were made in order to improve them. The local molecular enthalpy and the atomic source term were changed as follows. The local molecular enthalpy was approximated in [4] by

$$h_m \doteq h - c_a h_a^o \tag{15}$$

where c_a is the mass concentration of all the atoms present, added together. From this value of h_m the local temperature and other fluid properties are obtained. For $c_a \leq 0.2$ the program used the value of h_m^o for oxygen. For $c_a > 0.2$ the program used the value of h_a^o for nitrogen. This is equivalent to assuming that for $c_a > 0.2$ all of the atoms are nitrogen. As a result the local molecular enthalpy calculated is much lower than would be expected since h_N^o is much larger than h_O^o. Therefore (15) was replaced by

$$h_m \doteq h - c_O h_O^o - c_N h_N^o \tag{16}$$

The program calculates the atomic concentration c_a which includes all the atoms present. Therefore, the following scheme was devised in order to obtain c_O and c_N individually. For frozen flow, c_{O_e} and c_{N_e} are known and may be input to the program. Then

$$c_N = c_a/(1 + c_{O_e}/c_{N_e}) \tag{17a}$$

and

$$c_O = c_N \, (c_{O_e}/c_{N_e}) \tag{17b}$$

since c_O and c_N stay in constant proportion through the boundary layer. For dissociating air in equilibrium it is empirically known that the oxygen concentration remains relatively constant once the nitrogen has begun dissociating; oxygen dissociation is essentially complete at this time. For nonequilibrium flow a maximum value for c_O was put into the program. If c_a was greater than this maximum, the value of c_N was obtained from

$$c_N = c_a - c_{O_{max}} \tag{18a}$$

and

$$c_O = c_{O_{max}} \tag{18b}$$

If c_a was less than this maximum then

$$c_N = 0 \tag{18c}$$

and

$$c_O = c_a \tag{18d}$$

was used. This scheme will be best for near-equilibrium flow. The error will increase as the nonequilibrium flow proceeds away from equilibrium and toward frozen flow. A remedy for this is to add more species equations and calculate them individually, but this is another project in itself. The local molecular enthalpy obtained from (16) gave more reasonable fluid property values.

In order to be consistent with the above approach, the chemical source term was changed to use $\dot{w}_O$ in the oxygen range and $\dot{w}_N$ in the nitrogen range. The equation for $\dot{w}_a$ is (6.23) from [4]:

$$\frac{x}{c_{a_e}\rho u_e} \dot{w}_a = \frac{x}{c_{a_e} u_e} \bar{\psi} \frac{p}{R'T} \frac{N_A}{2} \left[(1 - c_{a_e} z) \, e^{-\frac{D}{kT}} - (c_{a_e} z)^2 \frac{\rho_e}{\rho_d} \frac{\rho}{\rho_e} \right] \tag{19}$$

where

$$\bar{\psi} = \frac{1}{2} \sqrt{\frac{2\pi R'T}{M_m}} \left[2 \left(\frac{\sigma_m + \sigma_a}{2} \right)^2 \sqrt{6} + \sigma_m^2 \sqrt{2} \right]$$

The constant values in (19) were obtained by averaging the values for oxygen and nitrogen from [6] and [7]. By substitution into (19) of the individual constant values for oxygen and nitrogen and the equations for ρ_d from [7], the equations for $\dot{w}_O$ and $\dot{w}_N$ were obtained for the present work as:

$$\frac{x}{c_{a_e}\rho u_e} \dot{w}_O = \frac{x}{c_{a_e} u_e} 0.266664 \times 10^8 \frac{p}{\sqrt{T}} \left[(1 - c_O) e^{-\frac{1.062 \times 10^5}{T}} - c_O^2 \frac{\rho_e}{\rho_{d_O}} \frac{\rho}{\rho_e} \right] \tag{20}$$

$$\frac{x}{c_{a_e}\rho u_e} \dot{w}_N = \frac{x}{c_{a_e} u_e} 0.316823 \times 10^8 \frac{p}{\sqrt{T}} \left[(1 - c_N) e^{-\frac{2.034 \times 10^5}{T}} - c_N^2 \frac{\rho_e}{\rho_{d_N}} \frac{\rho}{\rho_e} \right] \tag{21}$$

where

$$\rho_{d_0} = .454280 \left[\frac{\sqrt{T}(1 - \exp\{- 4014/T\})(5 + 3 \exp\{- 410.4/T\} + \exp\{- 588.6/T\})^2}{3 + 2 \exp\{- 20340/T\}} \right]$$

$$\rho_{d_N} = 7.203345 \sqrt{T} (1 - \exp \{-6012/T\})$$

Previously, ρ_d had been assumed constant, i.e.

$$\rho_d = 271.65 \quad \text{slugs/ft}^3$$

as indicated in [4].

General Method of Solution

The general method of solution of these equations consists of replacing the partial derivatives with respect to x by finite differences so that the partial differential equations become ordinary differential equations. The ordinary differential equations are solved simultaneously by numerical integration to obtain solutions at a given x station as calculation proceeds downstream. The details of solution are explained in [2] and [4]. If the boundary layer computer program includes an option for the type of fluid properties used, the choice must be specified prior to solution of the equations.

BOUNDARY LAYER CALCULATIONS

Hyperboloid of Revolution

The inviscid flow data was taken from [1]. The body geometry is shown in Fig. 2. Equilibrium, frozen and nonequilibrium expansions about the body were calculated for two free stream Reynolds numbers. The conditions for each case are listed in Table I. A more detailed discussion of the inviscid flow data and the

TABLE I

Case	$\bar{M}_\infty$	Re_∞/ft	p_∞,atm	T_∞,°R	T_w,°R	p_{t_n},atm	T_{t_n},°R
A	20.178	2.1579×10^6	1.0997×10^{-2}	408.56	2520.0	6.0352	12,592.8
B	21.744	5.1920×10^3	2.0074×10^{-5}	351.83	1800.0	0.0129	9,543.3

u_∞ = 20,000 ft/sec nose radius = 1.0 inch

preparation of it for input to the computer programs is presented in the appendix. The corresponding boundary layers on the body were calculated for cases A and B using the methods previously described.

The equilibrium cases were calculated using fluid properties in [3] where equilibrium dissociation is accounted for by an equivalent Prandtl number. The frozen and nonequilibrium cases were calculated using the modified binary model fluid properties. The chemical source term was suppressed for the frozen flow cases and was calculated as modified for the nonequilibrium cases. The $c_{0_{max}}$ used for each case is listed in Table II. These values were determined from the inviscid flow data. Approximately 30 x-wise stations were calculated for each case.

TABLE II

Case	Flow Type	$c_{0\ max}$
A	Frozen	0.22624
	Nonequilibrium	0.230*
B	Frozen	0.24682
	Nonequilibrium	0.234*

*Averaged over body length.

The resulting velocity profiles at x/r_n = 3.0, 10, 25 and 50 are presented in Fig. 3 for case A and case B. Comparison is made between equilibrium, frozen and nonequilibrium profiles at each station. The skin friction distributions along the body are shown in Fig. 4 and the displacement thickness distributions are shown in Fig. 5. The Stanton number based on the freestream conditions is shown in Fig. 6. The largest difference between the three types of flows shows up in the displacement thickness. This is due to the difference in density profiles in the boundary layer. The velocity and enthalpy profiles do not differ much, but each type of flow has a different profile of atomic concentration which results in different density values. All results look reasonable except for the nonequilibrium Case B. This case is close to frozen flow and the scheme in (18) has the largest error here.

A problem which occurred in the nonequilibrium cases was the fact that the atomic concentration calculated by the boundary layer program was not the same as that calculated in the inviscid flow for the same conditions. Therefore, there was a slight incompatibility in the atomic concentration profile near the edge of the boundary layer. The program did not calculate the same c_{a_e} as the value input to the program as obtained from [1]. A

remedy might be to recalculate c_{a_e} from the inviscid flow conditions using the boundary layer program chemical source term and fluid property relationships.

Three-Quarter Power-Law Body of Revolution

The inviscid flow data was taken from wind tunnel tests in [5]. Two models were tested at Mach 8 in equilibrium air. The model geometry is described by

$$r_o/L = \delta (X/L)^{3/4} \tag{22}$$

where $\delta = 0.235$ and $L = 3.19$ in. for the first model, and $\delta = 0.1$ and $L = 5$ in. for the second model. Data was measured on each model at three reservoir stagnation pressures in the tunnel for the test conditions listed in Table III. Experimental measurements were made of the surface pressure distributions and of the pitot pressure profiles at $X/L = 0.8$. The relationship

$$p/p_\infty \sim (\bar{M}/Re_\infty L)\,(X/L)^{-1/2} \tag{23}$$

was used to obtain the rest of the inviscid flow data. However, the conditions assumed in deriving (23) were violated by the experiment. The experimental scatter in the pressure distributions was smoothed out before the data was used.

TABLE III

Test Case	$\bar{M}_\infty$	p_{t_∞}, psig	T_∞, °R	T_∞, psf	Re_∞/ft
1	7.871	50	101.535	1.0605	0.304435×10^6
2	7.873	100	101.487	1.8769	0.539356×10^6
3	7.991	250	98.728	3.9330	1.201019×10^6

$T_{t_\infty} = 1350.6$ °R adiabatic wall

Corresponding boundary layer profiles were calculated on each model for each test case. Ideal gas fluid properties were used since the tunnel temperature was so low. The calculated boundary layer velocity profiles are presented in Fig. 7 for models 1 and 2. The experimental profiles from [5] are added for comparison. The calculated and experimental displacement thicknesses are shown in Fig. 8. The experimental and theoretical results do not agree well. This is mainly due to the fact that (23) is not valid for the conditions of the experiment. It would have been better to obtain experimental measurements for all of the necessary inviscid flow data and not to use a theoretical equation to fill in data needed.

ACKNOWLEDGMENT

The author wishes to thank Dr. Bradford Sturtevant, consultant from California Institute of Technology, for many helpful discussions during preparation of this work. This report summarizes work performed at the Aircraft Division under sponsorship of the Independent Research and Development Program of Douglas Aircraft Company, Inc.

APPENDIX

The inviscid flow data for the hyperboloid of revolution was taken from [1]. The pressure distribution on the body is shown in Fig. 9. Using this pressure distribution equilibrium, nonequilibrium and frozen flow expansions were calculated about the body. The resulting velocity distributions are shown in Fig. 10. In order to obtain the atomic concentrations, the oxygen and nitrogen atoms were added together. The resulting frozen and nonequilibrium concentrations are shown in Fig. 11.

In order to obtain the parameters

$$P = \frac{x}{u_e}\frac{du_e}{x}, \qquad S = \frac{x}{c_{a_e}}\frac{dc_{a_e}}{dx}$$

the distributions of c_{a_e} and u_e were differentiated numerically with respect to x, using 3-point Lagrange differentiation formulas. The values of P and S thus calculated were then smoothed since the accuracy of numerical differentiation is generally poor. The values of

$$R = \frac{x}{r_o}\frac{dr_o}{dx}$$

may be calculated in a similar manner if dr_o/dx is not readily available from the body geometry. The values of P, S and R are shown in Fig. 12, 13 and 14, respectively.

The inviscid flow data for the power-law body was taken from [5]. The geometry of the body is given by

$$r_o/L = \delta (X/L)^{3/4} \tag{24}$$

Using (24) the surface distance on the body may be calculated. Since the surface element is

$$dx^2 = dr_o^2 + dx^2 \tag{25}$$

the surface distance on the body is

$$x = \int_o^X \sqrt{1 + (dr_o/dX)^2}\; dX$$

or $$\frac{x}{L} = \int_0^X \sqrt{1 + \left[\frac{3\delta}{4}(X/L)^{-1/4}\right]^2}\, d(X/L) =$$

$$\left[\sqrt{\frac{X}{L}} + \frac{9\delta^2}{32}\right]\left[\sqrt{\frac{X}{L}}\left(\sqrt{\frac{X}{L}} + \frac{9\delta^2}{16}\right)\right]^{1/2} - \frac{81\delta^4}{512}\log_e\left[\sqrt{\frac{16}{9\delta^2}\frac{X}{L}} + \sqrt{1 + \frac{16}{9\delta^2}\frac{X}{L}}\right] \qquad (26)$$

The relationship (24) also allows the parameter R to be calculated directly.

The experimental pressure distributions are taken from [5] and smoothed before using them. The relationship (23) and the pressures are used to obtain the local Mach number and, therefore, u_e. Enough additional data is supplied at X/L = 0.8 to obtain $\bar{M}$ at this point and, therefore, the constant of proportionality in (23). $\bar{M}$ and u_e may then be calculated along the body. The parameter P is calculated as previously described and is shown in Fig. 15. The parameter S is not needed since these are equilibrium cases.

REFERENCES

[1] Lukasiewicz, J. Private Communication, von Karman Gas Dynamics Facility, ARO, Inc., April 7, 1967.

[2] Smith, A.M.O. and Clutter, D.W. "Machine Calculation of Compressible Boundary Layers." AIAA Journal, Vol. 3, No. 4, April 1965, pp. 637-647.

[3] Cohen, N.B. "Correlation Formulas and Tables of Density and Some Transport Properties of Equilibrium Dissociating Air for Use in Solution of the Boundary Layer Equations." NASA TN D-194, February 1960.

[4] Smith, A.M.O. and Jaffe, N.A. "General Method for Solving the Laminar Nonequilibrium Boundary Layer Equations of a Dissociating Gas." AIAA Journal, Vol. 4, No. 4, April 1966, pp. 611-629.

[5] Nagasu, Hideo. "Experimental Investigation on Viscous Hypersonic Flow Around Three-Quarter Power-Law Bodies of Revolution." Proceedings, Fourteenth Japan National Congress for Applied Mechanics, 1964.

[6] Scala, S.M. and Baulknight, C.W. "Transport and Thermodynamic Properties in a Hypersonic Laminar Boundary Layer." Aerophysics Research Memo 10, General Electric Missile and Ordnance Systems Division, Technical Information Series, Document No. 58D232, April 1958; also published in ARS Journal, Vol. 29, No. 1, January 1959, pp. 39-45.

[7] Wood, G.P. "Calculations of the Rate of Thermal Dissociation of Air Behind Normal Shock Waves at Mach Numbers of 10, 12, and 14." NACA TN 3634, April 1955.

NOMENCLATURE

c_{f_∞} skin friction, $\tau_w/\frac{1}{2}\rho_\infty u_\infty^2$

c_i mass concentration of species i, ρ_i/ρ

C $\rho\mu/\rho_e\mu_e$

C_p specific heat at constant pressure

D dissociation energy

D_{am} binary concentration coefficient of diffusion

D_a^T atom thermal-diffusion coefficient

f nondimensional stream function, $f = \psi/\rho_\infty\mu_\infty x\ u_e$

f' $\partial f/\partial n$, velocity, u/u_e

g enthalpy ratio, H/H_e

h local enthalpy, ft^2/sec^2

h_i local enthalpy of species i, ft^2/sec^2

h_i^o heat of formation per unit mass of atoms, ft^2/sec^2

H total enthalpy = h + 1/2 u^2, ft^2/sec^2

k Boltzman constant

L length of body, ft

Le Lewis number

M_i molecular weight of species i

$\bar{M}$ Mach number

N_A Avogadro number

p static pressure, lb/ft^2

p_t stagnation pressure, lb/ft^2

P $(x/u_e)(du_e/dx)$

Pr Prandtl number

q heat transfer at surface

r radial distance from axis of revolution, ft

r_o radius of body of revolution, ft

R $(x/r)(dr/dx)$

Re Reynolds number

R' universal gas constant

S $(x/c_{a_e})(dc_{a_e}/dx)$

St_∞ Stanton number, $-q_w/\rho_\infty u_\infty H_e(1 - g_w)$

T static temperature, °R

T_t stagnation temperature, °R

u x-component of velocity, ft/sec

v y-component of velocity, ft/sec

$\dot{w}_i$ net mass rate of formation of atoms per unit volume due to chemical reactions, $slugs/ft^3$ sec

x distance along body surface measured from stagnation point, ft

X axial distance from nose of body, ft

y distance normal to body surface, ft

z nondimensional atom mass fraction c_a/c_{a_e}

η transformed y-coordinate, Eq. (4)

μ viscosity, slugs/ft sec

ψ stream function, Eq. (5)

ρ density, slugs/ft^3

ρ_d parameter having dimensions of density in Eq. (19)

σ molecular radius of species i, ft

τ shear stress

Prime denotes differentiation with respect to η, except in R'

Subscripts

a value for atoms

e value at edge of boundary layer

m value for molecules

n value at the nose, x = 0

N value for nitrogen atoms

O value for oxygen atoms

∞ value at reference conditions

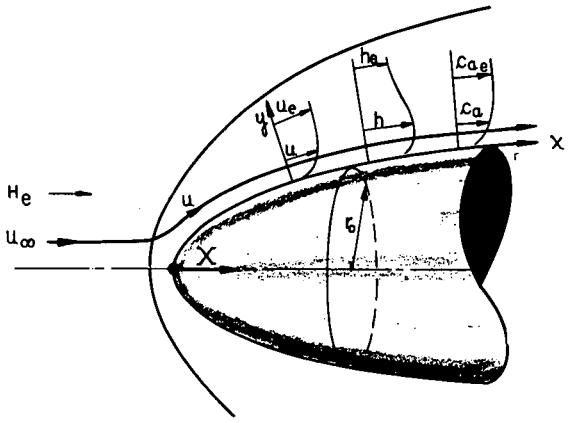

Fig.1 Boundary layer on a body of revolution. Coordinate system

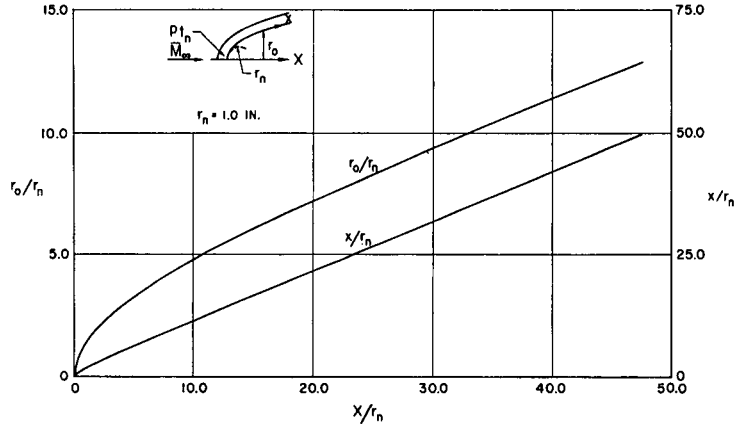

Fig.2 Hyperboloid of revolution. Body geometry

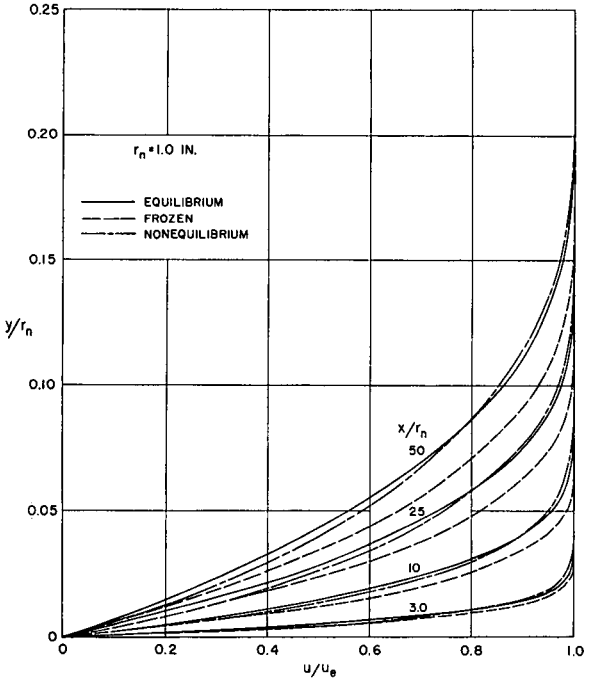

(a) Case A, $\bar{M}_\infty$ = 20, RE_∞/FT = 2.1579 x 10^6

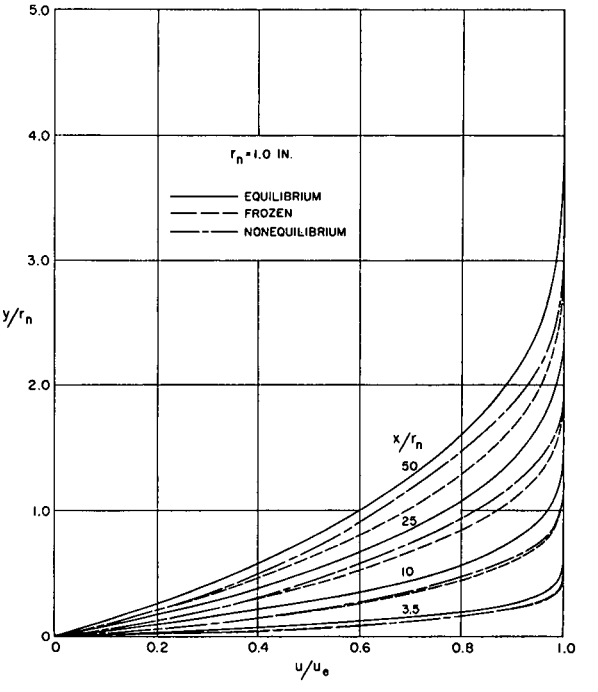

(b) Case B, $\bar{M}_\infty$ = 22, RE_∞/FT = 5.1920 x 10^3

Fig.3 Velocity profiles on the hyperboloid of revolution

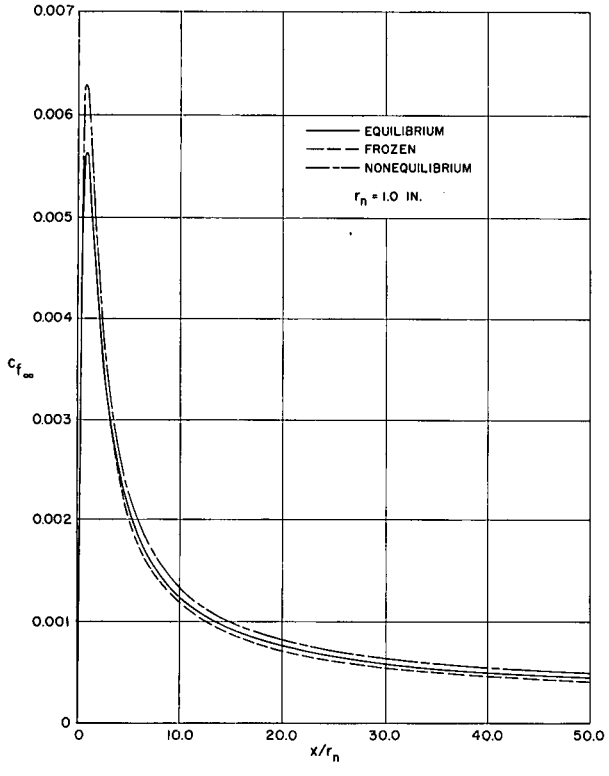

(a) Case A, $\bar{M}_\infty = 20$, $RE_\infty/FT = 2.1579 \times 10^6$

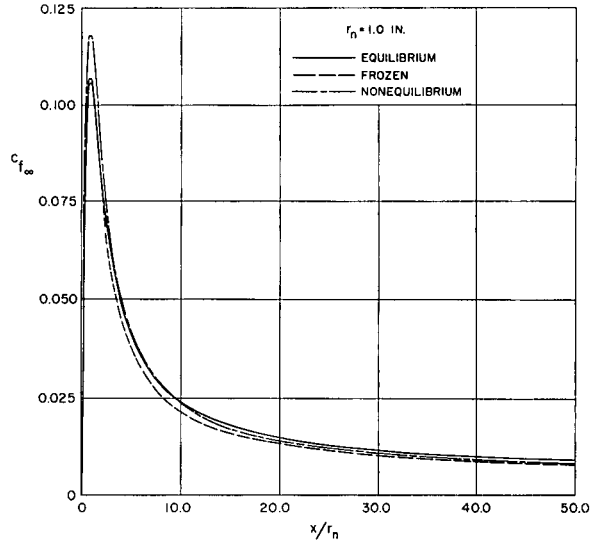

(b) Case B, $\bar{M}_\infty = 22$, $RE_\infty/FT = 5.1920 \times 10^3$

Fig.4 Skin-friction distributions on the hyperboloid of revolution

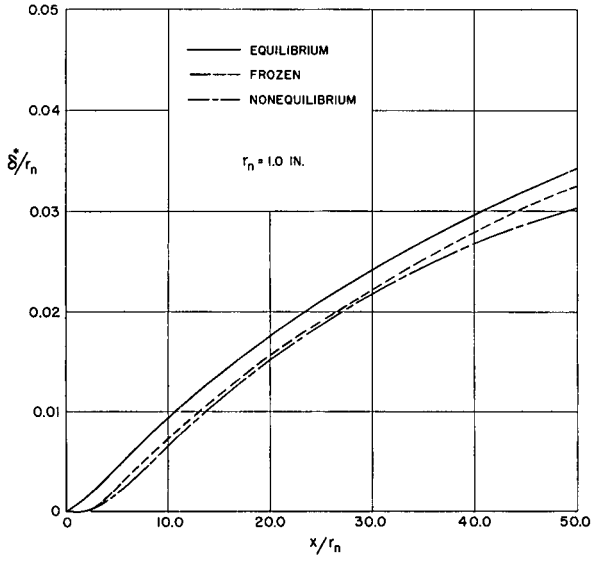

(a) Case A, $\bar{M}_\infty = 20$, $RE_\infty/FT = 2.1579 \times 10^6$

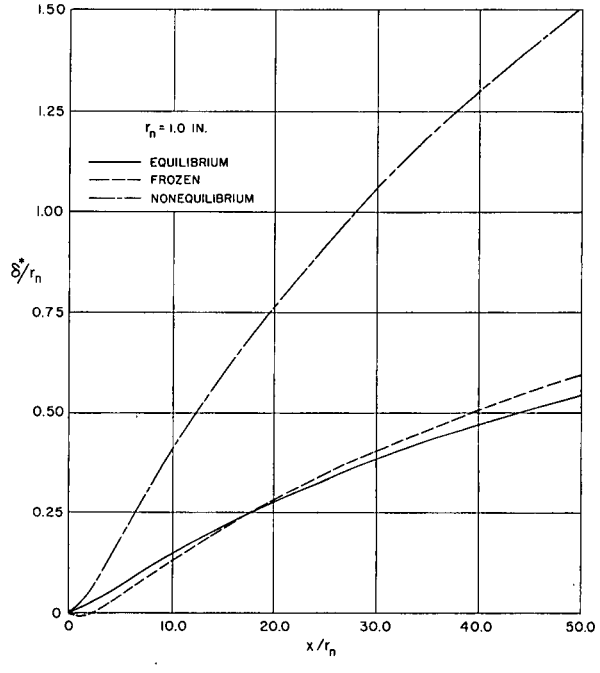

(b) Case B, $\bar{M}_\infty = 22$, $RE_\infty/FT = 5192$

Fig.5 Displacement-thickness distributions on the hyperboloid of revolution

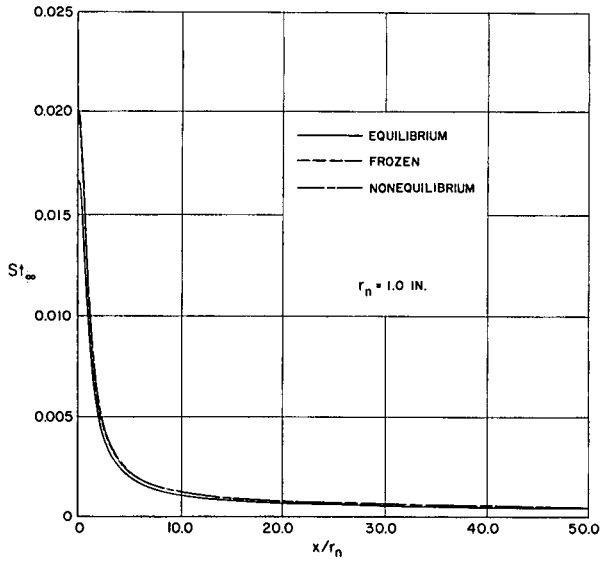

(a) Case A, $\bar{M}_\infty = 20$, $RE_\infty/FT = 2.1579 \times 10^6$

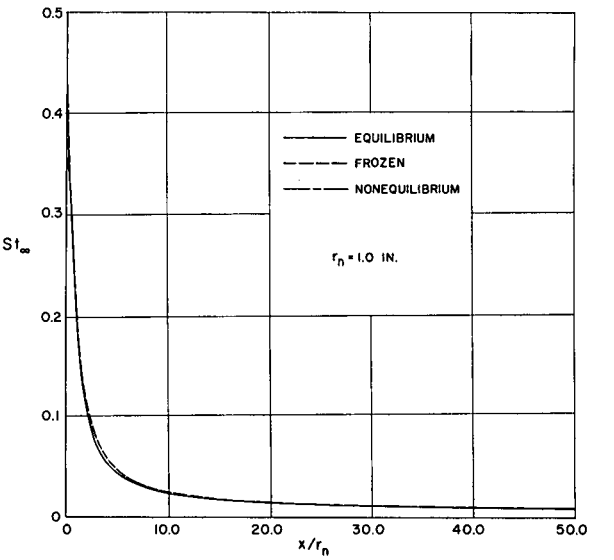

(b) Case B, $\bar{M}_\infty = 22$, $RE_\infty/FT = 5.1920 \times 10^3$

Fig.6 Stanton number distributions on the hyperboloid of revolution

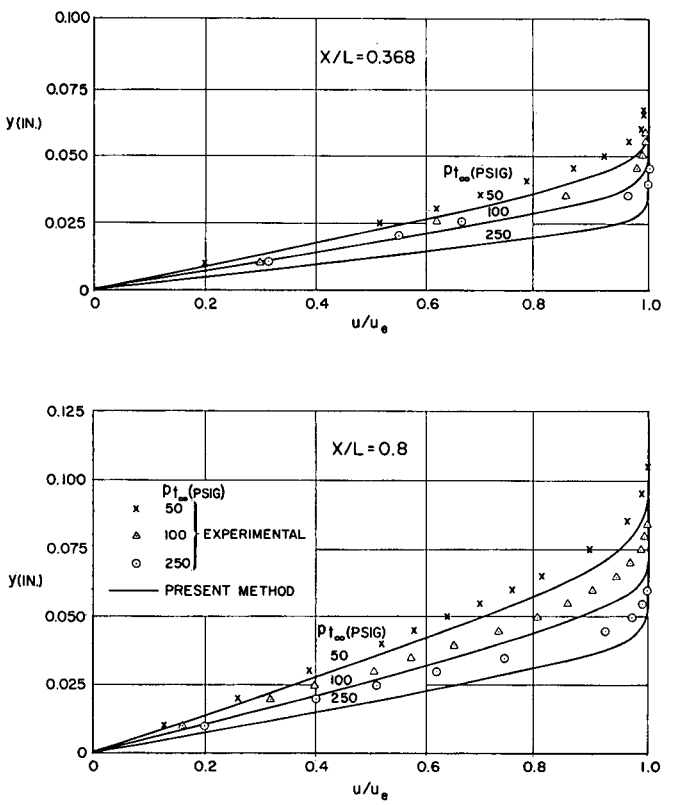

(a) Model 1, $\sigma = 0.235$, X/L = 0.368, 0.8

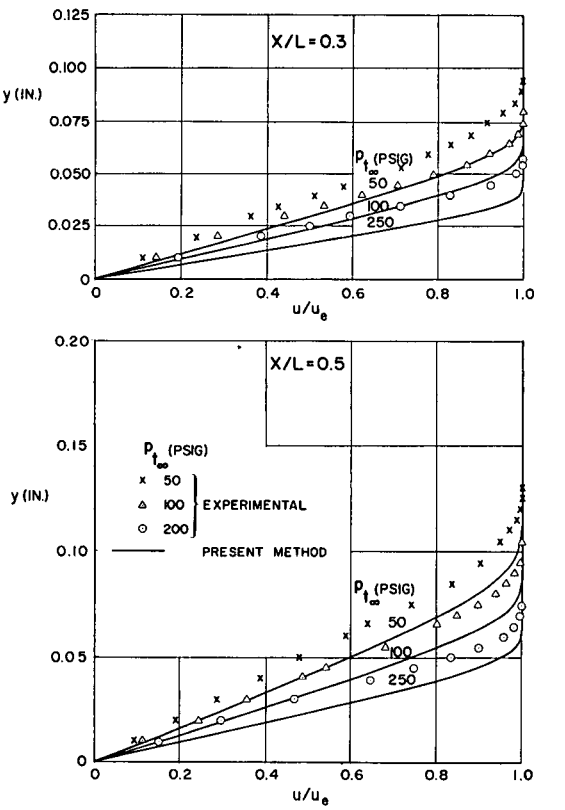

(b) Model 2, $\sigma = 0.1$, X/L = 0.3, 0.5

Fig.7 Velocity profiles on the three-quarter power-law body

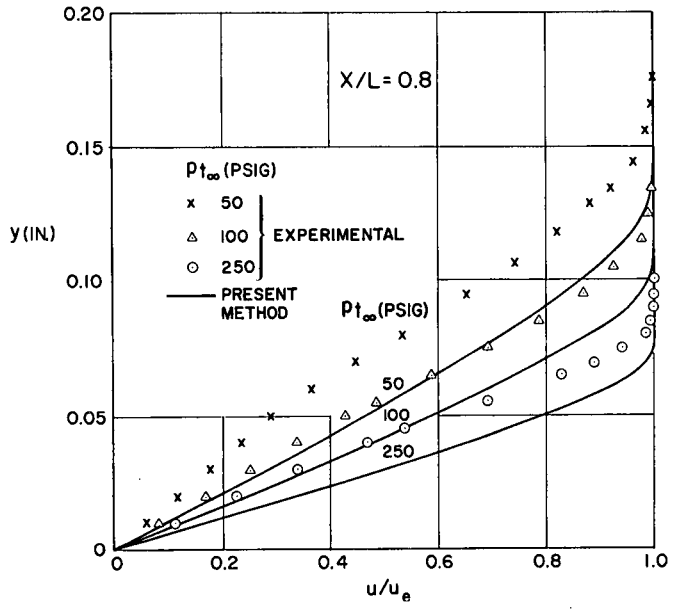

(c) Model 2, σ = 0.1, X/L = 0.8

Fig.7 (concluded) Velocity profiles on the three-quarter power-law body

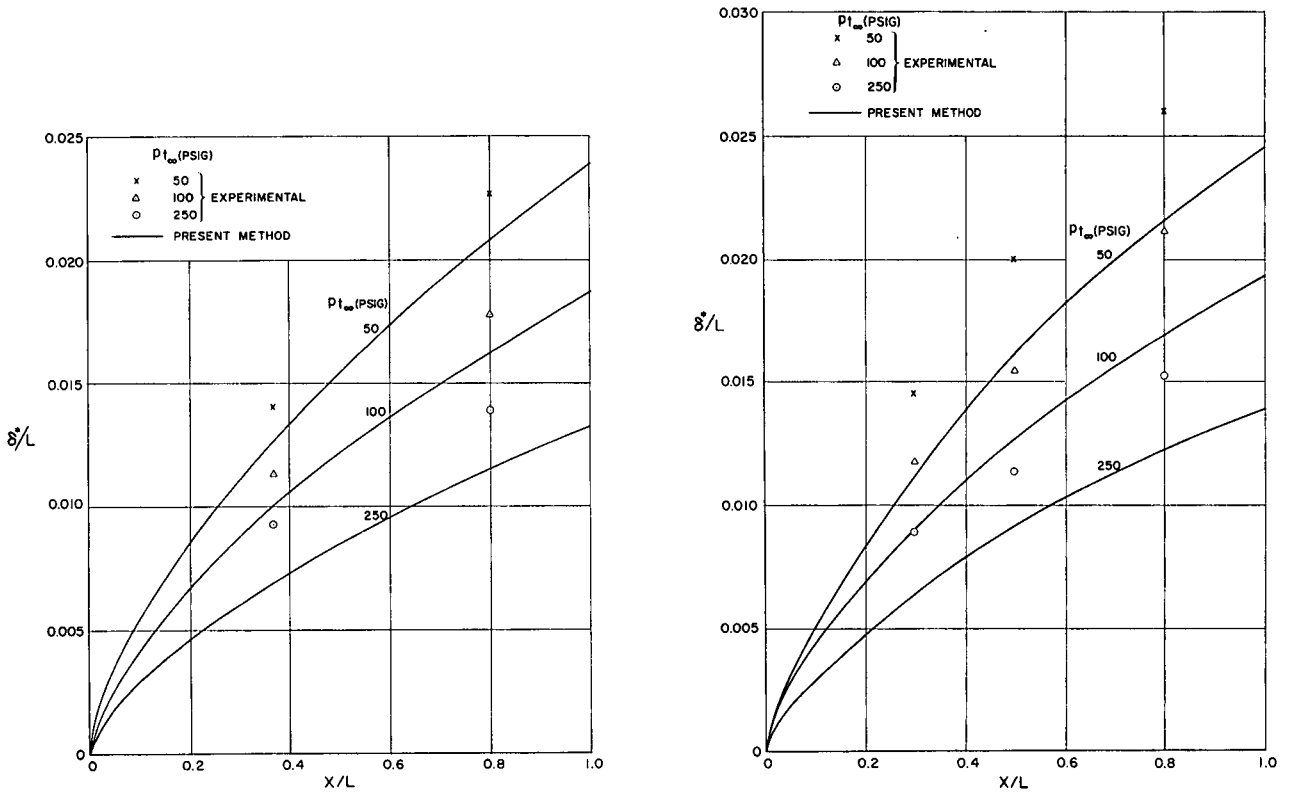

(a) Model 1, σ = 0.235

(b) Model 2, σ = 0.1

Fig.8 Displacement-thickness distributions on the three-quarter power-law body

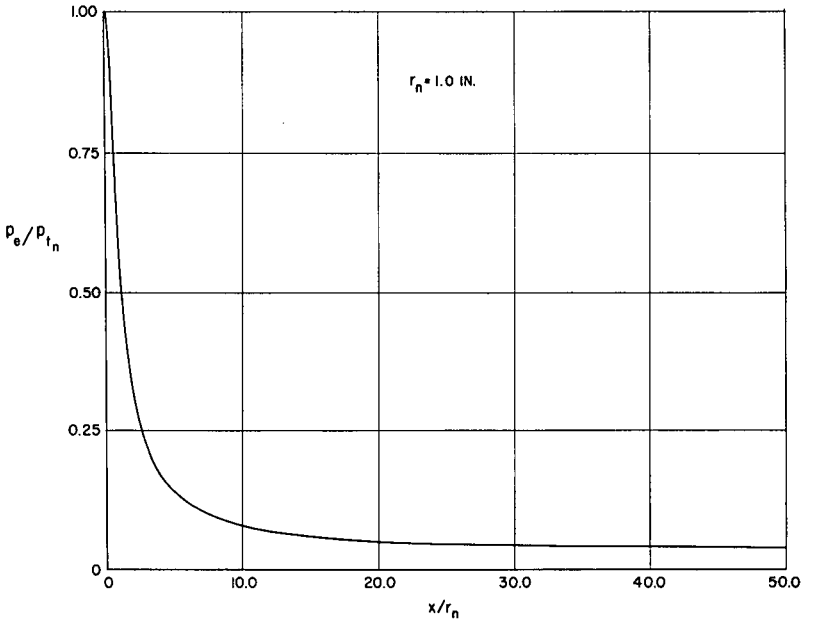

Fig.9 Pressure distribution on the hyperboloid of revolution

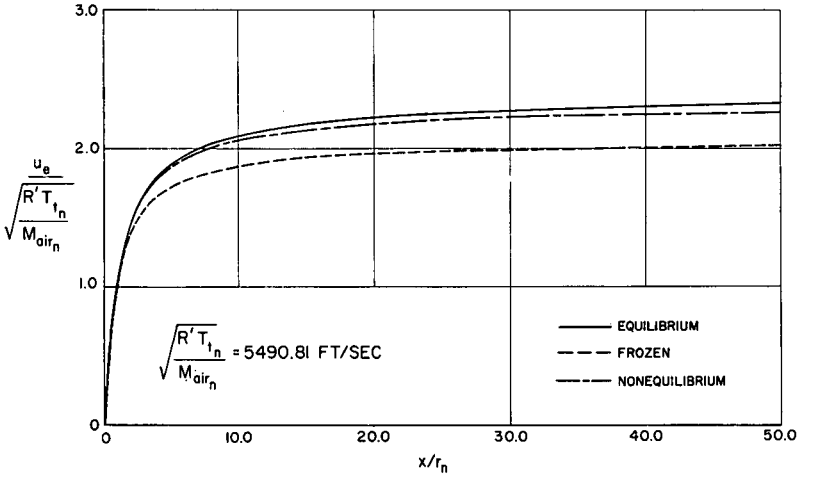

(a) $\bar{M}_\infty = 20$, $RE_\infty/FT = 2.1579 \times 10^6$

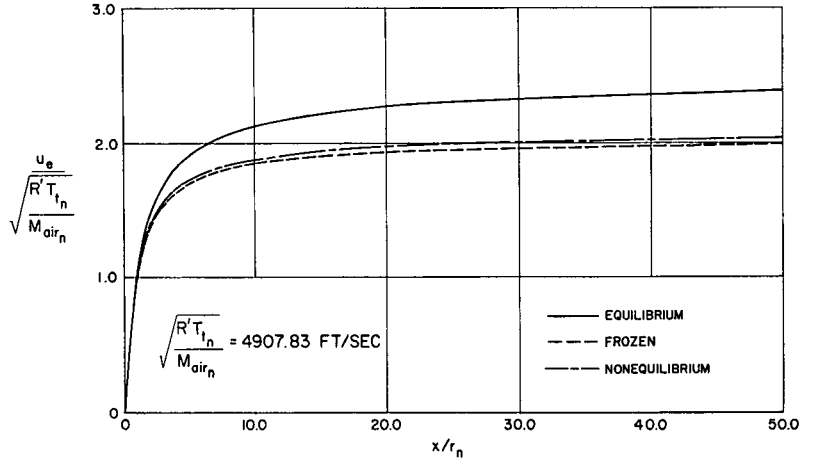

(b) $\bar{M}_\infty = 22$, $RE_\infty/FT = 5.1920 \times 10^3$

Fig.10 Inviscid velocity distributions on the hyperboloid of revolution

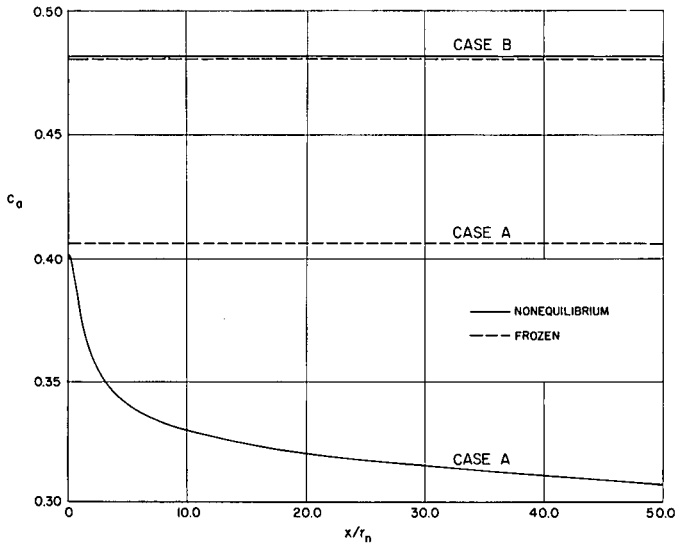

Fig.11 Inviscid atomic concentrations on the hyperboloid of revolution

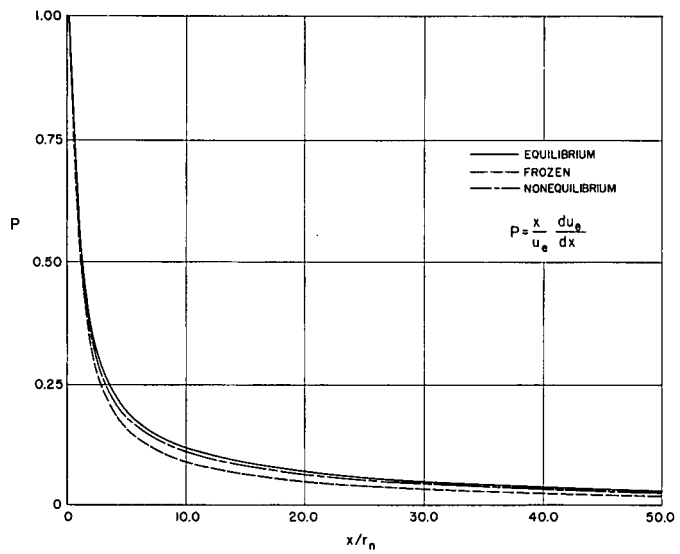

(a) Case A, $\bar{M}_\infty = 20$, $RE_\infty/FT = 2.1579 \times 10^6$

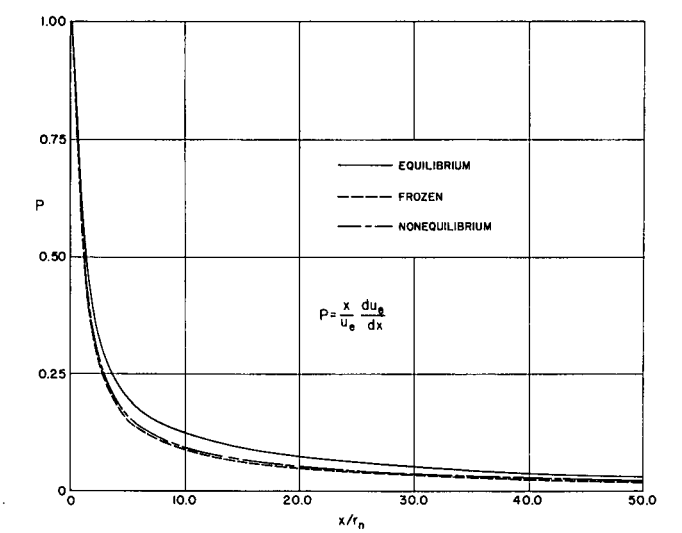

(b) Case B, $\bar{M}_\infty = 22$, $RE_\infty/FT = 5.1920 \times 10^3$

Fig.12 P VS X/R_N for the hyperboloid of revolution

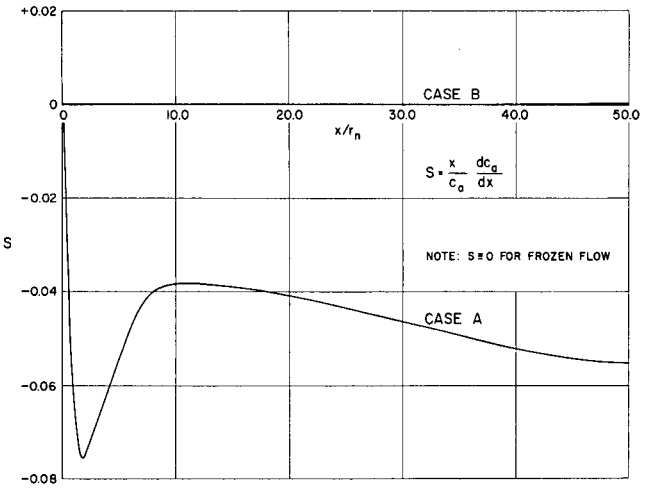

Fig. 13 S VS X/R_N for the hyperboloid of revolution. Nonequilibrium flow

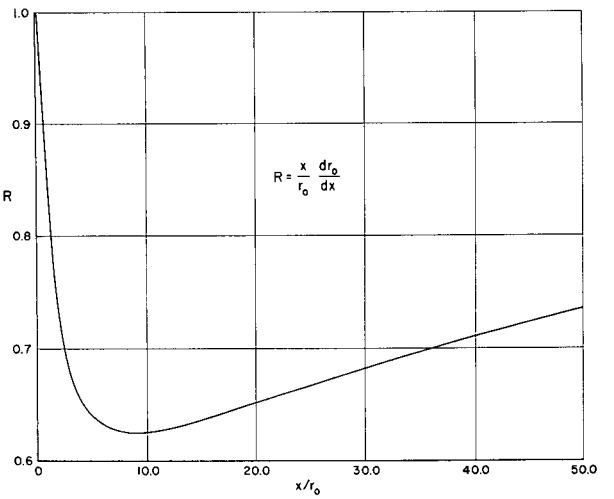

Fig. 14 R VS X/R_N for the hyperboloid of revolution

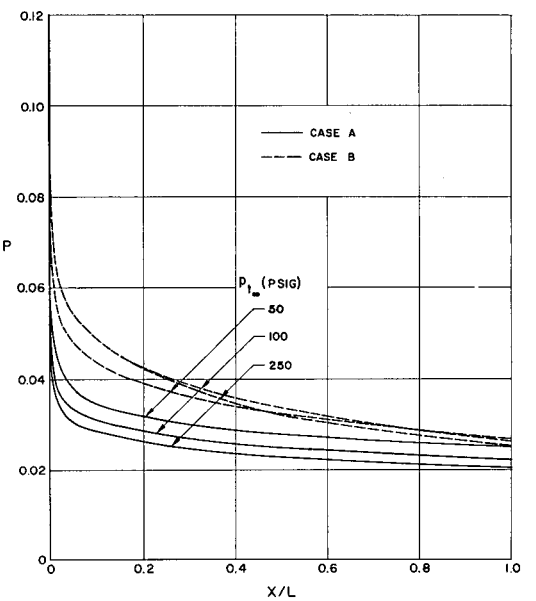

Fig. 15 P VS X/L for the three-quarter power-law body

SOLUTION OF THE VISCOUS SHOCK-LAYER EQUATIONS FOR A BINARY MIXTURE

by

R.T.Davis

Professor of Engineering Mechanics,
Virginia Polytechnic Institute,
Blacksburg, Virginia, USA

SOLUTION OF THE VISCOUS SHOCK-LAYER EQUATIONS FOR A BINARY MIXTURE

by R. T. Davis*

SUMMARY

The method of solution of the viscous shock-layer equations for a one component perfect gas discussed by Davis in this AGARDograph is extended to the case of a binary mixture consisting of oxygen atoms and molecules. Two altitude conditions are considered which correspond to either AGARD Case A or Cases B and C. The method of solution is identical to the method used to solve the one component perfect gas case except care must be taken in expressing the rate of production of atoms term in both the energy and species equations. Stanton number, wall pressure, and skin friction distributions are presented along with velocity, temperature, and atom concentration profiles.

INTRODUCTION

This paper presents a method for solving the viscous shock-layer equations for a binary mixture. The method of solution is almost identical to the method presented in another paper in this AGARDograph by Davis (1970a) for the perfect one component gas and therefore will not be discussed in detail here. Since another recent paper by Davis (1970b) has given extensive calculations for the binary mixture covering a range of altitude conditions, and using the same solution method as will be used here, we will not repeat those results here but will restrict ourselves to the AGARD cases. Much of the material which follows has been extracted from Davis (1970b). For more details one is referred to Davis (1970a,b).

The problem of calculating chemically reacting boundary layers is fairly well in hand. However, at lower Reynolds numbers where boundary-layer theory is not applicable, the same statement cannot be made. Even in the boundary-layer regime problems still exist in determining proper outer edge conditions for performing boundary-layer calculations.

For the reasons stated above, i.e. finding solutions at lower Reynolds numbers and examining outer edge conditions, it is desirable to develop a model which considers the whole shock layer about a blunt body at once rather than consider the flow field as a boundary layer plus an inviscid flow which exists outside of it.

Cheng (1963) formulated a set of viscous shock-layer equations which apply not only at the stagnation point but also downstream. He solved these equations for several flow cases involving a one component perfect gas using an inverse method which assumed the shock shape was given and determined the body shape as part of the solution. His method is also applicable but was not applied to the direct problem. Kang (1968) has solved Cheng's (1963) equations, using an integral method, for flows downstream on blunt bodies. He later (Kang (1969)) applied the same method to an ionized nonequilibrium flow past a blunt body. In both cases mentioned above, Kang's calculations extended a few nose radii downstream.

Davis and Flügge-Lotz (1964) proposed a set of equations which are quite similar to those of Cheng (1963) but which contain some curvature terms left out of Cheng's equations. Cheng was considering the case of a thin shock layer for which his equations are valid. However, as the shock layer becomes thicker the curvature terms will become more important. The equations proposed by Davis and Flügge-Lotz (1964) are valid even if the shock layer is thick, as long as the shock Reynolds number is high enough. Davis (1970a) developed a method of solution to these equations and applied the method to flows over several blunt bodies. The method used is an implicit finite-difference method similar to the method developed by Blottner and Flügge-Lotz (1963) for solving the compressible boundary-layer equations. In addition to using the viscous shock-layer equations to govern the flow, slip boundary conditions were used on the body surface, and the modified Rankine-Hugoniot (shock-slip) conditions of Cheng (1963) were used at the shock interface. The results compared favorably with the experimental results of Little (1969) for the drag on various hyperboloids at several shock Reynolds number conditions. Good agreement was found even for shock Reynolds numbers which were much lower than one would expect the equations to apply.

The present problem will be handled in exactly the same manner. The viscous shock-layer equations are developed for a binary mixture with finite rate chemical reactions. Pressure and thermal diffusion effects are neglected, but could be easily considered as well. Modified Rankine-Hugoniot (shock-slip) conditions are used at the shock and surface-slip conditions are used on the body surface.

With this formulation, characteristics of typical nonequilibrium chemically reacting flows have been studied for intermediate shock Reynolds number conditions, see Davis (1970b). The high shock Reynolds number cases have also been studied, but difficulties can be experienced if one uses constant step sizes since at high shock Reynolds numbers the boundary layer near the body becomes thin and the method requires a large number of steps in the normal direction across the shock layer in order to obtain sufficient accuracy. Variable grid spacings can be used in the normal direction to overcome this difficulty and the present method contains this option, see Davis (1970a). The 100,000 foot calculations presented in this paper were made using variable step sizes.

FORMULATION OF THE PROBLEM

The conservation equations for reacting, multicomponent gas mixtures can be found in numerous references, see Williams (1965) appendix C, or Bird, Stewart, and Lightfoot (1960) chapter 18 for example. For application to the present problem these equations are written in the coordinate system shown in Fig. 1 and nondimensionalized by variables which are of order one in the region near the body surface (boundary-layer) for large Reynolds numbers. The same set of equations are then written in variables which are of order one in the essentially inviscid region outside the boundary layer. Terms are kept in each set of equations up to

*Professor of Engineering Mechanics, Virginia Polytechnic Institute, Blacksburg, Virginia, U.S.A.

second order in the inverse square root of a Reynolds number. A comparison of the two sets of equations is then made and one set of equations is found from them which is valid to second-order in both the outer and inner regions. A solution to this set of equations is thus uniformly valid to second order in the entire shock layer.

The derivation described above is exactly the same as that given by Davis (1970a) and Davis and Flügge-Lotz (1964) except that the present case is for a mixture rather than a one component gas. The present equations are quite similar to those given by Cheng (1963), except that Cheng neglected some curvature and normal pressure gradient terms which are included in the present equations. These terms are small when the shock layer is thin, which was the case considered by Cheng. The present method will only be applied to problems where the shock layer is thin, therefore there would be little difference in the results if Cheng's equations were used. However, the present equations are valid even for thick shock layers if a suitable numerical method can be developed to solve them in that case.

We will refer to the present equations as the viscous shock-layer equations. Dimensionless variables are used as given in the Nomenclature. For a chemically reacting binary mixture of atoms and molecules they can be written as follows when thermal and pressure diffusion are neglected:

Governing Equations

Continuity Equation

$$[(r + n\cos\phi)^j \rho u]_s + [(1 + \kappa n)(r + n\cos\phi)^j \rho v]_n = 0 \quad , \tag{2.1}$$

s-Momentum Equation

$$\left(u\frac{u_s}{1+\kappa n} + vu_n + \frac{\kappa}{1+\kappa n}uv\right) + \frac{p_s}{1+\kappa n} = \frac{\varepsilon^2}{(1+\kappa n)^2(r+n\cos\phi)^j}[(1+\kappa n)^2(r+n\cos\phi)^j\tau]_n \tag{2.2a}$$

where

$$\tau = \mu\left(u_n - \frac{\kappa u}{1+\kappa n}\right) \quad , \tag{2.2b}$$

n-Momentum Equation

$$\rho\left(u\frac{v_s}{1+\kappa n} + vv_n - \frac{\kappa}{1+\kappa n}u^2\right) + p_n = 0 \quad , \tag{2.3}$$

Energy Equation

$$\rho\bar{C}_p\left(u\frac{T_s}{1+\kappa n} + vT_n\right) - \left(u\frac{p_s}{1+\kappa n} + vp_n\right) = \frac{\varepsilon^2}{(1+\kappa n)(r+n\cos\phi)^j}[(1+\kappa n)(r+n\cos\phi)^j k T_n]_n + \frac{\varepsilon^2}{\mu}\tau^2$$
$$+ \varepsilon^2(C_{pM} - C_{pA})j_{nA}T_n + (h_M - h_A)\dot{W}_A \quad , \tag{2.4a}$$

where

$$j_{nA} = -F_D C_{A_n} \tag{2.4b}$$

Species Conservation Equation

$$\rho\left(u\frac{C_{A_s}}{1+\kappa n} + vC_{A_n}\right) = -\frac{\varepsilon^2}{(1+\kappa n)(r+n\cos\phi)^j}[(1+\kappa n)(r+n\cos\phi)^j j_{nA}]_n + \dot{W}_A \quad , \tag{2.5}$$

Equation of State

$$p = \frac{R}{\bar{M}C^*_{p_\infty}}\rho T \quad , \tag{2.6a}$$

where

$$\bar{M} = \frac{1}{\frac{C_A}{M_A} + \frac{(1 - C_A)}{M_M}} \tag{2.6b}$$

In the above equation of state (2.6a) it is assumed that the gas consists of a mixture of perfect gases.

The specific heat at constant pressure for the binary mixture can be written as

$$\bar{C}_p = C_A(C_{pA} - C_{pM}) + C_{pM} \tag{2.7}$$

Boundary Conditions

At the body surface slip and temperature jump boundary conditions are used. The normal component of velocity at the surface is taken to be zero since no problems with mass injection at the wall will be considered. The conditions on slip and temperature jump are those given by Shidlovskiy (1967). The boundary condition on species concentration at the surface is given by various authors. We choose here a form which is essentially the same as that used by Cheng (1963). Cheng (1963) discusses how this boundary condition effects wall catalyticity as a function of Reynolds number.

Surface Conditions

$$v = 0 \quad , \tag{2.8a}$$

$$u = \varepsilon^2 a_1 \frac{\mu}{p}\sqrt{\frac{p}{\rho}}\frac{\partial u}{\partial n} \quad , \tag{2.8b}$$

$$T = T_w + \varepsilon^2 c_1 \frac{k}{p}\sqrt{\frac{p}{\rho}}\frac{\partial T}{\partial n} \tag{2.8c}$$

and

$$C_A = C_{Ae} + \varepsilon^2 \sqrt{\frac{\pi M_A}{2\bar{M}}}\left(\frac{2-\gamma_w}{\gamma_w}\right)\frac{F_D}{p}\sqrt{\frac{p}{\rho}}\frac{\partial C_A}{\partial n} \tag{2.8d}$$

The following values of the slip constants are used in (2.8b) and (2.8c) above:

$$a_1 = 1.2304 \tag{2.9a}$$

and

$$c_1 = 2.3071 \tag{2.9b}$$

The quantity γ_w in Eq. (2.8d) is the recombination efficiency, i.e. the probability for each atom to recombine after reaching the surface.

The conditions to be imposed at the shock are the modified Rankine-Hugoniot relations of Cheng (1963). In order to obtain these conditions it is necessary to assume that $\dot{W}_A$ (mass rate of formation of atoms) is negligible across the shock. Chung, Holt, and Liu (1968) have shown that the assumption of neglecting the $\dot{W}_A$ term may be a good one although caution should be used. This was shown by integrating the equations for a merged stagnation shock layer of nonequilibrium dissociating gas with the same properties as those of Cheng (1963). Their results obtained from integrating through the shock keeping the $\dot{W}_A$ term were very close to those obtained by Cheng using shock slip conditions and neglecting the $\dot{W}_A$ term.

With the coordinate system shown in Fig. 1 the shock slip conditions may be obtained. Since velocity components tangent and normal to the shock are not the same as those tangent and normal to the body surface we need transformations to relate these quantities. We let u'_{sh} and v'_{sh} denote shock quantities tangent and normal to the shock respectively. The variables u_{sh} and v_{sh} are quantities at the shock tangent and normal to the body surface respectively.

Conditions at the Shock

The transformations are given by:

$$u_{sh} = u'_{sh}\sin(\alpha+\beta) + v'_{sh}\cos(\alpha+\beta) \tag{2.10a}$$

and

$$v_{sh} = -u'_{sh}\cos(\alpha+\beta) + v'_{sh}\sin(\alpha+\beta). \tag{2.10b}$$

The modified Rankine-Hugoniot (shock-slip) conditions are given by:

$$\rho_{sh} v'_{sh} = -\sin\alpha \quad , \tag{2.11a}$$

$$\varepsilon^2 \mu_{sh}(u'_n)_{sh} + \sin\alpha\, u'_{sh} = \sin\alpha\cos\alpha \quad , \tag{2.11b}$$

$$P_{sh} - \sin\alpha\, v'_{sh} = \frac{P_\infty}{\rho_\infty U_\infty^2} + \sin^2\alpha \quad , \tag{2.11c}$$

$$\varepsilon^2 k_{sh}(T_n)_{sh} + \sin\alpha\,[C_{A_\infty} h_{A_{sh}} + (1-C_{A_\infty}) h_{M_{sh}}] - \frac{\sin\alpha}{2}[(u'_{sh}-\sin\alpha)^2 + \cos^2\alpha - v'^2_{sh}] = \sin\alpha\,[C_{A_\infty} h_{A_\infty} + (1-C_{A_\infty}) h_{M_\infty}] \quad , \tag{2.11d}$$

and

$$\varepsilon^2 F_{D_{sh}} \frac{\partial C_{A_{sh}}}{\partial n} + \sin\alpha\, C_{A_{sh}} = \sin\alpha\, C_{A_\infty} \quad . \tag{2.11e}$$

The quantity ρ_{sh} is determined from the equation of state (2.6a) after determining P_{sh}, T_{sh}, and $C_{A_{sh}}$ from Eqs. (2.11c), (2.11d), and (2.11e).

Gas Model

The binary mixture consists of oxygen atoms and molecules with the following thermodynamic properties. The specific heat and enthalpy include translational, rotational and vibrational energies. In dimensional form they are written as:

$$C^*_{pA} = \frac{5}{2}\frac{R}{M_A} \qquad (\mathrm{ft}^2/\mathrm{sec}^2\,{}^\circ\mathrm{R}) \quad , \tag{2.12}$$

$$C^*_{pM} = \frac{R}{M_M}\left[\frac{7}{2} + \left(\frac{\theta}{T^*}\right)^2 e^{\theta/T^*}\left(e^{\theta/T^*} - 1\right)^{-2}\right] \quad (ft/sec^2\ °R)\ , \tag{2.13}$$

$$h^*_A = \frac{5}{2}\frac{R}{M_A}T^* + 1.666 \times 10^8 \quad (ft^2/sec^2) \tag{2.14}$$

and

$$h^*_M = \frac{R}{M_M}T^*\left[\frac{7}{2} + \frac{\theta}{T^*}\left(e^{\theta/T^*} - 1\right)^{-1}\right] \quad (ft^2/sec^2) \tag{2.15}$$

where $\theta = 4014°R$ and T^* is the temperature in degrees Rankine.

The transport properties are also written in dimensional form. The viscosities of oxygen atoms and molecules have been given by Yun and Mason (1962). Dr. F. G. Blottner of Sandia Corporation has supplied curve fits to their data. These fits are good over a temperature range from 1,000 to 10,000 degrees Kelvin. They are written as:

$$\mu^*_A = e^{-11.692729\ TK^{(0.0184896\ \ln TK + 0.4558107)}} \quad (g/cm - sec) \tag{2.16}$$

and

$$\mu^*_M = e^{-9.550244\ TK^{(0.0389680\ \ln TK + 0.0094176)}} \quad (g/cm - sec) \tag{2.17}$$

where TK is the temperature in degrees Kelvin.

The thermal conductivities of the oxygen atoms and molecules are obtained from the Eucken (1913) semi-empirical formula which can be written as follows:

$$k^*_i = \frac{R\mu^*_i}{M_i}\left[\frac{C^*_{p_i} M_i}{R} + \frac{5}{4}\right] \tag{2.18}$$

After the viscosities and thermal conductivities of the individual species have been determined the corresponding properties of the mixture are determined from Wilke's (1950) semi-empirical formulas, see Bird, Stewart and Lightfoot (1960) pages 24 and 258.

The diffusion properties of the oxygen atoms and molecules are determined by assuming a constant value of the Lewis number which is defined by:

$$Le = \frac{\bar{C}^*_p \rho^* \mathcal{D}^*_{AM}}{k^*} \tag{2.19}$$

The Lewis number is taken to be 1.4 for both the oxygen atoms and molecules which make up the mixture.

The rate of production of atoms for a binary mixture can be written as:

$$\frac{\dot{W}^*_A}{\rho^*} = \dot{W}^{*0}_A - \dot{W}^{*1}_A C_A \quad (1/sec) \tag{2.20a}$$

where

$$\dot{W}^{*0}_A = \frac{\bar{\rho}}{M_A}\left[\frac{(1 - C_A)}{2} k_{f1} + k_{f2} C_A\right] \tag{2.20b}$$

and

$$\dot{W}^{*1}_A = \dot{W}^{*0}_A + \frac{2\bar{\rho}^2}{M_A^2} C_A \left[\frac{(1 - C_A)}{2} k_{b1} + k_{b2} C_A\right] \tag{2.20c}$$

where the units used in the constants k_{f1} etc. are such that $\bar{\rho}$ is in g/cm^3. The quantities k_{f1}, k_{f2}, k_{b1}, and k_{b2} are determined from the following expressions:

$$k_{fr} = TK^{C2_r} \exp\left(CO_r + Cl_r/TK\right) \tag{2.21a}$$

and

$$k_{br} = TK^{D2_r} \exp\left(DO_r + Dl_r/TK\right) \tag{2.21b}$$

Considerable difference in the results for atom concentration, for example, can be experienced depending upon whose constants are used in the above equations. This will be demonstrated later.

Shock Layer Characteristics

Once a solution has been obtained, important wall quantities such as skin friction and heat transfer can be obtained. These are given in dimensionless form (see Nomenclature) by a skin friction coefficient and Stanton number defined by:

$$C_f = \frac{2\tau^*_w}{\rho_\infty U^2_\infty} \tag{2.22}$$

and

$$St = - \frac{q_w^*}{\rho_\infty U_\infty (H_\infty^* - H_{w_e}^*)} \quad . \tag{2.23}$$

In dimensionless form these relations (2.22) and (2.23) become:

$$C_f = 2\varepsilon^2 \mu (u_n - \kappa u)_{n=0} \tag{2.24}$$

and

$$St = - \frac{q_w}{H_\infty - H_{w_e}} \tag{2.25}$$

where q_w is the dimensionless surface heat transfer given by

$$q_w = - \varepsilon^2 \left[kT_n + \mu u u_n + (h_A - h_M) F_D C_{A_n} \right]_{n=0} \tag{2.26}$$

and H is the dimensionless total enthalpy defined by

$$H = \frac{u^2 + v^2}{2} + C_A h_A + (1 - C_A) h_M \quad . \tag{2.27}$$

METHOD OF SOLUTION

The method of solution is essentially the same as that used by Davis (1970a) for solving the viscous shock-layer equations for a one component perfect gas. We will not go into the details of the method of solution here but will indicate briefly differences and modifications which have been made to develop the present method.

As in the one component perfect gas case described by Davis, new variables are defined by dividing all physical variables by their local values at the shock. The solution for the binary mixture then proceeds in exactly the same way as before for the one component gas except a species equation is included now which is solved in the same way as the other equations. For numerical solution the equations are uncoupled as before. The species equation is solved first followed in order by the energy, s-momentum, continuity, and n-momentum equations. The same iteration method is used as was used by Davis (1970a) on the shock slope and the v terms in the normal momentum equation.

Two problems were encountered in getting the method to converge for the binary mixture which did not occur in the one component case. Blottner (1970) comments on a method for handling these problems.

The first problem was handled by writing the rate of production of atoms term as shown in Eq. (2.20a). This form allows C_A, the atom concentration, to appear as one of the unknowns in the species equation (2.5). Blottner (1970) comments on why the particular forms for Eqs. (2.20b) and (2.20c) are chosen. If these forms are not used, one will have difficulty in getting the species equations to converge.

A similar difficulty is encountered in the energy equation (2.4a), again with the term which involves $\dot{W}_A$, the rate of production of atoms. To overcome this the term involving the $\dot{W}_A$ term in the energy equation is written in a form such that T, the temperature, appears as one of the unknowns. This is done by expanding the $\dot{W}_A/\rho$ term in a series as follows:

$$\left(\frac{\dot{W}_A}{\rho} \right)_{k+1} = \left(\frac{\dot{W}_A}{\rho} \right)_k + \left[\frac{\partial}{\partial T} \left(\frac{\dot{W}_A}{\rho} \right) \right]_k (T_{k+1} - T_k) \tag{3.1}$$

where k denotes the number of the iteration for which the solution is known and k+1 the iteration number for which we wish to obtain a new solution.

It was found that if an expression of the type (3.1) was not used which allowed T, the temperature, to appear as an unknown in the energy equation the method would not converge at low altitude conditions where the gas was approaching equilibrium conditions. Again, Blottner (1970) has commented on the necessity of using an expression like Eq. (3.1).

DISCUSSION OF RESULTS

Davis (1970b) has discussed the effect of the values of the rate constants in Eqs. (2.21a,b) on the solutions. The values that one uses can have a significant effect on the results. We choose to use the values of Bortner (1968) here. They are given as follows:

Constants for K_{fr} and K_{br} in Eqs. (2.21a,b)

$$r = 1 : O_2 + O_2 \rightleftarrows 2O + O_2$$

$$r = 2 : O_2 + O \rightleftarrows 2O + O$$

Reaction	CO_r	$C1_r$	$C2_r$	DO_r	$D1_r$	$D2_r$
r = 1	44.92777	-59,400	-1.0	37.83461	0	-0.5
r = 2	45.94634	-59,400	-1.0	38.85627	0	-0.5

Based on the constants used in the present problem stagnation-point solutions can be calculated. This has been done and the resulting shock Reynolds number determined. The AGARD cases for the present calculations then turn out to be:

Flow Conditions for Flow Past the 20° AGARD Hyperboloid

AGARD Case	Alt (ft)	T_∞(°R)	$\rho_\infty(\frac{\#\text{-sec}^2}{ft^4})$	$P_\infty(\frac{\#}{ft^2})$	Re_s	$T_r = U_\infty^2/C^*_{p_\infty}$	T_w(°R)
A	100 K	408.57	3.318×10^{-5}	2.105×10^{1}	9355.0	7.350×10^{4}	2520
B,C	250 K	351.83	7.033×10^{-8}	3.842×10^{-2}	23.4	7.357×10^{4}	1800

In All Cases:

U_∞ = 20,000 ft/sec $\quad \rho_r = \rho_\infty$

a = 1/12 ft $\quad P_r = \rho_\infty U_\infty^2$

$C_{A_\infty} = 0.0$ $\quad R = 4.9686 \times 10^4$

$\gamma_w = 1.0$ $\quad M_A = 16.0$

$U_r = U_\infty$ $\quad M_M = 32.0$

For the present calculations the value of the recombination efficiency, γ_w, is chosen to be one in Eq. (2.8d). Calculations were then made including both shock and body slip. The fact that both of these effects are important at the high altitude condition (250 K) has already been established by Davis (1970a).

Figs. 2 - 11 show the results for AGARD Case A. Figure 7 shows atom concentration profiles across the shock layer. Calculations were made which determined the equilibrium atom concentration which would exist at the pressure and temperature given by the nonequilibrium calculations. This showed that the flow outside the boundary layer along the stagnation streamline was essentially in equilibrium. Downstream from the stagnation point the flow did not remain as near to equilibrium conditions. One should therefore be careful in determining when equilibrium conditions exist based on stagnation-point calculations.

Fig. 7 shows that the use of Eq. (2.8d) along with a value of recombination efficiency γ_w of one results in an essentially catalytic wall condition for AGARD Case A.

Fig. 6 shows an outer overshoot in the temperature profile at ten and twenty-five nose radii which has also been previously observed by Davis (1970b). This outer overshoot exists in the inviscid portion of the flow field. The effect is found to be more pronounced at lower altitude conditions. An explanation for this is that the total enthalpy is nearly constant over the outer portion of the flow field. At ten nose radii the static enthalpy is a small portion of the total enthalpy and thus a small change in velocity results in a fairly large percentage change in temperature. Starting at the shock and proceeding toward the body, this explains why the temperature in Fig. 6 is increasing at first even though the velocity is decreasing slowly. Down to n/n_{sh} of about 0.6 there is essentially no dissociation. Below this point this is not the case and the temperature profile bends inward since energy is being used in dissociation of the oxygen molecules. Near the wall a final bump occurs, and this is due to viscous dissipation.

Figs. 12 - 21 show results for AGARD Case B-C. Fig. 17 shows that the flow is essentially frozen and thus there is good agreement between these results and those computed by Davis (1970a) for the one component perfect gas case. Some of the difference is due to the gas properties used here which are different from those used by Davis (1970a).

Fig. 17 shows that the wall is not as close to the catalytic conditions as it was in Case A. In fact far downstream the wall condition is near to the noncatalytic case.

Fig. 16 does not demonstrate the double overshoot which was found in Case A. This is because the viscous effects are felt across the entire shock layer and viscous dissipation is a large enough effect to overcome the tendency for temperature to decrease outside the boundary layer as it did in Case A.

ACKNOWLEDGEMENT

This research was supported by Sandia Corporation, Sandia Laboratories, Albuquerque, New Mexico, under Contract 48-7795.

REFERENCES

Bird, R.B., Stewart, W.E. and Lightfoot, E.N. (1960) Transport Phenomena, John Wiley, New York.

Blottner, F.G. and Flügge-Lotz, I. (1963) "Finite-Difference Computation of the Boundary-Layer with Displacement Thickness Interaction," Journal de Mecanique, Vol. 11, No. 4.

Blottner, F.G. (1970) "Finite-Difference Methods of Solution of the Boundary-Layer Equations," AIAA Journal, Vol. 8, No. 2, pp. 193-206.

Bortner, M.H. (1968) "A Review of Rate Constants of Reactions in Re-Entry Flow Fields," G.E. TIS R68SD13.

Cheng, H.K. (1963) "The Blunt-Body Problem in Hypersonic Flow at Low Reynolds Number," IAS Paper No. 63-92; Cornell Aeronautical Lab. Report No. AF-1285-A-10.

Chung, P.M., Holt, J.F. and Liu, S.W. (1968) "Merged Stagnation Shock Layer of Nonequilibrium Dissociating Gas," Aerospace Report No. TR-0158(3240-10)-8.

Davis, R.T. and Flügge-Lotz, I. (1964) "Second-Order Boundary-Layer Effects in Hypersonic Flow Past Axisymmetric Blunt Bodies," J. Fluid Mechanics, Vol. 20, Part 4, pp. 593-623.

Davis, R.T. (1970a) "The Hypersonic Fully Viscous Shock-Layer Problem," Presented at the AGARD Seminar on "Numerical Methods for Viscous Flows," National Physical Laboratory, Teddington, England, Sept. 18-21, 1967.

Davis, R.T. (1970b) "Hypersonic Flow of a Chemically Reacting Binary Mixture Past a Blunt Body," to be presented at the AIAA 3rd Fluid and Plasma Dynamics Conference, Los Angeles, California, June 29 - July 1, 1970.

Kang, S.W. (1968) "Studies of Hypersonic Viscous Flows Over a Blunt Body at Low Reynolds Number," Cornell Aeronautical Lab. Report No. Al-2187-A-9.

Kang, S.W. (1969) "Analysis of an Ionized Merged-Layer Hypersonic Flow over a Blunt Body," Cornell Aeronautical Lab. Report No. Al-2187-A-12.

Little, H.R. (1969) "An Experimental Investigation of Surface Conditions on Hyperboloids and Paraboloids at a Mach Number of 10," AIAA Paper No. 70-182.

Shidlovskiy, V.P. (1967) Introduction to Dynamics of Rarefied Gases, American Elsevier Publishing Company, New York.

Wilke, C.R. (1950) J. Chem. Phys., Vol. 18, pp. 517-519.

Williams, F. (1965) Combustion Theory, Appendix C, Addison Wesley.

Yun, K.S. and Mason, E.A. (1962) "Collision Integrals for the Transport Properties of Dissociating Air at High Temperature," The Physics of Fluids, Vol. 5, No. 4, pp. 380-386.

NOMENCLATURE

a_1 slip constant, taken to be 1.2304

a^* body nose radius of curvature

c_1 slip constant, taken to be 2.3071

C_A atom concentration, ρ_A^*/ρ^*

C_f skin friction coefficient, $2\tau_w^*/(\rho_\infty^* U_\infty^{*2})$

C_p specific heat at constant pressure, $C_p^*/C_{p_\infty}^*$

F_D diffusion coefficient, $\rho^* \mathcal{D}_{AM}^*/\mu^*(U_\infty^{*2}/C_{p_\infty}^*)$

H total enthalpy, H^*/U_∞^{*2}

h static enthalpy, h^*/U_∞^{*2}

j_{nA} diffusion flux vector defined by Eq. (2.4b)

k thermal conductivity, $k^*/[\mu^*(U_\infty^{*2}/C_{p_\infty}^*)\, C_{p_\infty}^*]$

Le Lewis number defined by Eq. (2.19)

M molecular weight

n coordinate measured normal to the body, n^*/a^*

p pressure, $p^*/(\rho_\infty^* U_\infty^{*2})$

q heat transfer, $q^*/(\rho_\infty^* U_\infty^{*3})$

R universal gas constant

r radius measured from the asix of symmetry to a point on the body surface, r^*/a^*

s coordinate measured along the body surface, s^*/a^*

St Stanton number defined by Eq. (2.23)

T temperature, $T^*/(U_\infty^{*2}/C_{p_\infty}^*)$

u velocity component tangent to the body surface, u^*/U_∞^*

v velocity component normal to the body surface, v^*/U_∞^*

$\dot{W}_A$ rate of production of atoms defined by Eq. (2.20)

α shock angle, see Fig. 1

β angle defined in Fig. 1

γ_w recombination efficiency

ε Reynolds number parameter, $\varepsilon = \left[\dfrac{\mu^*(U_\infty^{*2}/C_{p_\infty}^*)}{\rho_\infty^* U_\infty^* a^*}\right]^{1/2}$

κ surface curvature, $\kappa^* a^*$

μ coefficient of viscosity, $\mu = \mu^*/\mu^*(U_\infty^{*2}/C_{p_\infty}^*)$

ρ density, ρ^*/ρ_∞^*

τ shear stress, $\tau^*/(\rho_\infty^* U_\infty^{*2})$

ϕ body angle defined in Fig. 1

Superscripts

j defined to be 0 for plane flow and 1 for axisymmetric flow

$*$ dimensional quantities

Subscripts

A	atom
e	equilibrium value
M	molecule
n,s	differentiation with respect to a coordinate
sh	value behind the shock
r	reference value
w	wall value

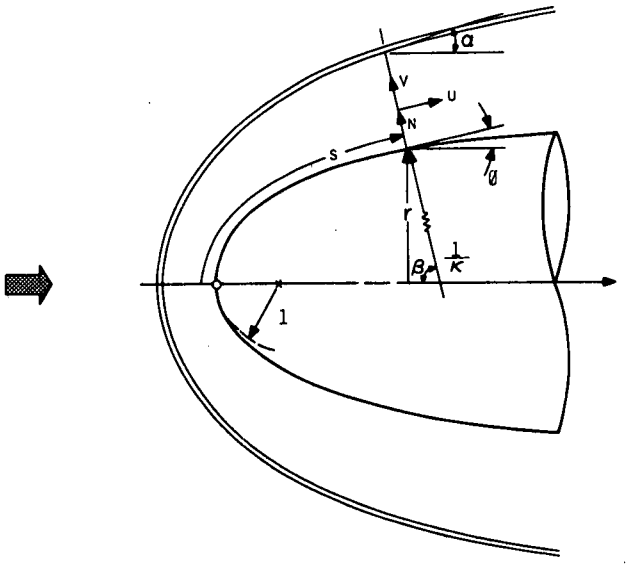

Fig.1 Coordinate system

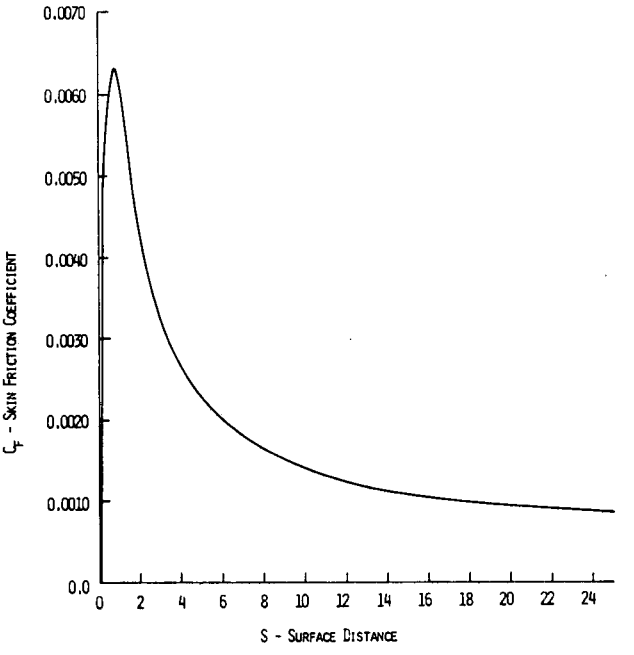

Fig.2 Skin friction coefficient for AGARD Case A

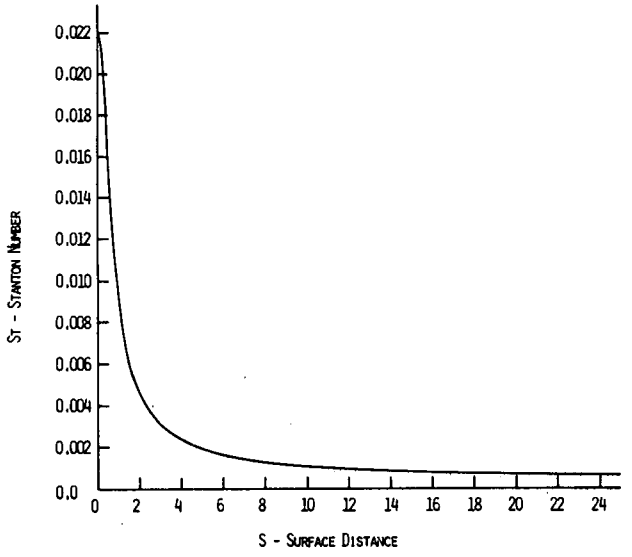

Fig.3 Stanton number for AGARD Case A

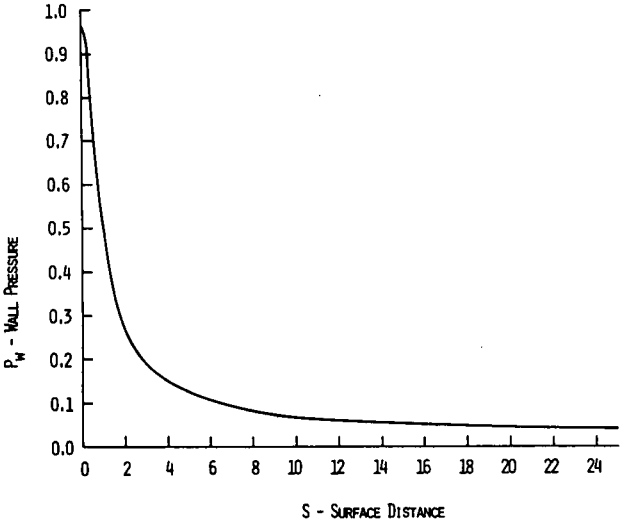

Fig.4 Wall pressure for AGARD Case A

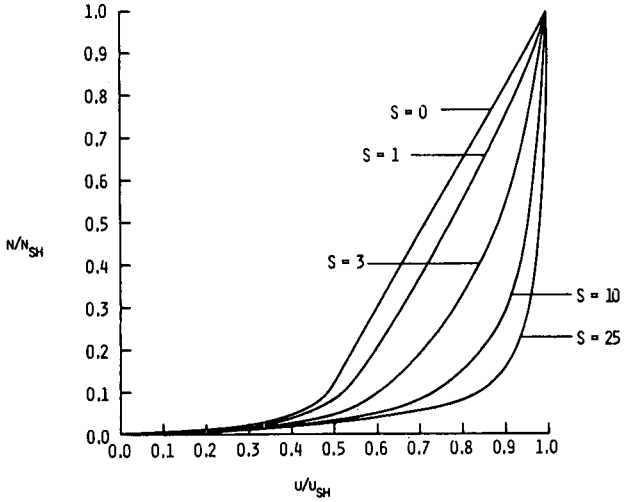

Fig.5 Velocity profiles for AGARD Case A

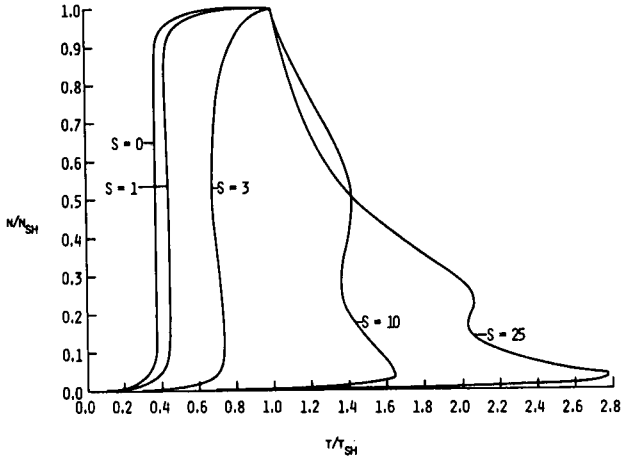

Fig.6 Temperature profiles for AGARD Case A

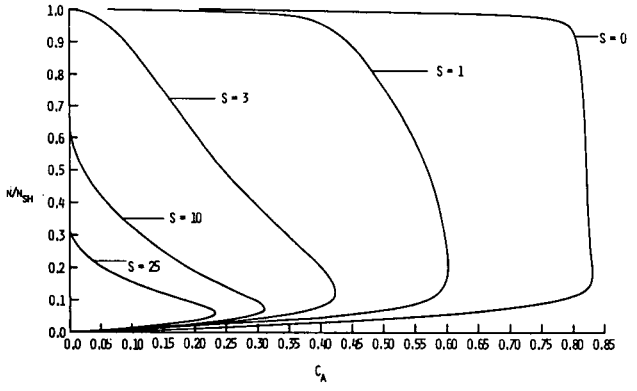

Fig.7 Atom concentration profiles for AGARD Case A

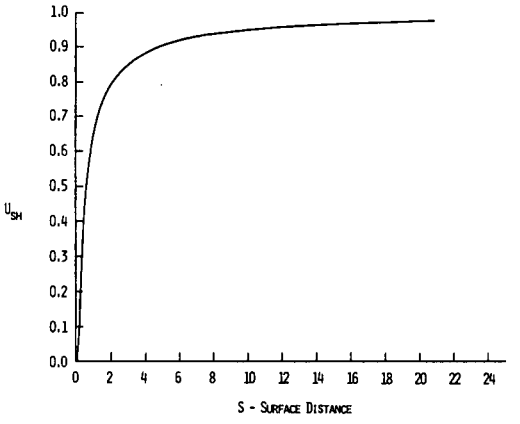

Fig.8 Shock velocity distribution for AGARD Case A

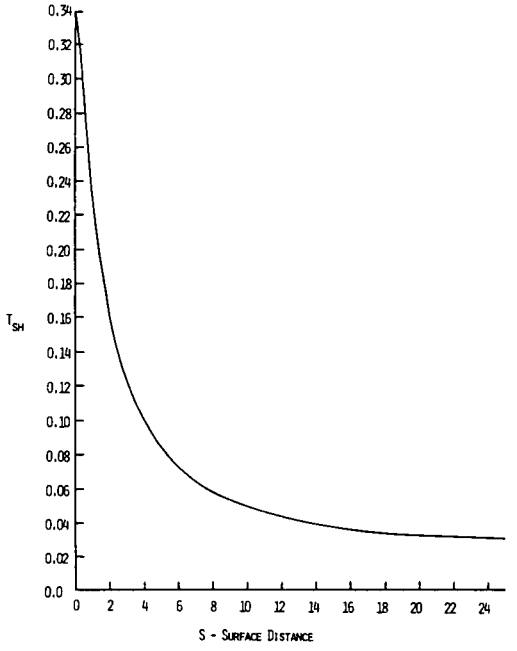

Fig.9 Shock temperature for AGARD Case A

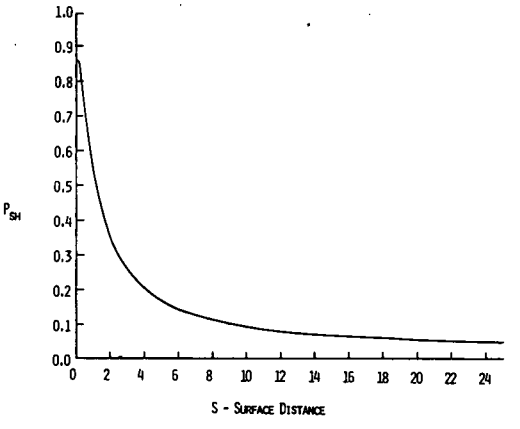

Fig.10 Shock pressure for AGARD Case A

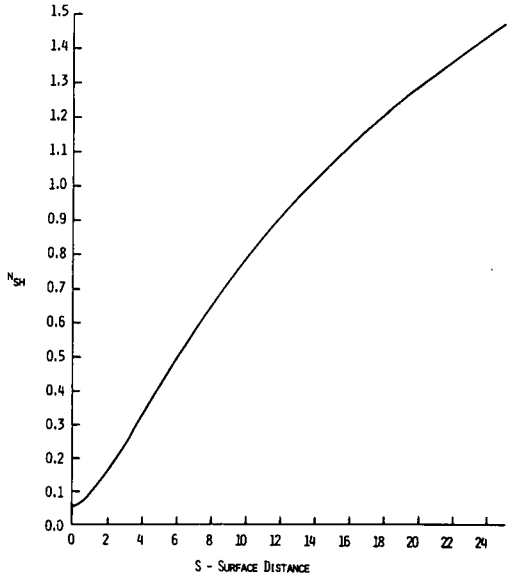

Fig.11 Shock stand-off distance for AGARD Case A

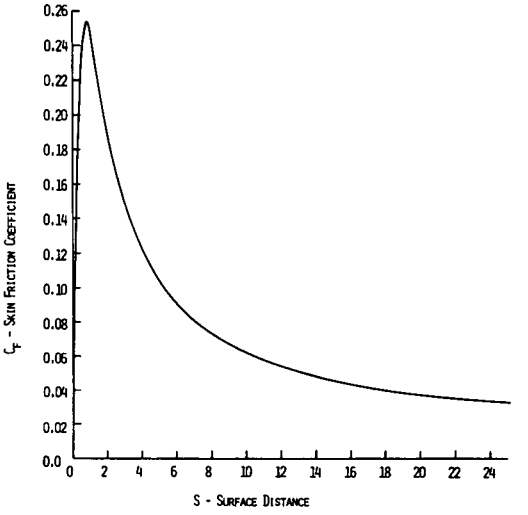

Fig.12 Skin friction coefficient for AGARD Case B-C

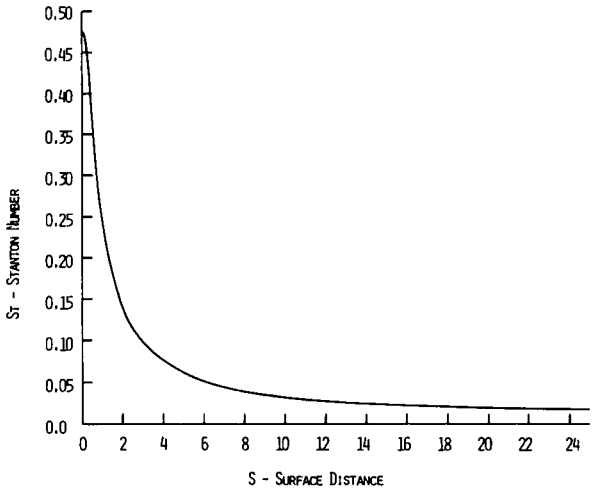

Fig.13 Stanton number for AGARD Case B-C

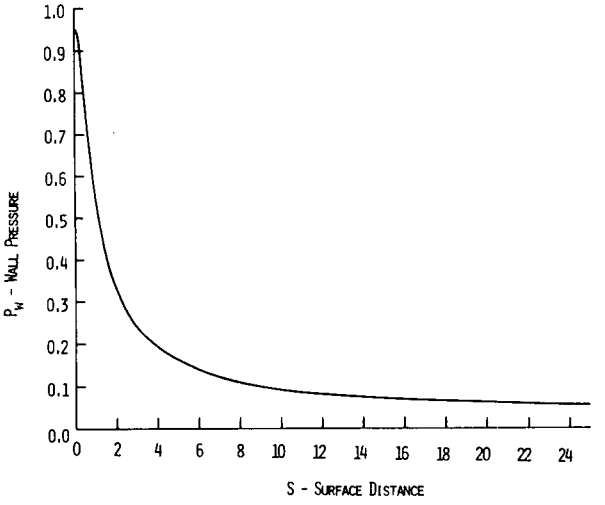

Fig.14 Wall pressure for AGARD Case B-C

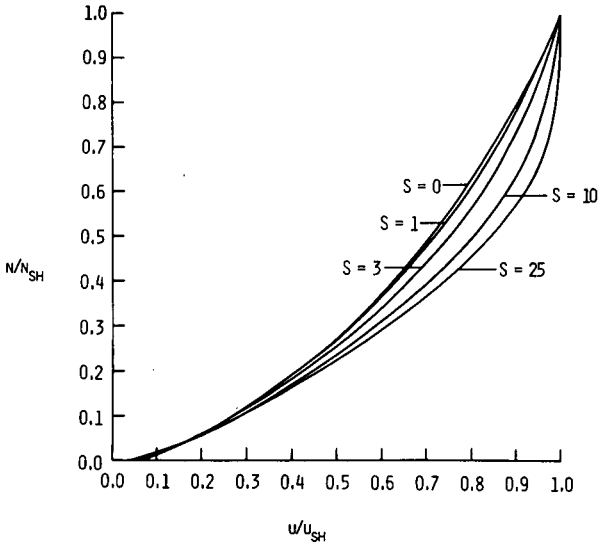

Fig.15 Velocity profiles for AGARD Case B-C

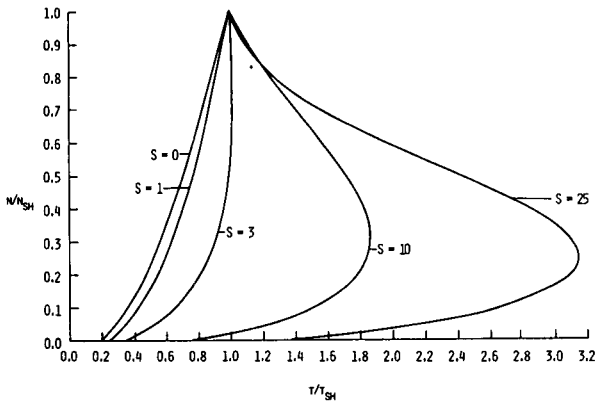

Fig.16 Temperature profiles for AGARD Case B-C

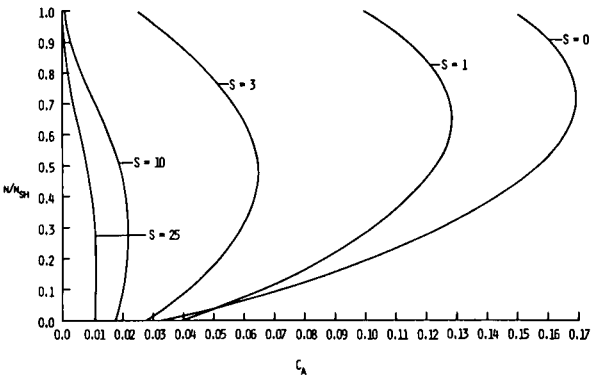

Fig.17 Atom concentration profiles for AGARD Case B-C

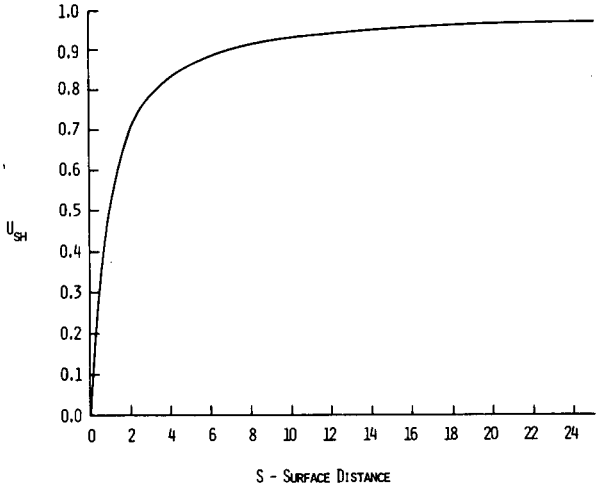

Fig.18 Shock velocity distribution for AGARD Case B-C

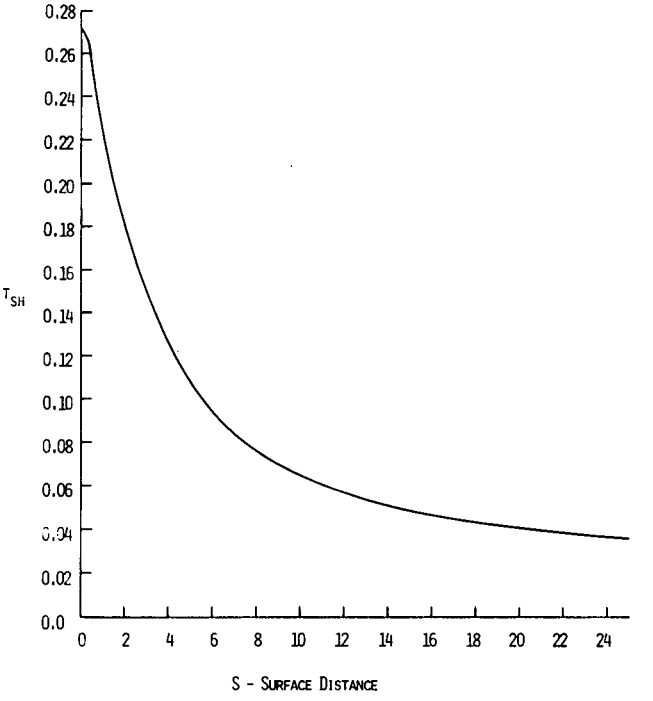

Fig.19 Shock temperature for AGARD Case B-C

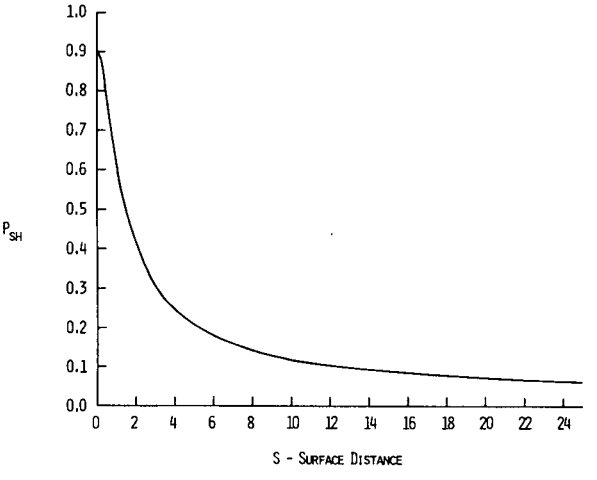

Fig.20 Shock pressure for AGARD Case B-C

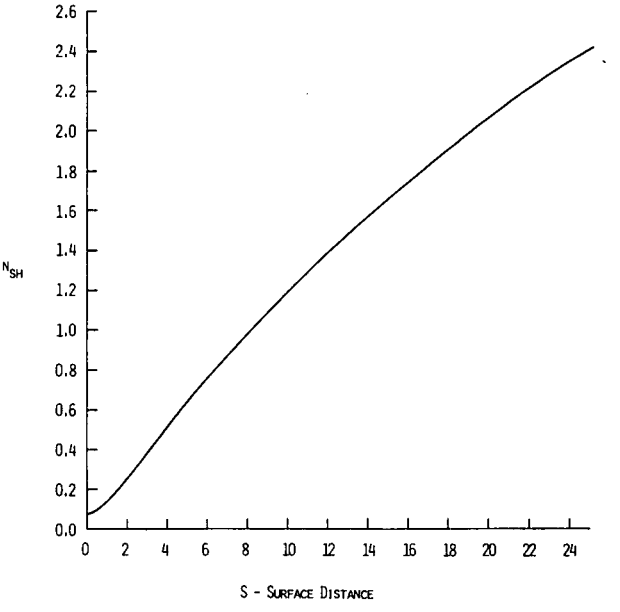

Fig.21 Shock stand-off distance for AGARD Case B-C

VISCOUS SHOCK-LAYER PROBLEM FOR THE STAGNATION POINT OF A BLUNT BODY

by

F.G.Blottner

Staff Member, Aero and Thermodynamics Department,
Sandia Corporation, Albuquerque, New Mexico 87115

VISCOUS SHOCK-LAYER PROBLEM FOR THE STAGNATION POINT OF A BLUNT BODY

by F. G. Blottner*

SUMMARY

A finite-difference method and a nonlinear overrelaxation method are investigated for solving the viscous shock layer at the stagnation point of a blunt body. An air gas model is employed with finite reaction rates and accurate thermodynamic and transport properties. For a body with a 1-inch nose radius and at a velocity of 20 Kfps, the present results at 100, 150, 200, and 250 Kft show that boundary-layer theory is appropriate for some altitude below 150 Kft. When the altitude is 250 Kft, the effects of shock slip must be included in the viscous shock-layer solution. For this case, the air is only slightly dissociated and ionized.

INTRODUCTION

At the stagnation point of a blunt body, the Navier-Stokes equations can be reduced to ordinary differential equations with two-point boundary conditions. This problem is often considered easier to solve than the partial differential equations for a thin shock layer or a boundary-layer flow around the body. However, for flows with many chemical species and fast reaction rates, the ordinary differential equation can be exceedingly difficult to solve. Also, to start the solution of the partial differential equations, the stagnation-point ordinary differential equations must be solved to provide initial profiles of the dependent variables. The solution of the same type of ordinary differential equations occurs for initial profiles for boundary-layer flows at the tip of a sharp body such as a cone or wedge.

The purpose of this paper is to investigate and develop techniques for solving the viscous shock-layer flow at the stagnation point of a blunt body for air with chemical reactions occurring at finite rate. At the same time, the solution for boundary-layer flows at a stagnation point, or a tip of a cone or wedge, will be considered. In the problems of interest, there can occur many chemical species as a result of the dissociation of air and the ablation products. Initial profiles at the tip of a sharp body are easiest to obtain, as the term involving the chemical production term is zero and the governing equations are the same as those for chemically frozen flow. The initial profiles at a stagnation point with finite rates are exceedingly difficult to obtain, being similar to the problems encountered in obtaining locally similar solutions along a wall [1]. Two techniques for solving ordinary differential equations with two-point conditions are investigated. These methods of solution are much more satisfactory than previous initial value techniques with iteration of guessed boundary conditions.

The flow in the stagnation region of a blunt body has been classified into a number of regimes by Probstein [2], and these results have been rearranged into Fig. 1. Also shown in this figure, as given by Inger [3], is the value of the shock Reynolds number at which the Rankine-Hugoniot relations break down and the inviscid flow is no longer in equilibrium. As this figure shows, the boundary-layer theory can be employed only at the lower altitudes, but the appropriate altitude increases as the nose radius becomes larger. The present investigation will consider the regimes from boundary-layer flow through the viscous layer flow.

The thin, viscous shock-layer equations, as developed by Ho and Probstein [4] and further simplified by Cheng [5], are the ones considered in this study. These equations are the same as the first-order boundary-layer equations, except a normal momentum equation must be included. The difference between the boundary-layer theory and the thin-shock-layer theory is in the manner the boundary conditions are applied at the outer edge. For the shock layer, the Rankine-Hugoniot shock conditions are applied at a finite distance from the surface, which is determined by matching the appropriate velocity behind the shock wave. In the paper by Cheng [5], modified Rankine-Hugoniot relations are employed which take into account a shock transition zone, but the gas is assumed frozen across this region. With the modified Rankine-Hugoniot relations the thin-shock-layer analysis can be extended into the merged layer regime, but this does not seem appropriate if one is interested in flows with finite chemical reactions. The more consistent approach is to solve the flow throughout the viscous shock layer and shock transition zone, as has been done by Lee and Zierten [6]. The present investigation is restricted to the domains pertaining to the viscous layer, vorticity interaction, and boundary layer where chemical nonequilibrium effects are more important.

There have been a number of papers concerned with the viscous, thin-shock-layer theory at the stagnation point of a blunt body. A complete review of the viscous hypersonic blunt-body problem was made recently by Cheng [7]. Many of the papers have employed a perfect gas model, such as [4, 8-14], or equilibrium air, such as [15-18]. Also there have been several papers [5,19-23] concerned with the viscous shock layer for a binary gas mixture with a finite chemical reaction rate. The papers by Stoddard [22] and Buckmaster [23] are even more restrictive, as the analytical solutions presented require a small degree of dissociation and negligible recombination rate. Also, most of these papers employ simplified thermodynamic and transport properties. The paper by Lee and Zierten [6] has employed the most complete chemistry; however, the species equations are decoupled from the other thin-shock-layer equations. This brief review is intended to show that a significant amount of work has been devoted to the understanding of the fluid dynamics of the viscous hypersonic blunt-body problem, but there is a need for solutions of this problem with realistic gas models. It is the intention of the present investigation to help provide these types of results.

GOVERNING EQUATIONS

The general equations for a multicomponent chemically reacting gas mixture are given in [24] and these can be written for the shock layer in a manner similar to Cheng [5]. The resulting partial differential equations are the same as those employed in boundary-layer studies in [25], except the normal momentum equation

$$\frac{dp}{dy} + \kappa_c \rho u^2 = 0 \tag{1}$$

*Staff Member, Aero and Thermodynamics Department, Sandia Corporation, Albuquerque, New Mexico 87115.

must be included. The governing equations are transformed by introducing new independent variables

$$\xi(x) = \int_0^x (\rho\mu)_r u_e r_b^{2j}\, dx \tag{2a}$$

$$\eta(x,y) = \frac{u_e r_b^j}{\sqrt{2\xi}} \int_0^y \rho\, dy \tag{2b}$$

and new dependent variables

$$f' = u/u_e \tag{2c}$$

$$\theta = T/T_e \tag{2d}$$

The resulting equations are given in [25] with $\bar{\bar{e}} = -1$ (see Eq. (5)). For the case $\xi = 0$, which corresponds to a stagnation point or the tip of a sharp body, the equations become, for continuity,

$$\frac{dV}{d\eta} + f' = 0 \tag{3a}$$

for tangential momentum,

$$\frac{d}{d\eta}\left(\ell \frac{df'}{d\eta}\right) - V \frac{df'}{d\eta} - \beta\left[\frac{\bar{M}_e}{\bar{\bar{M}}\bar{\bar{e}}}\theta + (f')^2\right] = 0 \tag{3b}$$

for normal momentum

$$\frac{dp}{d\eta} + \frac{\kappa_c u^2 \sqrt{2\xi}}{u_e r_b^j} = 0 \tag{3c}$$

for energy

$$\frac{1}{\bar{c}_p}\frac{d}{d\eta}\left(\frac{\ell \bar{c}_p}{Pr}\frac{d\theta}{d\eta}\right) - V\frac{d\theta}{d\eta} + \frac{u_e^2}{\bar{c}_p T_e}\left[\ell\left(\frac{df'}{d\eta}\right)^2 + \frac{\beta \bar{M}_e}{\bar{\bar{e}}\bar{\bar{M}}} f\theta\right]$$
$$+ \sum_{i=1}^{NI} \frac{c_{p_i}\ell}{\bar{c}_p Pr}\left[Le_i \frac{dc_i}{d\eta} + \sum_{\substack{k=1 \\ k\neq i}}^{NI} \Delta\bar{\bar{b}}_{ik}\frac{dc_k}{d\eta}\right]\frac{d\theta}{d\eta} - \frac{2\xi}{\bar{c}_p T_e u_e d\xi/dx}\sum_{i=1}^{NI} h_i(w_i/\rho) = 0 \tag{3d}$$

for species continuity

$$\frac{d}{d\eta}\left[\frac{\ell}{Pr}\left[Le_i\frac{dc_i}{d\eta} + \sum_{\substack{k=1 \\ k\neq i}}^{NI}\Delta\bar{\bar{b}}_{ik}\frac{dc_k}{d\eta}\right]\right] - V\frac{dc_i}{d\eta} + \frac{2\xi}{u_e d\xi/dx}\left[\frac{W_i}{\rho}\right] = 0 \tag{3e}$$

where

$$\beta = \frac{2\xi}{u_e}\frac{du_e}{d\xi} \qquad \left(\text{at stagnation point } \beta = \frac{1}{1+j}\right)$$

$$\bar{\bar{e}} = \rho_e u_e \frac{du_e}{dx} \Big/ \frac{dp}{dx}$$

$$Le_i = \sum_{\substack{j=1 \\ j\neq i}}^{NI} \frac{c_j}{M_j} \Big/ \sum_{\substack{j=1 \\ j\neq i}}^{NI} \frac{c_j}{M_j L_{ij}}$$

$$\Delta\bar{\bar{b}}_{ik} = Le_i - \left[\frac{M_i}{\bar{M}} L_{ik} + \left[1 - \frac{M_i}{M_k}\right]\sum_{j=1}^{NI} L_{ij} c_j\right]$$

If the binary Lewis-Semenov numbers, L_{ij}, are constant for all the species or if a trace species is being considered, the term $\Delta\bar{\bar{b}}_{ik}$ is zero. In the above equation, the pressure and thermal diffusion terms are neglected due to the boundary-layer assumption; and the force diffusion term is assumed zero. The equation of state is also required and is written as

$$\rho = \frac{p_e}{RT \sum_{i=1}^{NI} (c_i/M_i)} = \frac{p_e \bar{M}}{RT} \tag{4}$$

where it is assumed the gas consists of a mixture of chemically reacting perfect gases and the pressure change across the layer is neglected as a result of Eq. (3c). However, there is a variation of the rate of change of the tangential pressure gradient across the layer at the stagnation point, which can be determined from Eq. (3c). When the pressure is solved from Eq. (3c) and differentiated with respect to x, the following is obtained at the stagnation point.

$$\bar{\bar{e}} = \rho_s u_s \frac{du_s}{dx} \Big/ \frac{dp}{dx} = -\frac{1}{2\varepsilon} \left\{ \frac{(1-\varepsilon)}{\left[1 - \varepsilon\left(1 - \frac{1}{s}\right)\right]^2} + \frac{\int_{\eta}^{\eta_s} (f')^2 \, d\eta}{\{(i+j)Re_s \varepsilon[s(1-\varepsilon)+\varepsilon]\}^{1/2}} \right\}^{-1} \tag{5}$$

where

$$s = \frac{R_N}{R_s}\left[1 + \frac{\Delta}{R_N}\right]$$

For the boundary-layer problem, the value of $\bar{\bar{e}} = -1$ when the flow for the body streamline is used at the edge conditions.

The conditions at the surface and outer edge of the boundary layer determine the necessary boundary conditions for the foregoing equations. At the wall, it is assumed that the tangential velocity is zero and the surface temperature is specified. These conditions are expressed as

$$u(0) = 0 \tag{6a}$$

$$T(0) = T_b \tag{6b}$$

In addition, the boundary condition on the mass flux of a species "i" at the surface, $(\rho_i v_i)_b$, is

$$(\rho_i v_i)_b = \dot{m}_i = (c_i \rho v)_b + (j_i)_b \tag{6c}$$

The mass flux of a species at the surface, $\dot{m}_i$, depends on the surface material and how it interacts with the gases in the boundary layer. In the present study, only the extreme case of a fully catalytic surface is considered. For a fully catalytic wall, the gas is assumed undissociated and un-ionized. The total mass flux at the surface is zero for this case.

The flow at the edge of the shock layer is obtained from the Rankine-Hugoniot relations

$$p_s = p_\infty + \rho_\infty V_\infty^2 \left[1 - \frac{v_s}{V_\infty}\right] \tag{7a}$$

$$h_s = h_\infty + \frac{1}{2} V_\infty^2 \left[1 - \left[\frac{v_s}{V_\infty}\right]^2\right] \tag{7b}$$

$$T_s = \left[h_s - \sum_{i=1}^{NI} c_i \Delta h_i^F\right] \Big/ \sum_{i=1}^{NI} c_i c_{l_i} \tag{7c}$$

$$\frac{v_s}{V_\infty} = \frac{\rho_\infty}{\rho_s} = \frac{p_\infty T_s}{p_s T_\infty} \tag{7d}$$

An iteration process is used to solve the above equations where, initially, (v_s/V_∞) is assumed zero and the denominator in Eq. (7c) is taken equal to 7000. The mass fraction of species across the shock are taken constant. The use of the Rankine-Hugoniot relations (7) rather than the modified relations as employed by Cheng [5] will limit the applicability of the analysis to shock-layer Reynolds numbers greater than approximately 100. The boundary conditions at the outer edge of the shock layer are expressed as

$$V(\eta_e) = -\varepsilon\{Re_s/(1+j)[s(1-\varepsilon)+\varepsilon]\}^{1/2} \tag{8a}$$

$$f'(\eta_e) = 1 \tag{8b}$$

$$\theta(\eta_e) = 1 \tag{8c}$$

$$c_i(\eta_e) = c_{i_e} = c_{i_s} = c_{i_\infty} \tag{8d}$$

For the shock-layer flow, the value of $\eta_e = \eta_s$ must be varied until condition (8a) is satisfied.

When the shock-layer Reynolds number becomes large, the solution of Eq. (3) from the body to the shock is not necessary. In this case, the boundary-layer approach can be followed where the edge conditions are obtained from the inviscid flow at the surface where the air is assumed in chemical equilibrium. For the boundary-layer approach, the value of $\eta_e \approx 6$ and condition (8a) is not required.

THERMODYNAMIC AND TRANSPORT PROPERTIES, AND CHEMICAL KINETICS

The thermodynamic properties of enthalpy and specific heat of the individual species (O_2, N_2, O, N, NO, NO^+) are obtained from tabulated values as given by Browne [26-28]. The thermodynamic and transport properties based on the air model employed in this paper have been determined for an equilibrium composition at a pressure of 1 atmosphere and temperatures up to 20,000°K. The present results for enthalpy have been compared with predictions of Predroditelev [29] and Hansen [30]. These authors are in close agreement except at temperatures around 4000°K. The present frozen specific heat at constant pressure has been compared to the results of Hansen. The present results for enthalpy and specific heat are in good agreement with the predictions of these authors except at temperatures above 10,000°K. This is expected, as the present gas model is valid only when there is a slight amount of ionization.

The viscosity and thermal conductivity of the gaseous mixture is calculated from Wilke's semiempirical relations (see pages 24 and 258 of [24]). The viscosities of the individual species are those given by Yun and Mason [31]. The viscosity of NO^+ is assumed equal to that of NO. The present frozen thermal conductivity and viscosity of equilibrium air at atmospheric pressure have been compared to results of Hansen [30] and Yos [32]. These properties are in reasonable agreement with the predictions of Yos when the temperature is less than 10,000°K.

The thermodynamic and transport properties employed in the shock-layer solution in this paper are more accurate than is indicated by the equilibrium properties. When the temperature behind the shock is very high, the predominant species are molecular oxygen and nitrogen which are included in the gas model with reasonable accuracy. The temperature decreases toward the body, and probably no significant amounts of ionized atomic and molecular species have time to be produced. Therefore, the present gas model is considered reasonable for the cases investigated in this paper.

The net mass rate of production of a chemical species per unit volume is obtained from the usual relations as given in [25]. The following chemical reactions are used for the pure air gas model:

$$r = 1 \quad O_2 + M_1 \rightleftarrows 2O + M_1 \tag{9a}$$

$$2 \quad N_2 + M_2 \rightleftarrows 2N + M_2 \tag{9b}$$

$$3 \quad N_2 + N \rightleftarrows 2N + N \tag{9c}$$

$$4 \quad NO + M_3 \rightleftarrows N + O + M_3 \tag{9d}$$

$$5 \quad NO + O \rightleftarrows O_2 + N \tag{9e}$$

$$6 \quad N_2 + O \rightleftarrows NO + N \tag{9f}$$

$$7 \quad N + O \rightleftarrows NO^+ + e^- \tag{9g}$$

The forward reaction rates for the above reactions are expressed as

$$k_{f_r} = T_K^{C2_r} e^{(\ln CO_r - Cl_r \times 10^3/T_K)}$$

where the backward rate is the same form as the forward, with the constants C replaced with D's. The values of these reaction-rate coefficients as obtained from Bortner [33] are given in Table I. The corresponding third body efficiencies relative to argon are given in Table II.

METHOD OF SOLUTION

From previous experience with initial value techniques and the resulting difficulties encountered, a finite difference method was initially chosen as the method of solution. The finite difference equations were made linear in the unknown variables and any coupling between the equations was eliminated. If coupling between the equations is allowed (this is required for the quasilinearization technique as defined by Bellman and Kulaba [34]), the resulting system of algebraic equations for a gas mixture with many chemical species

requires an excessive amount of rapid-access computer storage. Therefore, the present scheme uncouples the conservation equations.

The governing equations (3) are written in the following form:

$$\frac{d^2W}{d\eta^2} + \alpha_1 \frac{dW}{d\eta} + \alpha_2 W + \alpha_3 = 0 \tag{10}$$

where for the tangential momentum equation,

$$W = f' \qquad \alpha_1 = (\ell' - V)/\ell \tag{11a}$$

$$\alpha_2 = -2\beta f'/\ell \tag{11b}$$

$$\alpha_3 = \frac{-\beta}{\ell}\left[\frac{\bar{M}_e}{M}\frac{\theta}{\bar{\bar{e}}} - (f')^2\right] \tag{11c}$$

for the energy equation,

$$W = \theta \qquad \alpha_1 = [\bar{c}' - \bar{c}_p(V + d + b)]/\bar{c} \tag{12a}$$

$$\alpha_2 = \left\{\frac{\alpha\beta}{\bar{\bar{e}}}\bar{c}_p\frac{\bar{M}_e}{\bar{M}} f' - \sum_{i=1}^{NI}\left[\bar{W}_i c_{l_i} + \frac{eh_i}{T_e}\frac{\partial}{\partial\theta}\left[\frac{w_i}{\rho}\right]\right]\right\}\Big/\bar{c} \tag{12b}$$

$$\alpha_3 = \left\{\alpha\ell\bar{c}_p\left[\frac{\partial f'}{\partial\eta}\right]^2 - \frac{1}{T_e}\sum_{i=1}^{NI}\left[\bar{W}_i\Delta h_i^F - eh_i\theta\frac{\partial}{\partial\theta}\left[\frac{w_i}{\rho}\right]\right]\right\}\Big/\bar{c} \tag{12c}$$

for the species equation,

$$W = c_i \qquad i = 1, 2, \ldots NI \qquad \alpha_1 = [b_i' - V]/b_i \tag{13a}$$

$$\alpha_2 = -eW_i^1/b_i \tag{13b}$$

$$\alpha_3 = \left[eW_i^O + \bar{b}_i\right]/b_i \tag{13c}$$

where

$$\frac{\partial}{\partial\theta}\left[\frac{w_i}{\rho}\right] = \frac{M_i}{\theta}\sum_{r=1}^{NI}(\beta_{ri} - \alpha_{ri})\left[\left[C2_r + \frac{C1_r}{T_K} - \alpha_r\right]L_{f_r} - \left[D2_r + \frac{D1_r}{T_K} - \beta_r\right]L_{b_r}\right]$$

The other quantities introduced into the above expressions are given below.

$$\alpha = u_e^2/(\bar{c}_p T_e)$$

$$\beta = \frac{1}{(1 + j)}$$

$$\bar{\bar{e}} = \rho_e u_e \frac{du_e/dx}{dp_e/dx} = \begin{cases} -1 \text{ (boundary layer)} \\ \text{See Equation 5 (shock layer)} \end{cases}$$

$$e = \frac{2\xi}{u_e d\xi/dx} = \begin{cases} 0 \text{ (tip of cone)} \\ \dfrac{1}{(1 + j)du_e/dx} \text{ (stagnation point)} \end{cases}$$

$$b_i = \ell Le_i/Pr$$

$$\bar{b}_i = \frac{\ell}{Pr}\sum_{\substack{k=1 \\ k\neq i}}^{NI}\Delta\bar{\bar{b}}_{ik}\frac{\partial c_k}{\partial\eta}$$

$$b = -\sum_{i=1}^{NI} c_{p_i} \bar{b}_i / \bar{c}_p$$

$$\frac{w_i}{\rho} = W_i^0 - W_i^1 c_i$$

$$\bar{W}_i = e(w_i/\rho)$$

$$\bar{c} = \ell \bar{c}_p / Pr$$

$$\frac{du_e}{dx} = \begin{cases} \frac{1}{R_N}\left[2\left[p_{e_s} - p_\infty\right]/\rho_{e_s}\right]^{1/2} & \text{(boundary layer)} \\ \frac{V_\infty}{R_N}\left[s(1-\varepsilon)+\varepsilon\right] & \text{(shock layer)} \end{cases}$$

$$d = -\sum_{i=1}^{NI} \frac{c_{p_i}}{\bar{c}_p} b_i \frac{\partial c_i}{\partial \eta}$$

$$(\,)' = \frac{\partial(\,)}{\partial \eta}$$

The ordinary differential equation (10) is written in finite difference form, with the usual difference quotients involving three points. The resulting equations are linear algebraic equations and, with the boundary conditions, give a system of the tridiagonal form. An efficient method of solution* for computers is available. If the ordinary differential equation is nonlinear, then α_1, α_2 and α_3 must be approximated by assuming an initial distribution of the independent variable W. Then the solution can be obtained to give a new value of W. This procedure can be repeated until the assumed value of W is the same or nearly the same as the calculated value of W. For some problems it is necessary to weigh the assumed and calculated solution to obtain a new assumed solution for the next iteration.

For the iteration procedure to converge and to have a reasonable rate of convergence, several items have been found important in the method of solution. How the chemical production terms are written is very important. The linearization technique employed in [25] cannot be used in this case, since that procedure involves a Taylor's-series expansion of all of the species and the temperature. When this procedure is followed, all the species and energy equations would be coupled together. As indicated above, the production term is written as

$$\frac{w_i}{\rho} = W_i^0 - W_i^1 c_i \tag{14}$$

where, for a binary mixture of oxygen, the only reaction is Eq. (9a) and

$$W_0^0 = 2M_0 k_{f_1} \bar{\rho} \gamma_{O_2} \gamma_{M_1} \tag{15a}$$

$$W_0^1 = k_{b_1} \bar{\rho}^2 \gamma_O \gamma_{M_1} \tag{15b}$$

For the case of an air mixture, reactions 4, 5, 6 and 7 contribute to the chemical production term of atomic oxygen. In each reaction, either the forward or backward term involves the mass fraction of atomic oxygen and allows the chemical production term to be expressed as relation (14). Similar comments can be made about the production term for other species. For rapid convergence of the finite-difference solution, it is desirable that the terms W_i^0 and W_i^1 be as nearly constant as possible. For the case of oxygen, the value of W_0^0 is proportional to γ_{O_2} and, when the oxygen is highly dissociated, the value of γ_{O_2} changes rapidly for a small change in γ_O, since $\gamma_{O_2} = (1 - c_O)/M_{O_2}$. Therefore, it was found better to write the terms W_0^0 and W_0^1 for oxygen as

$$W_0^0 = 2M_0 k_{f_1} \bar{\rho} \gamma_{M_1}\left[\gamma_{O_2} + \frac{1}{2}\gamma_O\right] = k_{f_1} \bar{\rho} \gamma_{M_1} \tag{16a}$$

$$W_0^1 = k_{b_1} \bar{\rho}^2 \gamma_O \gamma_{M_1} + k_{f_1} \bar{\rho} \gamma_{M_1} \tag{16b}$$

*This method apparently has been developed by several authors, but Bruce, Peaceman, Rachford, and Rice are generally given the credit in this country (see [35]). In Russia, this procedure is known as the "chasing" or double-sweep method, which was developed by Gelfund and Lokutsievski (see [36]).

For the case of the air mixture, the terms W_i^0 and W_i^1 were expressed in a similar manner to relations (15). Then the W_i^0 and W_i^1 for atomic oxygen were modified by adding $M_0 k_{f_1} \bar{\rho} \gamma_{M_1} \gamma_0$ and $k_{f_1} \bar{\rho} \gamma_{M_1}$, respectively, to these terms, as has been done in relations (16).

When the conservation equations are uncoupled and the dependent variables are solved one at a time, the order in which the variables f', θ, and c_i's are solved must be chosen. The present investigation has shown that the species equations should be solved before the energy equation. The mass fraction of species obtained from the solution of the species equations are used in Eq. (14) to evaluate the chemical production term which is required in the energy equation. The terms W_i^0 and W_i^1 are not recalculated in Eq. (14). The transformed velocity V is obtained from the integration of Eq. (3a).

The method of nonlinear overrelaxation (see [37]) has also been used to solve Eq. (10). An investigation was made for a binary gas of oxygen to compare the nonlinear overrelaxation method with the finite-difference procedure. It appears that the finite-difference procedure generally converges faster, as one would expect. For example, for a linear ordinary differential equation, the finite-difference procedure would give the solution directly, while the nonlinear overrelaxation method would still require an iteration procedure. The nonlinear overrelaxation method, however, will probably give convergent solutions for cases when the finite-difference method diverges.

DISCUSSION OF RESULTS

In the AGARD seminar it was requested that two flight environments be investigated, which are called Case A and Case B, and the conditions are given in Table III. When Fig. 1 is used, Case A should correspond to a boundary-layer flow with equilibrium inviscid flow at the edge, while Case B is in the merged layer regime. The computer program that solves the viscous shock layer also will solve the boundary-layer equations which are needed to investigate Case A. Since the present viscous shock-layer solution uses the Rankine-Hugoniot relations, the resulting solutions cannot be expected to be completely valid for Case B where shock slip effects are important. Three other cases are also investigated as indicated in Table III. With the aid of Fig. 1, Case 1 with boundary-layer theory should not be appropriate, while cases 2 and 3 with shock-layer theory should be a reasonable approach.

In the present solutions, the binary Lewis-Semenov numbers have all been assumed equal to 1.4. It is also assumed that the shock is concentric with the body, which makes s = 1. At the wall the gas is undissociated and un-ionized, which corresponds to a fully catalytic wall when the wall temperature is low.

The tangential velocity gradient at the stagnation point is given for the shock-layer solutions in Fig. 2. For the 150- and 200-Kft altitude cases, there is a boundary-layer region. For the 250-Kft case, a boundary layer cannot be readily identified. The tangential velocity gradient for the two boundary-layer cases are also presented. It should be noticed that the boundary-layer results are nondimensionalized by the tangential velocity gradient at the body surface, which is smaller than the tangential velocity gradient behind the shock which is used for the shock-layer results.

The temperature across the shock layer as obtained from the boundary-layer and shock-layer theories are given in Fig. 3. The temperature is high behind the shock and decreases as the gas dissociates toward the body. This situation is especially true for the 150-Kft case, but the gas has not reached equilibrium before the boundary layer is entered. The temperature close to the body surface is nearly the same for both the shock-layer and boundary-layer results for the 150-Kft case. This figure indicates that a well-defined boundary layer occurs at some altitude below 150 Kft.

The mass fractions of the various chemical species are given in Fig. 4-7. For the 250-Kft case, the air is slightly dissociated, but for the other cases, there is an appreciable amount of dissociated species. The conditions corresponding to the edge of the boundary layer in the shock-layer solution at 150 Kft indicates that the gas has not reached chemical equilibrium. Therefore, the assumption that the inviscid flow is in equilibrium for the 150-Kft case is not correct. This agrees with the information presented in Fig. 1. The electron number density is given in Fig. 8, where the shock-layer and boundary-layer results are nearly the same for the 150-Kft case. For the 250-Kft case, there is only a slight amount of ionization.

The present results obtained for Stanton number are compared to various theories in Fig. 9. In this figure, additional results to the five cases given in Table III are presented to make the plot more complete. The free molecule results are for infinite Mach number and complete accommodation. The boundary-layer results are based on the work of Fay and Riddell [38], and the enthalpy at the wall is taken as $0.025V_\infty^2$. The viscous shock-layer solution of Cheng [5] for a perfect gas is also given in this figure. The analysis of Cheng includes body and shock slip effects which have been neglected in the present analysis. The present results for small-shock Reynolds numbers are not accurate, due to the neglect of the shock and body slip effects.

ACKNOWLEDGEMENT

This work was supported by the United States Atomic Energy Commission.

REFERENCES

[1] Blottner, F.G. "Similar and Nonsimilar Solutions of the Nonequilibrium Laminar Boundary Layer." AIAA Journal, Vol. 1, No. 9, Sept, 1963, pp. 2156-2157.

[2] Probstein, R.F. "Shock-Wave and Flow Field Development in Hypersonic Re-entry." ARS Journal, Vol. 31, No. 2, Feb. 1961, p. 185.

[3] Inger, G.R. "Nonequilibrium Hypersonic Stagnation Flow with Arbitrary Surface Catalycity Including Low Reynolds Number Effects." Int. J. Heat Mass Transfer, Vol. 9, 1966, pp. 755-772.

[4] Ho, Hung-Ta, and Probstein, R.F. "The Compressible Viscous Layer in Rarefied Hypersonic Flow." Rarefied Gas Dynamics, edited by L. Talbot, Academic Press, Inc., New York, 1961, pp. 525-552.

[5] Cheng, H.K. "The Blunt-Body Problem in Hypersonic Flow at Low Reynolds Number." presented at IAS 31st Annual Meeting, New York, Jan. 21-23, 1963, IAS Paper No. 63-92; also Cornell Aero. Lab. Rep. AF-1285-A-10, 1963.

[6] Lee, R.H.C. and Zierten, T.A. "Merged Layer Ionization in the Stagnation Region of the Blunt Body." Proceedings, 1967 Heat Transfer and Fluid Mechanics Institute, edited by Paul A. Libby, Daniel B. Olfe, and Charles W. Van Atta, Stanford University Press, Stanford, California, June 1967, pp. 452-468.

[7] Cheng, H.K. "Viscous Hypersonic Blunt-Body Problems and the Newtonian Theory." Fundamental Phenomena in Hypersonic Flow, edited by J. G. Hall, Cornell University Press, Ithaca, New York, 1966.

[8] Cheng, H.K. "Hypersonic Shock-Layer Theory of the Stagnation Region at Low Reynolds Number." Proceedings, 1961 Heat Transfer and Fluid Mechanics Institute, Stanford University Press, Stanford, California, 1961, p. 161.

[9] Kao, H.C. "Hypersonic Viscous Flow Near the Stagnation Streamline of a Blunt Body: II. Third Order Boundary-Layer Theory and Comparison with Other Methods." AIAA Journal, Vol. 2, No. 11, 1964, pp. 1898-1906.

[10] Bush, W.B. "On the Viscous Hypersonic Blunt-Body Problem." J. Fluid Mechanics, Vol. 20, No. 3, Nov. 1964, p. 353.

[11] Chen, S.Y., Aroesty, J. and Mobley, R. "The Hypersonic Viscous Shock Layer with Mass Transfer." RM-4631-PR, May 1966, the RAND Corporation (to be published in International Journal of Heat and Mass Transfer).

[12] Levinsky, E.S. and Yoshihara, H. "Rarefied Hypersonic Flow Over a Sphere." Hypersonic Flow Research, edited by F. R. Riddell, Academic Press, New York, 1962, p. 81.

[13] Chen, S.Y., Baron, J. and Mobley, R. "Stagnation Region Gas Injection in Low Reynolds Number Hypersonic Flow." Proceedings, 1967 Heat Transfer and Fluid Mechanics Institute, edited by Paul A. Libby, Daniel B. Olfe, and Charles W. Van Atta, Stanford University Press, Stanford, California, June 1967, pp. 34-57.

[14] Cheng, H.K. and Chang, A.L. "Stagnation Region in Rarefied High Mach Number Flow." AIAA Journal, Vol. 1, 1963, pp. 231-233.

[15] Howe, J.T. and Viegas, J.R. "Solutions of the Ionized Radiating Shock Layer, Including Reabsorption and Foreign Species Effects, and Stagnation Region Heat Transfer." NASA TR R-159, 1963.

[16] Edelman, R. and Hoffman, J. "Viscous Hypersonic Flow in the Vicinity of the Stagnation Point of Axisymmetric Blunt Bodies - Calculations and Results for Equilibrium Air." Technical Report No. 498, May 1965, General Applied Science Laboratory, Inc., Westbury, New York.

[17] Goldberg, L. and Scala, S. "Mass Transfer in the Hypersonic Low Reynolds Number Viscous Layer." IAS Paper 62-80, January 1962.

[18] Hoshizaki, H., Neice, S. and Chen, K.K. "Stagnation Point Heat Transfer Rates at Low Reynolds Numbers." IAS Paper 60-68, June 1960.

[19] Chung, P.M. "Hypersonic Viscous Shock Layer of Nonequilibrium Dissociated Gas." NASA TR R-109, 1961.

[20] Shih, W.C.L. and Krupp, R.S. "Viscous Nonequilibrium Blunt-Body Flow." AIAA Journal, Vol. 5, No. 1, Jan. 1967, pp. 16-25.

[21] Inger, G.R. "Nonequilibrium Hypersonic Stagnation Flow at Low Reynolds Numbers." SSD-TDR-64-118, September 1964, Aerospace Corp.

[22] Stoddard, F.J. "Closed-Form Solutions for the Hypersonic Viscous Shock Layer with Finite-Rate Chemistry." Proceedings, 1963 Heat Transfer and Fluid Mechanics Institute, Stanford University Press, California, 1963, pp. 120-141.

[23] Buckmaster, J.D. "The Effects of Ambient Dissociation on Frozen Hypersonic Stagnation Flow." AEDC-TDR-64-142, June 1964, Cornell Aero. Lab.

[24] Bird, R.B., Stewart, W.E. and Lightfoot, E.N. Transport Phenomena, John Wiley & Sons, 1960.

[25] Blottner, F.G. "Nonequilibrium Laminar Boundary Layer Flow of Ionized Air." AIAA Journal, Vol. 2, No. 11, Nov. 1964, pp. 1921-1927.

[26] Browne, W.G. "Thermodynamic Properties of Some Atoms and Atomic Ions." and "Thermodynamic Properties of Some Diatomic and Linear Polyatomic Molecules." MSD Engineering Physics Technical Memorandum Nos. 2 and 3, General Electric Company.

[27] Browne, W.G. "Thermodynamic Properties of Some Ablation Products from Plastic Heat Shields in Air." MSD Aerospace Physics Memorandum 11, March 15, 1964, General Electric Company.

[28] Browne, W.G. "Thermodynamic Properties of Some Diatoms and Diatomic Ions at High Temperature." and "Thermodynamic Properties of the Species CN, C_2, C_3, C_2N_2, and C^-," MSD Advanced Aerospace Physics Technical Memorandum Nos. 8 and 9, May 14, 1962, General Electric Company.

[29] Predroditelev, A.S., et al. "Tables of Thermodynamic Functions of Air." translated and published by Associated Technical Services, Inc., Glen Ridge, N.J., 1962.

[30] Hansen, C.F. "Approximations for the Thermodynamic and Transport Properties of High-Temperature Air." NACA TN 4150, March 1958.

[31] Yun, K.S. and Mason, E.A. "Collision Integrals for the Transport Properties of Dissociating Air at High Temperatures." Physics of Fluids, Vol. 5, No. 4, 1962, pp. 380-386.

[32] Yos, J.M. "Transport Properties of Nitrogen, Hydrogen, Oxygen, and Air to 30,000°K," RAD-TM-63-7, March 1963, AVCO Corp.

[33] Bortner, M.H. "Suggested Standard Chemical Kinetics for Flow Field Calculations - A Consensus Opinion." AMRC Proceedings, Vol. 14, Part 1, 1966.

[34] Bellman, R.E. and Kulaba, R.E. Quasilinearization and Nonlinear Boundary-Value Problems, American Elsevier Publishing Company, Inc., New York, 1965.

[35] Richtmyer, R.D. Difference Methods for Initial-Value Problems, Interscience Publishers, Inc., New York, 1957, pp. 101-104.

[36] Godunov, S.K. and Ryabenki, V.S. Theory of Difference Schemes, North-Holland Publishing Company, Amsterdam, 1964.

[37] Ames, W.F. Nonlinear Partial Differential Equations in Engineering, Academic Press, New York, 1965.

[38] Fay, J.A. and Riddell, F.R. "Theory of Stagnation Point Heat Transfer in Dissociated Air." J. of the Aero Sciences, Vol. 25, No. 2, Feb. 1958, pp. 73-85.

NOMENCLATURE

c_i	mass fraction of species i, ρ_i/ρ
c_{p_i}	specific heat at constant pressure of species i, $ft^2/(sec^2\ °R)$
$\bar{c}_p$	frozen specific heat at constant pressure of the mixture, $\sum_i c_i c_{p_i}$, $ft^2/(sec^2\ °R)$
D_{ij}	multicomponent diffusion coefficient, ft^2/sec
$\mathcal{D}_{ij}$	binary diffusion coefficient, ft^2/sec
f'	velocity ratio, u/u_e
h	enthalpy, $\sum_i h_i c_i$, ft^2/sec^2
h_i	enthalpy of species i, ft^2/sec^2
j_i	mass flux relative to the mass-average velocity, slug/(ft^2 - sec)
k	thermal conductivity of mixture, lb/(sec °R)
k_{f_r}, k_{b_r}	forward and backward rate constants
ℓ	density-viscosity product, $\rho\mu/(\rho\mu)_r$
L_{ij}	multicomponent Lewis-Semenov number, $\bar{c}_p \rho D_{ij}/k$
$\mathcal{L}_{ij}$	binary Lewis-Semenov number, $\bar{c}_p \rho \mathcal{D}_{ij}/k$
$\bar{M}$	molecular weight of the mixture, $1/\left(\sum_i c_i/M_i\right)$, lb/lb-mole
M_i	molecular weight of species i, lb/lb-mole
NI	number of chemical species
Pr	Prandtl number, $\bar{c}_p\ \mu/k$
p	pressure, lb/ft^2
R	universal gas constant, lb ft^2/(lb-mole sec^2 °R)
R_N	nose radius, ft
Re_s	shock Reynolds number, $\rho_\infty V_\infty R_N/\mu_s$
r	distance from axis in axisymmetric problems, ft
T	temperature, °R
T_K	temperature, °K
u,v	velocity components tangential and normal to body surface, ft/sec
V	transformed normal velocity (Eq. (3a))
V_∞	freestream velocity, fps
w_i	mass rate of formation of species i, lb $sec^2/(ft^4$ sec)
x	distance along surface from leading edge or stagnation point, ft
y	distance along normal from surface, ft
ε	density ratio across shock, ρ_∞/ρ_s
η	transformed y coordinate
ξ	transformed x coordinate, $lb^2\ sec^2/ft^{2(2-j)}$
$\Delta\eta, \Delta\xi$	step sizes in transformed coordinates
θ	temperature ratio, T/T_e
κ_c	curvature of body, 1/ft
μ	viscosity, lb sec/ft^2
ρ	density, lb sec^2/ft^4
ρ_i	density of species i, lb sec^2/ft^4

Δ	shock standoff distance, ft

Subscripts

b,w	conditions at body surface
e	conditions at outer edge of shock layer or boundary layer
r	quantities evaluated at some reference condition
s	conditions behind shock wave
∞	freestream conditions

Superscripts

j=0	two-dimensional body
j=1	axisymmetric body

TABLE I

Reaction Rate Coefficients

Reaction	CO(r)	C1(r)	C2(r)	DO(r)	D1(r)	D2(r)
r = 1	3.61×10^{18}	59.4	-1.0	3.01×10^{15}	0	-0.5
2	1.92×10^{17}	113.1	-0.5	1.09×10^{16}	0	-0.5
3	4.15×10^{22}	113.1	-1.5	2.32×10^{21}	0	-1.5
4	3.97×10^{20}	75.6	-1.5	1.01×10^{20}	0	-1.5
5	3.18×10^{9}	19.7	1.0	9.63×10^{11}	3.6	0.5
6	6.75×10^{13}	37.5	0	1.50×10^{13}	0	0
7	9.03×10^{9}	32.4	0.5	1.80×10^{19}	0	-1.0

TABLE II

Third Body Efficiencies Relative to Ar

$Z_{(j\text{-}NI)i}$	O_2	N_2	O	N	NO	NO^+
	i = 1	2	3	4	5	6
(j-NI) = 1 e^-	0	0	0	0	0	1
M_1^2	9	2	25	1	1	0
M_2^3	1	2.5	1	0	1	0
M_3^4	1	1	20	20	20	0

TABLE III

Conditions for Example Investigated

Case	Altitude	Theory[a]	T_w (°K)	Re_s	p_e (psf)	T_e (°R)
A	100K	BL	1400	1.43×10^4	12772	12603
1	150K	BL	1000	1.54×10^3	1377	11330
2	150K	SL	1000	9.31×10^2	-	-
3	200K	SL	1000	1.38×10^2	-	-
B	250K	SL	1000	1.99×10^1	-	-

V_∞ = 20 Kfps, R_N = 1 inch } for all cases

a_{BL} = boundary layer; SL = shock layer.

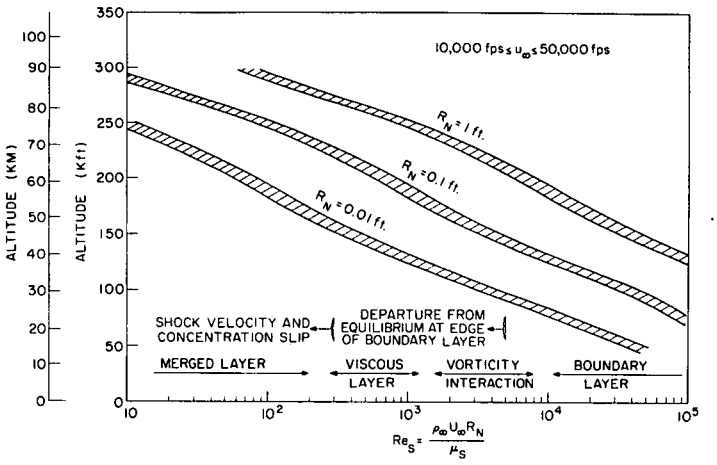

Fig.1 Flow regimes

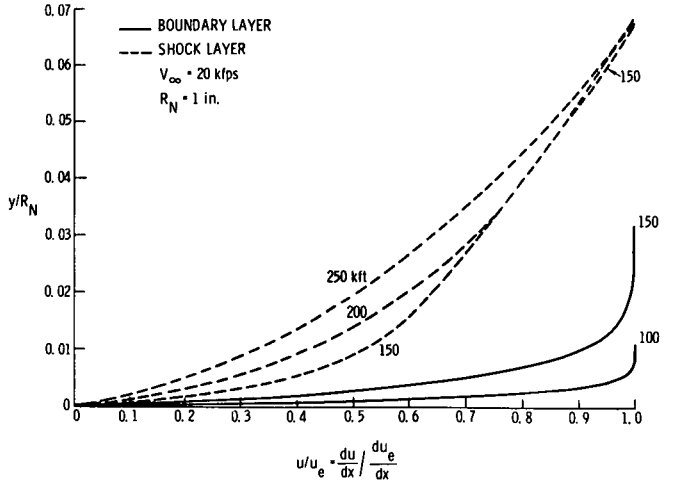

Fig.2 Tangential velocity gradient across shock layer

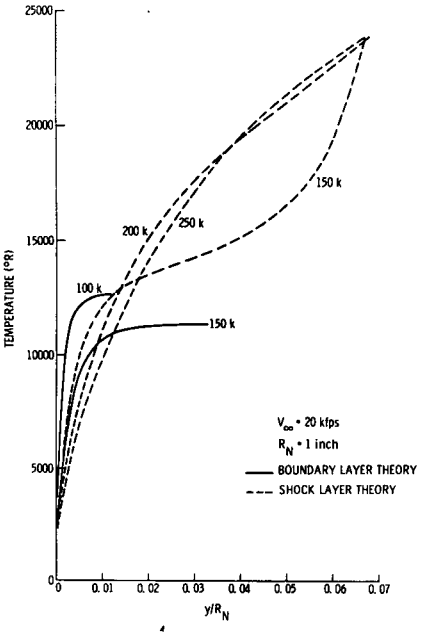

Fig.3 Temperature across shock layer

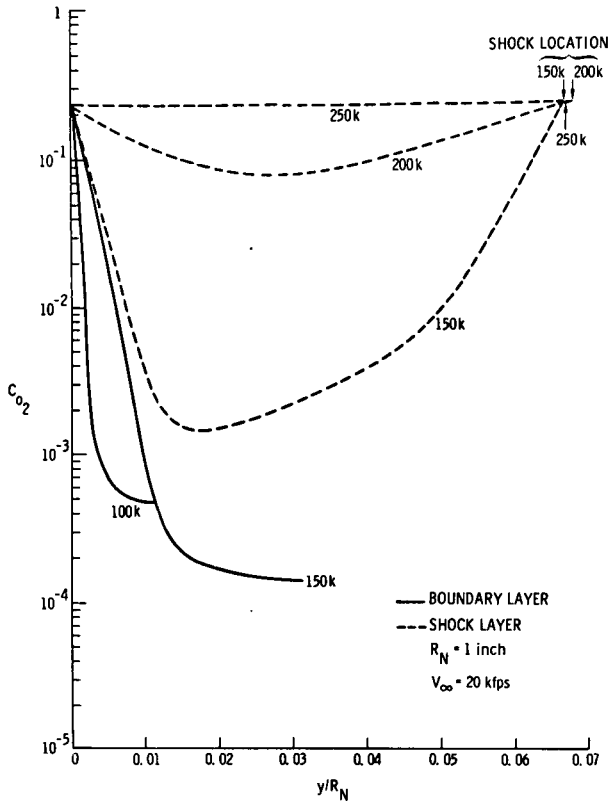

Fig.4 Mass fraction of molecular oxygen across shock layer

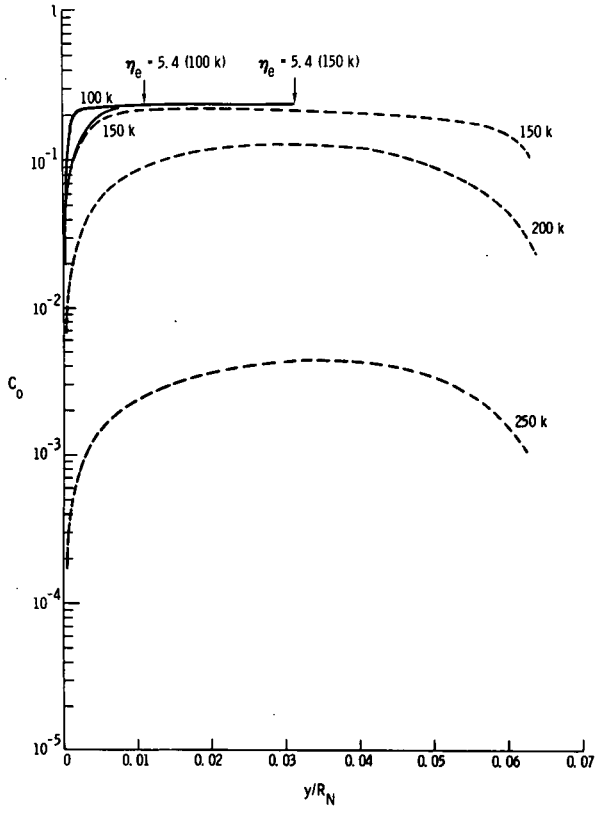

Fig.5 Mass fraction of atomic oxygen across shock layer

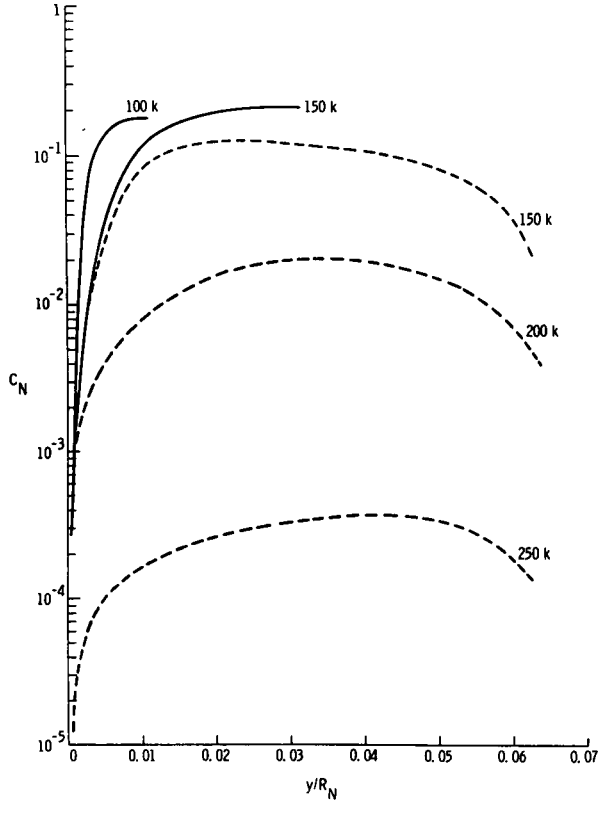

Fig.6 Mass fraction of atomic nitrogen across shock layer

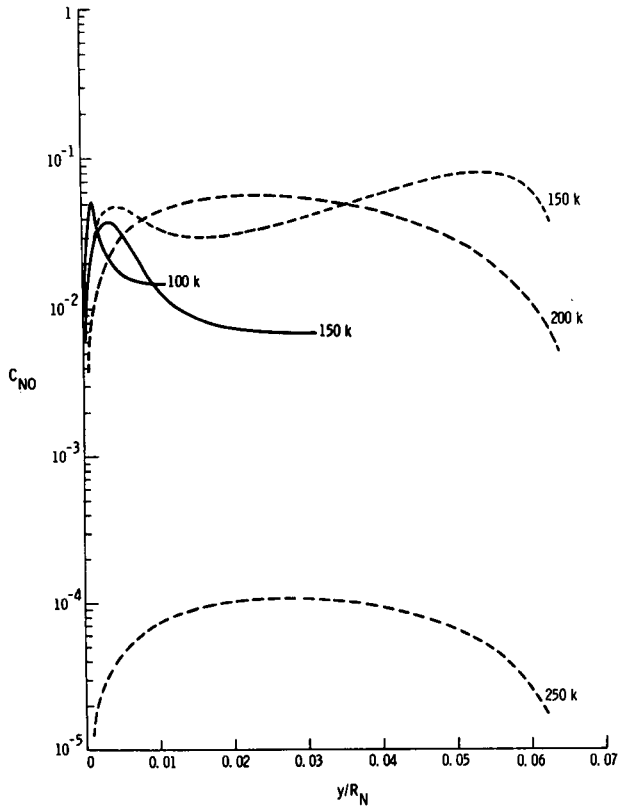

Fig.7 Mass fraction of nitric oxide across shock layer

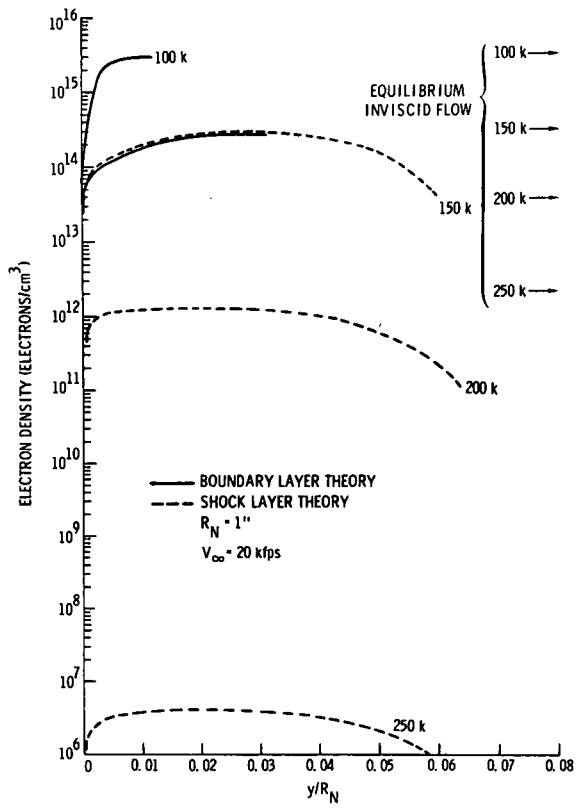

Fig.8 Electron number density across shock layer

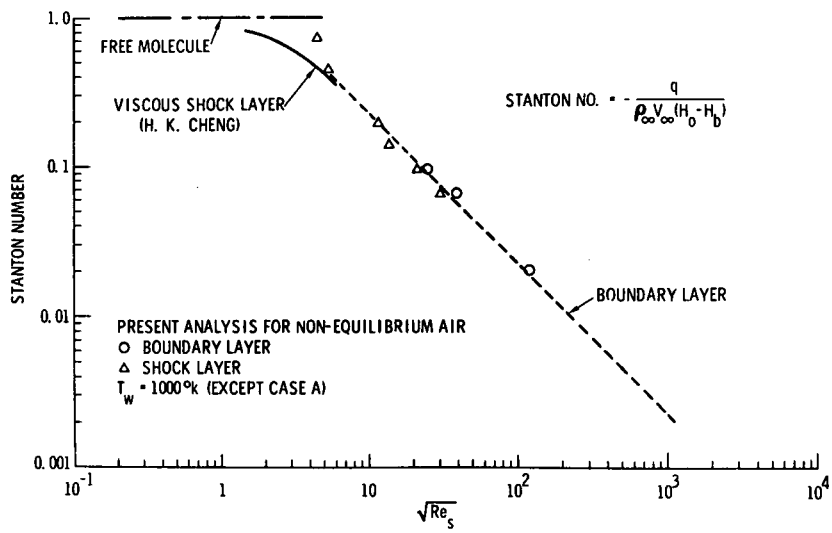

Fig.9 Stanton number variation with Reynolds number

CHEMICALLY REACTING BOUNDARY LAYER EFFECTS FOR THE AGARD ENGINEERING APPLICATIONS BODY AND FLOW CONDITIONS

by

John C. Adams, Jr

Supervisor, Theoretical Gas Dynamics Section,
Hypervelocity Branch, Aerophysics Division,
von Karman Gas Dynamics Facility, ARO, Inc.,
Arnold Air Force Station, Tennessee

CHEMICALLY REACTING BOUNDARY LAYER EFFECTS FOR THE AGARD ENGINEERING APPLICATIONS BODY AND FLOW CONDITIONS

by John C. Adams, Jr.*

SUMMARY

Numerical results for chemical nonequilibrium boundary-layer flow at the AGARD Case B condition (flight in the earth's atmosphere at 250,000 ft and 20,000 ft/sec) are presented for the AGARD 10.0° asymptotic half-angle hyperboloid having a nose radius of 1.0 inch and a wall temperature of 1800.0°R. The boundary-layer model allows multicomponent diffusion and both catalytic and noncatalytic walls. Also presented are stagnation point results for the above body and flight conditions using a thin viscous shock layer analysis allowing chemical nonequilibrium and shock merging effects for both wall conditions including multicomponent diffusion. Analysis of the results reveals that boundary-layer theory is not applicable to the AGARD Case B flow condition, and that only the merged thin viscous shock layer stagnation point analysis may be expected to have any physical meaning. However, boundary-layer results are presented over the entire body as requested by AGARD so as to facilitate comparison with other theoretical and numerical solutions for the same body and flow conditions.

INTRODUCTION

The present paper is devoted to documenting results presented by the author at the AGARD Seminar in the Engineering Application Section using computer programs developed by the von Karman Gas Dynamics Facility of the Arnold Engineering Development Center. The body (a hyperboloid of 10.0° asymptotic half-angle) and the flow conditions (see Table 1) were completely specified by AGARD [1]. All results presented in the present report are for the AGARD Case B flow condition using chemical nonequilibrium, laminar boundary-layer theory for ionized, multicomponent air.

CHEMICALLY REACTING FLOW SOLUTIONS (AGARD CASE B)

Theoretical Considerations and Description of Computer Program

All of the results for the real gas AGARD Case B condition were obtained by application of the chemical nonequilibrium, laminar boundary-layer theory for ionized, multicomponent air as formulated by Blottner [2]. In the present work all basic portions of Blottner's analysis have been retained, e.g., consideration of the diffusive mass flux for a multicomponent mixture of perfect gases and expressing the net mass rate of production for each species in a form especially suited for numerical computation. For further details on the theoretical formulation of the governing equations, see Blottner [3,4] and Lenard [5]. The following guidelines were followed in the course of the study: (a) The complete flow field was considered to be in the continuum flow regime. (b) The basic gas model was assumed to be a multicomponent mixture of chemically reacting perfect gases made up of seven chemical species: N, O, N_2, O_2, NO, NO^+, and e^-. (c) The gas was assumed to be in vibrational equilibrium but in chemical nonequilibrium as controlled by an eleven chemical reaction model using the rates of Bortner [6] tabulated in Table 2. (d) Multicomponent diffusion between species was allowed in the viscous region. For the ionized species, ambipolar type of diffusion was employed. Thermal diffusion was neglected for all species. The method of Moore [7] was used to calculate the required binary diffusion coefficients. (e) Thermodynamic properties of enthalpy and specific heats for the individual species were taken from Browne [8]. (f) Multicomponent transport properties of viscosity and thermal conductivity for the mixture were obtained from Wilke's formula [9] using individual species properties computed by the method of Moore [7]. (g) Radiation phenomena were not considered. (h) Mass transfer effects were not considered. (i) Effects of wall surface conditions were considered by examining both noncatalytic and equilibrium walls. (j) The angle of attack of the body relative to the freestream was specified by AGARD to be zero. (k) The flow field analyses, both viscid and inviscid, were accomplished by computerized numerical techniques utilizing a minimum number of simplifying assumptions.

The governing boundary-layer equations in physical variables were first transformed using the Lees-Dorodnitsyn transformation [9] and then solved in the transformed plane using an implicit finite-difference scheme of the Crank-Nicolson type; details of this procedure may be found in the report by Blottner [4]. The conditions at the wall and the outer edge of the boundary layer determine the necessary boundary conditions for these equations. At the wall, it was assumed that the normal and tangential velocities were zero, the wall temperature was specified by AGARD to be 1800.0°R, and the wall was taken to be either completely noncatalytic with respect to atom recombination or in local chemical equilibrium at the gas-solid interface. These catalytic conditions at the wall were based on the thesis by Moore [10] which includes the effects of foreign gas injection. The validity of Moore's formalism for cases without mass injection has been discussed by Adams, et al. [11]. At the outer edge of the boundary layer, inviscid conditions were specified by AGARD based on an inviscid chemically reacting streamtube expansion using modified Newtonian theory for prediction of the pressure distribution over the body. These outer edge conditions were recorded on magnetic tape for input to the boundary-layer program. The outer edge of the boundary layer was hence taken to coincide with the inviscid body streamline, and thus no attempt was made to account for viscous interaction such as treated by Adams, et al. [11] and Kaplan [12].

In addition to the wall and outer edge boundary conditions, initial conditions are required to completely determine the resulting downstream solution. In order to obtain the correct initial conditions, the system of boundary-layer equations (which are nonlinear partial differential equations) were reduced to the limiting form of ordinary nonlinear differential equations with two-point boundary conditions at the stagnation point. Such two-point boundary value problems are extremely difficult to solve using the more common "shooting" method since so many species equations are involved. Hence, a finite-difference method was developed such that the two-end conditions were always satisfied; the fundamentals of this technique may be found in Chapter

*Supervisor, Theoretical Gas Dynamics Section, Hypervelocity Branch, Aerophysics Division, von Karman Gas Dynamics Facility, ARO, Inc., Arnold Air Force Station, Tennessee.

VII of the book on numerical analysis by Conte [13]. More details of this finite-difference technique applied to the solution of nonlinear equations may be found in the papers by Holt [14] and Fay and Kaye [15]. Basically, the nonlinear ordinary differential equations were written in linearized finite-difference form so that the resulting linear algebraic equations were of tridiagonal form and a sweeping method of solution was used. Iteration was then applied until successive solutions ($f'(\eta)$, $\theta(\eta)$, and $c_i(\eta)$) were sufficiently close to each other. This procedure was found to converge rapidly for all cases in the present study.

Using the above obtained initial conditions, solutions to the complete nonsimilar boundary-layer equations were obtained in a step-by-step procedure marching downstream using the implicit finite-difference method by Blottner mentioned previously. No stability problems were encountered for the conditions studied.

Considerations were also given to the possibility that a boundary-layer type analysis may not be valid under the conditions of the present study. It may be that nonequilibrium and viscous effects have equal importance over the entire shock layer, especially in the nose region of the body. In order to examine this possibility, an analysis was performed where the entire shock layer at the stagnation point was treated as viscous. As shown by Cheng [16], Chung [17], Howe and Viegas [18], and Lee and Zierten [19], the governing equations for such an analysis are identical in form with the boundary-layer equations under the restrictions that the shock layer be thin, i.e. $\Delta/r_N \ll 1$, with all curvature effects neglected. Recent work by Howe and Sheaffer [20], Goldberg [21], Goldberg and Scala [22], and Chen, Aroesty, and Mobley [23], has further shown the validity of such an analysis for cases with mass injection at the wall.

The basic thin, hypersonic shock layer model as formulated by Cheng [16] assumes a strong bow shock wave of negligible thickness that is concentric with the body at the stagnation line. Across the shock, the static pressure and normal velocity components are discontinuous according to the usual Rankine-Hugoniot relations; in addition, the so-called "shock slip" effects (discontinuities in composition, tangential velocity, and total enthalpy) are allowed immediately behind the shock. Between the shock and the body there is assumed a thin ($\Delta/r_N \ll 1$) layer of continuum, viscous reacting gas flow. In this layer, the influence of body curvature and surface slip phenomena is also neglected in comparison to the shock-layer vorticity and "shock slip" effects, providing that the body surface is highly cooled. An important consequence of this thin, hypersonic shock-layer model is that the governing Navier-Stokes equations reduce to the familiar parabolic partial differential equations of boundary-layer theory as mentioned previously.

A modification of the above model was proposed by Chung [17]. Across the shock, the static pressure, enthalpy, and normal velocity component are taken to be discontinuous according to the Rankine-Hugoniot conditions for a real gas. However, through the shock the chemical composition is taken as frozen at the free-stream conditions. Furthermore, stagnation or total enthalpy is taken as constant across the shock. Hence, none of the so-called "shock-slip" effects are considered in this model. Other than this all other features of the thin-hypersonic shock layer are retained including the centrifugal effects due to a normal pressure gradient across the layer. Between the shock and the body the flow is considered to be in chemical nonequilibrium with the shock standoff distance determined as part of the solution.

Both of the above described models were applied in the present work. The programs are basically the same as the stagnation point boundary-layer program described previously since the only modifications were determination of the shock standoff distance and inclusion of the normal pressure gradient terms. The manner of iterative solution was exactly the same as in the boundary-layer stagnation case.

DISCUSSION OF RESULTS

The results presented in this section were obtained from an investigation into the effects of chemical nonequilibrium upon the boundary layer and viscous shock layer for the specified AGARD hyperboloid of 10.0° asymptotic half-angle at zero angle of attack under the specified AGARD Case B conditions as discussed previously. Particular emphasis was placed upon presenting results for different wall catalytic conditions and boundary-layer outer edge conditions in terms of quantities of interest such as the local wall heat transfer and skin friction. Only in this manner can one properly assess the influence of each of these parameters on the resultant solution.

Shown in Fig. 1 are the inviscid outer edge conditions as specified by AGARD [1] for the Case B condition. Reference to the altitude-velocity tables of Lewis and Burgess [24] shows that the Case B conditions correspond to flight at 250,000 ft with a velocity of 20,000 ft/sec. It is to be noted from Fig. 1 that both the nonequilibrium and frozen results for U_e and T_e are identical. Equilibrium flow yields higher values for U_e and T_e with a resulting decrease in the local edge Reynolds number, $Re_{s,e}$. Figure 2 shows the corresponding inviscid outer edge species distribution. The important point to recognize from Fig. 2 is that the flow field is essentially frozen over the entire body. The only chemical nonequilibrium effects are seen in the NO, NO^+, and O_2 distributions, and these species all have a mass fraction less than 10^{-3}. The inviscid stagnation point is taken to be in chemical equilibrium which results in total dissociation of O_2 and about 40 percent dissociation of N_2 so that the major species in the flow are O, N, and N_2. These species remain frozen over the body, and hence no influence of chemical nonequilibrium is reflected by the major species; equilibrium flow has only a slight influence in decreasing N with a corresponding increase in N_2 due to forced recombination.

Table 3 is a tabulation of stagnation point data for the AGARD Case B. Shown are boundary-layer solutions which assume the outer edge to be in a state of chemical equilibrium, thin viscous shock-layer solutions which take the species immediately behind the shock to be the same as the nondissociated free-stream conditions, i.e., a frozen shock with no "shock-slip", and merged thin viscous shock-layer solutions which allow the shock and the viscous layer to merge according to the "shock-slip" conditions. Noting that the shock Reynolds number is very low, $Re_s = 19.40$, the merged thin viscous shock-layer solution is the only approach of those presented expected to be physically valid under these flow conditions; both the boundary layer and thin viscous shock layer are not applicable to this flow. Such is apparent by examination of the stagnation point heat-transfer rates. Boundary-layer theory for a noncatalytic wall yields results which indicate a tremendous reduction in heat transfer as compared to the equilibrium catalytic wall; this is due to the frozen state of the boundary layer so that recombination does not occur unless forced by the catalytic wall condition. Also note that the outer edge location of the boundary layer is a factor of two larger than the shock

standoff distance predicted by the viscous shock-layer analysis. Hence the boundary-layer edge is outside the shock layer; such can be clearly seen in Figs. 3, 4, and 5. The fully viscous character of the shock layer is obvious from the velocity and temperature profiles in Figs. 3 and 4; note that the catalytic condition of the wall has almost no effect on the viscous shock-layer velocity and temperature profiles. Figure 5 re-emphasizes the frozen state of the shock layer as well as the gross error in using the boundary layer with equilibrium outer edge conditions. This is an important point to note since many prior boundary-layer investigations have used equilibrium outer edge conditions with no regard to their validity.

The above discussion has shown clearly that a boundary-layer analysis is definitely not applicable to the AGARD Case B flow under examination. However, as requested by AGARD, boundary-layer results over the entire body will be presented for sake of comparison with other methods. It is not apparent how relevant these results are for the physical problem.

Figure 6 shows the displacement thickness distribution over the body, while Fig. 7 presents the local skin friction. Edge conditions and catalytic condition of the wall influence the displacement thickness but have little effect on the skin friction. Shown in Figs. 8, 9, 10, and 11 are the heat-transfer results. As expected, the noncatalytic wall produces a substantial reduction in heat transfer as compared to the equilibrium catalytic wall. Recall from Fig. 2 the recombination of N to N_2 forced by the equilibrium outer edge; the effects of this recombination can be seen in the noncatalytic wall, equilibrium outer edge results of Figs. 8, 10, and 11. With respect to Fig. 9, the Stanton number is defined as

$$St_\infty = \frac{-\dot{q}_w}{\rho_\infty V_\infty (H_o - h_w)} \tag{1}$$

where, in a chemically reacting flow, the wall enthalpy, h_w, is a function of the catalytic condition of the wall. Such is reflected in Fig. 9 with the noncatalytic wall, equilibrium outer edge results. Hence, one must be extremely careful in interpretation of Stanton number in a chemically reacting flow with catalytic and noncatalytic wall conditions.

Figures 12 and 13 present the boundary-layer velocity and temperature profiles at specified body locations defined by AGARD [1]. The corresponding species profiles are given in Fig. 14. Regarding Fig. 13 recall from Fig. 1 that T_e for the equilibrium outer flow is higher than for the nonequilibrium and frozen outer flow; such influences the character of the equilibrium outer edge temperature profiles. This also causes the equilibrium outer edge boundary-layer thickness to be larger than for the nonequilibrium and frozen flows.

Another quantity of interest is the integrated skin-friction and pressure drag coefficients over the specified AGARD body. The results are shown in Table 4 where the reference area is taken to be the base cross-sectional area at $s/r_N = 50.0$. These quantities have no true physical meaning for this flow because of the failure of boundary-layer theory as discussed previously.

A few words should be said in conclusion as to the computer time requirements and character of numerical solutions for this investigation. The program itself was written in FORTRAN 63 for solution on a CDC 1604-B computer. Computation time including printout averaged 60 seconds per iteration for the stagnation point solutions with approximately 60 iterations required for convergence; hence, a total of approximately 60 minutes was required to obtain a stagnation point solution. Computation time including printout for the boundary-layer solutions over the body averaged 38 seconds per station with a total of 250 stations required to traverse the AGARD body of 50 nose radii in length; hence, a total of 160 minutes was required for a complete boundary-layer solution. Using Lees-Dorodnitsyn variables results in the solution being obtained in the transformed (ξ,η) plane; for the present investigation the following step sizes were chosen:

	Thin Viscous Shock Layer	Boundary Layer
η_{max}	η_{shock}	6.0
$\Delta\eta$	0.10	0.20

For the boundary-layer solution, the following s/r_N step sizes were used:

$$\Delta(s/r_N) = 0.05,\ 0.10,\ 0.20,\ 0.40$$

where a procedure for doubling the s/r_N step size was built into the program; hence, the s/r_N step size was doubled a total of 4 times over the body of interest in this work. Such a step size change is highly advantageous in reducing the total computing time requirements. The implicit finite-difference scheme proved to be inherently stable in all cases and repetition of the calculations with a halved step size in $\Delta\eta$ as well as an increase in η_{max} to 8.0 showed no change in the numerical results. All in all, the method must be described as highly satisfactory in the numerical sense.

SUMMARY

The present report is devoted to documenting numerical results for the AGARD Engineering Applications Case B using thin viscous shock layer and boundary-layer theory for a multicomponent gas in chemical nonequilibrium. The purpose of this report is to present these results in a manner specified by AGARD so as to facilitate comparison with other theoretical and numerical solutions from the same body and flow conditions. No attempt has been made to fully analyze the present solutions. The reader of this report is free to make his own judgment relative to other methods. In all fairness, however, the reader should keep in mind the

important point that boundary-layer theory in general is not applicable to the Case B flow condition. Only the merged thin viscous shock layer stagnation point analysis including "shock slip" may be expected to have any physical meaning.

ACKNOWLEDGEMENT

This work was sponsored by the Arnold Engineering Development Center (AEDC), Air Force Systems Command, U.S. Air Force, under Contract F40600-69-C-0001 with ARO, Inc., Contract Operator, AEDC. The author wishes to thank D. H. Wurst and M. Brown, Jr., ARO, Inc., for their help in performing the numerical calculations.

REFERENCES

[1] AGARD - Letter from Dr. J. Lukasiewicz, Member, AGARD Fluid Dynamics Panel, April 7, 1967.

[2] Blottner, F.G. -- "Nonequilibrium Laminar Boundary Layer Flow of Ionized Air." AIAA Journal, Vol. 2, No. 11, 1964, pp. 1921-1927.

[3] Blottner, F.G. "Nonequilibrium Laminar Boundary Layer Flow of a Binary Gas." General Electric TIS R63SD17, 1963.

[4] Blottner, F.G. "Nonequilibrium Laminar Boundary Layer Flow of Ionized Air." General Electric TIS R64DS56, 1964.

[5] Lenard, M. "Chemically Reacting Boundary Layers." General Electric TIS R64SD14, 1964.

[6] Bortner, M.H. "Chemical Kinetics in a Re-entry Flow Field." General Electric TIS R63SD63, 1963.

[7] Moore, J.A. "Transport Properties for Slightly Ionized Gas Mixtures." TRW Doc. No. 09823-6719-RO-00, 1968.

[8] Browne, W.G. General Electric Company, Missile and Space Division, Re-entry Systems Department, Personal Communication.

[9] Dorrance, W.H. Viscous Hypersonic Flow, McGraw-Hill, New York, 1962.

[10] Moore, J.A. "Chemical Nonequilibrium in Viscous Flows." Ph.D. Dissertation, State University of New York at Buffalo, 1967.

[11] Adams, J.C., Jr., Lewis, C.H., Brahinsky, H.S. and Marchand, E.O. "Effects of Chemical Nonequilibrium, Mass Transfer, and Viscous Interaction on Spherically Blunted Cones at Hypersonic Conditions." AIAA Preprint 69-168, 1969.

[12] Kaplan, B. "The Nonequilibrium Air Boundary Layer on a Blunt-Nosed Body." General Electric TIS 68SD227, 1968.

[13] Conte, S.D. Elementary Numerical Analysis. McGraw-Hill, New York, 1965.

[14] Holt, J.F. "Numerical Solution of Nonlinear Two-Point Boundary Problems by Finite Difference Methods." Assoc. for Computing Mach. Communications, Vol. 7, No. 6, pp. 366-373, 1964.

[15] Fay, J.A. and Kaye, H. "A Finite-Difference Solution of Similar Nonequilibrium Boundary Layers." AIAA Journal, Vol. 5, No. 11, pp. 1949-1954, 1967.

[16] Cheng, H.K. "The Blunt-Body Problem in Hypersonic Flow at Low Reynolds Number." Cornell Aeronautical Laboratory, Inc. AF-1285-A-10, 1963.

[17] Chung, P.M. "Hypersonic Viscous Shock Layer of Nonequilibrium Dissociated Gas." NASA TR R-109, 1961.

[18] Howe, J.T. and Viegas, J.R. "Solutions of the Ionizing Radiating Shock Layer, Including Reabsorption and Foreign Species Effects, and Stagnation Region Heat Transfer." NASA TR R-159, 1963.

[19] Lee, R.H.C. and Zierten, T.A. "Merged Layer Ionization in the Stagnation Region of a Blunt Body." Aerospace Corp. TR-1001 (S2240-10)-1, 1967.

[20] Howe, J.T. and Sheaffer, Y.S. "Mass Addition in the Stagnation Region for Velocity up to 50,000 Feet Per Second." NASA TR R-207, 1964.

[21] Goldberg, L. "The Structure of the Viscous Hypersonic Shock Layer." General Electric TIS R65SD50, 1965.

[22] Goldberg, L. and Scala, S.M. "Mass Transfer in the Low Reynolds Number Viscous Layer Around the Forward Region of a Hypersonic Vehicle." General Electric TIS R65SD27, 1965.

[23] Chen, S.Y., Aroesty, J. and Mobley, R. "The Hypersonic Viscous Shock Layer with Mass Transfer." Rand Memorandum RM-4631-PR, 1966.

[24] Lewis, C.H. and Burgess, E.G. III. "Altitude-Velocity Table and Charts for Imperfect Air." Arnold Engineering Development Center TDR-64-214, 1965.

NOMENCLATURE

A_b base cross-sectional area

C_{D_f} skin-friction drag coefficient referenced to base area

C_{D_p} pressure drag coefficient referenced to base area

$C_f = 2\tau_w/\rho_\infty V_\infty^2$ skin-friction coefficient

c_i mass fraction of species i

c_p specific heat at constant pressure

$f' = u/U_e$ velocity ratio

H_o stagnation enthalpy

h enthalpy

M_∞ free-stream Mach number

P inviscid pressure

P'_o free-stream normal shock pitot pressure

Pr Prandtl number

P_s inviscid pressure behind normal shock

$\dot{q}_w$ wall heat flux

$Re_s = \rho_\infty V_\infty r_N/\mu_s$ shock Reynolds number

$Re_\infty = \rho_\infty V_\infty r_N/\mu_\infty$ Reynolds number based on nose radius and free-stream conditions

r_N nose radius, 1,0 in.

$St_\infty = -\dot{q}_w/\rho_\infty V_\infty (H_o - h_w)$ Stanton number based on free-stream conditions

s surface distance measured from stagnation point

T temperature

T_e temperature at edge of boundary layer

T'_o free-stream normal shock stagnation temperature

T_s temperature behind normal shock

U_e inviscid tangential velocity at edge of boundary layer

u tangential velocity component

V_∞ free-stream velocity

y distance normal to the surface

Δ shock-layer thickness

δ boundary-layer thickness

δ^* boundary-layer displacement thickness

$\varepsilon = \rho_\infty/\rho_s$ normal shock density ratio

$\theta = T/T_e$ temperature ratio

μ viscosity

ξ, η transformed coordinates defined by Blottner [2]

ρ density

Subscripts

BL boundary layer

ECW equilibrium catalytic wall

EQUIL equilibrium

e conditions at outer edge of boundary layer

MTVSL merged thin viscous shock layer with "shock slip"

NCW noncatalytic wall

NEQ nonequilibrium

o stagnation conditions

s normal shock conditions

TVSL thin viscous shock layer without "shock slip"

w wall

$( )'_o$ normal shock stagnation conditions

∞ free-stream conditions

TABLE 1

Conditions for AGARD Engineering Applications Section
Hyperboloid (10.0° Asymptotic Half-Angle)

Case	Altitude (ft)	M_∞	U_∞ (ft/sec)	T_∞ (°K)	P_∞ (atm)	Re_∞ (Based on nose radius of $r_N = 1.0$ in.)	P_0' (atm)	T_0' (°K)	T_w (°K)	T_w/T_0'	$\epsilon^\ddagger$
A	100,000.0	20.178	20,000.0	226.98	1.0997×10^{-2}	179,828.5	6.0352*	6,996.0*	1,400.0	0.2001	0.0103
B	250,000.0	21.744	20,000.0	195.46	2.0074×10^{-5}	430.9	0.0129*	5,301.9*	1,000.0	0.1886	0.2237
C	250,000.0	21.744	20,000.0	195.46	2.0074×10^{-5}	430.9	0.01223†	18,678.2†	1,000.0	0.0535	0.2237

*Normal Shock Equilibrium Stagnation Conditions

†Normal Shock Ideal Gas ($\gamma = 1.40$) Stagnation Conditions

$$\ddagger \quad \epsilon = \left\{ \frac{1 + 112/T_\infty}{Re_\infty \left[(\gamma - 1)M_\infty^2 + 112/T_\infty\right]} \left[(\gamma - 1)M_\infty^2\right]^{3/2} \right\}^{1/2}$$

(Based on Sutherland Viscosity Law)

TABLE 2

Chemical Reactions and Rates

Reaction	Catalytic Body (M)	C_f	a_f	$e_{o,f}/k$ (°K)	C_b	a_b	$e_{o,b}/k$ (°K)
$O_2 + O_2 \rightleftarrows 2O + O_2$		2.3×10^{19}	-1	59,400	1.9×10^{16}	-1/2	0
$O_2 + O \rightleftarrows 2O + O$		8.5×10^{19}	-1	59,400	7.1×10^{16}	-1/2	0
$O_2 + M \rightleftarrows 2O + M$	N, N_2, NO, Inert	3.0×10^{18}	-1	59,400	2.5×10^{15}	-1/2	0
$N_2 + N_2 \rightleftarrows 2N + N_2$		3.8×10^{19}	-1	113,200	2.0×10^{18}	-1	0
$N_2 + N \rightleftarrows 2N + N$		1.3×10^{20}	-1	113,200	7.0×10^{18}	-1	0
$N_2 + M \rightleftarrows 2N + M$	O, O_2, NO, Inert	1.9×10^{19}	-1	113,200	1.0×10^{18}	-1	0
$NO + M \rightleftarrows N+O+M$	O, O_2, N, N_2, Inert	2.4×10^{17}	-1/2	75,500	6.0×10^{16}	-1/2	0
$NO + O \rightleftarrows O_2 + N$		4.3×10^{7}	3/2	19,100	1.8×10^{8}	3/2	3020
$N_2 + O \rightleftarrows NO + N$		6.8×10^{13}	0	37,750	1.5×10^{13}	0	0
$N_2 + O_2 \rightleftarrows 2NO$		2.0×10^{14}	0	61,600	1.0×10^{13}	0	40,000
$N + O \rightleftarrows NO^+ + e^-$		1.3×10^{8}	1	31,900	2.0×10^{19}	-1	0

Note: Reaction rates are from Bortner, M. H. "Chemical Kinetics in a Re-entry Flow Field." GE TIS R63SD63, August 1963.

$k_f = C_f T^{a_f} \exp(-e_{o,f}/kT)$, cm^3/mole sec $\qquad k_b = C_b T^{a_b} \exp(-e_{o,b}/kT)$

T in °K

k is Boltzmann's constant

TABLE 3

Stagnation Point Data for AGARD Case B

Boundary Layer Solution

	Nonequilibrium BL Equilibrium Outer Edge		Frozen BL Equilibrium Outer Edge	
	ECW	NCW	ECW	NCW
$-q_w]_o$ (Btu/ft^2-sec)	145.00	42.07	145.76	42.00
δ^*/r_N	-0.00516	0.00005	-0.00805	-0.00001
δ/r_N (@ f'=0.995)	0.1228	0.1246	0.1225	0.1246
P_o' (lb$_f$/ft^2)	27.299 →			
T_o' (°R)	9543.3 →			

Species Mass Fractions			EQUIL		
C_i	ECW	NCW	Outer Edge	ECW	NCW
O	5.16-10	2.35-01	2.34-01	5.13-10	2.34-01
O_2	2.50-01	7.78-06	1.64-05	2.47-01	1.64-05
NO	5.94-05	1.17-04	1.70-03	5.91-05	1.70-03
N	1.23-21	2.46-01	2.47-01	1.23-21	2.47-01
NO^+	4.81-25	1.25-04	2.72-04	4.80-25	2.72-04
N_2	7.50-01	5.19-01	5.17-01	7.53-01	5.17-01

Thin Viscous Shock Layer Solution

	Nonequilibrium		Frozen	
	ECW	NCW	ECW	NCW
$-\dot{q}_w]_o$ (Btu/ft^2-sec)	249.35	247.55	249.33	249.31
Δ/r_N	0.0642	0.0643	0.0644	0.0644
P_s (lb$_f$/ft^2)	24.818 →			
T_s (°R)	24494.8 →			

Species Mass Fractions

C_i	ECW	NCW	Outer Edge	ECW	NCW
O	5.24-10	3.69-03	0	5.24-10	0
O_2	2.34-01	2.28-01	2.35-01	2.34-01	2.35-01
NO	5.81-05	2.17-03	0	5.81-05	0
N	1.30-21	2.78-04	0	1.30-21	0
NO^+	5.00-25	1.34-09	0	5.00-25	0
N_2	7.65-01	7.66-01	7.65-01	7.65-01	7.65-01

Merged Thin Viscous Shock Layer Solution

	Nonequilibrium	
	ECW	NCW
$-\dot{q}_w]_o$ (Btu/ft^2-sec)	178.02	172.08
Δ/r_N	0.0617	0.0615
P_s (lb$_f$/ft^2)	25.498	25.541
T_s (°R)	19960.0	19620.0

Species Mass Fractions	ECW		NCW	
C_i	Shock	Wall	Shock	Wall
O	4.47-03	5.18-10	7.75-03	9.97-03
O_2	2.28-01	2.35-01	2.25-01	2.21-01
NO	2.05-03	5.81-05	3.28-03	4.68-03
N	3.52-04	1.29-21	4.52-04	4.09-04
NO^+	2.74-09	4.93-25	1.18-08	1.63-08
N_2	7.65-01	7.65-01	7.63-01	7.64-01

Additional Information:

r_N = 0.083333 ft

T_w = 1800.0 °R

ϵ = 0.1194 (Frozen Normal Shock Crossing)

Re_s = 19.40

TABLE 4

Integrated Skin-Friction and Pressure Drag Coefficients

	C_{D_p}	C_{D_f}
Nonequilibrium Outer Edge		
Equilibrium Catalytic Wall	0.114	0.0547
Noncatalytic Wall	0.114	0.0520
Equilibrium Outer Edge		
Equilibrium Catalytic Wall	0.114	0.0625
Noncatalytic Wall	0.114	0.0602
Frozen Outer Edge		
Equilibrium Catalytic Wall	0.114	0.0549
Noncatalytic Wall	0.114	0.0521

Conditions

AGARD Case B

$$C_D = \frac{\text{Drag Force}}{1/2\ \rho_\infty V_\infty^2 A_b}$$

where $A_b = 3.62206\ ft^2$ at $s/r_N = 50.0$

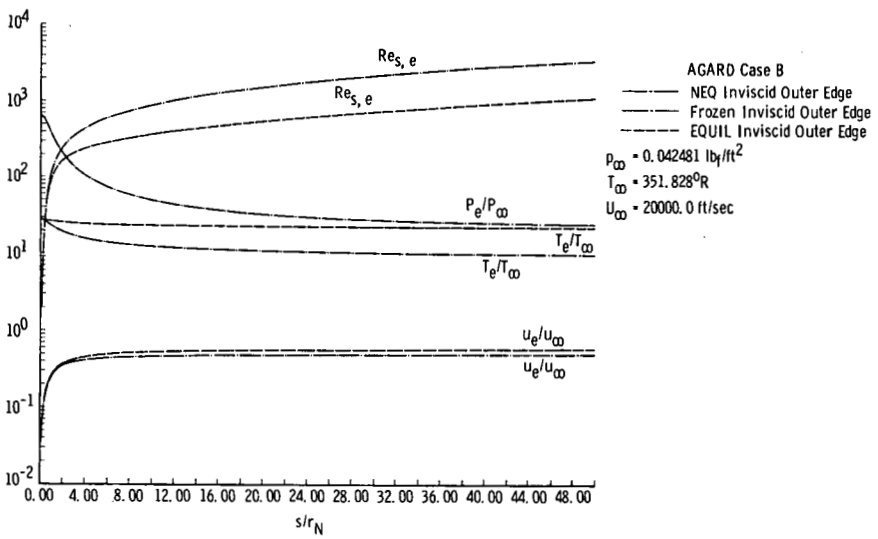

Fig. 1 Inviscid outer edge conditions

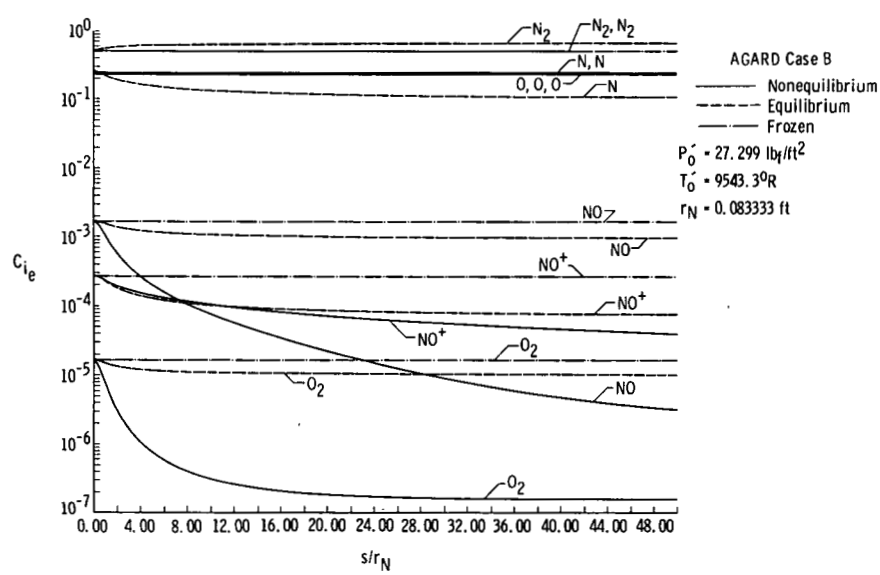

Fig. 2 Outer edge species distribution using inviscid streamtube expansion

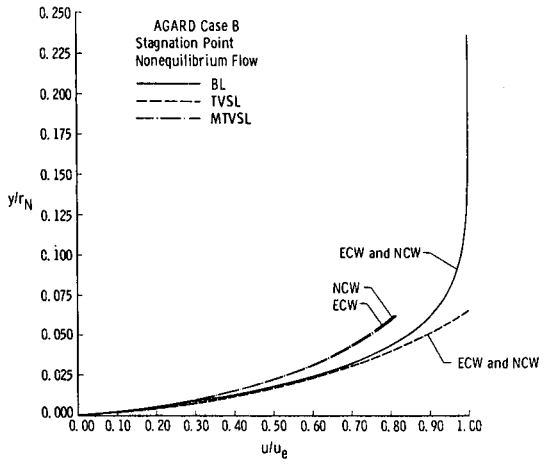

Fig. 3 Stagnation point velocity profiles

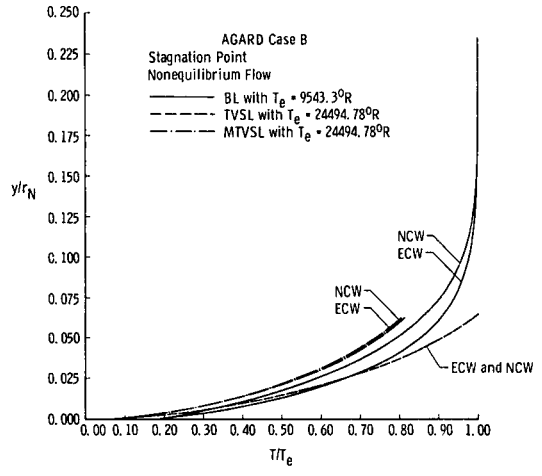

Fig. 4 Stagnation point temperature profiles

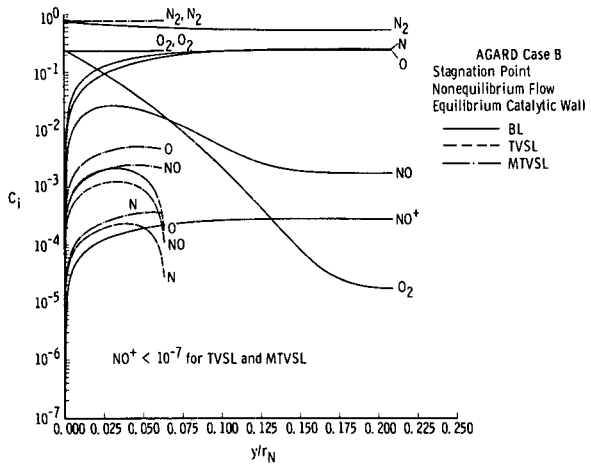

Fig. 5(a) Stagnation point species profiles

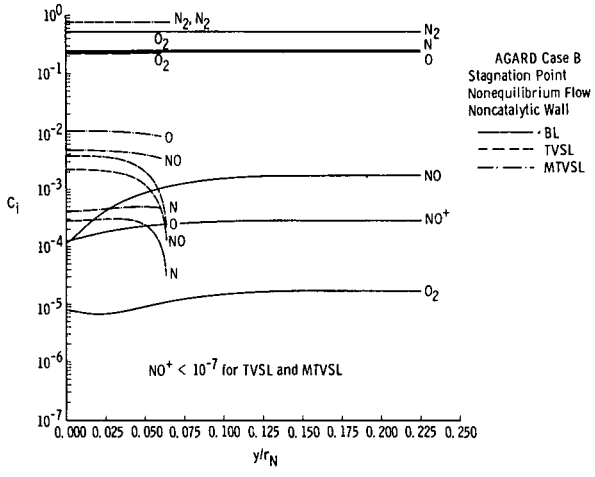

Figure 5(b)

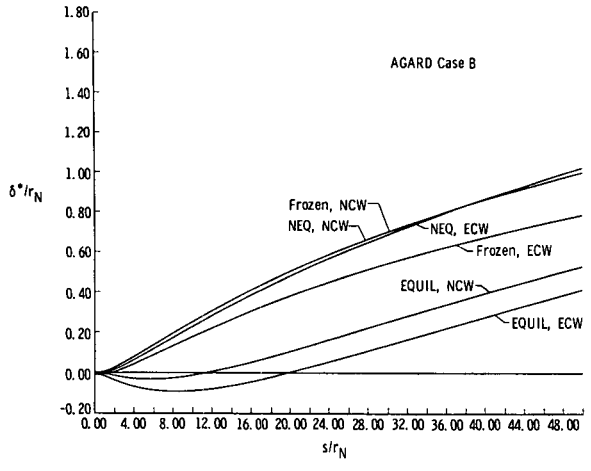

Fig. 6 Displacement thickness distribution

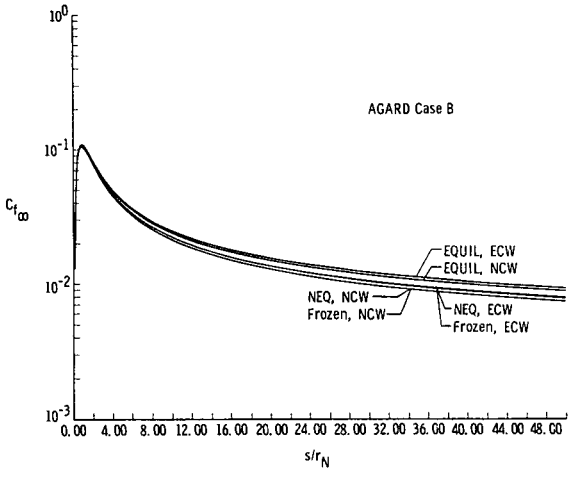

Fig. 7 Skin friction distribution

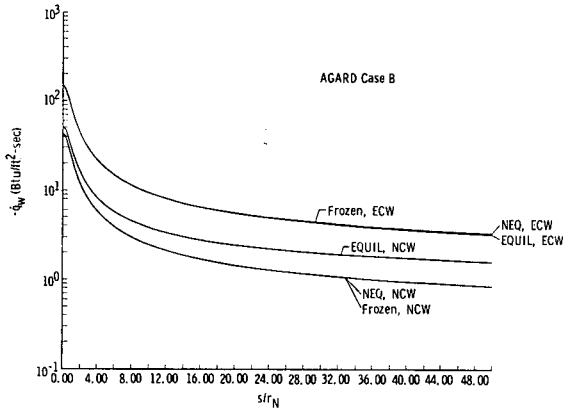

Fig.8 Dimensional surface heat transfer distribution

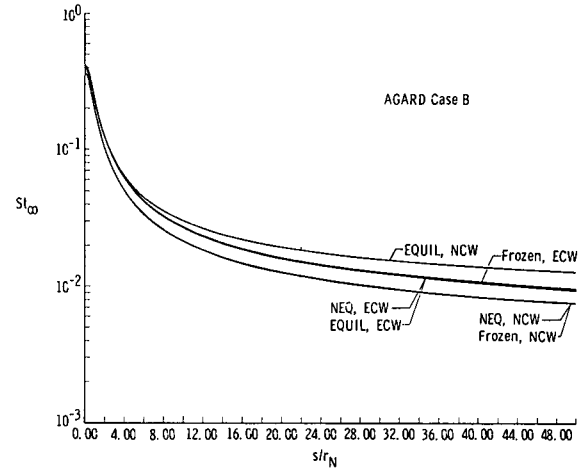

Fig.9 Stanton number distribution

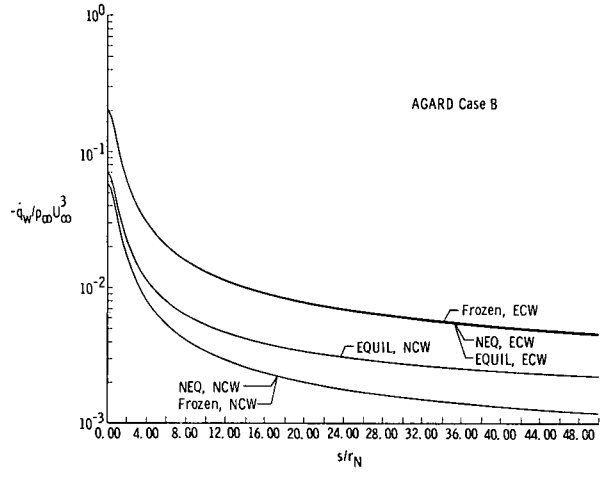

Fig.10 Surface heat transfer distribution

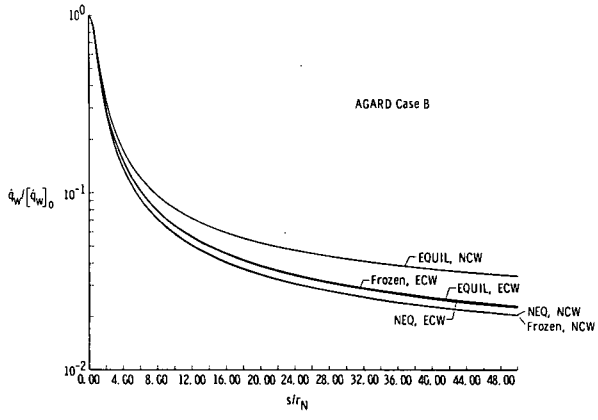

Fig.11 Surface heat transfer ratio distribution

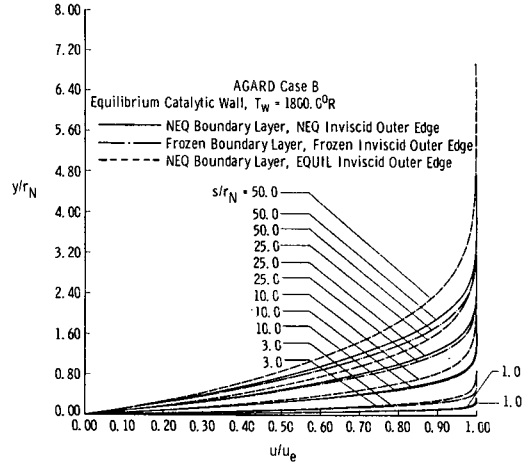

Fig.12(a) Boundary layer velocity profiles

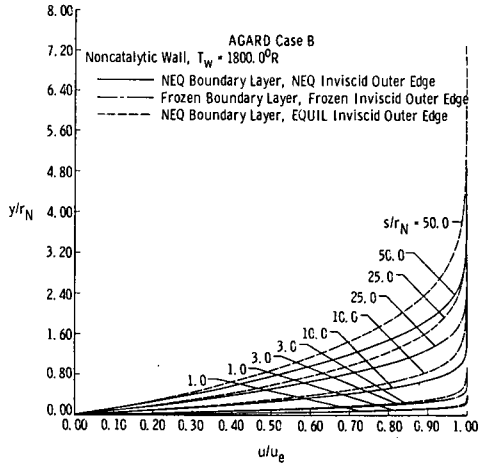

Figure 12(b)

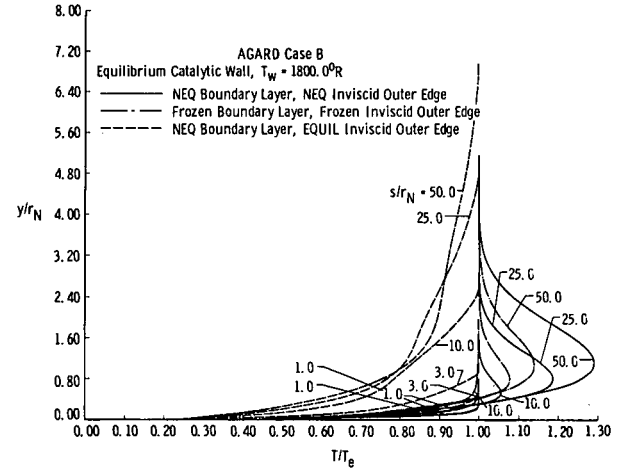

Fig. 13(a) Boundary layer temperature profiles

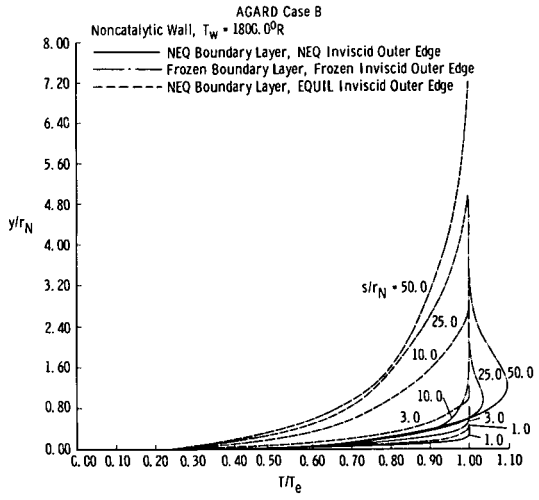

Figure 13(b)

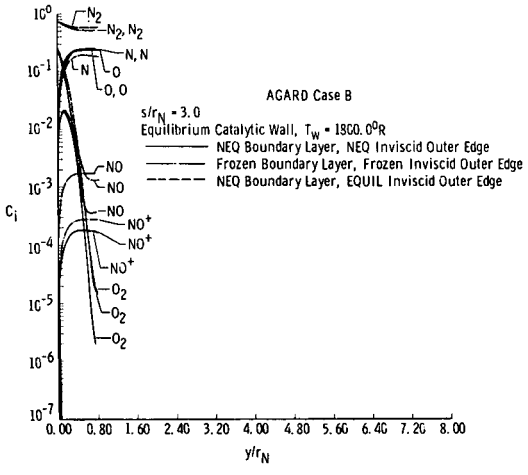

Fig. 14(a) Boundary layer species profiles

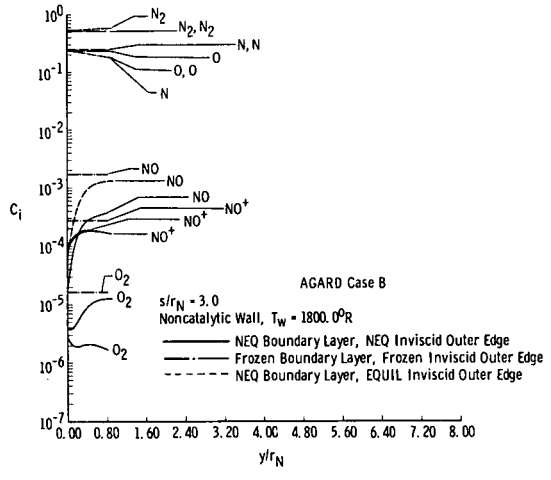

Figure 14(b)

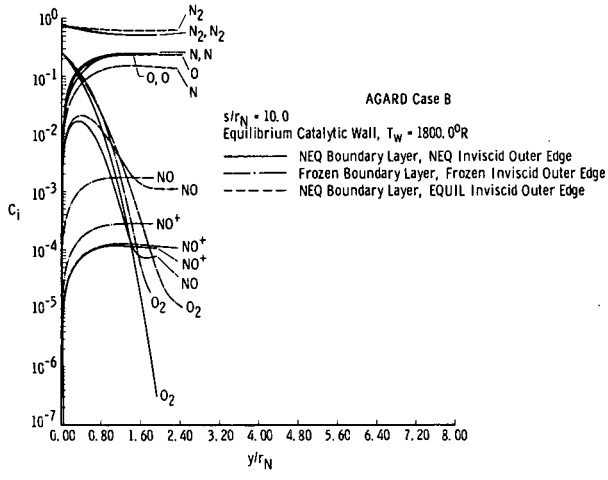

Figure 14(c)

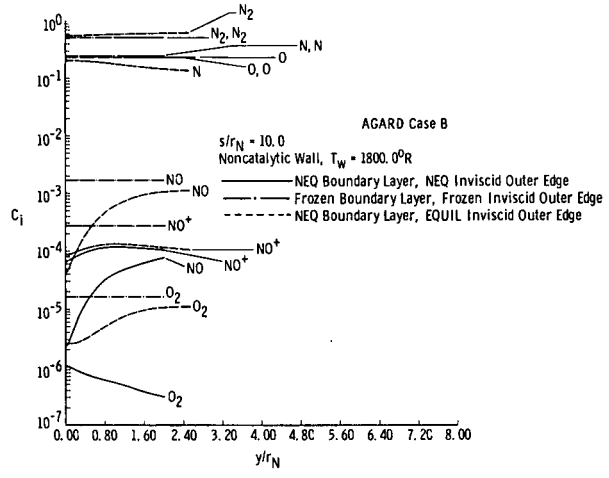

Figure 14(d)

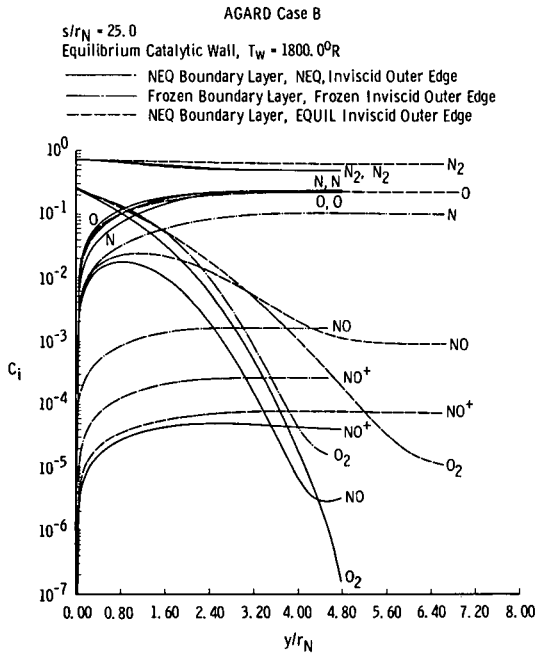

Figure 14(e)

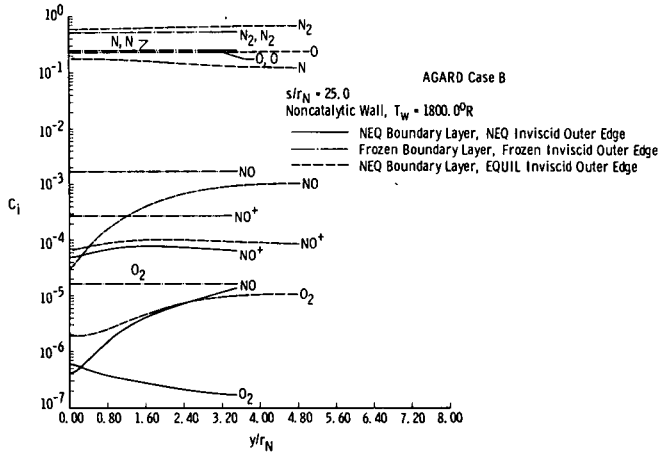

Figure 14(f)

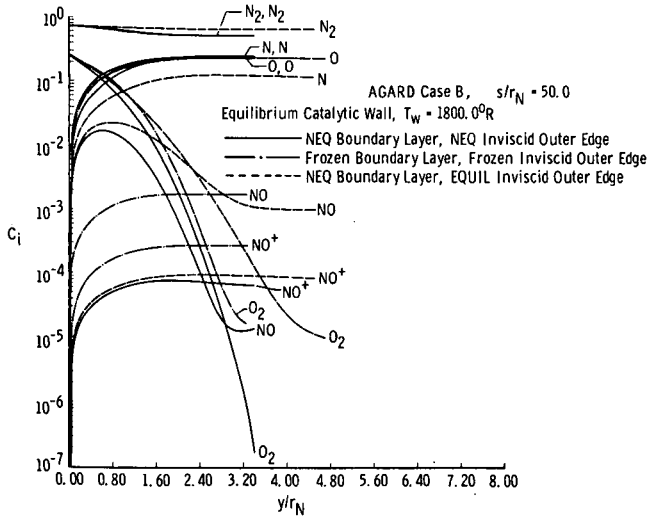

Figure 14(g)

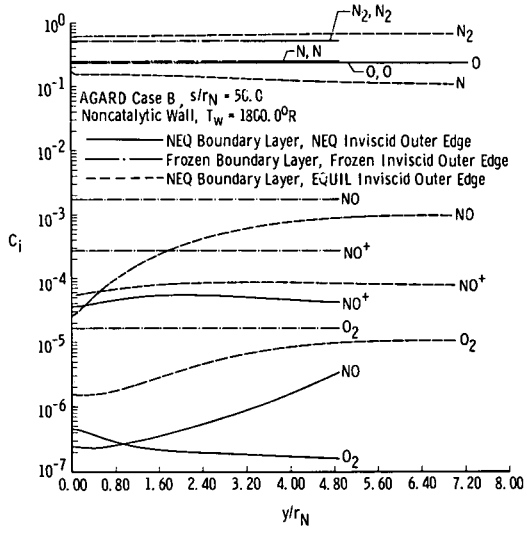

Figure 14(h)

COMPUTATION OF HIGHER-ORDER BOUNDARY-LAYER EFFECTS WITH A FIRST-ORDER TREATMENT AND COMPARISON WITH EXPERIMENTAL DATA

by

Clark H.Lewis

Professor, Aerospace Engineering,
Virginia Polytechnic Institute,
Blacksburg, Virginia

COMPUTATION OF HIGHER-ORDER BOUNDARY-LAYER EFFECTS WITH A FIRST-ORDER TREATMENT AND COMPARISON WITH EXPERIMENTAL DATA

by Clark H. Lewis*

SUMMARY

The effects of transverse curvature, shock generated external vorticity, boundary-layer displacement, and wall slip and temperature jump are considered as first-order boundary-layer effects. The classical boundary-layer equations were modified to include the higher-order effects, and flows over a 9-deg half-angle blunt cone were considered at M_∞ = 9 and 18. Comparisons are made with second-order theory and experimental data. Primary interest is given to predicting the higher-order effects on zero-lift drag and comparison with experimental data. Range of applicability of higher-order boundary-layer theory is indicated based upon the ability to predict zero-lift drag. Vorticity was the dominant higher-order effect, and the theory is most applicable to relatively short slender bodies. At very low Reynolds numbers, strong coupling of the higher-order effects was found to exist.

INTRODUCTION

Experimental data from wind tunnel tests have provided the incentive for a study of higher-order boundary-layer effects under nearly perfect gas conditions. Several years ago the strong influence of higher-order viscous effects was experimentally observed on the drag of slender cones at M_∞ = 10 to 20 [1]. Since that time a study of theoretical and numerical methods has been made to analyze and predict observed experimental trends. To date the best available theoretical models and numerical methods have not been successful in predicting the observed results over the entire ranges of Mach and Reynolds numbers experimentally studied.

The purpose of the present paper is to indicate the results of the application of first- and second-order boundary-layer theories to a sphere-cone for a range of Reynolds numbers at M_∞ = 9 and 18. The intent is to focus attention on some interesting results from the application of the theoretical models and methods, and the comparisons indicate where one might expect the theoretical to be applicable.

Lewis and Whitfield [1] presented some of the early work done in von Karman Gas Dynamics Facility (VKF) where they applied iterated inviscid-viscous flow field models to predict pressure and heat-transfer distributions and zero-lift drag of a 9-deg half-angle, spherically blunted cone at M_∞ = 9 and 18. In that work an inverse blunt body and characteristics solution for the inviscid outer flow was iterated with a first-order boundary-layer solution which included approximate transverse curvature terms. The blunt body and characteristics method used was due to Inouye, Rakich, and Lomax [2] and the boundary layer method of Clutter and Smith [3]. In many respects the results of the predictions of Lewis and Whitfield were in surprisingly good agreement with the experimental results since the effects of shock-generated external vorticity and slip and temperature jump were not considered and the effects of transverse curvature and displacement were only approximately treated.

Davis and Flügge-Lotz [4] considered second-order boundary-layer effects on hyperboloids, paraboloids, and spheres at infinite Mach number and ten, respectively. The theory of Van Dyke [5] was used with an implicit finite-difference scheme originally proposed by Flügge-Lotz and Blottner [6] for treating the classical first-order boundary-layer equations for two-dimensional flows. As will be shown in this paper, the theory of Van Dyke when coupled with the implicit finite-difference method of Davis and Flügge-Lotz gives a powerful tool for extending classical boundary-layer theory to lower Reynolds number.

In addition to the second-order treatment based on Van Dyke-Davis and Flügge-Lotz, a first-order treatment of vorticity, displacement, transverse curvature (TVC), and slip and temperature jump (STJ) is developed in the present paper based on a modification of the first-order boundary-layer method of Clutter and Smith. The treatment of vorticity is based on the suggestion of Hayes and Probstein [7] where the outer boundary condition is changed to account for an increase in velocity and a nonzero velocity gradient.

To emphasize some of the more interesting results obtained with the first- and second-order methods, only general descriptions of the methods will be made and attention will be focused on results such as skin-friction coefficients, and pressure and friction-drag coefficients. These data will then be compared with experimental data, and some general conclusions will be drawn.

HIGHER-ORDER BOUNDARY-LAYER THEORY

Second-Order Effects

Since the second-order boundary-layer theory has been treated in detail elsewhere by Van Dyke [5], Davis and Flügge-Lotz [4], and Adams [10] and Marchand, Lewis and Davis [11], only those numerical methods which have been recently developed will be discussed in detail. Those interested in the second-order theory are referred to the above papers for a detailed presentation of the theory and solution method used to solve the second-order boundary-layer problem. Van Dyke [12] has recently surveyed higher-order boundary-layer theory.

The second-order effects of external vorticity, displacement, transverse and longitudinal curvatures, and slip and temperature jump were identified by Van Dyke [5] and a method of solution developed by Davis and Flügge-Lotz [4]. The division of effects due to vorticity and displacement is arbitrary. From Van Dyke's second-order theory [5], the second-order inviscid outer-flow pressure gradient is

$$P_{2x} = -R_1(U_1U_2)_x - R_2U_1U_{1x} + r_w^j R_1^2 V_2(T_1S_1' - H_1') \qquad (1)$$

*Professor, Aerospace Engineering, Virginia Polytechnic Institute, Blacksburg, Virginia.

where prime denotes derivatives with respect to the stream function. The interaction between displacement and vorticity arises through the last term in Eq. (1). The inviscid vorticity is $\Omega_1 = r_w{}^j R_1 (T_1 S_1' - H_1')$ at y = 0. Davis and Flügge-Lotz obtained the expression $V_2 = (r_w{}^j R_1 U_1 \delta^*)_x / r_w{}^j R_1$ which shows the dependence of V_2 on the displacement thickness δ^*. Van Dyke called the effect "displacement speed" if the last term in Eq. (1) is considered as a vorticity effect; it was called "displacement pressure" if the term is treated as a displacement effect. The resulting sum of both effects is independent of the two classifications; however, it is important to note the coupling between the two effects and to consider the sum of both effects since the resulting separate effects are strongly affected by the treatment (see Adams [10] and Lewis [13]).

In what is presented in this paper and denoted as second-order displacement effect, the displacement pressure notation applies. In general, this division of effects reduces the vorticity effect and correspondingly increases the displacement effect.

The second-order contribution due to longitudinal curvature was approximately computed from the second-order theory and found to be very small, and thus is not considered further [11]. The effect of the discontinuity in surface curvature is important for this small effect, but a more accurate numerical treatment does not appear to be warranted.

The second-order effect due to slip and temperature jump follows Van Dyke.

FIRST-ORDER EFFECTS

Transverse Curvature

The original treatment of Clutter and Smith [3] included an error in the transverse curvature terms arising from the transformations and evaluation of the stream function. The error would be difficult to correct without a reformulation in terms of a more appropriate set of transformations. In the revised version of the report, Clutter and Smith termed the transverse curvature as approximate (which indeed it must be), and the degree of approximation was never determined to this writer's knowledge. Because of the extensive use which has been made of the various forms of the Douglas programs, some comparisons will be given here to illustrate the degree of approximation which one might expect from using the so-called "approximate" Clutter and Smith formulation.

A new and correct formulation of the first-order transverse curvature effect has recently been given by Jaffe, Lind, and Smith [9]. In this more recent work, the Levy-Lees and Probstein and Elliott transformations were combined so that the resulting transformed momentum and energy-equations are quite similar in form to the Clutter and Smith equations with additional terms. Attention is drawn to this later work since in addition to correction of the error in transverse curvature certain other difficulties and deficiencies with the original Clutter and Smith treatment have been eliminated, and the new method is capable of treating nonreacting binary gas boundary layers which are of considerable current interest.

Slip and Temperature Jump

The first-order slip and temperature jump boundary conditions are given in Appendix A.

Displacement Effects

The effects of displacement were based upon the now standard approach [1, 11, 13, 17]. The geometric sphere-cone was perturbed by adding the boundary-layer displacement thickness. The resulting "effective" body was curve fitted, and the inviscid blunt body and characteristics solutions were obtained for the "effective" body geometry [11, 13]. In this paper, the inviscid-viscous flow field was not iterated; a procedure consistent with second-order boundary-layer theory [13]. The significant difference between the first- and second-order treatments is in the normal pressure gradient. In the second-order theory, the second-order normal momentum equation was used to extrapolate the pressure along the effective wall to the geometric wall or body surface. Consistent with the original first-order boundary-layer theory, the normal component of momentum was not considered in the first-order treatment, and the pressure was assumed constant throughout the boundary-layer normal to the surface. Therefore, in the first-order treatment the perturbed inviscid outer flow pressure is impressed upon the first-order boundary layer as the edge pressure.

The comparative effects on the first- and second-order solutions are as follows:

First, over the nose where the longitudinal curvature $\kappa = 1$, the pressure on the surface may be either increased or decreased from the effective wall value, depending on whether the displacement thickness is negative (highly cooled wall) or positive. Over the conical afterbody where $\kappa = 0$, the first- and second-order treatments yield the same surface pressure, assuming equivalent displacement thicknesses. However, because of the effects of the inviscid vorticity along the wall, the velocity at the surface is always less over the conical afterbody based upon the second-order theory. This effect due to inviscid vorticity is *independent* of inclusion or exclusion of the vorticity effect in the second-order boundary-layer treatment.

Secondly, the first-order displacement treatment always produces an increase in friction and pressure drags. The second-order effects may be either positive or negative, depending on the sign and magnitude of displacement thickness and longitudinal curvature and that of inviscid external vorticity.

These two major factors can cause the first- and second-order displacement treatments to yield substantially different effects on such global quantities as drag and total heat transfer; however, for the length of the cone and other conditions treated here, the first- and second-order treatments predicted induced-drag effects in good agreement.

External Vorticity

Hayes and Probstein [7] defined a vorticity interaction parameter as

$$\Omega = \frac{\text{vorticity at the outer edge of boundary layer}}{\text{average vorticity across the boundary layer}}$$

Using the expressions derived by Van Dyke [5] for the vorticity at the outer edge and the Clutter and Smith transformations, it is shown in Appendix B that the outer boundary condition for the first-order momentum equation is $f'(\infty) = 1 + \Omega \int_0^{\eta_\infty} (\rho_e/\rho) d\eta$. The Clutter and Smith method was modified to permit the use of this voriticty interaction boundary condition [13].

Because of the implicit relationship between the inviscid entropy layer and the boundary layer, a vorticity interaction model is only applicable where the entropy layer is thick with respect to the boundary layer (such as the nose region of a blunt body). For long slender axisymmetric bodies, the entropy layer becomes thin with respect to the boundary layer and some adjustment should be made in the outer boundary condition on the boundary layer. Some models have been proposed which permit the boundary layer to "swallow" the entropy layer and thereby reduce the edge velocity and its gradient from that consistent with second-order theory. This model, however, is highly approximate since some physical boundary-layer edge and its corresponding stream function are required to determine the outer boundary condition. Also, it is not uncommon to find at low Reynolds numbers that the first-order boundary-layer thickness is greater than the inviscid shock-layer thickness (see, e.g. Lewis and Whitfield [1]). Under these conditions it is not clear how such matching is to be accomplished.

NUMERICAL RESULTS AND DISCUSSION

The results of the first-order treatment of higher-order boundary-layer effects will first be tested by comparison with results from the second-order theory [5,4,10,11]. Comparisons of transverse curvature, vorticity, slip and temperature jump (as a single effect), and displacement will be presented. A sensitive quantity for such comparisons is the effect on zero-lift drag, and this will be used primarily for comparisons of numerical results and experimental data. The effects of viscosity law are also easily shown by comparison of second-order solutions in physical variables using a square-root viscosity law and solutions in transformed Levy-Lees variables using the Sutherland viscosity law. All solutions used perfect gas ($\gamma = 1.4$), constant Prandtl number ($Pr = 0.71$), uniform wall temperature ($T_w/T_o = 0.2$ at $M_\infty = 9$ and 0.066 at $M_\infty = 18$), and identical pressure distributions from ideal-gas blunt body and characteristics solutions at $M_\infty = 9$ or 18.

The second-order solutions for each vorticity and displacement based upon displacement pressure treatment were found to be *nonunique*. The solutions were affected by both Δy or $\Delta\eta$ step sizes and η_∞ or its equivalent in physical variables. It has been shown, however, that the sum of both displacement and vorticity was unique and was equal to the displacement speed treatment of the sum of both effects [10]. Since the sum of the two effects is unique, no loss in accuracy is involved when comparisons are made with their combined effects.

Transverse Curvature Effects

A comparison of the transverse-curvature-induced friction drag at $M_\infty = 18$ is shown in Fig. 1. The differences are small between second-order solutions with different viscosity laws; however, the approximate treatment of Clutter and Smith predicts an increment about 30 percent less. This is a significant error, and the Clutter and Smith treatment cannot be recommended. As noted earlier, TVC was correctly treated by Jaffe, Lind, and Smith [9].

Vorticity Interaction Effects

Figure 2 shows the local skin-friction coefficient predicted by first- and second-order methods. Good agreement exists for about 8.5 nose radii from the stagnation point. Beyond that point the first-order prediction increases whereas the second-order result remains approximately constant to the base of the cone ($x = 16.4$).

The effects of both Δx and $\Delta\eta$ step sizes were investigated for the first-order solutions. It was found that the solutions were sensitive to $\Delta\eta$ but insensitive to Δx step sizes. This is explained as follows: First, the transformations used by Clutter and Smith are such that without vorticity effects the classical boundary layer was substantially reduced from $\eta_\infty \simeq 6$ at $x = 0$ to $\eta_\infty \simeq 2$ over much of the conical afterbody (for longer bodies or bodies with more favorable pressure gradient, $\eta_\infty < 1$ was not uncommon). The variation in boundary-layer thickness is less in the Levy-Lees transformed plane than in either the physical or Clutter and Smith transformed plane. Therefore, for classical boundary-layer solutions, the Clutter and Smith transformation is not optimum for bodies with strong favorable pressure gradients. Secondly, and more importantly, the extent of the first-order boundary layer with vorticity interaction is limited by a line of maximum velocity $f'_{max} = 1/(1 - h_e/H_e)^{1/2}$. Along this line $T_i = 0$ and $\rho_i \to \infty$. This limiting velocity, coupled with the increasing $f'(x)$ at constant η, substantially reduced η_∞ below the allowed classical solution value [13]. It was therefore necessary to occasionally reduce the $\Delta\eta$ step size as the solution proceeded along the body. The data normal to the surface were interpolated so that a minimum of 200 η points were used to integrate the momentum and energy equations. The solutions were accepted when similar calculations were made with reduced step size and no significant changes were observed in f_w'' and g_w'. Similar reduction of Δx-stepsize significantly increased machine time without affecting the solution. Examination of the $f'(\eta)$ profiles showed they asymptotically approached a linear variation as $\eta \to \eta_\infty$ [13].

The good agreement in C_{f_∞} for $x < 8.5$ is gratifying and might have been expected; however, to the author's knowledge, this is the first time the essential agreement between first- and second-order solutions has been demonstrated.

Displacement Effects

First- and second-order displacement-induced pressure and friction-drag increments are shown on Fig. 3. Perturbed inviscid outer-flow solutions were obtained for four values of ε at $M_\infty = 9$ and three values at $M_\infty = 18$. The two predictions for displacement-induced pressure drag differ only by the effect of the normal pressure gradient over the nose; the effect is included in the second-order but not in the first-order treatment.

The differences between the two treatments of displacement-induced friction drag are larger, and the results are more interesting. In the first-order treatment, only the effect of displacement of the inviscid outer flow-field pressure is included. In the second-order solutions, however, the effects of inviscid vorticity on the outer edge velocity and temperature are also present.

Caution must be used when trying to generalize the results shown in Fig. 3. The second-order results for displacement-induced pressure and friction-drag increments were not simply linearly and quadratically dependent, respectively, on ε. It is interesting to note, however, that the first-order friction-drag results were quadratically dependent. For other bodies under different conditions, negative second-order displacement-induced friction drag has been found. The effects of geometry (both surface slope and length), wall-to-stagnation temperature ratio, and viscosity law used had the strongest influence on second-order wall shear-stress distribution. For the conditions treated here, the effects of wall-to-stagnation temperature ratio caused small differences in the induced-drag increments for both first- and second-order treatments.

Slip and Temperature Jump Effects

The slip-and-temperature-jump-induced friction-drag results are shown in Fig. 4. At the highly cooled wall conditions at $M_\infty = 18$, the second-order solution in physical variables was Δy-step size dependent, and we were unable to obtain an acceptable solution for this effect at these conditions using physical variables [11]. In either the Clutter and Smith or Levy-Lees transformed planes, the highly cooled wall presented no difficulty, and stable solutions were obtained with reasonable ($\Delta\eta = 0.025$ or 0.05) step sizes. Both first- and second-order treatments evaluated the properties in the slip velocity and temperature jump consistent with those theories. The differences between first- and second-order treatments are large for this separate effect. However, since this drag component is small compared with other second-order effects, the difference between the two treatments of this separate effect was not an important influence on the total drag prediction for $\varepsilon < 0.2$.

Coupled Effects

The first-order treatment of higher-order effects on skin-friction coefficient at $M_\infty = 9$ is shown in Fig. 5. The results are shown for a large value of the expansion parameter $\varepsilon = 0.533$ in order to magnify some of the effects and clearly establish the strong coupling influence between certain effects.

The individual effects of transverse curvature (TVC), vorticity (vort), displacement (disp), and slip and temperature jump (STJ) on the skin-friction coefficient are seen by comparison with the classical first-order axisymmetric result. The bumps in the curves including displacement were caused by a displacement-induced compression region over the effective body and the resulting displaced inviscid outer flow. Although at the conditions considered in Fig. 5 each separate higher-order effect had a significant influence on the skin-friction distribution, the separate effect of vorticity was clearly dominant. The strong effect of coupling displacement and vorticity can be seen by comparison of the results of these combined effects with the sum of the independent effects. We see that coupling displacement with vorticity roughly doubled the vorticity-induced skin-friction coefficient. The displacement-induced pressure strongly affected the vorticity index Ω which in turn controlled the vorticity effect. Coupling TVC with displacement and vorticity increased the coupled effect of the latter two by about the increment due to transverse-curvature-induced skin friction only.

The most surprising result was found when slip and temperature jump effects were coupled with displacement, vorticity, and transverse curvature. Near the end of the body the effects of coupling STJ were larger than the combined effects of displacement and transverse curvature! The trends clearly indicate if the body were longer the effects of slip and temperature jump would have offset not only the effects of displacement and transverse curvature but vorticity as well. Elsewhere [13] it was shown that $f'(\eta = 0) \propto f''(\eta = 0)$. Vorticity increased f_w'' which in turn increased the slip velocity $f'(\eta = 0)$ which reduced the velocity gradient $f''(\eta = 0)$. This coupling between vorticity and slip can be seen by comparison of the almost linear increase in the vorticity-induced skin-friction coefficient with the almost linear decrease in the combined total effects including STJ.

The results for the coupled higher-order effects are clearly not linearly independent as are the second-order effects of transverse and longitudinal curvatures, vorticity, and slip and temperature jump according to Van Dyke's theory [5]. The obvious result here is that small separate higher-order effects can have a strong influence when coupled with other higher-order effects, and a simple linear combination of each first-order effect is not justified and can lead to erroneous results.

Range of Applicability

The range of applicability of the first- and second-order theories must finally be determined by comparisons with experimental data; however, it is instructive to consider the range of applicability predicted from the numerical results.

The first-order boundary layer-to-shock layer thickness ratio over the cone at $M_\infty = 18$ is shown in Fig. 6. The boundary-layer thickness is defined to be the normal distance from the wall where $f' = u/u_e = 0.995$ and y_{shock} is the first-order (non-perturbed) inviscid shock-layer thickness from the blunt body and

characteristics solution. The variation of δ/y_{shock} is small over the entire body (see Fig. 6), and a region is indicated between $\varepsilon = 0.11$ and 0.16 where $\delta/y_{shock} \approx 1$. Beyond this region the shock-layer was fully viscous and boundary-layer theory is not applicable.

Since the boundary-layer thickness was arbitrarily defined, the effect of the definition of the boundary-layer thickness on δ/y_{shock} was investigated and found to have a negligible influence on the results shown in Fig. 6 [13].

COMPARISON OF NUMERICAL RESULTS AND EXPERIMENTAL DATA

We now wish to compare the results of the first- and second-order treatments with some available experimental data on pressure and heat-transfer distributions and zero-lift drag of a sphere-cone at $M_\infty = 9$ and 18.

Pressure Distributions

The displacement-induced pressure over a spherically blunted cone at $M_\infty \approx 20$ is shown in Fig. 7. The first-order iterated results of Lewis and Whitfield [1] and the second-order results using Van Dyke-Davis and Flügge-Lotz at $M_\infty = 18$ are compared with the experimental data of Lewis [14] and Griffith and Lewis [15]. It is obvious that the trends of the experimental results are not predicted by either first- or second-order treatments. The nonlinear character of the first-order results of Lewis and Whitfield is due to the effects of iterating the inviscid outer flow and the viscous boundary-layer flow fields. The effect of this iteration is always to reduce the displacement-induced pressure.

The poor agreement between numerical results and experimental pressure data is not understood. The experimental data lie in a range where the second-order theory should be applicable, and the errors due to approximations in the numerical treatments and experimental scatter are believed to be small deviations.

The lack of agreement between theories and experiment shown on Fig. 7 should be contrasted with the good agreement found by Pappas and Lee [16] who compared their experimental data with predictions by Lewis, Adams, and Gilley [17] for the displacement-induced pressure distributions over a spherically blunted cone at low density hypersonic conditions with and without surface mass transfer. In general, the agreement between predicted pressure and heat-transfer distributions and experimental data were good even for moderately strong blowing rates [16].

Heat-Transfer Distribution

Fig. 8 shows a comparison of first- and second-order heat transfer to a sphere-cone at $M_\infty \approx 18$. In contrast with the pressure data comparisons, the second-order heat-transfer results are in excellent agreement with the experimental data of Griffith and Lewis [15]. Again predictions by Lewis, Adams and Gilley [17] using procedures identical to those used in the present paper but including iteration of the inviscid-viscous flow fields were in good agreement with the experimental heat-transfer data of Pappas and Lee [16].

Zero-Lift Drag

The final and most instructive comparisons between first- and second-order numerical results and experimental data are given in Fig. 9 and 10. The total drag predicted by the two treatments is compared with the experimental data of Whitfield and Griffith [18]. For $M_\infty \approx 18$ and $\varepsilon < 0.15$ we find good agreement between numerical results and the available experimental data. For $\varepsilon > 0.2$ the agreement is poor. If we recall that in the second-order theory [5] it was assumed that $\varepsilon \ll 1$, one should expect that as ε increases at some value the theory will no longer be applicable. For these conditions, this point appears to be near $\varepsilon = 0.15$. From this comparison the range of applicability of the theory is consistent with the range predicted from consideration of boundary layer-to-shock layer thickness ratio, δ/y_{shock} (cf. Fig. 6).

The previous first-order results of Lewis and Whitfield [1] are also shown for comparison. The apparently good agreement is simply fortuitous since only approximate transverse curvature (Clutter and Smith) and displacement (iterated inviscid-viscous flow fields) were included. The comparisons of transverse-curvature-induced friction drag showed that the approximate Clutter and Smith treatment led to an error of about 30 percent in that component. Also, iteration of the inviscid-viscous flow fields reduced the displacement-induced pressure and friction drag. In a first-order sense, it can be argued that iteration is allowable until there is negligible change in $P(x)$. The fact remains, however, that in earlier work a sizable error existed in the transverse curvature term and the important contribution of external vorticity was not considered.

The comparison of drag data at $M_\infty \approx 9$ is shown in Fig. 10. Here the experimental data were in the range $\varepsilon = 0.26$ to 0.54, and for this range, the first- and second-order results substantially overpredicted the zero-lift drag. Again the prediction of Lewis and Whitifield was in fortuitously good agreement with the experimental data.

Because of the much lower Reynolds number for much of the $M_\infty \approx 9$ data, the treatment of the outer flow as inviscid with a simple Rankine-Hugoniot shock wave is highly suspect. Van Dyke [5] notes that third-order boundary-layer theory requires treating the outer flow as viscous rather than inviscid which is consistent with the second-order theory. The substantial disagreement between second-order results and experiment indicates the need for substantial improvement in the theoretical model.

CONCLUSIONS

Based upon a comparison of first- and second-order treatments of transverse curvature, vorticity, displacement, and slip and temperature jump, a comparison of numerical results with experimental data, the following conclusions are drawn: (i) The approximate treatment of transverse curvature by Clutter and Smith led to errors in wall shear stress which in turn led to errors in transverse-curvature-induced friction drag

of about 30 percent. (ii) The first- and second-order treatments of vorticity interaction were in substantial agreement over the forward half of the body, and the first-order treatment predicted higher wall shear and thus higher total vorticity-induced friction drag than the second-order results gave. Also, a coupling between entropy and boundary layers is needed in the first-order treatment for more realistic predictions of wall shear stress and displacement effects. (iii) The first- and second-order treatments of slip and temperature jump led to significant differences in slip velocity and temperature jump but small differences in local (total) shear stress. The differences in the friction-drag predictions for the two treatments were significant for this separate effect, but the effect on the linear combination of effects was not large. A strong effect of first-order slip and temperature jump was observed when coupled with all other higher-order effects at very low Reynolds number. However, in the range of applicability of the theory, the effects of coupling were small. (iv) The first- and second-order treatments predicted substantially the same displacement-induced friction drag. This difference was attributed to the effects of normal pressure gradient and external vorticity on the second-order outer-edge velocity and temperature since these effects were neglected in the first-order treatment. (v) Both first- and second-order treatments substantially overpredicted the experimentally measured pressure distribution for a sphere-cone at $M_\infty \simeq 18$. These differences are not understood since the comparisons were made under conditions where the second-order theory should be applicable. More extensive experimental data are needed to clearly establish the differences. (vi) The agreement between second-order predictions of Stanton number and experimental data was excellent for $M_\infty \simeq 18$. (vii) For $M_\infty \simeq 18$ and $\varepsilon < 0.15$, good agreement was found between second-order prediction of zero-lift drag and experimental results. For $\varepsilon > 0.2$ at both $M_\infty \simeq 9$ and 18, the second-order treatment substantially overpredicted the total drag. Higher-order effects are needed to improve agreement between theory and experiment. (viii) For the conditions treated, the range of applicability of first- and second-order boundary-layer theories as predicted theoretically ($\delta/y_{shock} \lesssim 1$) and from comparison with experimental zero-lift drag data was found to be $\varepsilon < 0.2$.

In summary, it has been shown that except for the pressure data in the expected range of applicability of the second-order theory ($\varepsilon << 1$), first- and second-order treatments are in substantial agreement with the experimental data. For $\varepsilon > 0.2$, the predictions from the numerical treatments were substantially in error. From these comparisons it is clear that higher-order boundary-layer treatments are not the correct approach. A theoretical model is needed which properly takes into account all higher-order effects such as viscous "external" flow and the effects of transport properties on the shock wave.

ACKNOWLEDGEMENT

This work was partially supported by the Arnold Engineering Development Center (AEDC) under contract F40600-69-C-0001 with ARO, Inc. The author acknowledges the assistance of J. C. Adams and E. O. Marchand who furnished the second-order boundary-layer solutions.

REFERENCES

[1] Lewis, C.H. and Whitfield, J.D. "Theoretical and Experimental Studies of Hypersonic Viscous Effects," Recent Developments in Boundary Layer Research, AGARD Specialists' Meeting, Naples, Italy, May 1965, AGARDograph 97, Part III; also AEDC-TR-65-100, May 1965, Arnold Engineering Development Center.

[2] Inouye, M., Rakich, J.V. and Lomax, H. "A Description of Numerical Methods and Computer Programs for Two-Dimensional and Axisymmetric Supersonic Flow over Blunt-Nosed and Flared Bodies," NASA TN D-2970, August 1965, Washington, D.C.

[3] Clutter, D.W. and Smith, A.M.O., "Solution of the General Boundary-Layer Equations for Compressible Laminar Flow, Including Transverse Curvature," Douglas Aircraft Company Report LB 31088, February 1963 and revised October 1964, Long Beach, California.

[4] Davis, R.T. and Flügge-Lotz, I., "Laminar Compressible Flow Past Axisymmetric Blunt Bodies (Results of a Second-Order Theory)," Stanford University Report 143, December 1963, Stanford, California.

[5] Van Dyke, M. "Second-Order Compressible Boundary-Layer Theory with Application to Blunt Bodies in Hypersonic Flow," Hypersonic Flow Research, ed. F. R. Riddell, Academic Press, New York, 1962, pp. 37-76.

[6] Flügge-Lotz, I. and Blottner, F.G. "Computation of the Compressible Laminar Boundary-Layer Flow Including Displacement-Thickness Interaction Using Finite-Difference Methods," Stanford University Report No. 131, January 1962, Stanford, California.

[7] Hayes, W.D. and Probstein, R.F. Hypersonic Flow Theory, Academic Press, New York, 1959, Chapter 9, Section 6, pp. 370f.

[8] Van Dyke, M. "Higher Approximations in Boundary-Layer Theory, Part 1," Journal of Fluid Mechanics, Vol. 14, 161-177, 1962.

[9] Jaffe, N.A., Lind, R.C., and Smith, A.M.O., "Solution to the Binary Diffusion Laminar Boundary Layer Equations Including the Effect of Second-Order Transverse Curvature," Douglas Aircraft Company Report LB 32613, January 1966; also AIAA Journal, Vol. 5, No. 9, pp. 1563-1569, September 1967.

[10] Adams, J.C., "Higher-Order Boundary-Layer Effects on Analytic Bodies of Revolution," AEDC-TR-68-57, April 1968, Arnold Engineering Development Center, Tennessee.

[11] Marchand, E.O., Lewis, C.H., and Davis, R.T., "Second-Order Boundary-Layer Effects on a Slender Blunt Cone at Hypersonic Conditions," AIAA Paper 68-54, January 1968.

[12] Van Dyke, M., "Higher-Order Boundary-Layer Theory," Annual Review of Fluid Mechanics, Vol. 1, ed. by W. R. Sears and M. Van Dyke, Annual Reviews, Inc., Palo Alto, California, 1969, pp. 265-292.

[13] Lewis, C.H., "Comparison of a First-Order Treatment of Higher-Order Boundary-Layer Effects with Second-Order Theory and Experimental Data," Ph.D. Dissertation, University of Tennessee, June 1968; also AEDC-TR-68-148, Arnold Engineering Development Center, Tennessee.

[14] Lewis, C.H., "Pressure Distribution and Shock Shape Over Blunted Slender Cones at Mach Numbers from 16 to 19," AEDC-TN-61-81, August 1961, Arnold Engineering Development Center, Tennessee.

[15] Griffith, B.J. and Lewis, C.H., "Laminar Heat Transfer to Spherically Blunted Cones at Hypersonic Conditions," AIAA Journal, Vol. 2, No. 3, March 1964, pp. 438-444.

[16] Pappas, C.C. and Lee, G., "Effects of Mass Addition of Various Gases on the Heat Transfer and Surface Pressures on a Blunt Cone in Hypersonic Flow," AIAA Paper 69-716, June 1969.

[17] Lewis, C.H., Adams, J.C. and Gilley, G.E., "Effects of Mass Transfer and Chemical Nonequilibrium on Slender Blunted Cone Pressure and Heat-Transfer Distribution at $M_\infty = 13.2$," AEDC-TR-68-214, November 1968, Arnold Engineering Development Center, Tennessee.

[18] Whitfield, J.D. and Griffith, B.J., "Hypersonic Viscous Drag Effects on Blunt Slender Cones," AIAA Journal, Vol. 2, No. 10, October 1964, pp. 1714-1722 and "Viscous Drag Effects on Slender Cones in Low-Density Hypersonic Flow," AIAA Journal, Vol. 3, No. 6, June 1965, pp. 1165-1166.

APPENDIX A

FIRST-ORDER SLIP AND TEMPERATURE JUMP BOUNDARY CONDITIONS

For second-order boundary-layer theory, Van Dyke [5] shows that the slip-flow boundary conditions are

$$u(0) = \mu/p(\pi RT/2)^{1/2}(\partial u/\partial y)_w$$

$$T(0) = T_w + (15/8)\ \mu/p(\pi RT/2)^{1/2}(\partial T/\partial y)_w$$

when the billiard-ball model is used to evaluate the coefficients.

Transforming the equations to the x,η-plane and expressing in terms of convenient variables for inclusion in the Clutter and Smith numerical scheme gives

$$f'(\eta=0) = C(\rho_*/\rho)F_s f''(\eta=0)$$

$$h(\eta=0) = h_w + (15/8)C(\rho_*/\rho)F_s\ \partial h/\partial\eta$$

where

$$F_s = [\pi(\gamma/\gamma-1)(u_*^2/2h_{ref})(h_{ref}/h_w)(u_e/u_*)1/Re_*)1/x]^{1/2}$$

Here, as elsewhere, subscript w denotes properties evaluated at the no-slip wall conditions, and all other properties are evaluated at the slip temperature $T(\eta = 0)$. Thus, the boundary conditions must be found by iteration. This poses no problems for inclusion within the Clutter and Smith iterative solution method for the coupled momentum and energy equations. Moreover, no problems were experienced with numerical stability or significantly changing rate of convergence of the momentum and energy equation iteration loop.

APPENDIX B

FIRST-ORDER VORTICITY BOUNDARY CONDITIONS

The first-order momentum and energy equations are

$$1/C_*(1/r)(\partial/\partial\eta(Crf'')) + P[(\rho_e/\rho) - f'^2] + \left[\frac{P+1}{2} + R\right] ff'' - x[f'\partial f'/\partial x - f''\partial f/\partial x] = 0$$

and

$$\frac{1}{C_*}\frac{1}{r}\frac{\partial}{\partial\eta}\left\{r\left[\frac{C}{Pr}g + \frac{u_e^2}{H_e}C\left(1 - \frac{1}{Pr}\right)f'f''\right]\right\} = \left[\frac{P+1}{2} + R\right] fg' + x\left[f'\frac{\partial g}{\partial x} - g'\frac{\partial f}{\partial x}\right]$$

where

$$C = \rho\mu/\rho_e\mu_e\ ,\quad C_* = \rho_*\mu_*/\rho_e\mu_e\ ,\quad P = (x/u_e)\ du_e/dx\ ,\quad R = (x/r)\ dr/dx\ ,\quad \eta = (u_e/\rho_*\mu_* x)^{1/2}\ \rho\ dy$$

and all other symbols have the usual meaning.

Inclusion of vorticity does not alter the basic equations but only the boundary conditions. Hayes and Probstein [7] define a vorticity parameter

$$\Omega = \frac{\zeta_i}{\rho_i u_i} \int_0^{\eta=1} \rho dy$$

where ζ is the inviscid vorticity, and subscript i denotes the inviscid conditions in the absence of boundary layers. From Crocco's law in terms of Van Dyke's variables,

$$\zeta_w = (\partial U_i^*/\partial y^*)_w = (U_\infty^*/r_n^*)\ \partial U_1/\partial y = -(U_\infty^*/r_n^*)\ r^j R_1 T_1 S_1$$

where for $\gamma = 1.4$ one finds

$$S_1' = \frac{-1.6(M_\infty^2 - 1)^2 \alpha^2}{(2.8M_\infty^2 - 0.4)(2 + 0.4M_\infty^2)}$$

with $\alpha = r_n/r_s$. A second-order expansion of the (viscous) velocity leads to

$$u(s,y;\varepsilon) = u_1(x,y) + \varepsilon u_2(x,y) \sim U(x,o) - y r_w^j R_1 T_1 S_1'$$

Dividing by $U = U_i^*/U_\infty^*$ and introducing the η transformation leads to

$$f'(\infty) = 1 + \Omega \int_0^{\eta_\infty} (\rho_e/\rho)\ d\eta$$

for the outer boundary condition on the momentum equation with external vorticity. Without mass transfer or slip and temperature jump, the wall boundary conditions are the usual ones: $f(0) = f'(0) = 0$. The boundary conditions on the energy equation are unchanged from the usual case: $g(\infty) = 1$ and $g(0)$ or $g'(0)$ are prescribed functions of x.

The vorticity index Ω can be written as

$$\Omega = K\, r_w^j [(H_e/u_*^2) - 1/2\ (u_e/u_*)^2]\ (x)^{1/2} (u_*/u_e)^{3/2}$$

where

$$K = -(\rho_*/\rho_\infty)(u_*/u_\infty)\ S_1'/(Re_*)^{1/2}$$

independent of x.

NOMENCLATURE

All lengths are nondimensionalized by the nose radius.

C = $\rho\mu/\rho_e\mu_e$, density-viscosity product ratio

C_{D_f} = friction-drag coefficient referenced to base area

C_{D_p} = pressure-drag coefficient referenced to base area

C_{f_∞} = $2\tau_w/\rho_\infty U_\infty^2$, skin-friction coefficient

f = dimensionless stream function

f' = u/u_e, velocity ratio

g = H/H_e, stagnation enthalpy ratio

h,H = static and stagnation enthalpy, respectively

h_{ref} = reference enthalpy

M = Mach number

P = inviscid outer flow pressure

Pr = Prandtl number

p,p_o' = static and free-stream pitot pressure, respectively

R = inviscid outer-flow density

Re_∞ = $\rho_\infty u_\infty r_n/\mu_\infty$, Reynolds number

Re_* = $\rho_* u_* r_n/\mu_*$, Reynolds number

r,r_n = body and nose radius, respectively

S_1' = enthropy derivative in basic inviscid flow

St_∞ = $q_w/\rho_\infty U_\infty H_0(1 - g_w)$, Stanton number

T = inviscid outer-flow temperature

U = tangential component, inviscid outer-flow velocity

U_∞ = free-stream velocity

u = tangential velocity

V = normal component, inviscid outer-flow velocity

x = surface distance from stagnation point

y = distance normal to surface

α = angle between tangent to surface and axis of symmetry; nose-to-shock radius ratio

γ = ratio of specific heats

δ^* = boundary-layer displacement thickness

ε = $(\mu^*(U_\infty^{*2}/C_p^*)/\rho_\infty^* U_\infty^* r_n^*)^{1/2}$, Van Dyke's expansion parameter

ζ = inviscid vorticity

η = transformation variable

κ = longitudinal curvature

μ = dynamic viscosity

ρ = density

τ = shear stress

Ω = vorticity index

Ω_1 = Van Dyke's inviscid vorticity

Subscripts

0 = stagnation conditions

1,2 = first- and second-order quantity, respectively

disp = displacement effect

e = at the edge of the boundary layer

i = inviscid

STJ = slip and temperature jump effect

TVC = transverse curvature effect

vort = vorticity effect

w = wall

x,y = derivative with respect to x- and y-coordinate

* = inviscid sonic conditions on the body

∞ = free-stream conditions

Superscripts

' = derivative with respect to independent variable

* = dimensional quantity in second-order theory

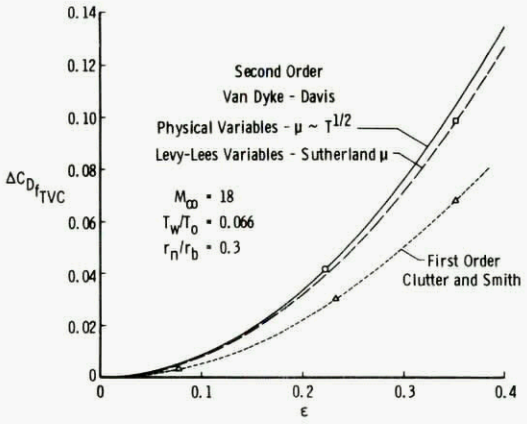

Fig. 1 Transverse-curvature-induced friction drag from first- and second-order theories

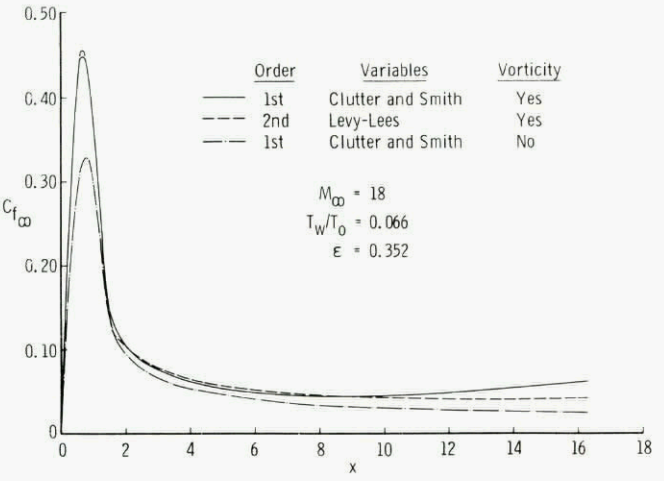

Fig. 2 Effects of shock generated vorticity interaction on skin-friction coefficient

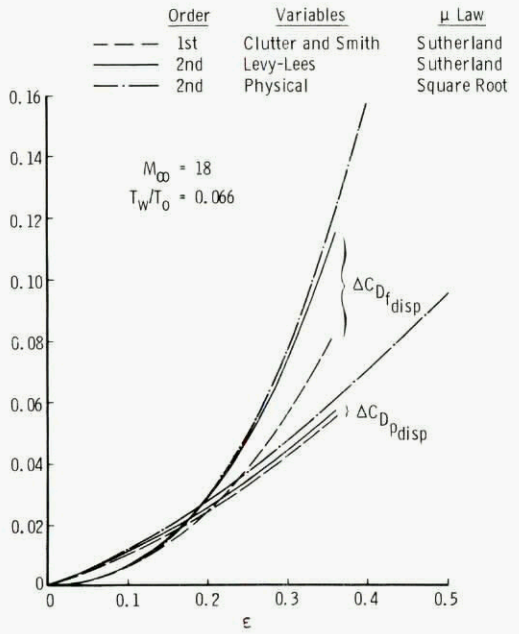

Fig. 3 First- and second-order predictions of displacement-induced pressure and friction drag

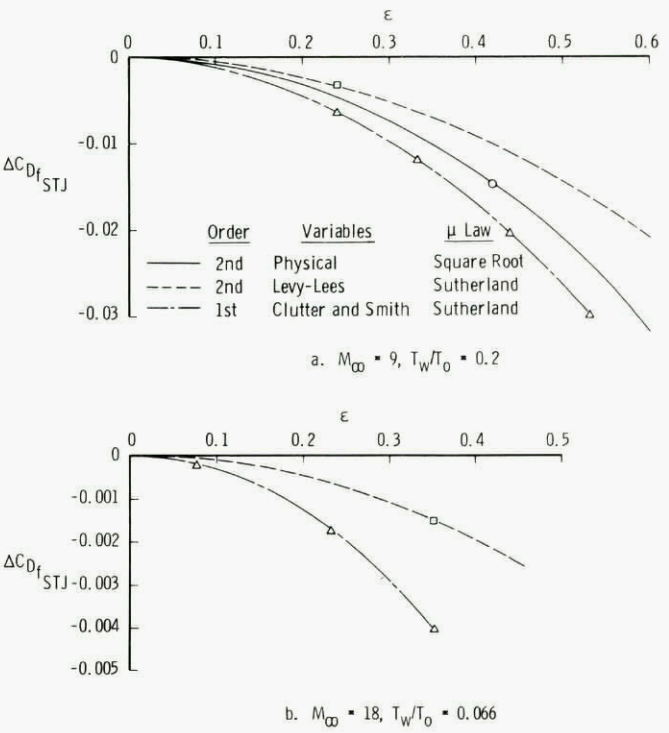

Fig. 4 First- and second-order slip and temperature jump-induced friction drag

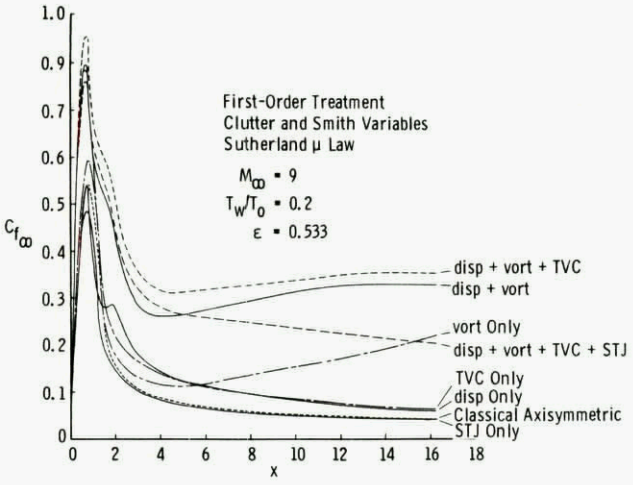

Fig.5 Effects of coupling higher-order effects on skin-friction coefficient

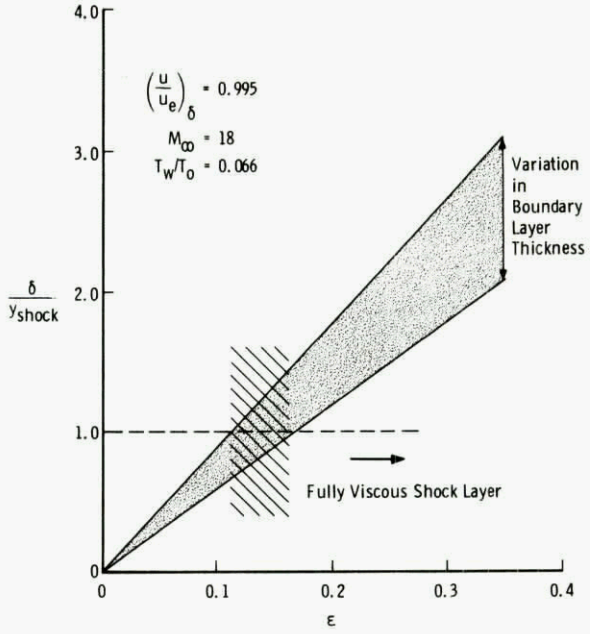

Fig.6 Boundary layer-to-shock layer thickness ratio over the cone at $M_\infty \simeq 18$. The total variation in boundary-layer thickness over the cone from the stagnation point to the base of the cone is shown

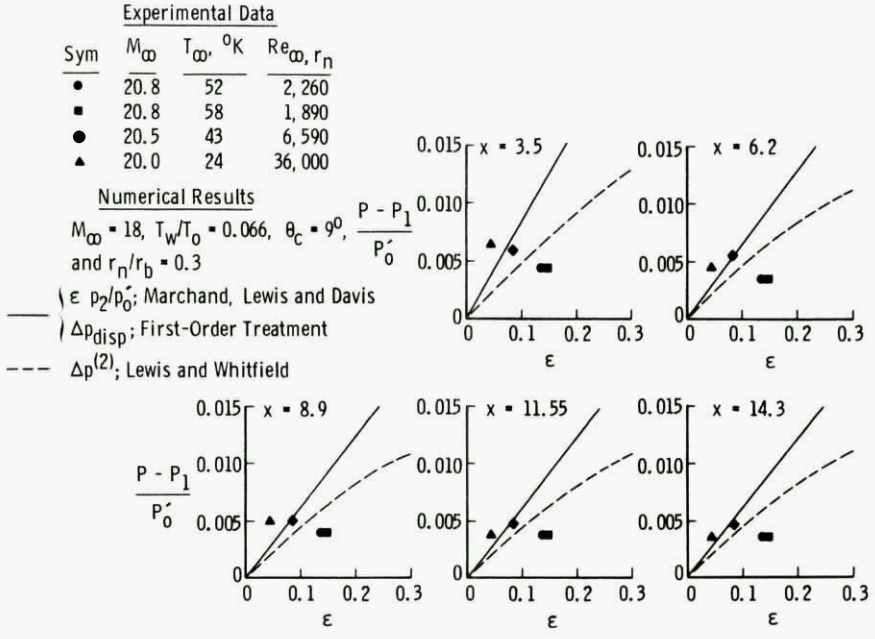

Fig.7 Displacement-induced pressure over a spherically blunted cone at $M_\infty \simeq 18$

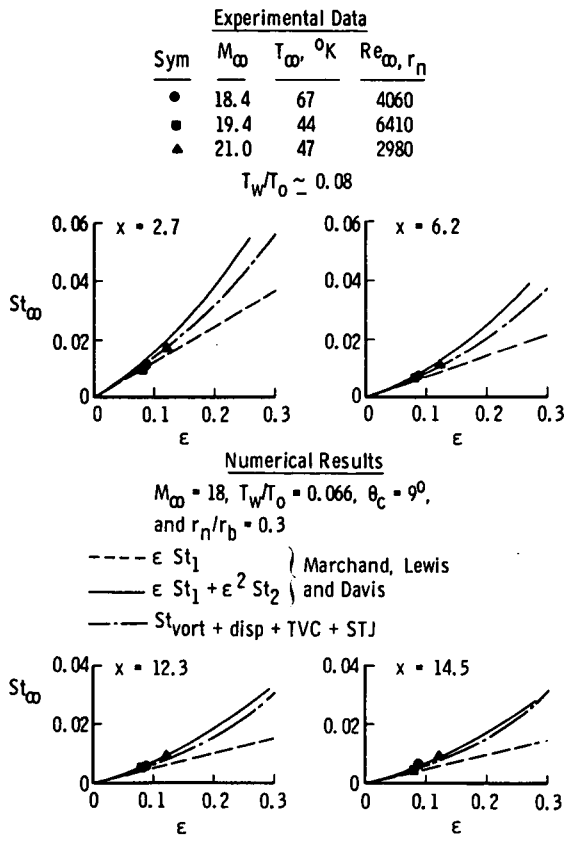

Fig.8 Heat transfer to a spherically blunted cone at $M_\infty \simeq 18$

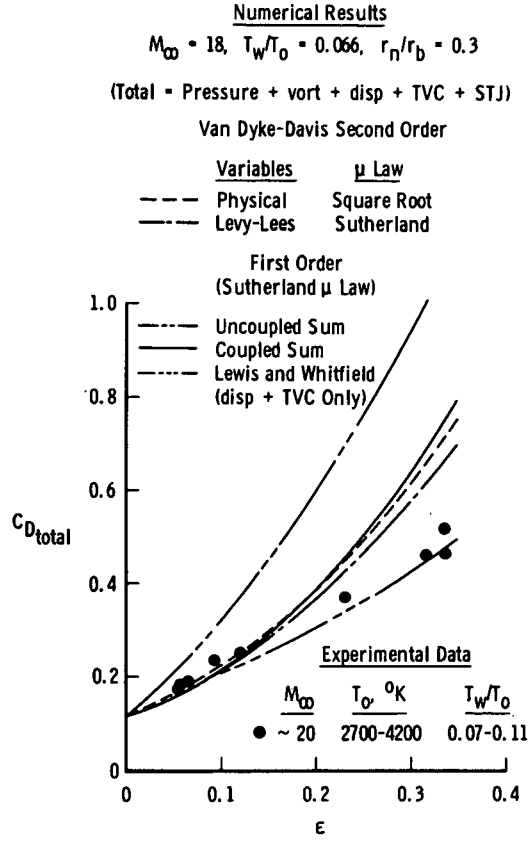

Fig.9 Total drag of a spherically blunted cone at $M_\infty \simeq 18$

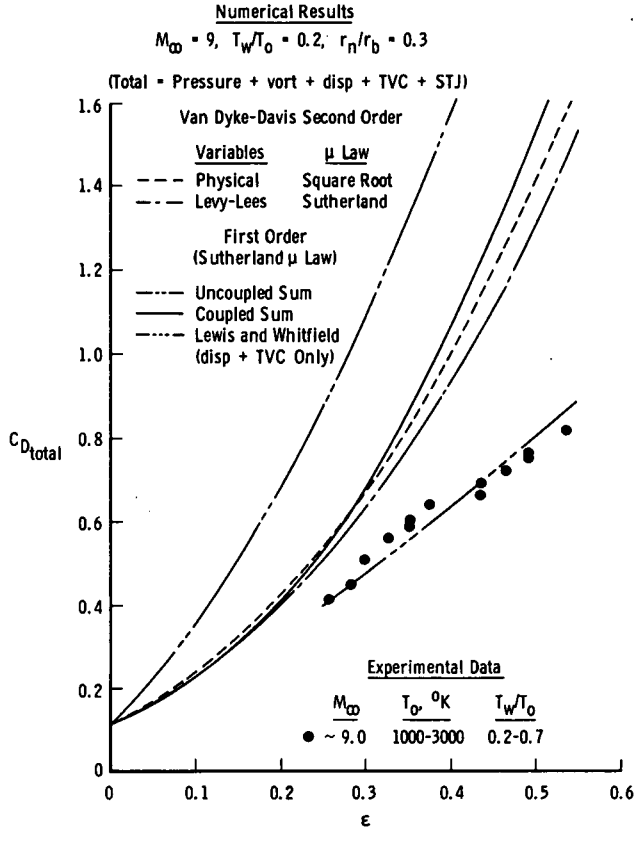

Fig.10 Total drag of a spherically blunted cone at $M_\infty \simeq 9$

HIGHER ORDER BOUNDARY-LAYER EFFECTS FOR THE AGARD ENGINEERING APPLICATIONS BODY AND FLOW CONDITIONS

by

John C. Adams, Jr

Supervisor, Theoretical Gas Dynamics Section,
Hypervelocity Branch, Aerophysics Division,
von Karman Gas Dynamics Facility, ARO, Inc.,
Arnold Air Force Station, Tennessee

HIGHER ORDER BOUNDARY-LAYER EFFECTS FOR THE AGARD ENGINEERING APPLICATIONS BODY AND FLOW CONDITIONS

by John C. Adams, Jr.*

SUMMARY

Numerical results for perfect gas boundary-layer flow at the AGARD Case C condition (M_∞ = 21.744, Re_∞, r_N = 430.9, and T_w/T_o = 0.0535) are presented for the AGARD 10.0° asymptotic half-angle hyperboloid. The boundary-layer model utilizes first- and second-order boundary-layer theory which accounts for displacement, external vorticity, longitudinal curvature, transverse curvature, slip, and temperature jump effects. Analysis of the results reveals that the AGARD Case C flow regime is such that second-order boundary-layer theory is not applicable since the boundary-layer thickness is much greater than the vortical (entropy layer) thickness so that correct asymptotic matching of the two layers is not possible. Hence the numerical results presented herein have little meaning relative to the physical problem; however, the results are presented in a manner specified by AGARD so as to facilitate comparison with other theoretical and numerical solutions for the same body and flow conditions.

INTRODUCTION

This paper is devoted to documenting results presented by the author at this AGARD Seminar in the Engineering Application Section using computer programs developed by the von Karman Gas Dynamics Facility of the Arnold Engineering Development Center. The body (a hyperboloid of 10.0° asymptotic half-angle) and the flow conditions (see Table 1) were completely specified by AGARD [1]. All results presented in the present report are for the AGARD Case C flow condition using first- and second-order compressible boundary-layer theory for a perfect gas.

PERFECT GAS SOLUTIONS (AGARD CASE C)

Theoretical Considerations and Description of Computer Program

All of the results for the perfect gas AGARD Case C condition were obtained by application of the second-order compressible boundary-layer theory derived by Van Dyke [2]. Basically, Van Dyke's approach involves solving first- and second-order boundary-layer equations which are found from the complete Navier-Stokes equations by an expansion in inverse powers of the square-root of a Reynolds number. The expansion procedure used is the method of inner and outer expansions and results in replacing the Navier-Stokes equations by two separate sets of equations, one set which is valid in the outer inviscid region and another set which is valid in the inner viscous (boundary-layer) region. By using Van Dyke's perturbation procedure the resulting second-order boundary-layer equations are linear and can be subdivided to exhibit several second-order boundary-layer effects, namely displacement, external vorticity, longitudinal curvature, transverse curvature, slip, and temperature jump. However, this theory is not universally applicable in that it should be applied in flow regimes where the expansion parameter ε is small but not so small that second-order terms in the parameter are negligible.

Numerous authors in addition to Van Dyke, e.g., Lenard [3], Maslen [4], and Davis and Flügge-Lotz [5], have obtained second-order boundary-layer solutions which are valid only in the stagnation-point region. The work by Davis and Flügge-Lotz [6] represents the first attempt at solutions of the second-order boundary-layer equations in regions removed from the nose. They employ an implicit finite-difference method and consider all second-order effects so that the resultant solutions represent a complete first- and second-order boundary-layer theory. They march the finite-difference solutions along the body surface and terminate them several nose radii downstream of the stagnation point; three different analytic bodies are considered, a paraboloid, a hyperboloid (22.5° asymptotic half-angle), and a sphere. The case of flow over the hyperboloid exhibits strong growth of vorticity interaction as the computation proceeds downstream and indicates that the effect of vorticity interaction will become a first-order effect at distances far downstream from the nose. This result is very interesting in that significant vorticity effects may be expected on certain slender blunt-nosed bodies which in turn can now be analyzed using this method.

In view of the ability of second-order boundary-layer theory to sort out the various second-order effects and their contribution to such quantities of interest as the viscous-induced drag increment, considerable attention has been devoted to this mathematical model. A computer program has been formulated to solve the governing first- and second-order boundary-layer equations in physical variables using the implicit finite-difference scheme of Davis and Flügge-Lotz discussed previously. Any combination of second-order effects may be considered for a specified body geometry; however, the pressure distribution along the body surface must be input to the program from a separate source, say an inviscid blunt body and method of characteristics solution. Further details of this work may be found in the paper by Lewis [7] presented at the AGARD Seminar as well as the later AIAA paper by Marchand, Lewis, and Davis [8].

Experience with this program has revealed several undesirable features connected with regions of strong boundary-layer growth (where an excessive number of points are used in the finite-difference scheme to traverse the boundary layer). It is interesting to note that Fannelop [9] has encountered precisely the same problem in treating the first-order boundary-layer equations with crossflow. With this deficiency in mind, and recalling that it is often advantageous to work with similarity variables when solving the boundary-layer equations by numerical methods, it was decided to transform the governing first- and second-order boundary-layer equations using the well-known Levy-Lees transformation [10] written in terms of first-order quantities. A computer program similar to that for the physical variables was written to solve the resultant set of transformed equations using a modification of the Davis and Flügge-Lotz implicit finite-difference scheme to

*Supervisor, Theoretical Gas Dynamics Section, Hypervelocity Branch, Aerophysics Division, von Karman Gas Dynamics Facility.

account for variable step size along the body in the transformed plane. Provisions were made in the program to allow solutions for either a Sutherland or power viscosity law as well as arbitrary (but constant) Prandtl number and specific heat ratio. The first-order stagnation point solution was obtained by use of a Runge-Kutta-Gill numerical integration routine in conjunction with an iterative correction scheme; all second-order quantities were set equal to zero at the stagnation point, and hence a forward marching of approximately twenty stations with a very small step size was required before the second-order solution became valid. Another feature included in the program was the capability of obtaining a first-order locally similar solution by setting the nonsimilar terms in the governing first-order equations equal to zero. The resultant set of coupled ordinary nonlinear differential equations was then solved by a successive approximation technique coupled to the same implicit finite-difference scheme used for the nonsimilar case. By this approach the accuracy and limitations of the oft-used locally similar approximation can properly be assessed using a common method of solution.

The present section is concerned solely with analyzing the various second-order boundary-layer effects on the specified AGARD body, a hyperboloid of 10.0° asymptotic half-angle at zero angle of attack; this body geometry and shock shape are shown in Fig. 1. The specified AGARD flow conditions are given in Table 1 where the present results are for the AGARD Case C which is a perfect gas, $\gamma = 1.40$ flow. As mentioned earlier the surface pressure distribution must be input to the program from an external source. For the present work modified Newtonian theory as deduced by Lees [11] was used for pressure prediction as specified by AGARD. The modified Newtonian theory turns out to be in good agreement with a more exact inviscid blunt body and method of characteristics solution as shown by Fig. 2.

Controversy has arisen in the past over the proper method for treating the second-order vorticity-displacement interaction effect; excellent discussions of this point may be found in the reviews by Van Dyke [12] and Cheng [13]. Following Van Dyke [14] one is free to choose either a "displacement speed" or "displacement pressure" treatment for the separate effects of second-order vorticity and displacement. Basically, the classification of displacement speed means that the second-order pressure gradient term attributable to vorticity interaction is treated as a vorticity effect in the second-order tangential momentum equation, whereas displacement pressure means that this pressure gradient term is considered as a displacement effect. Various authors have said that this term does not exist or that it is negligible, while other authors have said that it exists but then fail to include it. The question has been answered in the affirmative by Van Dyke [12] who shows in a very clear manner that this term does indeed exist and should properly be included in any second-order analysis. However, as speculated by Cheng [13], Van Dyke's classification of displacement speed should result in giving the second-order displacement and vorticity effects an unduly large value which is not representative of the actual magnitude for flows over blunt bodies. That such is indeed true has been shown by Adams [15], who concluded that one should properly interpret second-order vorticity and displacement as a combined effect (vorticity-displacement interaction). Such an approach will be followed in the present work; however results showing the separate effects of second-order vorticity and displacement treated in a displacement speed sense will also be presented. As discussed by Adams [15] this type of treatment is the only correct procedure for analyzing these separate effects using the second-order boundary-layer theory of Van Dyke [2].

The method developed by Davis and Flügge-Lotz [6] for treating the second-order displacement effect is limited in applicability to the extreme nose region of the body. Hence, Adams [15] formulated a new technique which is valid over the entire body and uses first-order inviscid theory. This approach is fully compatible with the second-order theory of Van Dyke [2] and has been used for the solutions presented herein.

DISCUSSION OF RESULTS

The results presented in this section were obtained from an investigation into second-order boundary-layer effects on the specified AGARD hyperboloid of 10.0° asymptotic half-angle at zero angle of attack under the specified AGARD Case C conditions as discussed previously. Particular emphasis was placed upon presenting results for different viscosity laws, Prandtl numbers, and types of solution in terms of quantities of interest such as the local skin-friction coefficient and Stanton number. Only in this manner can one properly assess the influence of each of these parameters on the resultant solution.

In this examination of the effect of various viscosity laws upon both first- and second-order boundary-layer solutions, three different relations were considered: Sutherland, square-root, and linear. A comparison of these laws is shown in Fig. 3 where it is seen that the Sutherland law is in excellent agreement with the square-root law in the temperature range of current interest. It is important to note that the linear law underpredicts the viscosity (as compared to the Sutherland value) by a substantial amount, approximately 60 percent maximum deviation. One must keep these discrepancies in mind when evaluating the numerical results of this investigation since the choice of viscosity law influences the boundary-layer character to a considerable extent as will now be shown.

In the past many boundary-layer investigations have been conducted under various assumptions, e.g., linear viscosity law, $Pr = 1.0$, locally similar solution, etc., without due consideration as to the effect of these assumptions on the resultant solution. An attempt has been made in the present study to define and clarify some of these effects by presentation of the results shown in Figs. 4 through 8. With respect to variation of viscosity law, Figs. 4 and 5 show that use of the linear viscosity law results in a severe underprediction of both skin-friction coefficient and Stanton number as compared to the square-root and Sutherland values, which are in good agreement. Hence, the choice of viscosity law can produce large variance in the resulting solution. Effects of Prandtl number and type of solution on the skin-friction coefficient and Stanton number are shown in Figs. 6 and 7 for the Sutherland viscosity law. It is seen that both of these effects are negligible for the present body and flow conditions. Such is of interest because many prior first-order boundary-layer investigations used a locally similar solution without justification.

One of the most sensitive boundary-layer quantities is the displacement thickness. Figure 8 presents such information using Davis and Flügge-Lotz [6], Eq. (2.33), for the two-dimensional form of the first-order displacement thickness. Again, the square-root viscosity law results are in good agreement with the Sutherland prediction, whereas the linear law underpredicts by a substantial amount. The large influence of Prandtl

number in changing from 0.70 to 1.0 is rather surprising; however, one must remember that the Prandtl number effectively controls the ratio of viscous shear work to thermal heat conduction, and hence a change in Prandtl number results in a redistribution of both the velocity and temperature profiles which in turn control the displacement thickness.

Turning now to specific consideration of second-order boundary-layer effects, Figs. 4 through 7 show the influence of including all second-order effects concurrently. The large influence of second-order effects is strikingly apparent, especially far downstream on the body where the first- and second-order results are approximately twice the first-order predictions. In order to properly interpret these results, one must in turn examine each second-order effect considered separately over the entire body range of interest. Figures 9 and 10 present such information. With respect to the increment in the local skin-friction coefficient as shown in Fig. 9, vorticity-displacement interaction is by far the dominant second-order effect. Note that the vorticity continues to grow with increasing distance along the hyperboloid; however, as pointed out by Adams [15], one must consider vorticity and displacement in a combined sense (vorticity-displacement interaction) when interpreting results. Hence, the displacement effect will tend to cancel the vorticity effect on the aft portion of the hyperboloid which can be seen in the character of the resultant total curve. Further, note that all other second-order quantities are essentially negligible (transverse curvature has a very small effect) with respect to their influence on the local skin-friction increment. With regard to the local Stanton number increment, one sees in Fig. 10 that all second-order effects are of the same order of magnitude for both bodies. One notes that here slip and temperature jump effects are of importance in the nose region. Furthermore, Fig. 10 shows that vorticity-displacement interaction is dominant on the aft portion of the hyperboloid.

Based on the above detailed investigation into second-order effects, one can safely say that vorticity-displacement interaction is the dominant factor in second-order boundary-layer theory. However, a word of caution must be injected as to the applicability of second-order theory in general and the present results in particular. It is assumed that the boundary-layer thickness is much smaller than the vortical (entropy layer) thickness so that the boundary conditions at the common boundary obtained by asymptotic matching of the two layers remain valid. Such may not be true on the aft portion of the body since the boundary layer is growing in thickness while the vortical layer is diminishing. What is needed is a "swallowing-type" boundary-layer analysis or a fully viscous shock-layer treatment of the same problem in order to clearly define where second-order boundary-layer theory becomes inapplicable with respect to position along the body. Such an analysis would permit one to properly assess the present results.

As mentioned previously, the second-order compressible boundary-layer theory of Van Dyke [2] is meant to be applied to flow regimes where the expansion parameter ε is small but not so small that second-order terms in the parameter are negligible. For the present AGARD Case C condition, Table 1 shows that $\varepsilon = 0.2237$ based on the Sutherland viscosity law. For this value of ε, Fig. 11 shows that the first-order boundary-layer thickness (defined to be the normal distance from the body surface where the velocity ratio $u_1/U_e = 0.995$) is between 1.3 to 1.8 times the inviscid shock standoff distance. Hence, the boundary layer more than fills the inviscid shock layer, which is a clear indication that classical boundary-layer theory is not valid for this flow condition. What is needed for analysis of this flow is a fully viscous shock layer treatment allowing the shock to merge with the viscous layer.

It is interesting to note from Fig. 11 that if $\varepsilon = 0.10$, the boundary layer would only fill approximately 60 to 80 percent of the inviscid shock layer; such is more clearly shown in Fig. 12. Hence, for the present flow condition, one would have to require $\varepsilon < 0.10$ in order to even consider the use of classical boundary-layer theory. In this connection Fig. 13 shows the variation of free-stream Reynolds number with respect to the perturbation parameter. From this figure it is seen that an order of magnitude increase in Re_∞ is required in order to produce an $\varepsilon < 0.10$. Since the altitude and flight conditions are fixed, this would require that the nose radius be increased by an order of magnitude, i.e. $r_N > 10.0$ inches, in order for $\varepsilon < 0.10$. From this discussion the utility of ε as a scaling parameter for blunt body flows should be apparent. Such has been exploited by Marchand, Lewis, and Davis [8] in their analysis of drag and heat transfer data on a spherically blunted cone. By comparison of results from second-order boundary-layer theory with experimental measurements, they concluded that $\varepsilon < 0.2$ appears to be the range of applicability for application of second-order boundary-layer theory.

Turning now to details of the flow field, Figs. 14 and 15 present velocity and temperature profiles, respectively, at selected locations along the body as specified by AGARD. Both first-order as well as first- and second-order results are shown. The overwhelming influence of second-order vorticity-displacement interaction is apparent, especially for the temperature which assumes negative values for body locations greater than about two nose radii downstream of the stagnation point. Such anomalous behavior can be traced to use of second-order boundary-layer theory in a flow regime where the asymptotic matching conditions are not applicable, i.e., the boundary-layer thickness is much greater than the vortical (entropy layer) thickness so that asymptotic matching of the two layers is not possible. As previously discussed, classical first-order boundary-layer theory is not even applicable to this flow (recall the boundary-layer thickness outside the inviscid shock layer) so that any of the current boundary-layer predictions, either first-order or first- and second-order must be regarded as suspect.

Another quantity of interest is the integrated skin-friction and pressure drag coefficients over the specified AGARD body. The results are shown in Table 2 where the reference area is taken to be the base cross-sectional area at $s/r_N = 50.0$. These quantities have no true physical meaning for this flow because of the failure of boundary-layer theory as discussed previously.

A few words should be said in conclusion as to the computer time requirements and character of numerical solutions for this investigation. The program itself was written in FORTRAN 63 for solution on a CDC 1604-B computer. Computation time including printout for both first- and second-order equations averaged 12 seconds per station in transformed variables with a total of 355 stations required to traverse the AGARD body of 50 nose radii in length; hence, a total of 71 minutes was required for the complete solution. Using Levy-Lees variables results in the solution being obtained in the transformed (ξ,η) plane; for the present investigation the following step sizes were chosen: $\eta_{max} = 6.0$, $\Delta\eta = 0.050$, $\Delta(s/r_N) = 0.0125, 0.0250, 0.0500, 0.1000, 0.2000,$

0.4000, where a procedure for doubling the s/r_N step size at any chosen location was built into the program; hence, the s/r_N step size was doubled a total of six times over the body of interest in this work. Such a step size change procedure is highly advantageous in reducing the total computing time requirements. Repetition of the calculations with a halved step size in $\Delta\eta$ as well as an increase in η_{max} to 9.0 showed no change in the numerical results. That the body in question is essentially independent of the $\Delta(s/r_N)$ step size is evidenced by the excellent agreement of the locally similar solution (which is independent of this step size). The implicit finite-difference scheme proved to be inherently stable in all cases, and any oscillations introduced by the second-order stagnation point treatment were quickly damped out. All in all, the method must be described as highly satisfactory in the numerical sense.

SUMMARY

The present paper is devoted to documenting numerical results for the AGARD Engineering Applications Case C using compressible first- and second-order boundary-layer theory for a perfect gas. The purpose of this report is to present these results in a manner specified by AGARD so as to facilitate comparison with other theoretical and numerical solutions for the same body and flow conditions. No attempt has been made to fully analyze the present solutions. The reader of this report is free to make his own judgment relative to other methods. In all fairness, however, the reader should keep in mind the important point that boundary-layer theory in general is not applicable to the Case C flow condition.

ACKNOWLEDGEMENT

This work was sponsored by the Arnold Engineering Development Center (AEDC), Air Force Systems Command, U.S. Air Force under Contract F40600-69-C-0001 with ARO, Inc., Contract Operator, AEDC. The author wishes to thank D. H. Wurst and M. Brown, Jr., ARO, Inc., for their help in performing the numerical calculations.

REFERENCES

[1] AGARD - Private Communication by Dr. J. Lukasiewicz, von Karman Gas Dynamics Facility, ARO, Inc., Arnold Air Force Station, Tennessee, April 7, 1967.

[2] Van Dyke, M. "Second-Order Compressible Boundary-Layer Theory with Application to Blunt Bodies in Hypersonic Flow." Hypersonic Flow Research, edited by F. R. Riddell, Academic Press, Inc., New York, 1962, pp. 37-76.

[3] Lenard, M. "Stagnation Point Flow of a Variable Property Fluid at Low Reynolds Numbers." Thesis, Cornell University, Graduate School of Aeronautical Engineering, 1961.

[4] Maslen, S.H. "Second-Order Effects in Laminar Boundary Layers." AIAA Journal, Vol. 1, 1963, pp. 33-40.

[5] Davis, R.T. and Flügge-Lotz, I. "The Laminar Compressible Boundary-Layer in the Stagnation Point Region of an Axisymmetric Blunt Body Including the Second-Order Effect of Vorticity Interaction." International J. Heat Mass Transfer, Vol. 7, 1964, pp. 341-370.

[6] Davis, R.T. and Flügge-Lotz, I. "Laminar Compressible Flow Past Axisymmetric Blunt Bodies (Results of Second-Order Theory)." Stanford University, Division of Engineering Mechanics TR-143, 1963.

[7] Lewis, C.H. "First- and Second-Order Boundary-Layer Effects at Hypersonic Conditions." Paper presented at AGARD Seminar on "Numerical Methods for Viscous Flows." National Physical Laboratory, Teddington, England, September 18-21, 1967.

[8] Marchand, E.O., Lewis, C.H. and Davis, R.T. "Second-Order Boundary-Layer Effects on a Slender Blunt Cone at Hypersonic Conditions." AIAA Paper No. 68-54, 1968.

[9] Fannelop, T.K. "A Method of Solving the Three-Dimensional Laminar Boundary-Layer Equations with Application to a Lifting Re-entry Body." Avco Missile Systems Division BSD-TR-66-209, 1966.

[10] Lees, L. "Laminar Heat Transfer Over Blunt-Nosed Bodies at Hypersonic Flight Speeds." Jet Propulsion, Vol. 26, pp. 259-269, 274, 1956.

[11] Lees, L. "Hypersonic Flow." Inst. Aero. Sci., Preprint No. 554, 1955.

[12] Van Dyke, M. "A Review and Extension of Second-Order Hypersonic Boundary-Layer Theory." Rarefied Gas Dynamics, Vol. II. Supplement 2, edited by J. A. Lauermann, Academic Press, Inc., New York, 1963, pp. 212-227.

[13] Cheng, H.K. "Viscous Hypersonic Blunt-Body Problems and the Newtonian Theory." Fundamental Phenomena in Hypersonic Flow, edited by J. Gordon Hall, Cornell University Press, Ithaca, New York, 1966, pp. 90-131.

[14] Van Dyke, M. "Higher Approximations in Boundary-Layer Theory, Part I." J. Fluid Mechanics, Vol. 14, 1962, pp. 161-177.

[15] Adams, J.C., Jr. "Higher Order Boundary-Layer Effects on Analytic Bodies of Revolution." Paper presented at AGARD Seminar on "Numerical Methods for Viscous Flows," National Physical Laboratory, Teddington, England, September 18-21, 1967. Also published as AEDC-TR-68-57, 1968.

NOMENCLATURE

$C_f = 2\tau_w/\rho_\infty U_\infty^2$	skin-friction coefficient
C_{D_f}	skin-friction drag coefficient referenced to base area
C_p	pressure drag coefficient referenced to base area
c	specific heat at constant pressure
M_∞	free-stream Mach number
P	inviscid pressure
P_o'	free-stream normal shock pitot pressure
Pr	Prandtl number
q_w	wall heat flux
$Re_\infty = \rho_\infty U_\infty r_N/\mu_\infty$	Reynolds number based on nose radius and free-stream conditions
r, r_N, r_s	radius, nose radius, shock radius, respectively
$St_\infty = -q_w/\rho_\infty U_\infty c_p(T_o - t_w)$	Stanton number based on free-stream conditions
s	surface distance measured from stagnation point
T_e, T_∞, T_o	inviscid temperature at edge of boundary layer, free-stream temperature, free-stream stagnation temperature, respectively
t, t_w	temperature, wall temperature, respectively
U_e, U_∞	inviscid tangential velocity at edge of boundary layer, free-stream velocity respectively
u	tangential velocity
Z	distance along physical body axis
γ	ratio of specific heats
Δ	inviscid shock standoff distance
δ	boundary-layer thickness (at $u_1/U_e = 0.995$)
δ^*	boundary-layer displacement thickness
ϵ	Van Dyke's expansion parameter [2]
ξ,η	transformed Levy-Lees coordinates [10]
μ	dynamic viscosity
ρ	density
τ_w	wall shear stress

Subscripts

o	stagnation conditions
1	first-order quantity
2	second-order quantity
e	at the edge of the boundary layer
N	at the nose
ref	reference condition
s	at the shock
w	at the physical wall
∞	at free stream conditions

TABLE 1

Conditions for AGARD Engineering Applications Section
Hyperboloid (10.0° Asymptotic Half-Angle)

Case	Altitude (ft)	M_∞	U_∞ (ft/sec)	T_∞ (°K)	P_∞ (atm)	Re_∞ (Based on nose radius of $r_N = 1.0$ in.)	P_0' (atm)	T_0' (°K)	T_w (°K)	T_w/T_0'	$\varepsilon^\ddagger$
A	100,000.0	20.178	20,000.0	226.98	1.0997×10^{-2}	179,828.5	6.0352*	6,996.0*	1,400.0	0.2001	0.0103
B	250,000.0	21.744	20,000.0	195.46	2.0074×10^{-5}	430.9	0.0129*	5,301.9*	1,000.0	0.1886	0.2237
C	250,000.0	21.744	20,000.0	195.46	2.0074×10^{-5}	430.9	0.01223†	18,678.2†	1,000.0	0.0535	0.2237

*Normal Shock Equilibrium Stagnation Conditions

†Normal Shock Ideal Gas ($\gamma = 1.40$) Stagnation Conditions

$$\ddagger \quad \varepsilon = \left\{ \frac{1 + 112/T_\infty}{Re_\infty \left[(\gamma - 1)M_\infty^2 + 112/T_\infty\right]} \left[(\gamma - 1)M_\infty^2\right]^{3/2} \right\}^{1/2}$$

(Based on Sutherland Viscosity Law)

TABLE 2

Integrated Skin-Friction and Pressure Drag Coefficients

First-Order (No Second-Order Effects)

$C_{D_p} = 0.10901$ $\qquad$ $C_{D_f} = 0.08671$

First- and Second-Order (All Second-Order Effects Included Concurrently)

$C_{D_p} = 0.12424$ $\qquad$ $C_{D_f} = 0.29626$

Conditions

AGARD Case C

$M_\infty = 21.744$, $\varepsilon = 0.2237$, $\gamma = 1.40$, $Pr = 0.70$, $T_w/T_0 = 0.0535$

Sutherland Viscosity Law

Perfect Gas

$$C_D = \frac{\text{Drag Force}}{\frac{1}{2} \rho_\infty U_\infty^2 A_b}$$

where $A_b = 3.62206$ ft^2 at $s/r_N = 50.0$

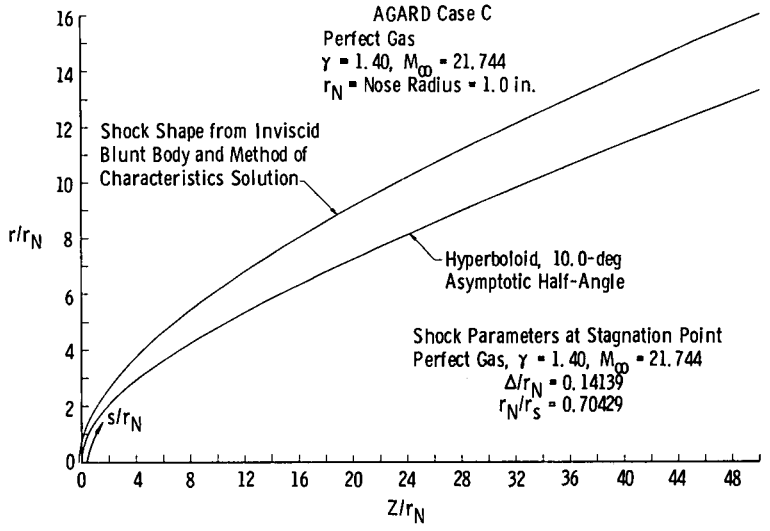

Fig.1 Body and shock geometry

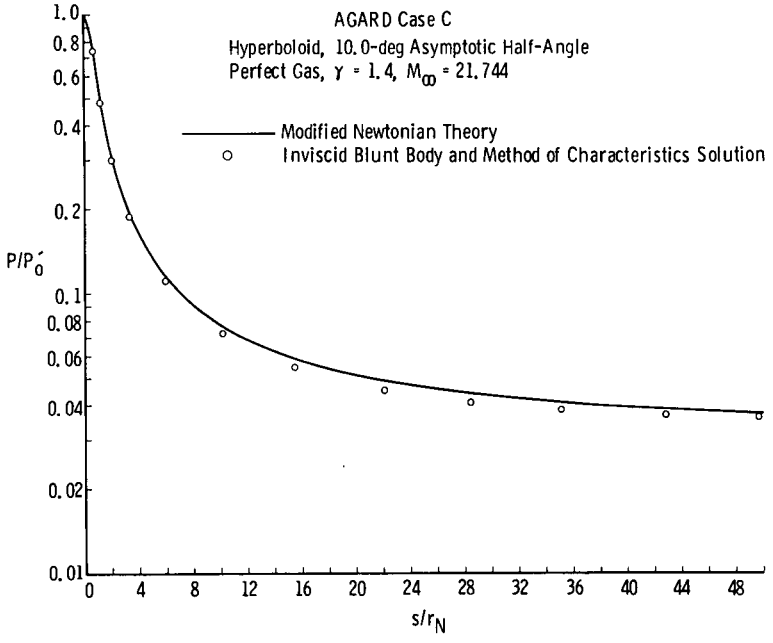

Fig.2 Pressure distribution

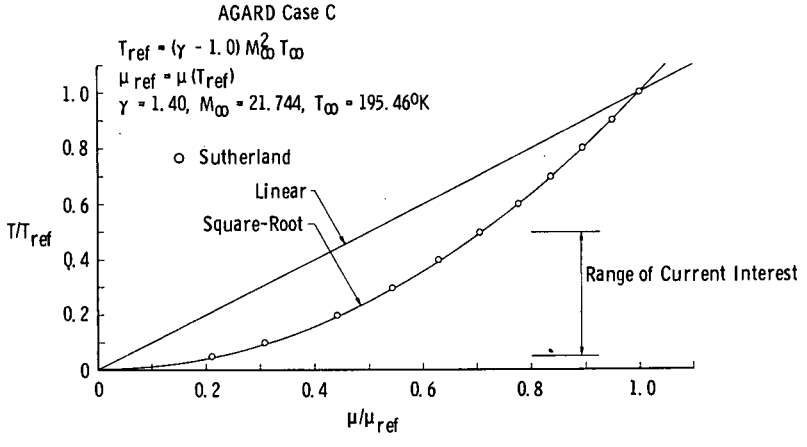

Fig.3 Comparison of various viscosity laws

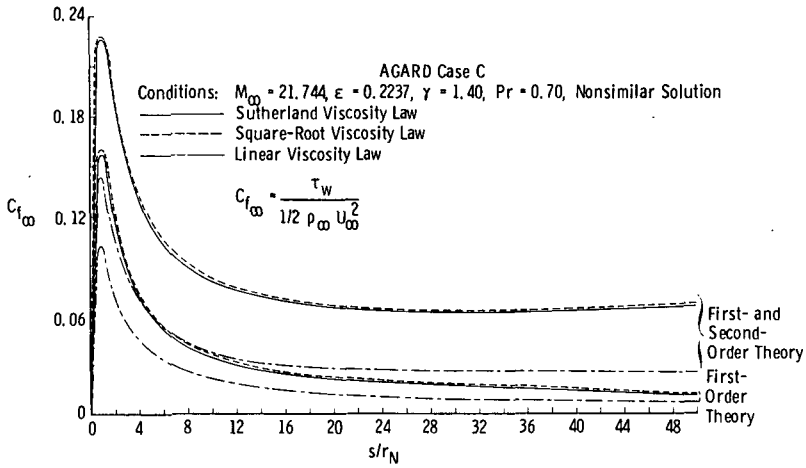

Fig. 4 Effects of viscosity law on first- and second-order local skin-friction coefficients

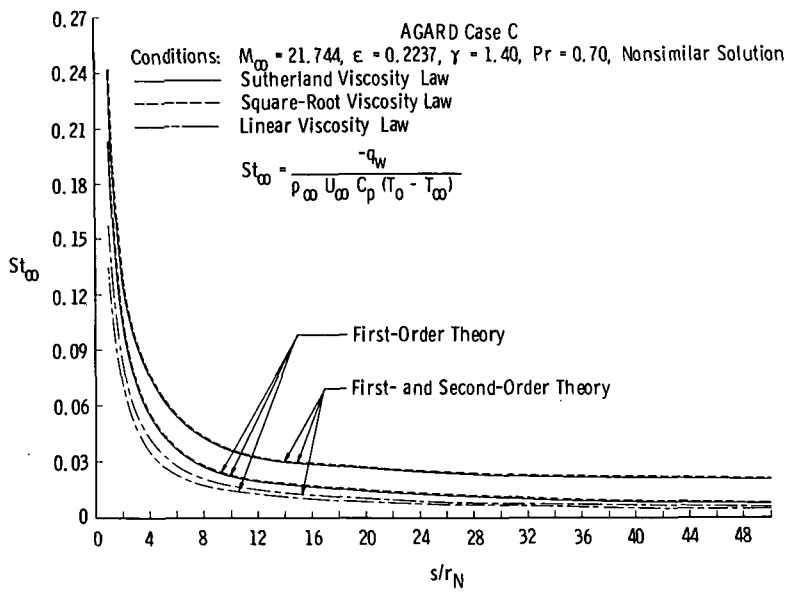

Fig. 5 Effects of viscosity law on first- and second-order local Stanton numbers

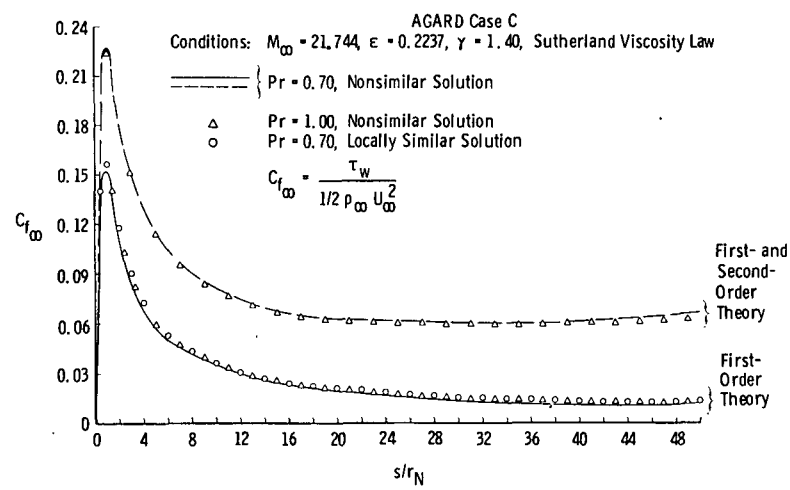

Fig. 6 Effects of Prandtl number and type of solution on first- and second-order local skin-friction coefficients

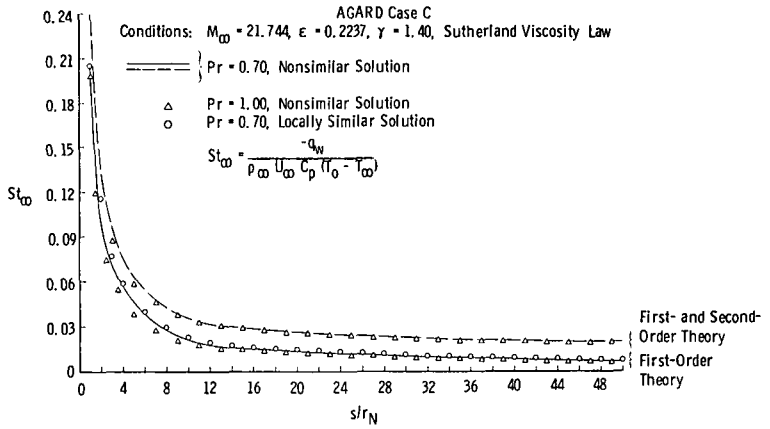

Fig.7 Effects of Prandtl number and type of solution on first- and second-order local Stanton numbers

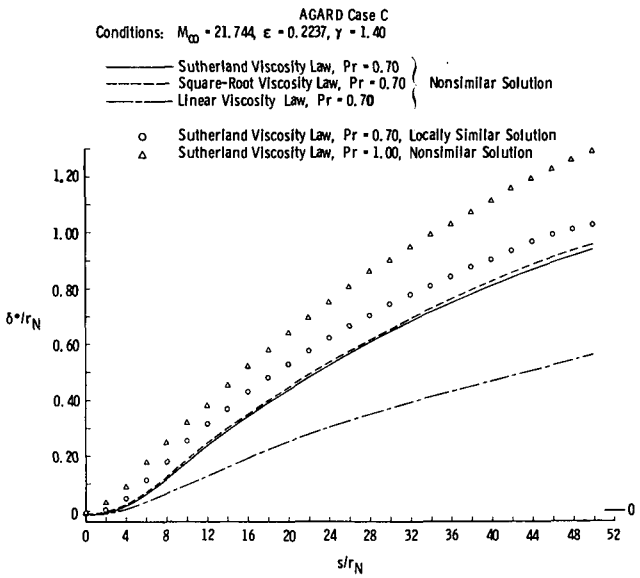

Fig.8 Comparison of first-order displacement thicknesses

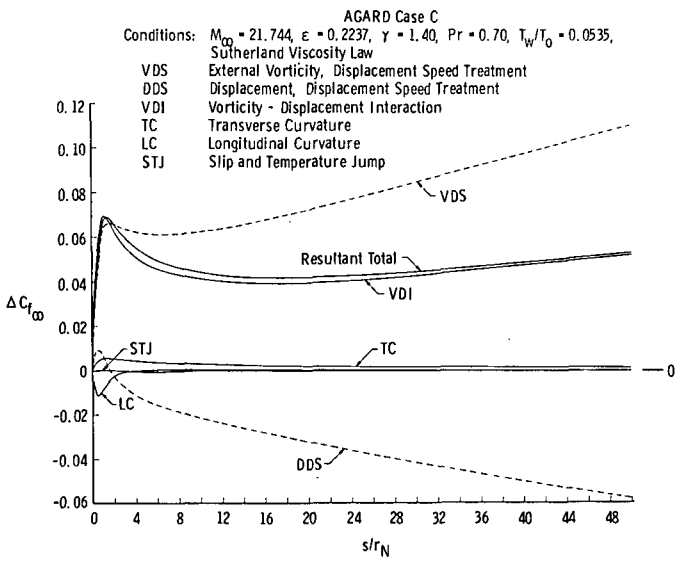

Fig.9 Increment in local skin-friction coefficient due to second-order effects

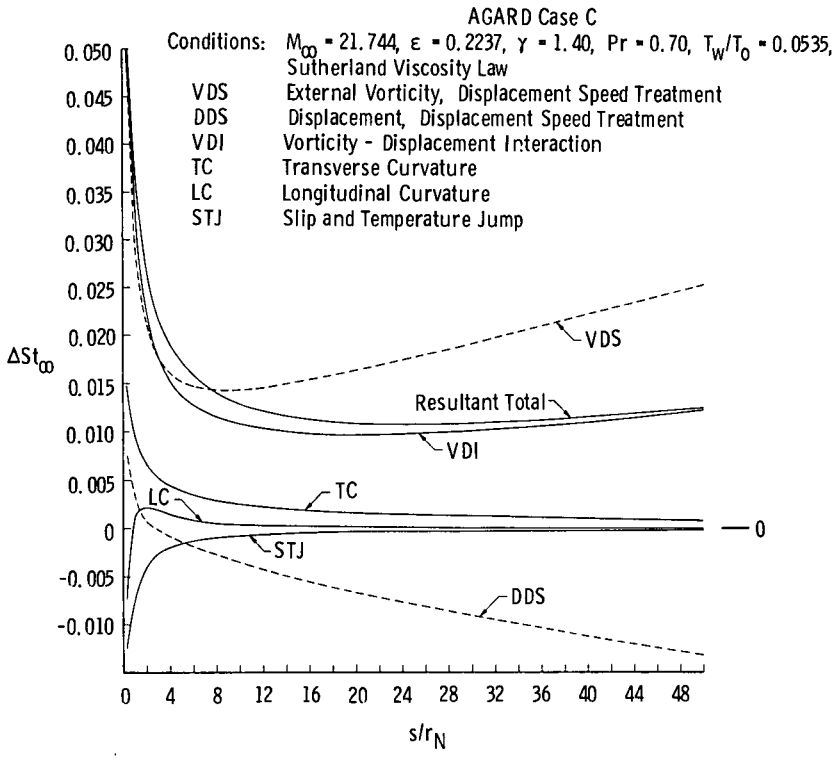

Fig.10 Increment in local Stanton number due to second-order effects

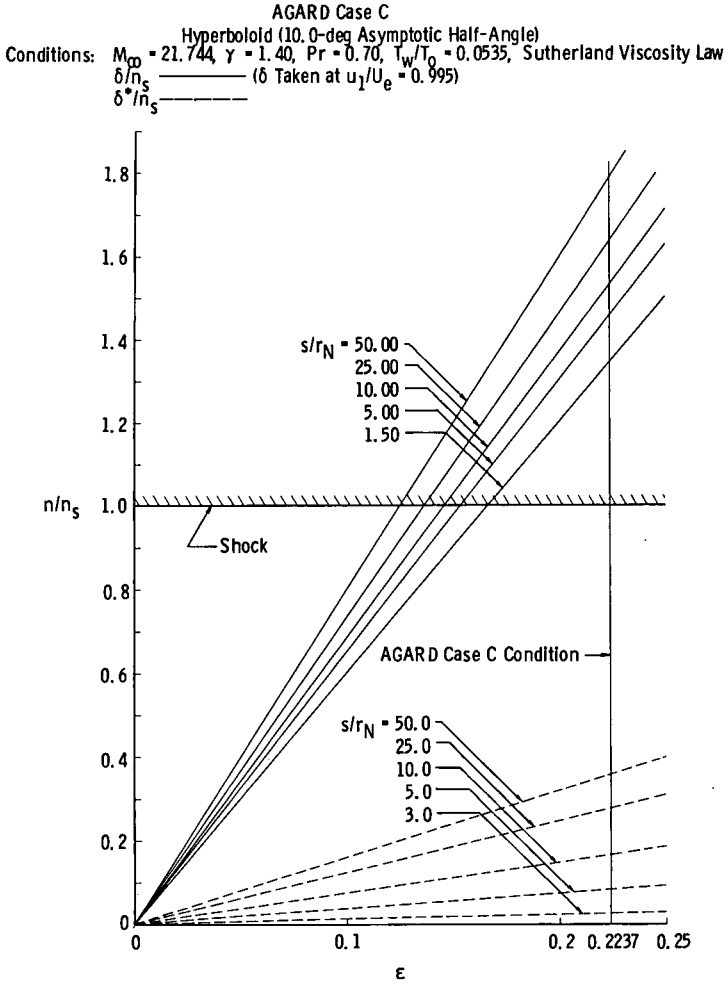

Fig.11 Variation of boundary-layer parameters δ and δ* with respect to perturbation parameter ε

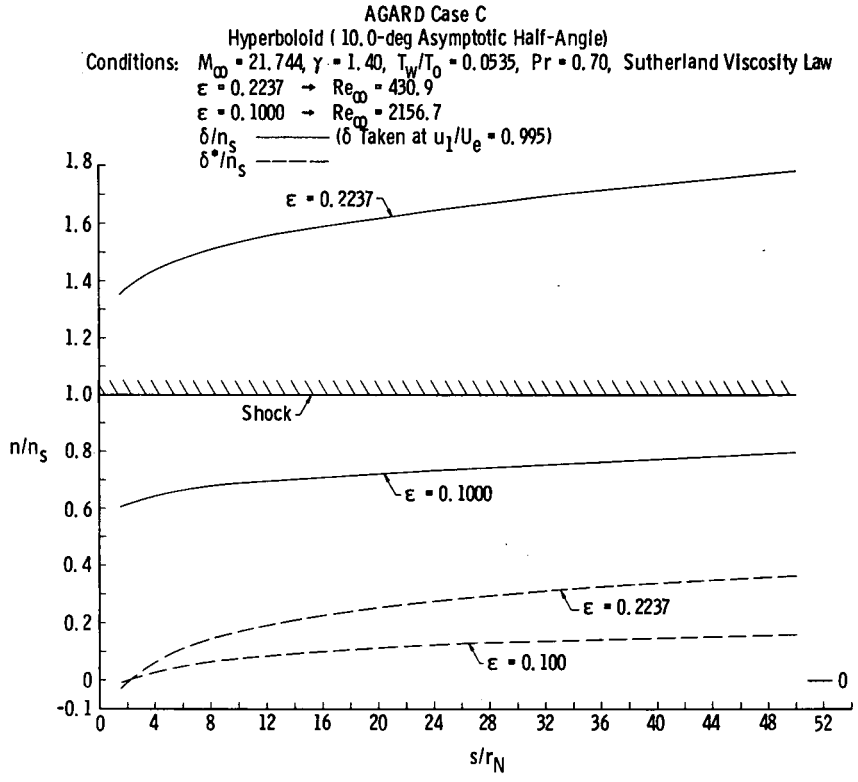

Fig.12 Variation of boundary-layer parameters δ and δ^* with respect to body surface location s/r_N

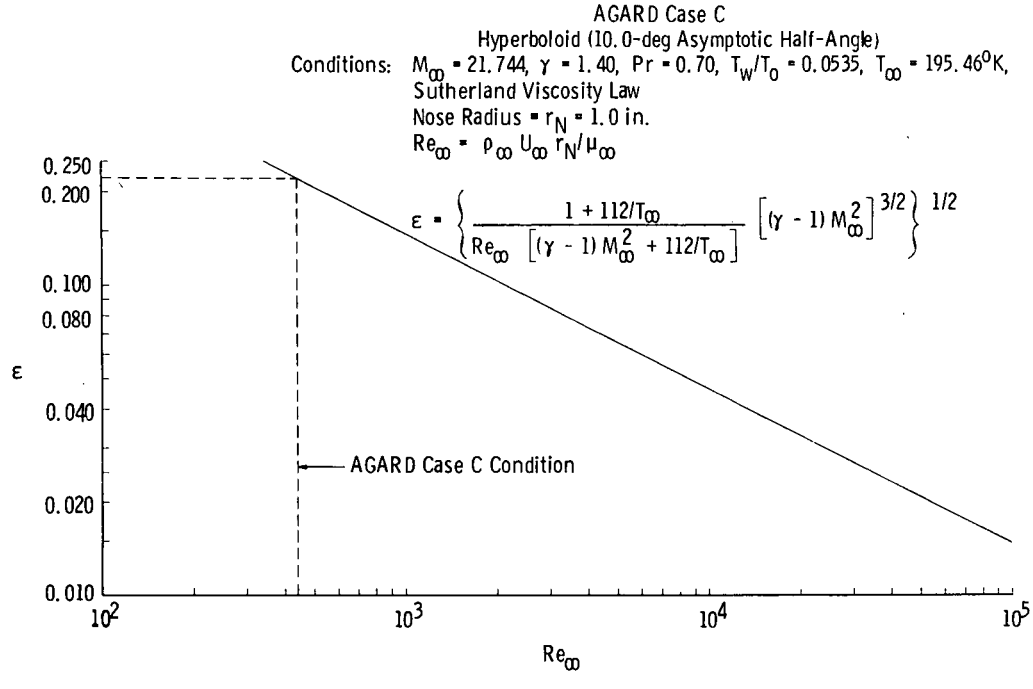

Fig.13 Variation of free-stream Reynolds number, Re_∞, with respect to perturbation parameter ϵ

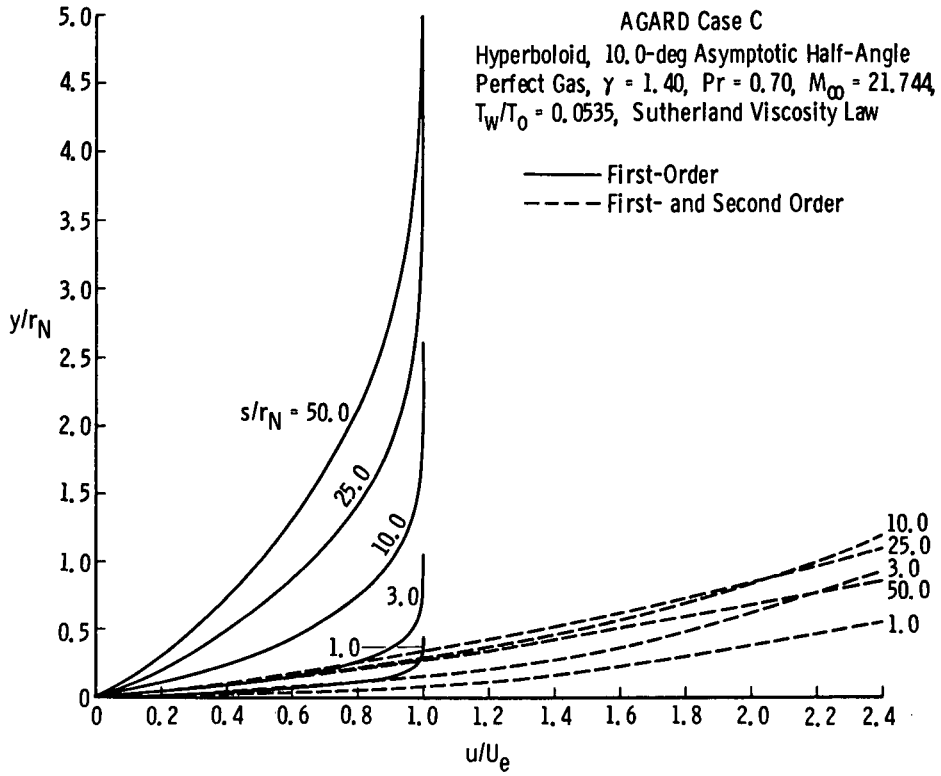

Fig.14 Velocity profiles

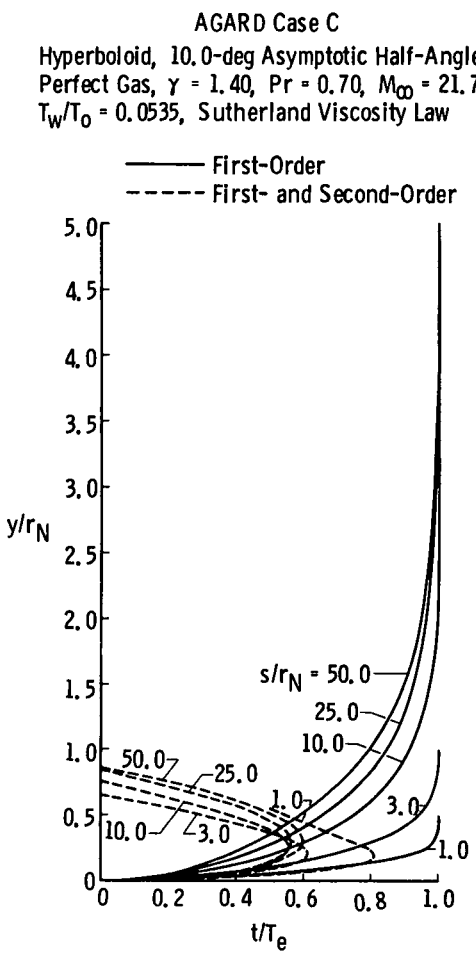

Fig.15 Temperature profiles

THE HYPERSONIC VISCOUS SHOCK-LAYER PROBLEM

by

R.T.Davis

Professor, Engineering Mechanics,
Virginia Polytechnic Institute,
Blacksburg, Virginia

THE HYPERSONIC VISCOUS SHOCK-LAYER PROBLEM

by R. T. Davis*

SUMMARY

Laminar flow past axisymmetric blunt bodies moving at hypersonic speeds is considered on the basis of a set of equations which govern the fully viscous shock-layer for moderate to high Reynolds numbers. The shock-layer equations are derived by writing the full Navier-Stokes equations in boundary-layer coordinates and performing an order of magnitude analysis on the terms in the equations. Terms are kept up to second-order in the inverse square root of the Reynolds number from both a viscous and an inviscid viewpoint, so that the simplified governing equations are uniformly valid to moderately low Reynolds numbers. To the order of the approximations involved the body surface conditions are given by slip and temperature jump conditions while a set of shock slip conditions are used to determine conditions behind the shock. The thin shock-layer approximation is then applied to the simplified set of governing equations, and the resulting equations are found to be of parabolic type. This is an important simplification as far as numerical solution of the problem is concerned since these equations can be solved by numerical methods similar to those developed for solving the boundary-layer equations. The numerical procedure consists of finding initial data at the stagnation-point and then integrating downstream using an implicit finite-difference method. The thin shock-layer approximation is then removed by iteration. Rather than work with the governing equations in the usual boundary-layer coordinates, it is found that it is more convenient to work with the equations in a transformed form. New dependent variables are defined by dividing the old dependent variables by their local values at the shock. In addition, a new normal independent variable is defined by dividing the old normal variable by the local distance from the body to the shock. Examples are presented to demonstrate the method and to compare with second-order boundary layer theory.

INTRODUCTION

The problem of computing the hypersonic laminar flow at moderate Reynolds numbers past axisymmetric blunt bodies is an interesting one and has attracted considerable interest due to the application to re-entry problems. One may approach the problem in several ways. Two of these methods are through numerical solution of the second-order boundary-layer equations and through numerical solution of the thin shock-layer equations.

The idea of using the second-order boundary-layer of Van Dyke [1] to compute the flow field is appealing; however, this approach can lead to considerable difficulty. This difficulty arises for two different reasons. First, the computing time from using second-order boundary-layer theory is excessive since one must compute the inviscid flow, first-order boundary-layer flow, flow due to displacement thickness and then the second-order boundary-layer flow. Second, one can experience difficulty on long axisymmetric blunt bodies since second-order boundary-layer theory in its present form does not properly take into account the effect of strong vorticity interaction which may occur far downstream on bodies of this type. In spite of this, Davis and Flügge-Lotz [2] have developed a numerical method, based on the earlier work of Blottner and Flügge-Lotz [3] for solving the first-order boundary-layer equations. Fannelop and Flügge-Lotz [16] have applied essentially the same method to plane problems. This method is successful as long as one does not have problems with strong vorticity interaction, and has access to a numerical method for solving for the first-order inviscid flow and for the second-order inviscid flow which arises due to displacement thickness. Davis and Flügge-Lotz [2] and Fannelop and Flügge-Lotz [16] used an approximate method to calculate the flow due to displacement thickness; however, later Marchand, Lewis and Davis [4] and Adams [5] calculated the flow due to displacement thickness exactly, and applied the method to a number of other flow problems.

Because of the difficulties mentioned above it is desirable to seek an alternate method of approach to the problem. The most appealing method is one originally suggested by Cheng [6] (see also Cheng [15]) for solving a set of equations valid in the entire shock-layer. Davis and Flügge-Lotz [2] have given a similar set of equations, but ones which contain some second-order curvature terms left out of Cheng's theory. Kaiser and Flügge-Lotz [14] have shown that these curvature terms have an influence on stagnation point shock stand-off distance and skin friction for $\gamma = 1.4$; however, as expected, the effect is small. The shock-layer equations contain all of the terms in the Navier-Stokes equations which contribute to second-order boundary-layer theory plus those which arise to second order in the outer inviscid flow. By making the thin shock-layer approximation on the resulting momentum equation normal to the body surface, these equations are reduced to a set of equations which are parabolic and can thus be solved numerically in a manner similar to the method of Blottner and Flügge-Lotz [3] for solving the first-order boundary-layer equations. This approximation is removed by iterating on the normal momentum equation which includes neglected terms.

Cheng's [6] equations are applicable to either the direct or inverse problem. However, he applied the method to only the inverse problem so that better accuracy could be gained. The method presented here is applied to the direct problem only and determines the shock shape if the body shape is given. The method is fast in terms of computer time and avoids the difficulty of strong vorticity interaction encountered in second-order boundary-layer theory.

We choose here to consider only the axisymmetric problem; however, the plane problem can be handled in exactly the same manner. We consider only the case of a perfect gas; however, no difficulties should be encountered in extending the method to chemically reacting flows.

The method to be discussed here is similar in idea, but represents a vast improvement in the method developed by Davis and Chyu [7] and Chen [8].

*Professor, Engineering Mechanics, Virginia Polytechnic Institute, Blacksburg, Virginia.

FORMULATION OF THE PROBLEM

The compressible Navier-Stokes equations are written in a boundary-layer coordinate system (see Fig. 1) and non-dimensionalized (see Nomenclature) by variables which are of order one in the region near the body surface (boundary layer) for large Reynolds numbers. This set of equations and variables are given by Van Dyke [1]. The same set of equations are then written in variables which are of order one in the essentially inviscid region outside the boundary layer. Terms in each set of equations are kept up to second order in the inverse square root of a Reynolds number. A comparison of the two sets of equations is then made and one set of equations is found from them which is valid to second order in both the outer and inner regions. A solution to this set of equations is thus uniformly valid to second order in the entire shock layer.

The shock-layer equations obtained from keeping terms up to second-order are of a hyperbolic-parabolic nature. If terms were kept up to third or higher order, the equations would be elliptic and thus very difficult to solve numerically.

A final approximation is made to the shock-layer equations by making the thin shock-layer approximation to the normal momentum equation. The purpose of this approximation is to make the equations totally parabolic. This final set of equations can then be solved by numerical methods similar to methods used in boundary-layer theory. An iteration method will be used to remove this approximation.

A more detailed discussion of the shock-layer equations can be found in a paper by Davis and Flügge-Lotz [2]. Weinbaum [9] has discussed the same set of equations, but applied to the near wake problem.

The viscous shock-layer equations are given by:

Continuity Equation

$$[(r + n\cos\phi)^j \rho u]_s + [(1 + \kappa n)(r + n\cos\phi)^j \rho v]_n = 0 , \tag{2.1}$$

s-Momentum Equation

$$\rho\left(u\frac{u_s}{1+\kappa n} + vu_n + \frac{\kappa}{1+\kappa n}uv\right) + \frac{p_s}{1+\kappa n} = \frac{\varepsilon^2}{(1+\kappa n)^2(r+n\cos\phi)^j}\left[(1+\kappa n)^2(r+n\cos\phi)^j\tau\right]_n , \tag{2.2a}$$

where $$\tau = \mu\left(u_n - \frac{\kappa u}{1+\kappa n}\right) , \tag{2.2b}$$

n-Momentum Equation

$$\rho\left(u\frac{v_s}{1+\kappa n} + vv_n - \frac{\kappa}{1+\kappa n}u^2\right) + p_n = 0 , \tag{2.3a}$$

where with the thin shock-layer approximation this equation (2.3a) becomes

$$p_n = \frac{\kappa}{1+\kappa n}\rho u^2 , \tag{2.3b}$$

Energy Equation

$$\rho\left(u\frac{T_s}{1+\kappa n} + vT_n\right) - \left(u\frac{p_s}{1+\kappa n} + vp_n\right) = \frac{\varepsilon^2}{(1+\kappa n)(r+n\cos\phi)^j}\left[(1+\kappa n)(r+n\cos\phi)^j q\right]_n + \frac{\varepsilon^2}{\mu}\tau^2 , \tag{2.4a}$$

where $$q = \frac{\mu}{\sigma}T_n , \tag{2.4b}$$

Equation of State

$$p = \frac{\gamma - 1}{\gamma}\rho T , \tag{2.5}$$

and

Viscosity Law

$$\mu = \frac{1 + c'}{T + c'}(T)^{3/2} , \tag{2.6a}$$

where $$c' = \frac{c^*}{(\gamma - 1)M_\infty^2 T_\infty^*} \tag{2.6b}$$

c^* is taken to be 198.6° R for air.

Consistent with the approximations used in the above set of equations the boundary conditions are given as below. Slip at the body surface is a second-order effect and is thus included here, we also consider the case of shock slip even though it is a third-order effect.

The conditions at the body surface are given by (see Fig. 1):

Surface Conditions

$$v = 0 \tag{2.7a}$$

$$u = \varepsilon^2 a_1 \frac{1}{p} \sqrt{\frac{\gamma - 1}{\gamma} T}\ \tau \ , \tag{2.7b}$$

$$p = p_w + \varepsilon^2 b_1 \frac{\sigma}{T} \sqrt{\frac{\gamma - 1}{\gamma} T}\ q \ , \tag{2.7c}$$

at $n = 0$

and

$$T = T_w + \varepsilon^2 c_1 \frac{\sigma}{p} \sqrt{\frac{\gamma - 1}{\gamma} T}\ q \ . \tag{2.7d}$$

In the above a_1, b_1 and c_1 are constants (see Shidlovskiy [10] and Nomenclature) and the subscript w refers to the body surface. The above boundary conditions can be modified to include mass injection at the boundary. Eq. (2.7c) is not used as a boundary condition, but is needed to obtain the surface pressure and to calculate the drag.

The conditions at the shock including slip are given by (see Fig. 1):

Shock Conditions

$$u_{sh} = u'_{sh} \sin(\alpha + \beta) + v'_{sh} \cos(\alpha + \beta) \tag{2.8a}$$

and

$$v_{sh} = - u'_{sh} \cos(\alpha + \beta) + v'_{sh} \sin(\alpha + \beta) \tag{2.8b}$$

where u'_{sh} and v'_{sh} are the components of velocity tangent and normal to the shock interface respectively and are given along with temperature, pressure, and density from the following expressions:

$$\rho_{sh} v'_{sh} = - \sin\alpha \ , \tag{2.8c}$$

$$\varepsilon^2 \mu_{sh} (u'_n)_{sh} + \sin\alpha\, u'_{sh} = \sin\alpha \cos\alpha \ , \tag{2.8d}$$

$$\varepsilon^2 \sigma^{-1} \mu_{sh} (T_n)_{sh} + \sin\alpha\, T_{sh} - \frac{\sin\alpha}{2} (u'_{sh} - \cos\alpha)^2 =$$

$$\frac{\sin\alpha}{2} \left[\frac{4\gamma}{(\gamma + 1)^2} \sin^2\alpha + \left(\frac{2}{\gamma - 1} - \frac{4(\gamma - 1)}{(\gamma + 1)^2} \right) \frac{1}{M_\infty^2} - \frac{4}{(\gamma + 1)^2 M_\infty^4 \sin^2\alpha} \right] \ , \tag{2.8e}$$

$$p_{sh} = \frac{2}{\gamma + 1} \sin^2\alpha - \frac{\gamma - 1}{\gamma(\gamma + 1) M_\infty^2} \ , \tag{2.8f}$$

and

$$\rho_{sh} = \gamma P_{sh} / (\gamma - 1) T_{sh} \ . \tag{2.8g}$$

The angles used in the shock conditions are shown in Fig. 1. Primes used with u_{sh} and v_{sh} denote components evaluated tangent and normal to the shock interface respectively. All other quantities used in the boundary conditions and governing equations are as defined in the Nomenclature. The conditions given are slightly different from those of Cheng [6,15] and Bush [17] in that they have been modified to give the exact shock relations for finite Mach number when slip is not present.

If one examines Eq. (2.1 - 2.6), it is found that the equations are parabolic if Eq. (2.3b) is used for the normal pressure gradient. These equations are quite similar to the compressible boundary-layer equations.

For ease in numerical computation a different form of Eq. (2.1 - 2.6) is used. This is done in the case of the independent normal variable in order to have a constant number of steps in the finite-difference grid between the body and the shock. This eliminates interpolation to determine the shock position and eliminates the problem of adding grid points in the normal direction as the computation proceeds downstream from the stagnation-point. The transformation is also important as far as the iteration method to determine the shock position is concerned. This will be discussed later. We also define new dependent variables by dividing the old dependent variables by their local values at the shock. The new dependent variables thus have the value one at the shock.

The new independent and dependent variables are defined by:

$$\eta = n/n_{sh} \ , \tag{2.9a}$$

$$\xi = s \ , \tag{2.9b}$$

$$\bar{u} = u/u_{sh} \ , \tag{2.9c}$$

$$\bar{v} = v/v_{sh} \ , \tag{2.9d}$$

$$\bar{t} = T/T_{sh} \ , \tag{2.9e}$$

$$\bar{p} = p/p_{sh} \ , \tag{2.9f}$$

$$\bar{\rho} = \rho/\rho_{sh} \ , \tag{2.9g}$$

and

$$\bar{\mu} = \mu/\mu_{sh} \ . \tag{2.9h}$$

The differential relations needed to transform Eq. (2.1 - 2.6) are given by:

$$\frac{\partial}{\partial s} = \frac{\partial}{\partial \xi} - \eta \frac{n'_{sh}}{n_{sh}} \frac{\partial}{\partial \eta} \ , \tag{2.10a}$$

$$\frac{\partial}{\partial n} = \frac{1}{n_{sh}} \frac{\partial}{\partial \eta} \ , \tag{2.10b}$$

and

$$\frac{\partial^2}{\partial n^2} = \frac{1}{n^2_{sh}} \frac{\partial^2}{\partial \eta^2} \ , \tag{2.10c}$$

where $n'_{sh} = \frac{dn_{sh}}{d\xi}$

The s-momentum and energy equations (2.2a, 2.4a) written in the transformed ξ,η plane can be written in the standard form for a parabolic equation as

$$\frac{\partial^2 w}{\partial \eta^2} + \alpha_1 \frac{\partial w}{\partial \eta} + \alpha_2 w + \alpha_3 + \alpha_4 \frac{\partial w}{\partial \xi} = 0 \tag{2.11}$$

where w equals $\bar{u}$ for the s-momentum equation, and $\bar{t}$ for the energy equation. The coefficients $\alpha_1 - \alpha_4$ can be written as follows:

s-Momentum Equation

$$\alpha_1 = \frac{\rho_{sh} u_{sh} n'_{sh}}{\varepsilon^2 \mu_{sh}} \frac{n_{sh}}{1 + \kappa n_{sh} \eta} \frac{\bar{\rho}\bar{u}\eta}{\bar{\mu}} - \frac{\rho_{sh} v_{sh} n_{sh}}{\varepsilon^2 \mu_{sh}} \frac{\bar{\rho}\bar{v}}{\bar{\mu}} + \frac{\bar{\mu}_\eta}{\bar{\mu}} + \frac{\kappa n_{sh}}{1 + \kappa n_{sh} \eta} + \frac{\cos\phi \, n_{sh}}{r + n_{sh}\eta \cos\phi} \tag{2.12a}$$

$$\alpha_2 = - \frac{\rho_{sh} u'_{sh} n_{sh}}{\varepsilon^2 \mu_{sh}} \frac{n_{sh}}{1 + \kappa n_{sh} \eta} \frac{\bar{\rho}\bar{u}\eta}{\bar{\mu}} - \frac{\rho_{sh} v_{sh} n_{sh}}{\varepsilon^2 \mu_{sh}} \frac{\kappa n_{sh}}{1 + \kappa n_{sh} \eta} \frac{\bar{\rho}\bar{v}}{\bar{\mu}} - \kappa \frac{n_{sh}}{1 + \kappa n_{sh} \eta} \frac{\bar{\mu}_\eta}{\bar{\mu}} - \left(\frac{\kappa n_{sh}}{1 + \kappa n_{sh} \eta} + \frac{\cos\phi \, n_{sh}}{r + n_{sh}\eta \cos\phi} \right) \frac{\kappa n_{sh}}{1 + \kappa n_{sh} \eta} \ , \tag{2.12b}$$

$$\alpha_3 = - \frac{p_{sh} n_{sh}}{\varepsilon^2 \mu_{sh}} \frac{n_{sh}}{1 + \kappa n_{sh} \eta} \frac{1}{\bar{\mu}} \frac{1}{u_{sh}} \left(\bar{p}_\xi - \frac{n'_{sh}}{n_{sh}} \eta \bar{p}_\eta + \frac{p'_{sh}}{p_{sh}} \bar{p} \right) \ , \tag{2.12c}$$

and

$$\alpha_4 = - \frac{\rho_{sh} u_{sh} n_{sh}}{\varepsilon^2 \mu_{sh}} \frac{n_{sh}}{1 + \kappa n_{sh} \eta} \frac{\bar{\rho}\bar{u}}{\bar{\mu}} \ , \tag{2.12d}$$

Energy Equation

$$\alpha_1 = \frac{\rho_{sh} u_{sh} n'_{sh} \sigma}{\varepsilon^2 \mu_{sh}} \frac{n_{sh}}{1 + \kappa n_{sh} \eta} \frac{\bar{\rho}\bar{u}\eta}{\bar{\mu}} - \frac{\rho_{sh} v_{sh} n_{sh} \sigma}{\varepsilon^2 \mu_{sh}} \frac{\bar{\rho}\bar{v}}{\bar{\mu}} + \frac{\bar{\mu}_\eta}{\bar{\mu}} + \frac{\kappa n_{sh}}{1 + \kappa n_{sh} \eta} + \frac{\cos\phi \, n_{sh}}{r + n_{sh}\eta \cos\phi} \ , \tag{2.13a}$$

$$\alpha_2 = - \frac{\rho_{sh} u_{sh} n_{sh} T'_{sh} \sigma}{\varepsilon^2 \mu_{sh} T_{sh}} \frac{n_{sh}}{1 + \kappa n_{sh} \eta} \frac{\bar{\rho}\bar{u}}{\bar{\mu}} \ , \tag{2.13b}$$

$$\alpha_3 = \frac{p_{sh} u_{sh} n_{sh} \sigma}{\varepsilon^2 \mu_{sh} T_{sh}} \frac{1}{\bar{\mu}} \left[\frac{n_{sh} \bar{u}}{1 + \kappa n_{sh} \eta} \left[\bar{p}_\xi - \frac{n'_{sh}}{n_{sh}} \eta \bar{p}_\eta + \frac{p'_{sh}}{p_{sh}} \bar{p} \right] + \frac{v_{sh}}{u_{sh}} \bar{v} \bar{p}_\eta \right] + \frac{u_{sh}^2 \sigma}{T_{sh}} \left(\bar{u}_\eta - \frac{\kappa n_{sh}}{1 + \kappa n_{sh} \eta} \bar{u} \right)^2 \tag{2.13c}$$

and

$$\alpha_4 = - \frac{\rho_{sh} u_{sh} n_{sh} \sigma}{\varepsilon^2 \mu_{sh}} \frac{n_{sh}}{1 + \kappa n_{sh} \eta} \frac{\bar{\rho}\bar{u}}{\bar{\mu}} \ . \tag{2.13d}$$

The remaining equations are written as follows:

Continuity Equation

$$[n_{sh} (r + n_{sh}\eta \cos\phi) \rho_{sh} u_{sh} \bar{\rho} \bar{u}]_\xi + [(r + n_{sh}\eta \cos\phi)\{(1 + \kappa n_{sh}\eta) \rho_{sh} v_{sh} \bar{\rho}\bar{v} - n'_{sh} \rho_{sh} u_{sh} \bar{\rho}\bar{u}\eta\}]_\eta = 0 \tag{2.14}$$

n-Momentum Equation

$$\frac{\bar{\rho}\bar{u}}{1+\kappa n_{sh}\eta}\left(\bar{v}_\xi - \frac{n'_{sh}}{n_{sh}}\eta\,\bar{v}_\eta + \frac{v'_{sh}}{v_{sh}}\,\bar{v}\right) + \frac{v_{sh}}{u_{sh}}\,\frac{\bar{\rho}\,\bar{v}}{n_{sh}}\,\bar{v}_\eta - \frac{\kappa}{1+\kappa n_{sh}\eta}\,\frac{u_{sh}}{v_{sh}}\,\bar{\rho}\bar{u}^2 + \frac{p_{sh}}{\rho_{sh}u_{sh}v_{sh}n_{sh}}\,\bar{p}_\eta = 0 \quad , \tag{2.15a}$$

where with the thin shock-layer approximation this equation becomes

$$\bar{p}_\eta = \frac{\kappa}{1+\kappa n_{sh}\eta}\,\frac{\rho_{sh}u^2_{sh}n_{sh}}{p_{sh}}\,\bar{\rho}\bar{u}^2 \quad , \tag{2.15b}$$

Equation of State

$$\bar{p} = \bar{\rho}\bar{t} \quad , \tag{2.16}$$

and

Viscosity Law

$$\bar{\mu} = \frac{T_{sh} + c'}{T_{sh}\bar{t} + c'}\,\bar{t}^{3/2} \tag{2.17}$$

where c' is as defined in Eq. (2.6b).

The boundary conditions become:

Surface Conditions

$$\bar{v} = 0 \quad , \tag{2.18a}$$

$$\left.\begin{aligned}\bar{u} &= \varepsilon^2 a_1 \frac{\mu_{sh}}{n_{sh}p_{sh}\bar{p}}\sqrt{\frac{\gamma-1}{\gamma}T_{sh}\bar{t}}\;\bar{\mu}\,(\bar{u}_\eta - \kappa n_{sh}\bar{u}) \quad , \\ \bar{t} &= \bar{t}_w + \varepsilon^2 c_1 \frac{\mu_{sh}}{n_{sh}p_{sh}\bar{p}}\sqrt{\frac{\gamma-1}{\gamma}T_{sh}\bar{t}}\;\bar{\mu}\bar{t}_\eta \quad ,\end{aligned}\right\} \quad \text{at } \eta = 0 \tag{2.18b, 2.18c}$$

and

and

Conditions at the Shock

$$\bar{u} = \bar{v} = \bar{t} = \bar{p} = \bar{\rho} = \bar{\mu} = 1 \qquad \text{at } \eta = 1 \tag{2.19a-2.19f}$$

The shock conditions are now involved in the governing equations (2.11 - 2.15) and are obtained from Eq. (2.8a-g). In the above equations (2.12-2.15) ( )' means d( )/dξ, which should not be confused with the primes in Eq. (2.8) which are defined differently.

An equation of mass conservation can be obtained from Eq. (2.14) by integrating from η = 0 (the body) to η = 1 (the shock) while holding ξ constant. This results in

$$\frac{dm}{d\xi} = (r + n_{sh}\cos\phi)\,[n'_{sh}\rho_{sh}u_{sh} - (1+\kappa n_{sh})\,\rho_{sh}v_{sh}] \tag{2.20}$$

where

$$m = \int_0^1 n_{sh}\,(r + n_{sh}\eta\cos\phi)\,\rho_{sh}u_{sh}\,\bar{\rho}\bar{u}\,d\eta \tag{2.21}$$

is proportional to the rate of mass flux between the body and shock at a given position on the body surface.

Eq. (2.20) and (2.21) will be used to determine the shock location in the numerical method which determines the flow field.

The dimensionless shear stress, heat transfer and wall pressure (see Nomenclature) are given by

$$C_f = 2\varepsilon^2\,\frac{\mu_{sh}u_{sh}}{n_{sh}}\,\bar{\mu}\left(\frac{\partial\bar{u}}{\partial\eta} - \kappa n_{sh}\bar{u}\right) \quad , \tag{2.22}$$

$$\left.\begin{aligned}q_w &= -\varepsilon^2\frac{\mu_{sh}T_{sh}}{n_{sh}\sigma}\,\bar{\mu}\,\frac{\partial\bar{t}}{\partial\eta} - \varepsilon^2\,\frac{\mu_{sh}u^2_{sh}}{n_{sh}}\,\bar{\mu}\bar{u}\,\frac{\partial\bar{u}}{\partial\eta} \quad , \\ p_w &= p - \varepsilon^2 b_1\frac{\mu_{sh}}{n_{sh}\bar{t}}\sqrt{\frac{\gamma-1}{\gamma}T_{sh}\bar{t}}\;\bar{\mu}\bar{t}_\eta \quad ,\end{aligned}\right\} \quad \text{at } \eta = 0 \tag{2.23, 2.24}$$

while the Stanton number is defined as

$$St = -\frac{q_w}{H_o - H_w} \quad . \tag{2.25}$$

The second term in Eq. (2.23) is a term which arises only in slip flow and is due to sliding friction (see Maslen [11]). If wall injection is present in slip flow, additional terms arise in these shear stress and heat transfer expressions.

STAGNATION-POINT SOLUTIONS

The governing equations (2.11 - 2.17) reduce to ordinary differential equations at the stagnation-point if Eq. (2.15b) is used for the normal pressure gradient. This can be done by expanding the shock conditions (2.8a-g) in power series. If Eq. (2.15b) is used for the normal momentum equation, no truncation of the series is required and the series can be integrated term by term indicating that the equations are parabolic. There is a difficulty with the boundary conditions, however. This can be demonstrated as follows. Assume a power series for the shock shape in the form

$$n_{sh} = n_{sh_1} + s^2 n_{sh_2} + \cdots \qquad (3.1)$$

Using this relation in the equation for u_{sh} (2.8a) along with Eq. (2.8c-g) and simplifying we can find an expression for u_{sh} in terms of a power series. For simplicity we consider here only the no slip case. The first term in the series is of the form

$$u_{sh} = \left[1 - \frac{2}{\gamma + 1}\left[1 - \frac{1}{M_\infty^2}\right]\frac{2n_{sh_2}}{1 + n_{sh_1}}\right] s + \cdots \qquad (3.2)$$

A similar expression results for the pressure behind the shock. This is given by

$$p_{sh} = \frac{2}{\gamma + 1} - \frac{\gamma - 1}{\gamma(\gamma + 1)M_\infty^2} - \frac{2}{\gamma + 1}\left(1 - \frac{2n_{sh_2}}{1 + n_{sh_1}}\right)^2 s^2 + \cdots \qquad (3.3)$$

v_{sh}, T_{sh} and ρ_{sh} do not involve n_{sh_2} in the first terms of their expansions.

The difficulty mentioned is that n_{sh_2} cannot be determined from the stagnation-point equations. It is a quantity that depends upon the flow downstream. We must therefore assume a value for n_{sh_2}. The usual assumption is to assume that it is zero. In order to find stagnation-point solutions we do this, but later we show how this assumption can be removed. It will be shown that the assumption that $n_{sh_2} = 0$ is included in the assumption of local similarity and can result in an error of about 20%. The influence of the downstream shock shape on the solution has the effect of making the problem elliptic rather than parabolic. Fortunately in some cases the problem is so weakly elliptic that the elliptic nature of the boundary conditions can be overcome by iteration. It may be possible to treat n_{sh_2} as an initial condition and determine it from the condition that the solution proceed downstream. This possibility has not been explored.

Fig. 2 - 9 are the results obtained from solving the governing equations at the stagnation-point. These results will be discussed later. The next section will deal with the method of solution of the equations.

METHOD OF SOLUTION

In this section we discuss the method of solution of the problem. The problem basically reduces to the solution of parabolic partial differential equations. There are many ways to solve this type of equation. The method that will be used here is similar to the method that Blottner and Flügge-Lotz [3] developed for solving the boundary-layer equations. This method has been shown to be stable and accurate. A few modifications have been made to the method to solve the present problem. Below we will give a brief discussion of the application of this method to the present problem.

The derivatives in Eq. (2.11) are replaced with finite-difference quotients. In order to handle high Reynolds number cases we allow for variable grid spacing in the η direction so that we can use many points in the region near the body surface where the variables are changing rapidly. Let the subscript m denote the station measured along the body surface and n denote the station measured normal to the body surface. It can then be shown by Taylor series expansions that central differences taken in the η direction at the point m,n are

$$\left(\frac{\partial w}{\partial \eta}\right)_{m,n} = \frac{\Delta\eta_{n-1}}{\Delta\eta_n(\Delta\eta_n + \Delta\eta_{n-1})} w_{m,n+1} + \frac{\Delta\eta_n - \Delta\eta_{n-1}}{\Delta\eta_n \Delta\eta_{n-1}} w_{m,n} - \frac{\Delta\eta_n}{\Delta\eta_{n-1}(\Delta\eta_n + \Delta\eta_{n-1})} w_{m,n-1} - \frac{1}{6}\left(\frac{\partial^3 w}{\partial \eta^3}\right)_{m,n} \Delta\eta_n \Delta\eta_{n-1}, \qquad (4.1)$$

and

$$\left(\frac{\partial^2 w}{\partial \eta^2}\right)_{m,n} = \frac{2}{\Delta\eta_n(\Delta\eta_n + \Delta\eta_{n-1})} w_{m,n+1} - \frac{2}{\Delta\eta_n \Delta\eta_{n-1}} w_{m,n} + \frac{2}{\Delta\eta_{n-1}(\Delta\eta_n + \Delta\eta_{n-1})} w_{m,n-1} - \frac{1}{12}\left(\frac{\partial^4 w}{\partial \eta^4}\right)_{m,n} \Delta\eta_n \Delta\eta_{n-1} - \frac{1}{3}\left(\frac{\partial^3 w}{\partial \eta^3}\right)_{m,n} (\Delta\eta_n - \Delta\eta_{n-1}) - \frac{1}{12}\left(\frac{\partial^4 w}{\partial \eta^4}\right)_{m,n} (\Delta\eta_n - \Delta\eta_{n-1})^2 . \qquad (4.2)$$

The subscript n on a step increment denotes the step from the n^{th} to the n plus first point.

The derivative in the ξ direction in Eq. (2.11) is handled in the usual way as a two-point difference. If the derivative $\partial w/\partial \xi$ is evaluated at the midpoint (m - 1/2, n) and the other terms are averaged we obtain the Crank-Nicolson scheme. If a backward difference is used for $\partial w/\partial \xi$ at the point (m,n) and all other quantities are evaluated at (m,n) also we obtain a purely implicit scheme. The implicit method is more stable than the Crank-Nicolson scheme; however, it was found that in the present problem both schemes were stable as long as shock slip was not included. When shock slip was included it was found that the Crank-Nicolson method could become unstable. This was probably due to the way in which the shock slip was handled. The truncation errors in the ξ direction in the Crank-Nicolson scheme are smaller than those in the implicit scheme, therefore one would expect more accurate results from the Crank-Nicolson scheme for a given step size $\Delta\xi$. The numerical results do not show much difference, however, between the two methods.

When the difference quotients are substituted into the differential equation (2.11) a difference equation of the following form results.

$$A_n W_{n-1} + B_n W_n + C_n W_{n+1} = D_n \tag{4.3}$$

The solution to this equation is straightforward once the boundary conditions are given. For the method of solution one is referred to Richtmyer [12]. The boundary conditions at the wall are given by writing the slip conditions (2.18b) or (2.18c) in three point forward difference form. Manipulation of this equation, Eq. (4.3), and the equation for the solution to the problem allows one to determine a condition to satisfy the wall conditions. The condition at the shock is given by W = 1; however, the shock conditions now appear as unknown coefficients in the Eq. (2.12) or (2.13).

The method of solution is then as follows. Start at the stagnation-point where $\partial w/\partial \xi = 0$. Eq. (2.11) then reduces to an ordinary differential equation. Care must be taken to evaluate the pressure gradient term properly at the stagnation-point. This can be done by series expansion. Make initial guesses for all of the flow profiles. Integrate, using the finite-difference method, the energy equation (2.11 and 2.13). Now evaluate all quantities related to temperature such as viscosity. Next, integrate, in the same manner, the s momentum equation (2.11 and 2.12) to determine a $\bar{u}$ velocity profile. Next integrate the continuity equation (2.14) to determine first the shock stand-off distance from Eq. (2.21) and then the $\bar{v}$ component of velocity from Eq. (2.14). At the stagnation-point these equations must also be handled with series expansions. Finally integrate Eq. (2.15) to determine the pressure. Evaluate the coefficients in the equations using the shock conditions (2.8) and the new value of n_{sh}. Repeat the above steps until the solution converges. Then step along the body surface and iterate at each step if necessary. The previous values of the profiles are used at each new step as a first guess. It was found that there was very little change after the second iteration at each step except at the stagnation-point where more iterations are needed.

In the first approximation we assume that n'_{sh} is equal to zero at each step on the body surface. We also use Eq. (2.15b) in the first approximation. In the second approximation, we use n'_{sh} calculated from the stand-off distance in the first approximation. We also use the $\bar{v}$ terms calculated in the first approximation to approximate the $\bar{v}$ terms in Eq. (2.15a) in the second approximation. Further iterations are performed until the solution converges. These approximations on n'_{sh} and the $\bar{v}$ terms in the normal momentum equation are necessary in order to make the equations parabolic.

The shock-slip conditions (2.8) were handled by simply evaluating the $(u'_n)_{sh}$ and $(T_n)_{sh}$ terms from the previous step in the iteration and then solving the resulting equations for the shock conditions. This was found to converge even for fairly small values of Reynolds number.

The option of using variable grid spacing in the η direction helps in high Reynolds number or cold wall cases. The computer program contains the variable spacing option, which has been used with success in decreasing the computation time while attaining high accuracy. If one looks at the truncation error terms in the η direction in Eq. (2.11) using Eq. (4.1) and (4.2) one finds that they are

$$\text{Relative Truncation Error} = \frac{\left[\frac{1}{12}\Delta\eta_n\,\Delta\eta_{n-1}\left(\frac{\partial^4 w}{\partial\eta^4} + 2\alpha_1\frac{\partial^3 w}{\partial\eta^3}\right)_{m,n} + \frac{1}{3}(\Delta\eta_n - \Delta\eta_{n-1})\left(\frac{\partial^3 w}{\partial\eta^3}\right)_{m,n}\right]}{\left(\frac{\partial^2 w}{\partial\eta^2} + \alpha_1\frac{\partial w}{\partial\eta}\right)_{m,n}}$$

We have neglected the last term in Eq. (4.2) since it will be small. From a constant step size calculation we can calculate the terms in the brackets. Then by setting the relative truncation error equal to a constant we can calculate the grid spacing $\Delta\eta_n$ that would produce the desired truncation error. Using this new step size distribution we can then recalculate a solution which, for the same number of steps in η, should be much more accurate. A calculation of this type done at the stagnation-point can save considerable computing time for a computation that goes far downstream. A method could be devised for changing the grid spacing as we go downstream also; however, in the present program the grid spacing determined at the stagnation-point is used at every downstream station.

DISCUSSION OF RESULTS

As a check on the method of solution, stagnation-point solutions were calculated to compare with some of the results of Cheng [13]. Cheng gives extensive results but only a few points are shown to point out the agreement that is obtained. Identical flow conditions were assumed. The results are shown in Fig. 2 for Stanton number. Even though the equations are slightly different from Cheng's, one sees that the results are almost identical. The K^2 parameter is a parameter defined by Cheng [13] and Re_s is the Reynolds number behind the shock on the stagnation streamline. The characteristic length taken in the shock Reynolds number is the body nose radius. The term n_{sh_2} in Eq. (3.1) is taken to be zero in the calculations. The influence of this assumption will be shown later.

Fig. 3 - 6 are stagnation-point results for a typical flow situation. Again n_{sh_2} is taken to be zero. The free stream conditions were taken to be standard atmospheric conditions at 250,000 feet with a free stream velocity of 20,000 feet per second. Prandtl number σ is taken to be 0.7, the ratio of specific heats γ is taken to be 1.4 and Sutherland's viscosity law is used. If the body nose radius of curvature is chosen to be one inch, then ε turns out to be 0.224.

The results shown in Fig. 3 and 4 indicate that for low Reynolds numbers, shock and body slip are large effects, in fact above values of ε of about 0.2, they should not be neglected. These two figures also give some indication of the range of validity of second-order boundary-layer theory. For both skin friction and Stanton number, second-order boundary-layer theory predicts an increase over first-order theory, therefore these curves should show an upward curvature initially as they do. The trend has already reversed at around an ε of about 0.3, so second-order boundary-layer theory appears to only be valid to an ε of about 0.2. If one looks at Fig. 5 and 6 one notices that this is about the value of ε when the viscous layer extends from

the body to the shock. One would not expect that even higher order boundary-layer theory would be valid when there is no distinct boundary-layer or outer inviscid flow. The velocity and temperature profiles shown in Fig. 5 and 6 are for the case when both shock slip and body slip are included.

A typical case was chosen to compare the present results with second-order boundary-layer theory. Complete second-order calculations have been made by Adams [5] for flow over a hyperboloid which is asymptotic to a cone of 45° total interior angle. For purposes of comparison the same flow conditions, viscosity law, etc. were chosen here. Free stream Mach number M_∞ is 10.0, ε is 0.1806, Prandtl number σ is 0.70, and the ratio of specific heats γ is 1.40. The ratio of wall to inviscid stagnation-point temperature is taken to be 0.2. Shock and body slip are included in all calculations.

Fig. 7 through 9 indicate the effect of various approximations at the stagnation-point. Fig. 10 and 11 show the solutions for one particular value of ε at points along the body surface. In the first approximation n'_{sh} is taken to be zero at every point along the body surface and the $\bar{v}$ terms are neglected in the normal momentum equation (2.15a). The lower curve in Fig. 7 shows the stand-off distance at the stagnation-point as a function of ε with these approximations. Fig. 11 shows the distribution of n_{sh} along the body surface for one particular value of ε. The values of n'_{sh} and $\bar{v}$ calculated from this approximation are put back into the equations and the equations are integrated again resulting in a new solution. In subsequent iterations the previous calculated values of the quantities n'_{sh} and $\bar{v}$ are used. As is shown in Fig. 10 and 11 the convergence is achieved in two steps. There is very little difference in the results in further iterations as the figures show. These results are also a good check of the assumption of local similarity at the stagnation-point. The effect of n'_{sh} being equal to zero represents an error of about 20% in itself at the stagnation-point in calculating skin friction as is shown in Fig. 8. This is found by comparing the two thin shock-layer calculations, one including the effect of n'_{sh}, the other not. The effect is not as pronounced on other flow quantities such as Stanton number shown in Fig. 9. Kaiser and Flügge-Lotz [14] have found similar results for flow past a sphere in using the method of series truncation. It is interesting to note that the shock stand-off distance at the stagnation-point converges to the exact inviscid value as ε goes to zero (i.e. Reynolds number goes to infinity). The value obtained at AEDC from an inviscid blunt-body solution using the Lomax Ames program gives a value of 0.1498 for the stagnation-point shock stand-off distance under identical free stream conditions. Fig. 7 shows that a value very close to this is being approached as ε goes to zero. Other flow field quantities show similar correct trends.

One reason that the method works so well is that the shock stand-off distance in the first approximation is quite close to the final result and therefore the n'_{sh} value calculated from the first approximation is quite accurate. Fig. 11 indicates this and also shows that the stand-off distance does not change after the second iteration.

Fig. 12 and 13 show velocity and temperature profiles at various stations along the body surface. These were obtained from the second iteration. One sees clearly how the linear type velocity profile is swallowed up as the outer flow becomes an inviscid cone type flow.

Second-order boundary-layer theory gives erroneous results when applied to a problem of this type. Fig. 14 shows the result of applying second-order boundary-layer theory to the problem. The effect of strong vorticity interaction is not taken care of properly by second-order boundary-layer theory. Fig. 15 and 16 show similar comparisons for Stanton number and surface pressure.

Fig. 17, 18 and 19 show a comparison of results obtained from the present method with experimental results obtained by Little [18]. The test cases were for a range of shock Reynolds numbers resulting in the different values of ε and for flows over hyperboloid shaped bodies of various lengths opening to asymptotic total interior angles of 90°, 45°, and 20°. The numerical calculations were performed including both shock and body slip.

Little [18] has mentioned that some of the data for the 90° hyperboloid cases is not applicable to the present calculations, especially for the short bodies, since the bodies were not long enough for the flow to reach a supersonic condition before the base of the body was reached. This should explain the scatter in the data for this case. The same type of scatter is not present in the other cases and the data seems to follow a definite trend. Use of values of θ_r and α_t in the slip conditions other than one would reduce the drag and would make the calculations agree better with the experiments. Little estimates his possible experimental error in drag at plus or minus seven percent. In general, the calculations fall within these error bounds. Pressure jump was included in calculating the drag, but had a small effect due to the warm body conditions.

AGARD CASE C

Sample numerical calculations were invited for a seminar "Numerical Methods for Viscous Flows" held at the National Physical Laboratory, Teddington, England, for the period of 18-21 September 1967. One of the cases considered was as follows: 20° Total Interior Angle Hyperboloid, Altitude = 250,000 ft., Freestream Velocity, U_∞ = 20,000 f/s, Wall Temperature, T_w = 1,800°R, Nose Radius, a = 1 in.

The parameters in the viscous shock layer method which result from these conditions are: Wall to Stagnation Temperature Ratio, T_w/T_o = 0.0535, Free Stream Mach Number, M_∞ = 21.75, Perturbation Parameter, ε = 0.2232.

Fig. 3 and 4 indicate how these conditions influence stagnation-point solutions. We see that we are in what might be called a second-order boundary-layer regime where slip effects are small. Fig. 20-25 show the solutions for fifty nose radii downstream on the hyperboloid. Unless otherwise noted, all slip effects are included. As in the previous case for a 45° hyperboloid, see Fig. 10 - 16, second-order boundary-layer theory is not valid far downstream where vorticity interaction effects are overpredicted by second-order boundary-layer theory. Fig. 22 indicates the influence of the pressure jump condition, Eq. (2.7c) and (2.24), on the wall pressure. For cold wall conditions such as AGARD CASE C this can be a significant effect. The effect has been overlooked in previous second-order boundary-layer and viscous shock-layer calculations.

The integrated drag effects have been calculated and are as shown in table 1. Table 1 also includes values for skin friction, Stanton number and wall pressure. The drag calculations include the pressure jump effect.

ACKNOWLEDGEMENT

This research was initiated under NASA Grant NGR-47-004-006 and continued while the author was a summer employee of Sandia Corporation. Some of the final calculations were made with the support of Sandia Contract #48-7795. An early version of the work was presented at the AGARD Seminar on "Numerical Methods for Viscous Flows," National Physical Laboratory, Teddington, England, Sept. 18-21, 1967.

REFERENCES

[1] Van Dyke, M., "A Review and Extension of Second-Order Hypersonic Boundary-Layer Theory," Rarefied Gas Dynamics, Fluid Symposium Supplement 2, Vol. II (J. A. Lauermann, ed.), Academic Press, New York, 1963.

[2] Davis, R.T. and Flügge-Lotz, I., "Second-Order Boundary-Layer Effects in Hypersonic Flow Past Axisymmetric Blunt Bodies," J. Fluid Mechanics, Vol. 20, Part 4, 1964, pp. 593-623.

[3] Blottner, F.G. and Flügge-Lotz, I., "Finite-Difference Computation of the Boundary-Layer with Displacement Thickness Interaction," J. de Mecanique, Vol. II, No. 4, 1963.

[4] Marchand, E.O., Lewis, C.H., and Davis, R.T., "Second-Order Boundary-Layer Effects on a Slender Blunt Cone at Hypersonic Conditions," AIAA Paper No. 69-54, Presented at the 6th Aerospace Sciences Meeting, New York, 1968.

[5] Adams, J.C., "Higher Order Boundary-Layer Effects on Analytic Bodies of Revolution," AEDC-TR-68-57, 1968.

[6] Cheng, H.K., "The Blunt-Body Problem in Hypersonic Flow at Low Reynolds Number," CAL Report AF-1285-A-10, 1963.

[7] Davis, R.T. and Chyu, W.J., "Laminar Flow Past a Sphere at High Mach Number," J. Fluid Mechanics, Vol. 24, Part 3, 1966, pp. 481-495.

[8] Chen, C.H., "Laminar Flow Past Axisymmetric Blunt Bodies at High Mach Number and Moderate Reynolds Number," Virginia Polytechnic Institute, Department of Engineering Mechanics Ph.D. Dissertation, 1967.

[9] Weinbaum, S., "Near Wake Uniqueness and a Re-Examination of the Throat Concept in Laminar Mixing Theory," AIAA Paper No. 67-65, Presented at the 5th Aerospace Sciences Meeting, New York, 1967.

[10] Shidlovskiy, V.P., "Introduction to Dynamics of Rarefied Gases," American Elsevier Publishing Company, New York, 1967.

[11] Maslen, S.H., "On Heat Transfer in Slip Flow," Journal of Aeronautical Sciences, Vol. 25, No. 6, 1958, pp. 400-401.

[12] Richtmyer, R.D., "Difference Methods for Initial-Value Problems," Interscience Publishers, Inc., New York, 1957.

[13] Cheng, H.K., "Hypersonic Shock-Layer Theory of the Stagnation Region at Low Reynolds Number," 1961 Heat Transfer and Fluid Mechanics Institute, Stanford Press, 1961.

[14] Kaiser, J.E. and Flügge-Lotz, I., "Viscous Hypersonic Flow Around a Blunt Body," Division of Engineering Mechanics, Stanford University, Technical Report No. 178, 1968.

[15] Cheng, H.K., "Viscous Hypersonic Blunt-Body Problems and the Newtonian Theory," in Fundamental Phenomena in Hypersonic Flow, J. G. Hall, ed., Cornell University Press, 1966, pp. 90-132.

[16] Fannelop, T.K. and Flügge-Lotz, I., "Viscous Hypersonic Flow Over Simple Blunt Bodies Including Second-Order Effects," Journal de Mecanique, Vol. 5, 1966, pp. 69-100.

[17] Bush, W.B., "On the Viscous Hypersonic Blunt Body Problem," Journal of Fluid Mechanics, Vol. 20, Part 3, 1964, pp. 353-367.

[18] Little, H.R., "An Experimental Investigation of Surface Conditions on Hyperboloids and Paraboloids at a Mach Number of 10," University of Tennessee M.S. Thesis, 1969.

NOMENCLATURE

a_1 = slip constant taken to be $1.2304\ (2 - \theta_r)/\theta_r$

a^* = body nose radius of curvature

b_1 = slip constant taken to be $1.1750\ (2 - \theta_r)/\theta_r$

c_1 = slip constant taken to be $2.3071\ (2 - \alpha_t)/\alpha_t$

C_D = drag coefficient based on the local cross sectional area, $2\ \text{Drag}/(\rho_\infty U_\infty^2 A)$

C_f = skin friction coefficient, $2\tau^*_w/(\rho^*_\infty U^{*2}_\infty)$

c^*_p = specific heat at constant pressure

H = total enthalpy, H^*/U^{*2}_∞

M_∞ = free stream Mach number

n = coordinate measured normal to the body, nondimensionalized by the body nose radius

p = pressure, $p^*/(\rho^*_\infty U^{*2}_\infty)$

q = heat transfer, $q^*/(\rho^*_\infty U^{*3}_\infty)$

r = radius measured from the axis of symmetry to a point on the body surface, nondimensionalized by the body nose radius

s = coordinate measured along the body surface, nondimensionalized by the body nose radius

St = Stanton number defined by Eq. (2.25)

T = temperature, $T = T^*/(U^{*2}_\infty/c^*_p)$

T^*_∞ = free stream temperature

u = velocity component tangent to the body surface u^*/U^*_∞

U^*_∞ = free stream velocity

v = velocity component normal to the body surface, v^*/U^*_∞

z = axial distance measured from the stagnation point

α = shock angle, see Fig. 1

α_t = thermal accommodation coefficient, taken to be 1

β = angle defined in Fig. 1

γ = ratio of specific heats

ε = perturbation parameter, $\varepsilon = \left[\dfrac{\mu^*(U^{*2}_\infty/c^*_p)}{\rho^*_\infty U^*_\infty a^*}\right]^{1/2}$

θ_r = fraction of incident molecules diffusely reflected, taken to be 1

κ = surface curvature, nondimensionalized by the inverse of the body nose radius

μ = coefficient of viscosity,

ρ = density, $\rho \approx \rho^*/\rho^*_\infty$

ρ^*_∞ = free stream density

τ = shear stress, $\tau^*/(\rho^*_\infty U^{*2}_\infty)$

ϕ = body angle defined in Fig. 1

Subscripts

w = wall value

o = stagnation-point value

sh = value behind the shock

∞ = free stream conditions

Superscripts

- = quantities divided by their shock values

* = dimensional quantities

j = 0 for plane flow and 1 for axisymmetric flow

TABLE 1

Drag and Stagnation Point Values for the AGARD Case C Hyperboloid

AGARD Case C

Drag Coefficients

	Pressure C_{D_P}	Friction C_{D_f}	Total $C_{D_{tot}}$
Shock + Body Slip	0.103	0.122	0.225
No Shock Slip	0.102	0.124	0.226

Stagnation Point Values

	C_f/s	St	P_w
Shock + Body Slip	0.491	0.383	0.628 With Jump 0.925 Without Jump
No Shock Slip	0.541	0.423	0.617 With Jump 0.924 Without Jump

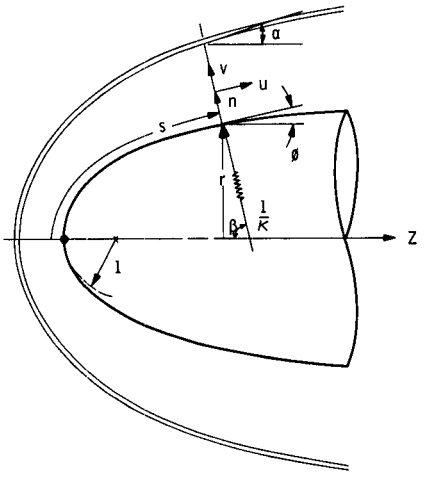

Fig.1 Coordinate system

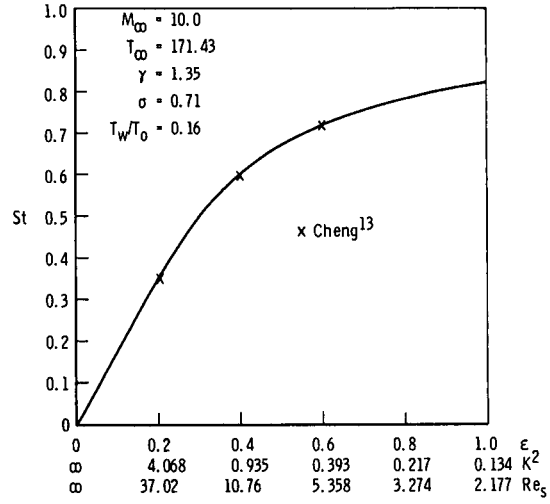

Fig.2 Comparison of the present results with those of Cheng[13]

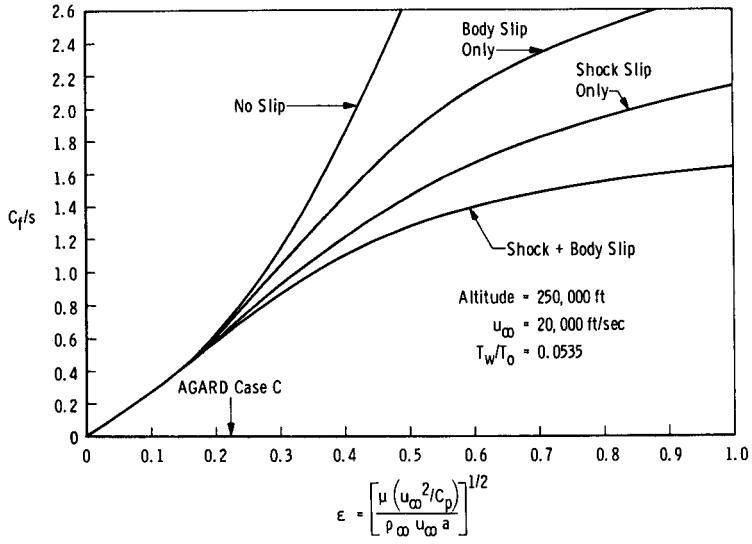

Fig.3 Skin friction at the stagnation point as a function of ϵ

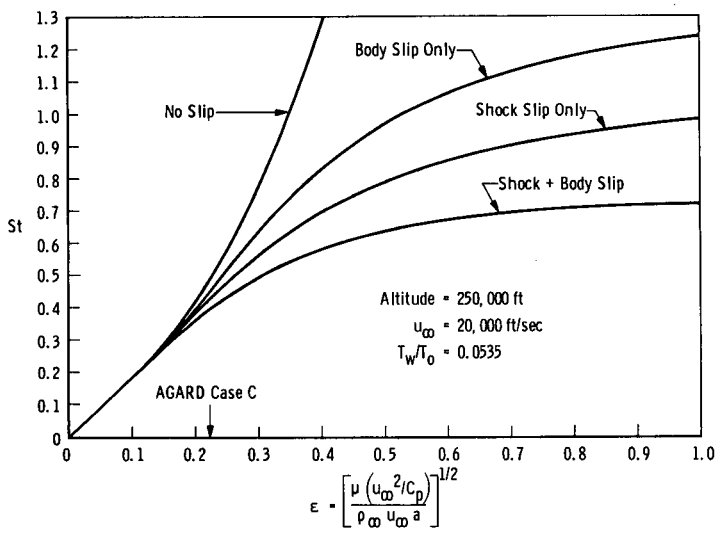

Fig. 4 Stanton number at the stagnation point as a function of ϵ

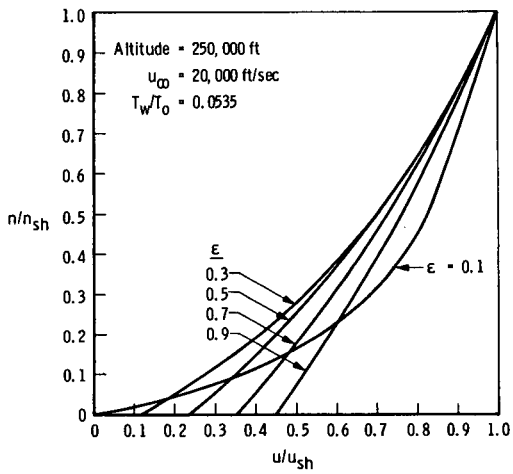

Fig. 5 Velocity profiles tangent to the body surface at the stagnation point as a function of ϵ

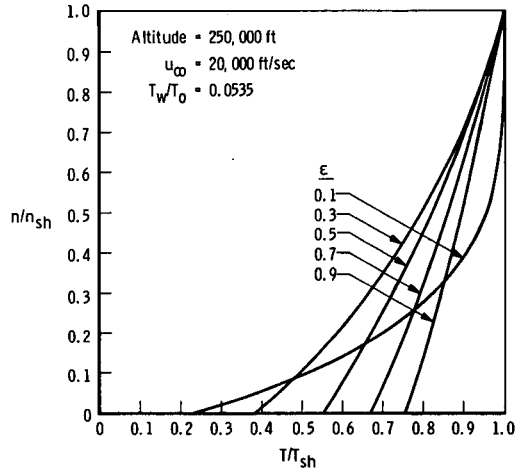

Fig. 6 Temperature profiles at the stagnation point as a function of ϵ

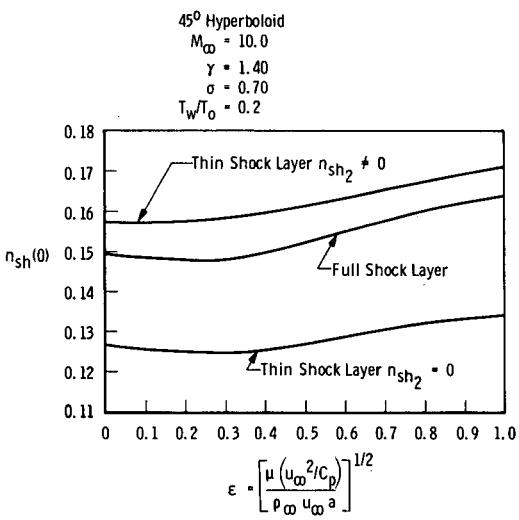

Fig. 7 Shock stand-off distance at the stagnation point as a function of ϵ

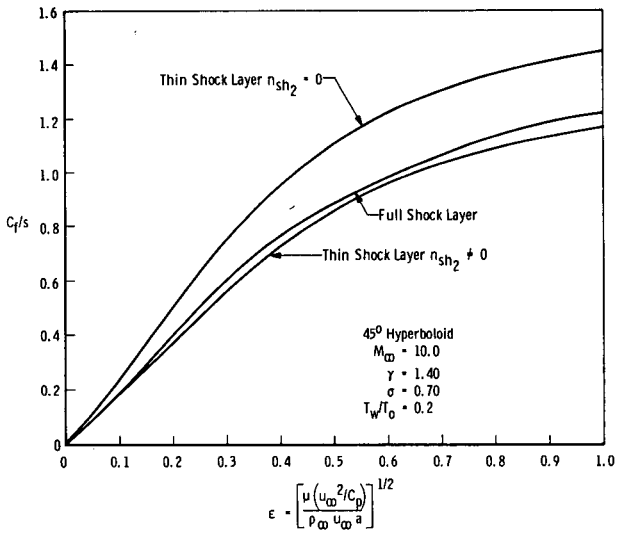

Fig. 8 Skin friction at the stagnation point as a function of ϵ

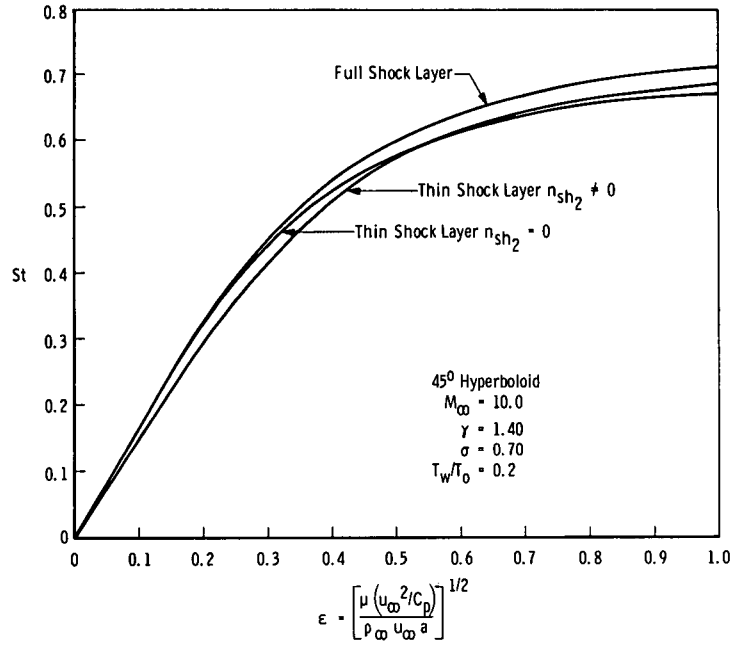

Fig.9 Stanton number at the stagnation point as a function of ϵ

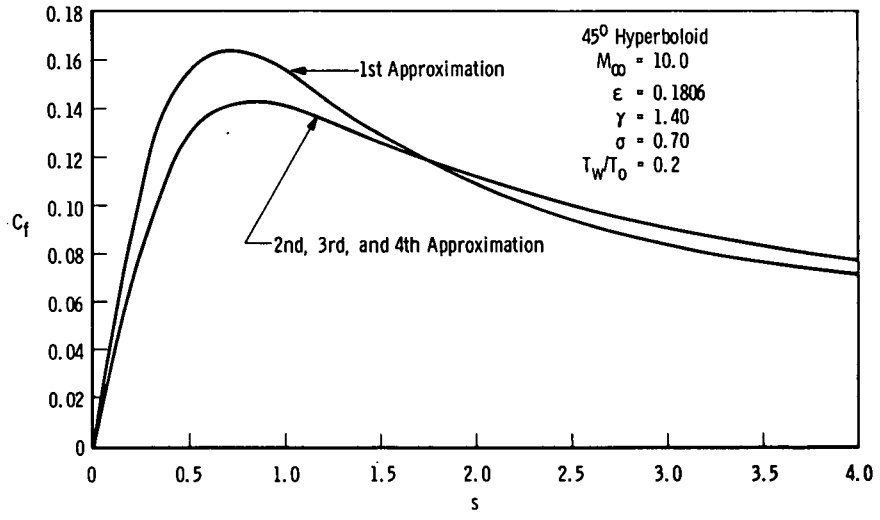

Fig.10 Skin friction on a hyperboloid

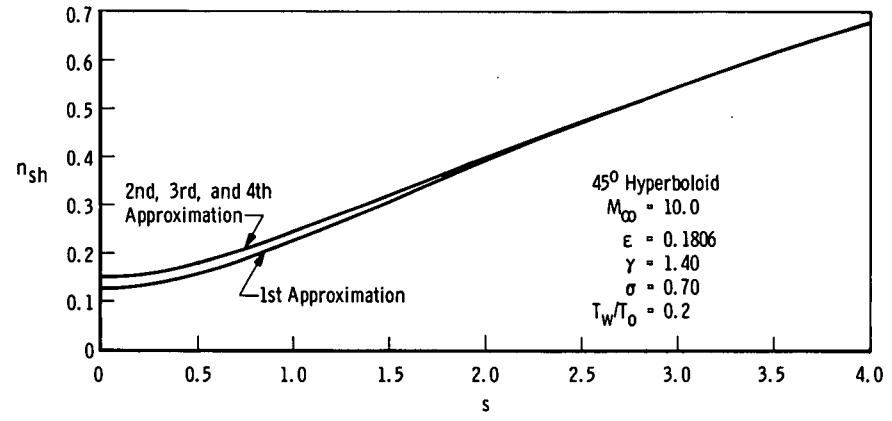

Fig.11 Shock stand-off distance on a hyperboloid

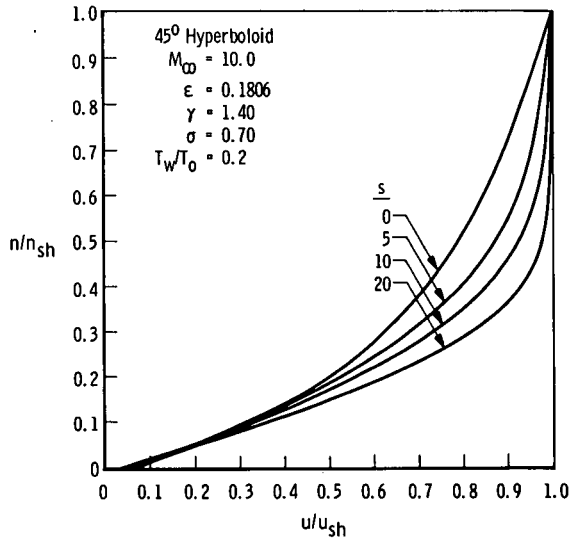

Fig.12 Velocity profiles tangent to the body surface of a hyperboloid

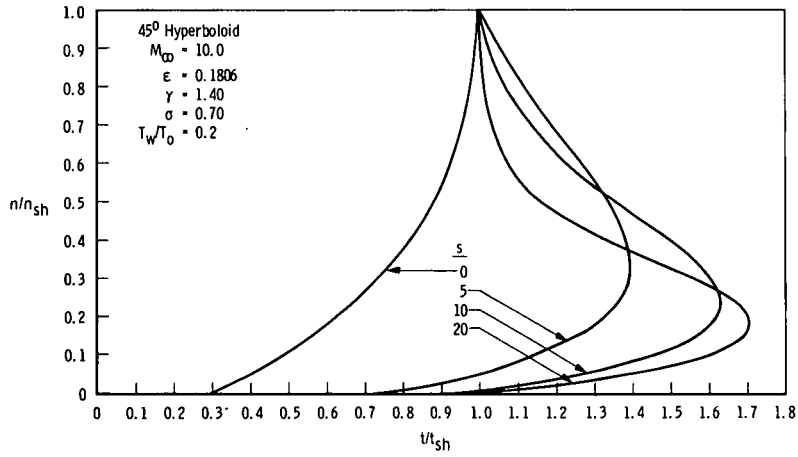

Fig.13 Temperature profiles normal to a hyperboloid surface

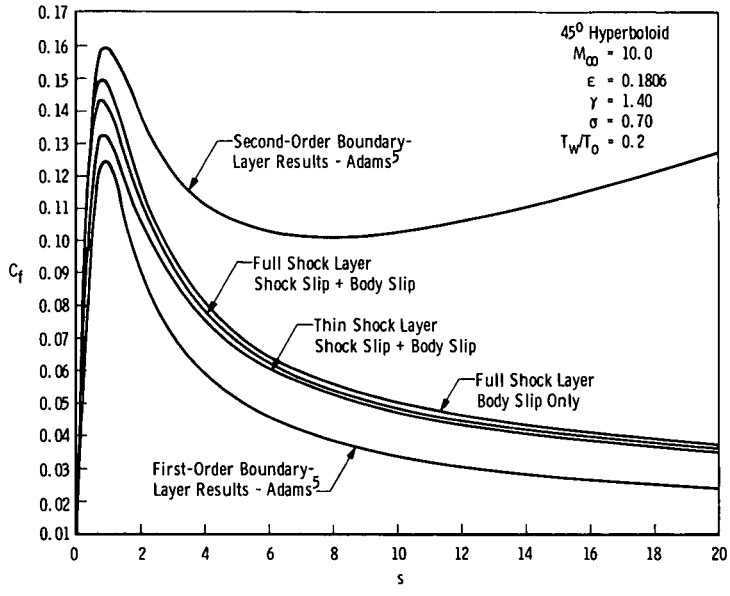

Fig.14 Skin friction on a hyperboloid

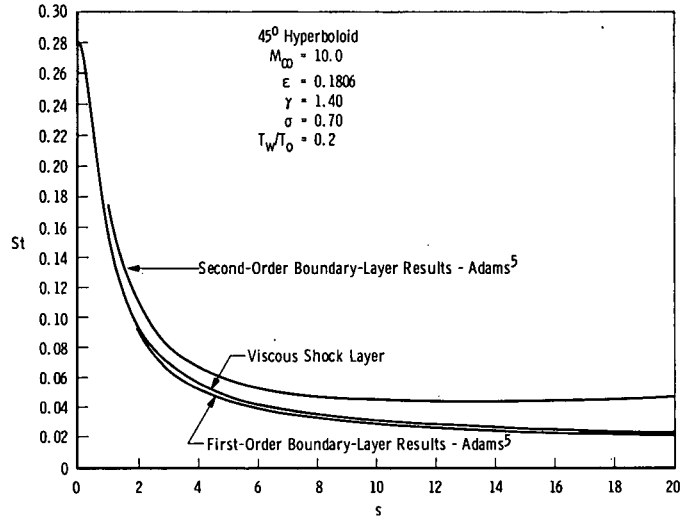

Fig.15 Stanton number on a hyperboloid

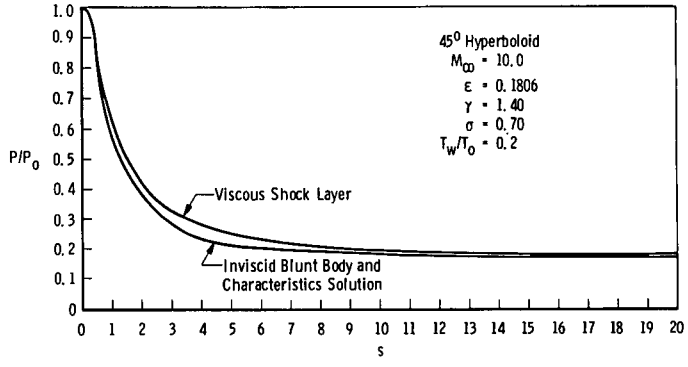

Fig.16 Pressure distribution on a hyperboloid

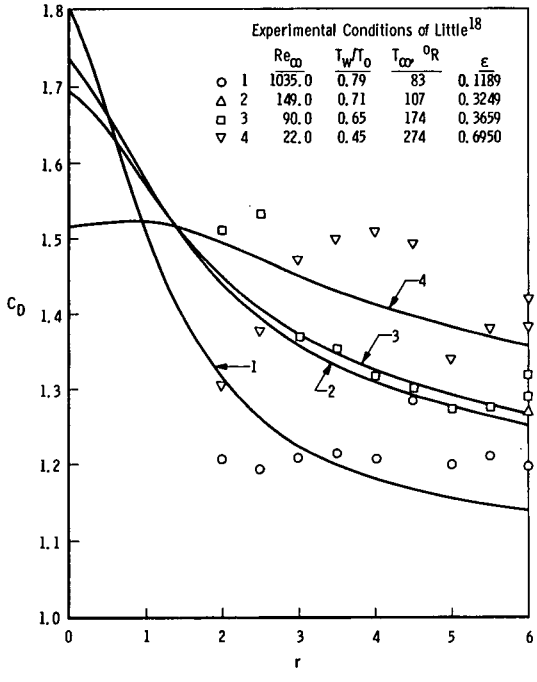

Fig.17 Drag coefficient for a 90° hyperboloid

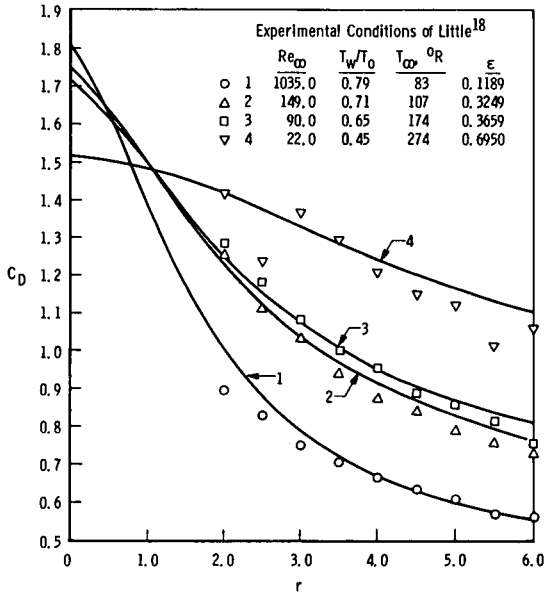

Fig.18 Drag coefficient for a 45° hyperboloid

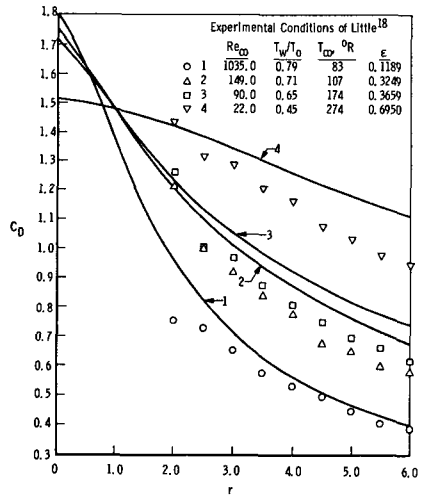

Fig.19 Drag coefficient for a 20° hyperboloid

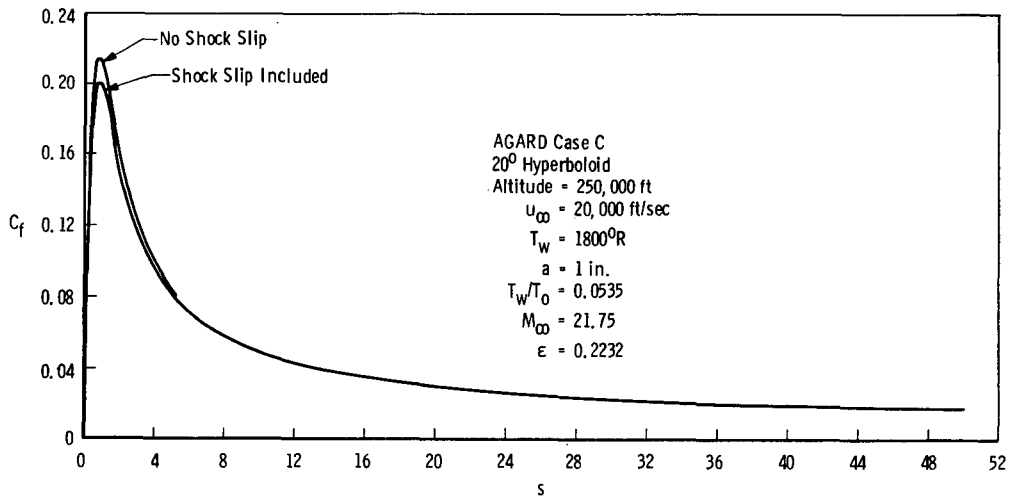

Fig.20 Skin friction on the AGARD Case C hyperboloid

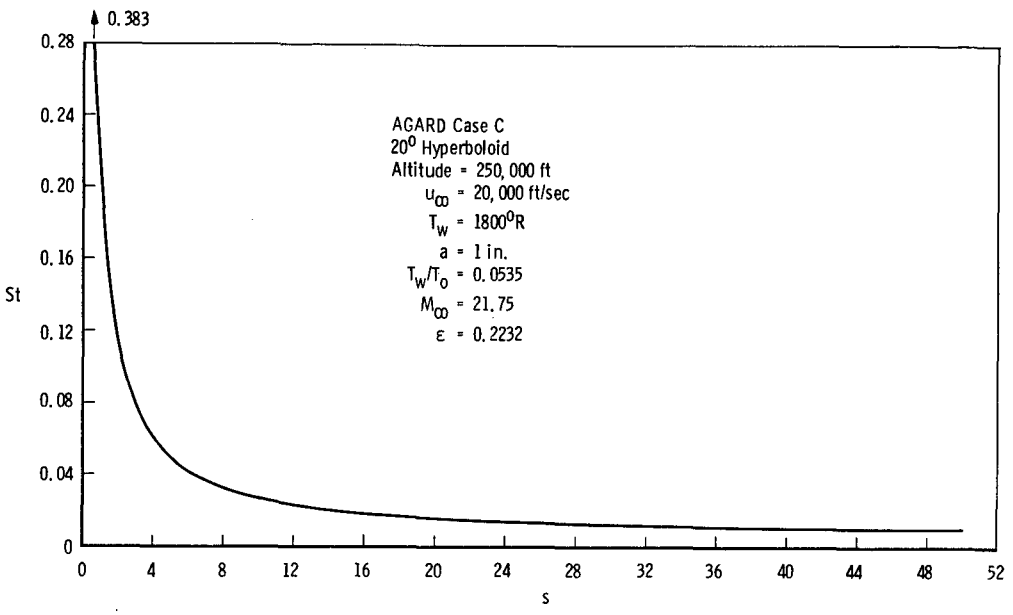

Fig.21 Stanton number on the AGARD Case C hyperboloid

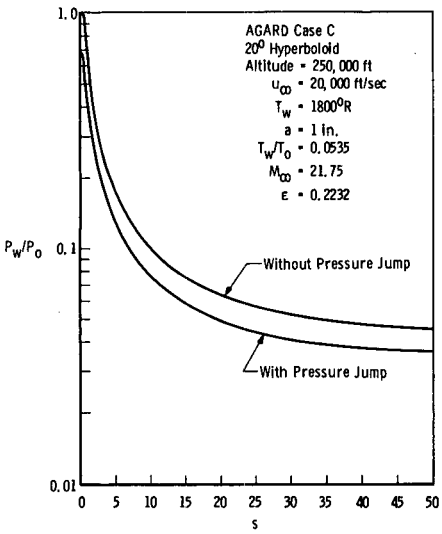

Fig. 22 Pressure distribution on the AGARD Case C hyperboloid

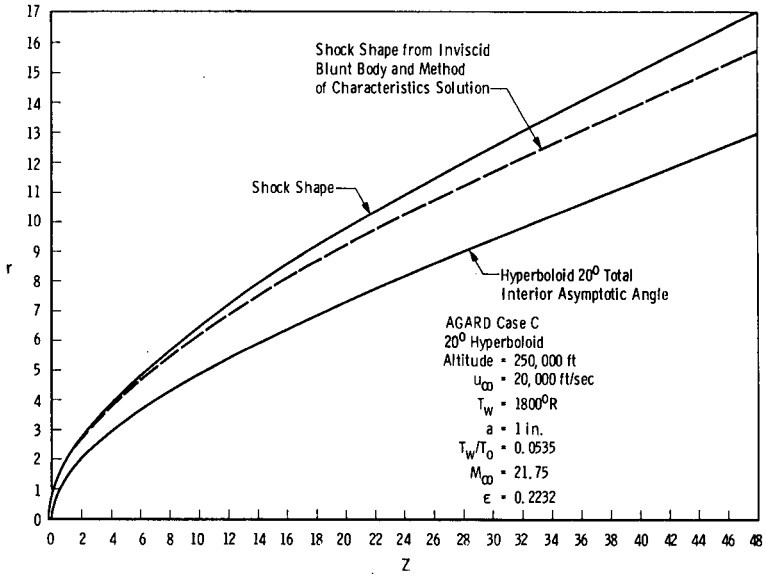

Fig. 23 Shock stand-off distance on the AGARD Case C hyperboloid

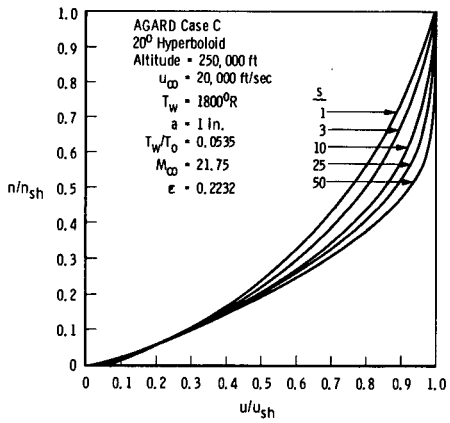

Fig. 24 Velocity profiles on the AGARD Case C hyperboloid

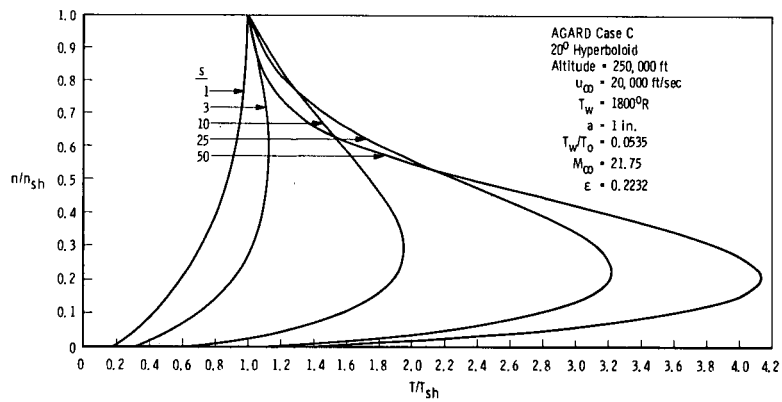

Fig. 25 Temperature profiles on the AGARD Case C hyperboloid

NUMERICAL METHODS FOR NONREACTING AND CHEMICALLY REACTING LAMINAR FLOWS - TESTS AND COMPARISONS

by

Clark H.Lewis

Professor of Aerospace Engineering,
Virginia Polytechnic Institute,
Blacksburg, Virginia

NUMERICAL METHODS FOR NONREACTING AND CHEMICALLY REACTING LAMINAR FLOWS - TESTS AND COMPARISONS

by Clark H. Lewis*

SUMMARY

Equilibrium, nonequilibrium and ideal gas ($\gamma = 1.4$) laminar boundary layers and viscous shock layers over a 10° half-angle hyperboloid 50 nose-radii long at three altitude-velocity conditions were computed by several investigators. Results of skin-friction and heat-transfer coefficients and displacement-thickness distributions over the body and property profiles across the layer at the ends of the body were compared. The conditions chosen test the ability of the numerical methods to compute nonequilibrium viscous layers near chemical equilibrium and the applicability of boundary-layer theory at low Reynolds number conditions. Results show that recently developed finite-difference methods are superior to earlier methods.

INTRODUCTION

During the past ten years a number of numerical methods have been developed for the solution of laminar boundary-layer flows of nonreacting and chemically reacting gases over two-dimensional and axisymmetric bodies at zero lift. In 1967 the Advisory Group for Aerospace Research and Development (AGARD) of the North Atlantic Treaty Organization sponsored a seminar on numerical methods in viscous flows at the National Physical Laboratory in Teddington, England. One objective of that seminar was to provide a forum for presentation of numerical methods and comparison of results for selected test cases. A body and set of conditions were chosen to test boundary-layer theory, computational methods and chemical models used by various investigators.

Preliminary results were given at the AGARD seminar of 1967; however, substantial extensions and improvements have been made since that time, and it is now possible to present comparisons from more complete calculations.

The purpose of the present paper is to present the results from those involved in the AGARD seminar for the specific set of test cases. It is thus possible to draw certain conclusions regarding higher-order boundary-layer effects and the effects of various chemical models on measurable quantities. It is also hoped that other investigators who were not involved previously and have developed operational methods will also use these results for further tests and comparisons.

The tests conditions will be described and the numerical methods and chemical models used by the various investigators will be indicated. Next, skin-friction, heat-transfer, and boundary-layer displacement-thickness distributions over the body will be presented and discussed for the various test cases. Higher-order boundary-layer effects on skin-friction and heat-transfer distributions will be presented and profiles of flow quantities through the shock layer will be compared at the end of the body. Finally, a comparison of the predicted stagnation heat transfer will be presented from the various methods and flow models.

The results presented in this paper should be useful to those interested in design applications since data are presented which permit comparison of various methods for the same test conditions. Because of the cost involved to perform the numerical calculations, a wider range of conditions was not considered feasible. Of course, the conditions chosen do not adequately test laminar boundary-layer theory with regard to either chemical effects or higher-order boundary-layer effects. It is necessary to keep these points in mind when considering the range of conditions specified for the test cases.

TEST CASE CONDITIONS

In this section the conditions of the test cases will be given. It is not possible, however, to include all data which were furnished to the various investigators. From what is given in this paper, it is possible to interpret the results presented and to perform nonreacting (perfect gas) laminar boundary-layer calculations.

Three test cases A, B, and C were defined and the conditions are shown in Table 1. A free-stream velocity of 20,000 ft/sec was specified for all conditions. Case A at 100,000 feet altitude was specified to test finite rate chemically reacting flow models at conditions near chemical equilibrium. Case B at 250,000 feet altitude can be compared with the results of Case C at the same altitude conditions but for perfect gas conditions. Methods have not been developed which include the effects of nonequilibrium chemistry and higher-order boundary-layer effects; therefore, Case C was designed as a perfect gas ($\gamma = 1.4$) test condition.

The body, a 10° half-angle hyperboloid 50 nose radii long with a nose radius of 1 inch, is shown in Fig. 1. A comparison was made between modified Newtonian pressure distribution and the results of a blunt body and characteristics solution for perfect gas flows over this analytic shape. It was found that the difference in pressure distribution was negligible (less than 5%); therefore, Newtonian pressure distribution was prescribed for all test conditions. For the chemically reacting viscous flow Cases A and B, frozen, equilibrium and nonequilibrium streamtube expansions were performed from the equilibrium stagnation conditions given in Table 1 and for the Newtonian pressure distribution along the body using the method of Lordi and Mates [1]. Complete tabulations of these inviscid expansion data were provided to each of the investigators, and these data can be provided to others interested in making comparisons with the data presented in this paper by writing to the author of the present paper. Fig. 2 shows the temperature distribution and oxygen concentration distribution from the inviscid streamtube expansion data. It can be seen from Fig. 2a that Case A is indeed near chemical equilibrium and Case B is near the chemically frozen limit. However, from Fig. 2b we see that the concentration of oxygen from the nonequilibrium expansions are not near the equilibrium or frozen limits. Therefore, it is desirable to use the complete set of nonequilibrium expansion data to determine the inviscid outer boundary-layer conditions.

*Professor of Aerospace Engineering, Virginia Polytechnic Institute, Blacksburg, Virginia.

The investigators involved in the AGARD competition were J. C. Adams, ARO, Inc.; F. G. Blottner, Sandia Corporation; R. T. Davis, Virginia Polytechnic Institute; A. M. O. Smith, McDonnell-Douglas Corporation; and W. Schönauer, University of Karlsruhe. The methods used and cases treated are indicated in Table 2. All investigators except Smith used an implicit finite difference method to solve the boundary-layer or viscous shock-layer equations. Papers describing the numerical methods are given in Refs. 2-5.

RESULTS AND DISCUSSION

Case A

The skin-friction, heat-transfer and boundary-layer displacement thickness distributions over the body are shown in Fig. 3-5. The nonequilibrium solutions of Blottner and Smith, the equilibrium solution of Schönauer, and for comparison the perfect gas ($\gamma = 1.4$) solutions of Adams are shown. All calculations were based upon the same free-stream conditions and modified Newtonian pressure distribution.

The skin-friction predictions of Blottner and Smith are within about 5% of each other over the entire body. Schönauer's equilibrium gas prediction is about 10% below and the perfect gas ($\gamma = 1.4$) prediction is about 10% above the nonequilibrium gas results.

The nonequilibrium heat-transfer predictions of Blottner and Smith are again within about 5% over the body. The equilibrium and perfect gas results are within about 10% of each other and both are about 25% below the nonequilibrium results. The nonequilibrium (NEQ), noncatalytic (NCW) wall results of Blottner are not shown, but the heat-transfer was reduced about 15%. The perfect gas heat-transfer prediction is therefore within about 10% of the NEQ,NCW prediction.

From Fig. 5 we see that the predictions of displacement thickness differed substantially from the various investigations. The nonequilibrium gas predictions of Blottner were about twice the values predicted by Smith, and the equilibrium gas prediction of Schönauer was about 25% below Smith's NEQ results. The perfect gas prediction was substantially above Blottner's predictions. Thus even though the skin-friction and heat-transfer predictions of Blottner and Smith were in good agreement, the prediction of displacement thickness differed substantially.

A comparison of species profiles at the end of the body ($s/r_n = 50$) is shown in Fig. 6 from the NEQ calculations of Blottner and the equilibrium gas results of Schönauer. The equilibrium gas model of Schönauer did not include ionization. Species concentrations near the wall were in good agreement, and the differences near the outer edge of the boundary layer are probably due mostly to differences in the inviscid boundary conditions from the equilibrium and nonequilibrium streamtube expansions.

The chemical model of Blottner is the most complete and exact, and his data are considered the reference condition for this case. It should also be noted that Adams tried to solve this nonequilibrium gas case and was unable to obtain a convergent solution since the flow was near equilibrium. Thus Blottner's ability to solve this case indicates the improvements made in nonequilibrium boundary-layer solution methods from 1967 to 1969.

Case B

The skin-friction, heat-transfer and displacement-thickness distributions are shown in Fig. 7-9. The nonequilibrium solutions from Smith, Blottner and Adams and for comparison the perfect gas results of Adams are shown.

The nonequilibrium skin-friction results of Blottner and Smith are shown as one curve since the differences were not plottable. Except for the stagnation region ($s/r_n < 1$), the results of all nonequilibrium solutions were within 5%. Adams' perfect gas prediction was about 60% above his nonequilibrium result.

The heat-transfer results are shown in Fig. 8. The effects of nonequilibrium catalytic (ECW) and noncatalytic (NCW) wall boundary conditions can be seen from the data shown. Adams' ECW prediction is 25% above his NCW results. For $s/r_n > 10$, Blottner's ECW is higher (as much as 15%) than Adams' results for the same wall conditions. This will be discussed in more detail below. Adams' perfect gas and NEQ,NCW results are within 5% of each other. Considering all calculations, the NEQ heat-transfer predictions differ as much as 50% for $s/r_n > 20$.

The displacement-thickness results are shown in Fig. 9 where the differences are even larger. Using Adams' NEQ,ECW prediction for reference, Blottner's results for the same chemical model is twice as large, Smith's result is 60% higher (but in good agreement with Adams' perfect gas prediction), and Schönauer's equilibrium result is about 50% below the reference value.

In concluding consideration of this case, it is of interest to compare separately the results of Adams and Blottner. Adams used the numerical methods developed by Blottner [7] in 1964. Both used 6 species, and Blottner and Adams used a 7 and 8 reaction, multicomponent gas model respectively. Adams used Bortner's 1963 reaction-rate coefficient [8] while Blottner used Bortner's 1966 data [9]. Lacking direct comparison from one investigator using both sets of rate data, the differences are not expected to be significant on heat-transfer and displacement-thickness results. The most significant difference between the methods used by Adams and Blottner is that Adams iterated his solution of the conservation equations at each step along the body until the velocity, temperature and all species profiles differed by less than 0.1% at all points across the boundary layer while Blottner did not iterate his solution. From Fig. 8 we see that Blottner and Adams heat-transfer predictions are identical for $s/r_n < 4$; however, beyond that point differences as large as 20% occur. Also for $s/r_n > 4$, large differences exist in displacement-thickness distribution. From these data it appears that s-stepwise iteration of the solution is required for accurate results.

Case C

A comparison of predicted skin-friction coefficient from first- and second-order boundary-layer theory and viscous shock-layer theory is shown in Fig. 10. We see that classical first-order theory underpredicts skin friction by about 30% over the entire body. Second-order theory is within about 10% of the viscous shock-layer result for one nose radii and thereafter increasingly overpredicts the skin-friction coefficient. Whereas the trends of the first-order prediction are correct over the entire body, the trends of the second-order theory are incorrect beyond 30 nose radii where the effects of vorticity are greatly overpredicted by the second-order theory.

The predicted heat-transfer distribution is compared in Fig. 11. Here we see that the first-order theory is within 10% of the viscous shock-layer result over the entire body whereas again the second-order theory overpredicts the viscous shock-layer result by as much as a factor of two at the end of the body. It is interesting to note that the first-order prediction of heat transfer is substantially in better agreement than the predicted skin-friction distribution upon comparison with the viscous shock-layer results. Also even though higher-order boundary-layer (low Reynolds number) effects are important, predictions based on classical first-order boundary-layer theory are sufficient for predictions of wall heat transfer.

For this case a comparison is possible for viscous effects on the surface pressure distribution, and the results are shown in Fig. 12. The effects of boundary-layer displacement on the inviscid (Newtonian) pressure distribution is compared with the viscous shock-layer prediction. Boundary-layer displacement increases the surface pressure distribution about 15 - 20% over most of the body whereas the viscous shock-layer result is about 40% above the inviscid result. Certainly this difference is large enough to measure experimentally, and such a comparison would be most interesting.

A comparison of predicted flow-field variables at the end of the body ($s/r_n = 50$) is shown in Fig. 13. The inviscid shock-layer results were computed by the author from a perfect gas ($\gamma = 1.4$) method of characteristics (MOC) solution. The first- and second-order boundary-layer results were computed by Adams and the viscous shock-layer results are from Davis. An additive composite expansion of the (inner) first-order boundary-layer results with the (outer) inviscid MOC results can be compared with the viscous shock-layer results. A composite expansion using the second-order results was not attempted since it is clear that second-order theory is not applicable at that location on the body. Also, the composite expansion for the first-order temperature is not shown since a negative temperature is predicted using the first-order boundary-layer result.

From the data shown in Fig. 13, we see that the composite expansion yields a velocity distribution in reasonably good agreement with the viscous shock-layer results; however, the prediction of all other flow-field variables is in poor agreement with the more complete theory.

Finally, for the conditions of this case, the predictions of boundary-layer theory are substantially in error upon comparison with the viscous shock-layer results. Although the first-order prediction of surface heat transfer was within 10%, the errors in skin friction (30%) and viscous-induced pressure (40%) predictions were substantial and the prediction of most flow-field variables were often in error by a factor of two.

Stagnation Point

Stagnation point velocity, temperature and species profiles for Case B multicomponent nonequilibrium boundary layer (BL), thin viscous shock layer (TVSL), and thin viscous shock layer with shock slip (TVSLSS) are shown in Fig. 14 for both noncatalytic (NCW) and equilibrium catalytic (ECW) wall conditions. The calculations were from Adams. The effects of shock-slip reduce the velocity and temperature behind the shock about 20% below the frozen shock-crossing values. The equilibrium inviscid stagnation conditions were used as the outer boundary conditions for the boundary-layer solution.

The stagnation point species distributions are shown in Fig. 14c for the three theoretical models. All species except N_2 are strongly affected by the shock-layer models. Including shock slip effects in the TVSL model reduced the concentrations of O, N and NO by about one order of magnitude just behind the shock. The effect could be important if gas radiation were to be considered for these conditions.

Also shown in Fig. 14c for comparison are the predictions of stagnation heat-transfer rate from the three theories. It is not obvious from the consideration of the temperature profiles in Fig. 14b that the viscous shock layer without shock slip should increase the heat-transfer rate to the surface by 70% and including the effects of shock slip should reduce the heat-transfer rate about 30%. From these data it is important to consider the effects of transport properties on the shock wave when predicting the stagnation heat-transfer rate under similar conditions.

Stagnation Heat Transfer

The final comparison of data is shown in Table 3 where the stagnation point Stanton number predictions from all available sources and for all conditions considered by the investigators are shown. For Case A the limited data available for NEQ,BL predictions are within 5%, and the EQ,BL predictions are within about 6%. For Case B, the NEQ,BL predictions are within 3% while the EQ,BL results differ by 15%.* For the perfect gas ($\gamma = 1.4$) Case C, the first- and second-order predictions were about 10% below and above, respectively, the viscous shock layer prediction, and the effects of shock slip reduced the heat-transfer rate by 12%. This is to be compared with the Case B results where the effects of shock slip reduced the heat-transfer rate by 23.5%. Therefore the effects of finite-rate chemistry and shock slip have a stronger influence on the stagnation heat-transfer rate than does shock slip alone in the perfect gas case.

*This case is not near chemical equilibrium and these EQ,BL results are shown only for purposes of comparing numerical results.

CONCLUSIONS

1. Blottner has recently made substantial improvements in numerical methods for computing laminar viscous flows with finite rate, multicomponent, nonequilibrium chemistry and was able to compute flow fields near chemical equilibrium.

2. For Case A (100,000 ft), predictions of skin-friction and heat-transfer distributions were within about 15% whereas displacement thickness differed by a factor of two. Equilibrium and nonequilibrium species profiles at 50 nose radii were controlled primarily by differences in edge conditions from the inviscid streamtube expansion.

3. For Case B (250,000 ft), nonequilibrium predictions of skin friction were within 10% while heat-transfer rates differed by as much as 50%, and differences in displacement thickness were again by a factor of two. Effects of iterating the solution of the conservation equations resulted in differences in heat transfer of 20% using similar numerical methods and chemical data.

4. For Case C (Perfect Gas 250,000 ft), first-order boundary-layer heat-transfer predictions were within 10% whereas prediction of skin-friction was 30% in error. Except in the nose region, second-order theory was not applicable, and the viscous shock-layer theory must be used for these conditions. Viscous-to-inviscid surface pressure ratio was about 1.4. Composite expansions of boundary-layer and inviscid (method of characteristics) results did not in general yield reliable shock-layer property profiles.

5. For similar chemical and viscous flow field models, stagnation point heat-transfer predictions were in good agreement among all investigators. Viscous shock-layer models with nonequilibrium chemistry with and without shock slip substantially affected the stagnation heat-transfer rate.

6. Finally, although the range of conditions covered by the test cases was not especially broad or severe it showed that substantial differences existed in results from the various prediction methods. Also, comparison with perfect gas results shows the need for adequate chemical and viscous flow-field models for predicting wall and viscous-layer measurable properties.

REFERENCES

[1] Lordi, J.A., Mates, R.E., and Moselle, Jr., "Computer Program for the Numerical Solution of Nonequilibrium Expansions of Reacting Gas Mixtures," Report AD-1689-A-6, June 1965, Cornell Aeronautical Lab., Buffalo, New York.

[2] Blottner, F.G., "Viscous Shock Layer at the Stagnation Point with Nonequilibrium Air Chemistry," AIAA Journal, Vol. 7, No. 12, Dec. 1969, pp. 2281-2288.

[3] Blottner, F.G., "Finite Difference Methods of Solution of the Boundary-Layer Equations," AIAA Journal, Vol. 8, No. 2, Feb. 1970, pp. 193-205.

[4] Keltner, G.L., "Laminar Boundary Layer Calculations on Bodies of Revolution in Hypersonic Flow," McDonnell-Douglas Report DAC-66719, March 1968, Long Beach, California.

[5] Davis, R.T., "The Hypersonic Fully Viscous Shock-Layer Problem," Sandia Report SC-RR-68-840, December 1968, Albuquerque, New Mexico.

[6] Adams, J.C., "Higher-Order Boundary-Layer Effects on Analytic Bodies of Revolution," AEDC-TR-68-57, April 1968, Arnold Engineering Development Center, Tennessee.

[7] Blottner, F.G., "Nonequilibrium Laminar Boundary Layer Flow of Ionized Air," AIAA Journal, Vol. 2, No. 11, Nov. 1964, pp. 1921-1927.

[8] Bortner, M.H., "Chemical Kinetics in a Re-entry Flow Field," General Electric TIS R63SD63, 1963.

[9] Bortner, M.H., "Suggested Standard Chemical Kinetics for Flow Field Calculations - A Consensus Opinion," AMRC Proceedings, Vol. 14, Part 1, 1966.

Case	A	B	C
Altitude, ft	100 K	250 K	250 K
Velocity, ft/sec	20,000	20,000	20,000
M_∞	20.178	21.744	21.744
T_∞, °K	226.98	195.46	195.46
P_∞, atm	1.0997	2.0074	2.0074
Re_∞/ft	2157943.	5192.	5192.
T_W, °K	1400	1000	1000
p_O', atm	6.0352[a]	0.0129[a]	0.01223[b]
T_O', °K	6996[a]	5302[a]	18,678[b]

Table 1. Test case conditions

[a]Equilibrium normal shock stagnation conditions

[b]Ideal gas (γ=1.4) normal shock stagnation conditions

Investigator	JCA	FGB	RTD	AMOS	WS
Gas Model					
Binary				A,B	
Multicomponent	B	A,B			A,B
Perfect Gas					
(γ = 1.4)	C		C		
Chemistry					
Frozen				A,B	
Equilibrium				A,B	A,B
Nonequilibrium	B	A,B		A,B	
Numerical Method					
Finite difference	*	*	•		*
Differential difference				*	

Table 2. Test cases computed and methods used

Source	Conditions	A	B	C
Adams	BL,NEQ,NCW	-	0.128	-
	BL,NEQ,ECW	-	0.44	-
	TVSL,ECW	-	0.706	-
	TVSL,NCW	-	0.705	-
	TVSLSS,NCW	-	0.52	-
	TVSLSS,ECW	-	0.54	-
	1st O.BL	-	-	0.38
	2nd O.BL	-	-	0.46
Blottner	BL,NEQ,NCW	0.0189	-	-
	BL,NEQ,ECW	0.0204	0.432	-
Davis	SL	-	-	0.421
	SLSS	-	-	0.373
Schönauer	BL,EQ	0.0177	0.417	-
Smith	BL,NEQ	0.0199	0.418	-
	BL,EQ	0.0166	0.354	-
	BL, Frozen	0.0201	0.427	-

Table 3. Stagnation point Stanton number

NOMENCLATURE

C_{f_∞}	$2\tau_w/\rho_\infty U_\infty^2$, skin-friction coefficient
C_i	species mass fraction, gm/gm-mixture or moles/gm-mixture
H	stagnation enthalpy
M	Mach number
p	static pressure
p_T	local pitot pressure through the shock layer
q	heat-transfer rate, Btu/ft^2-sec
r, r_n	radial distance normal to the axis and body nose radius, respectively
Re_∞	$\rho_\infty U_\infty/\mu_\infty$, free-stream unit Reynolds number
s	surface distance from forward stagnation point
St_∞	$q_w/\rho_\infty U_\infty(H_\infty - H_w)$, Stanton number
T	temperature
u	tangential velocity component
U_∞	free-stream velocity
γ	ratio of specific heats
δ^*	boundary-layer displacement thickness
ρ	mass density

Subscripts

w	wall
∞	free stream

Other Notation

$( )_0'$	free-stream normal shock stagnation conditions
BL	boundary layer
EQ	chemical equilibrium
ECW	equilibrium catalytic wall with species diffusion and convection
NCW	noncatalytic wall
NEQ	finite-rate chemical nonequilibrium
SL	viscous shock layer
SLSS	shock layer with shock slip
TVSL	thin viscous shock layer
TVSLSS	thin viscous shock layer with shock slip

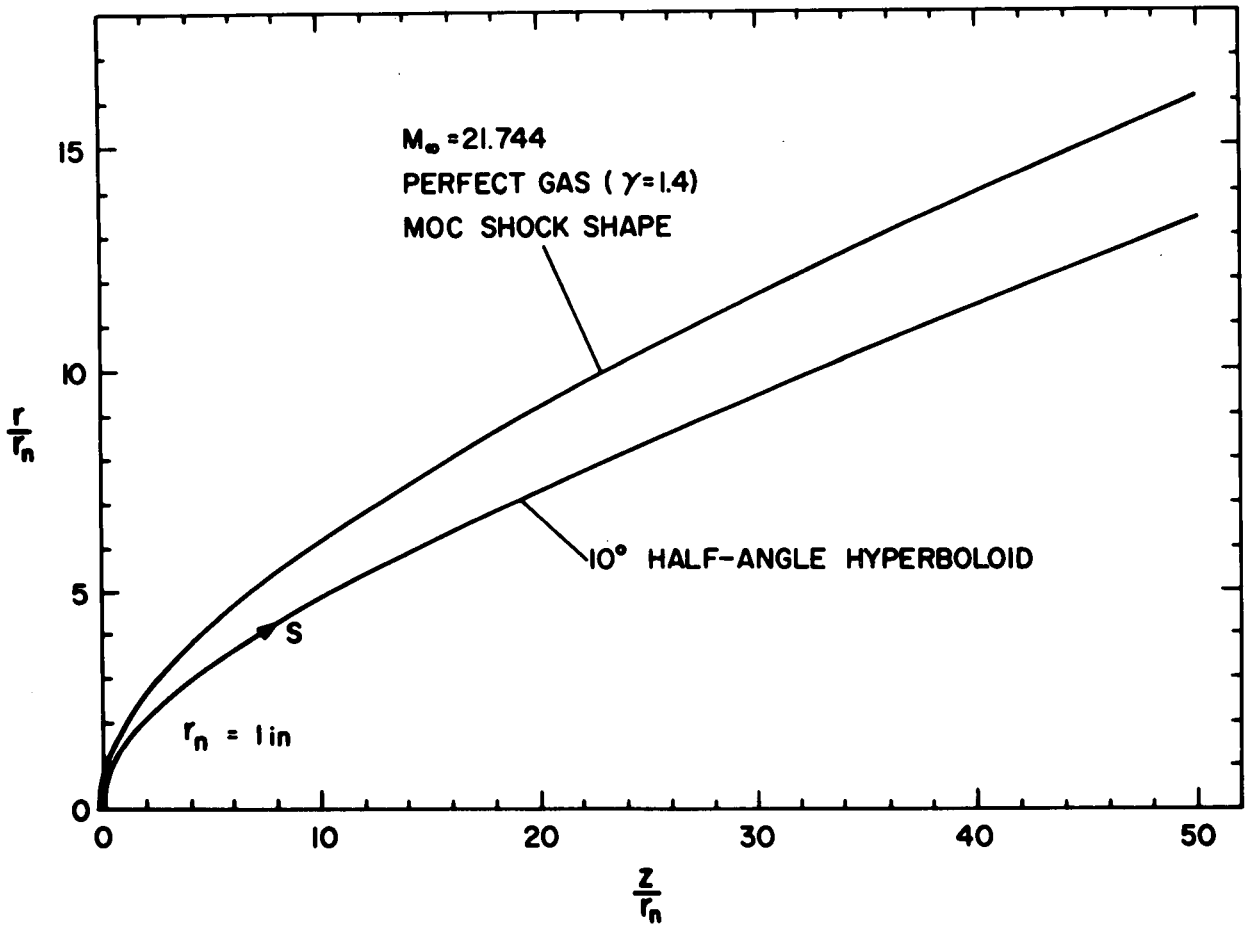

Fig.1 Hyperboloid geometry and perfect gas shock wave

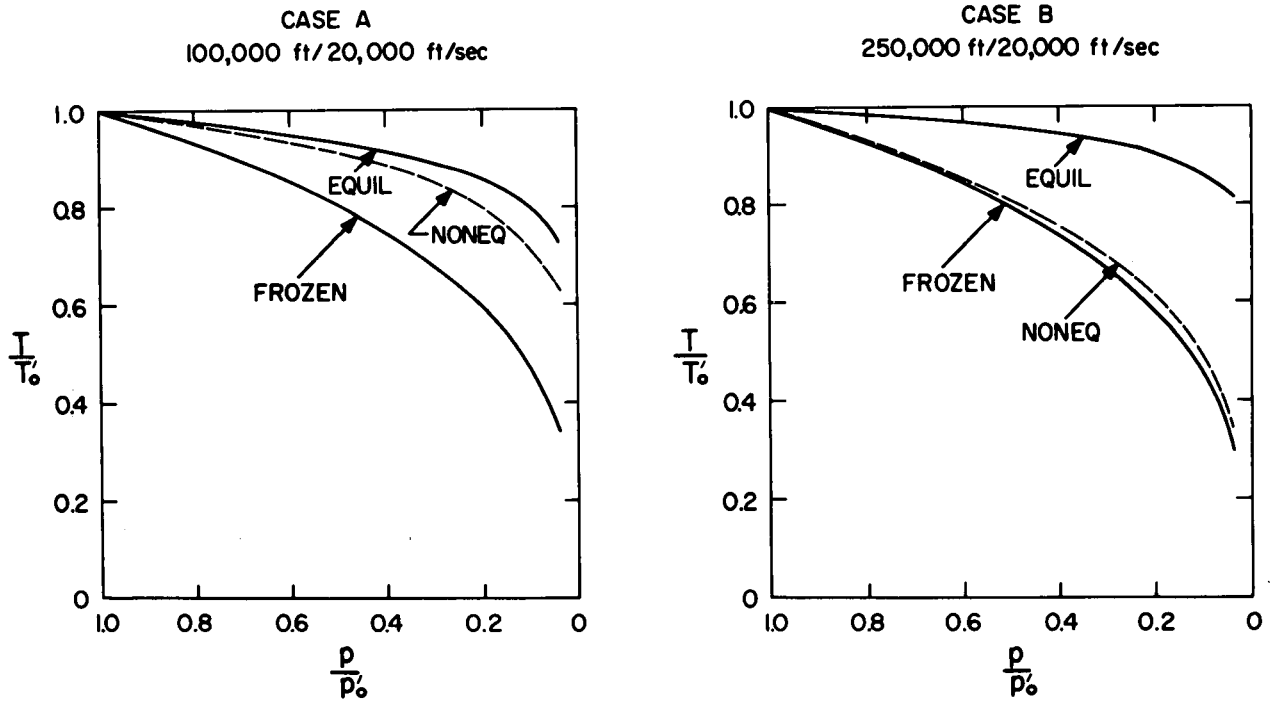

Fig.2(a) Inviscid streamtube temperature distribution

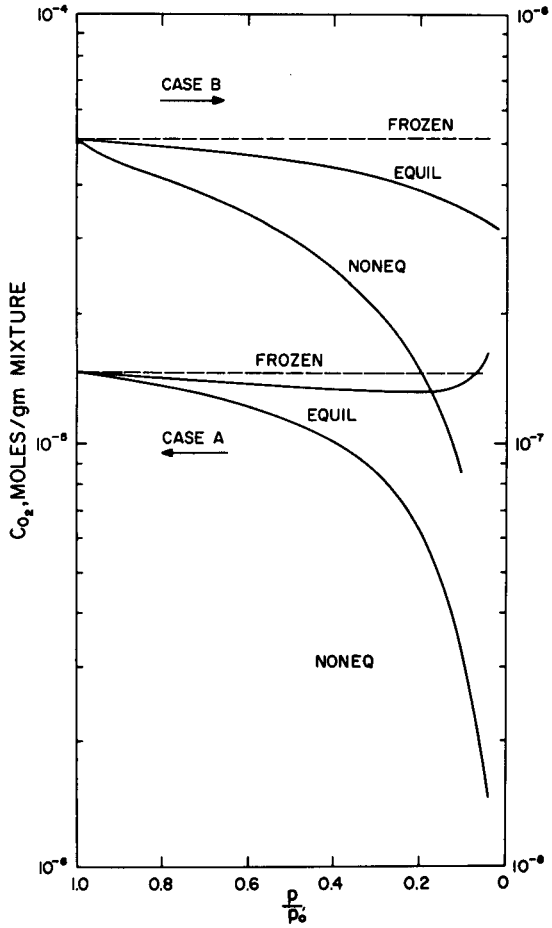

Fig.2(b) Oxygen concentration distribution from the inviscid streamtube expansions

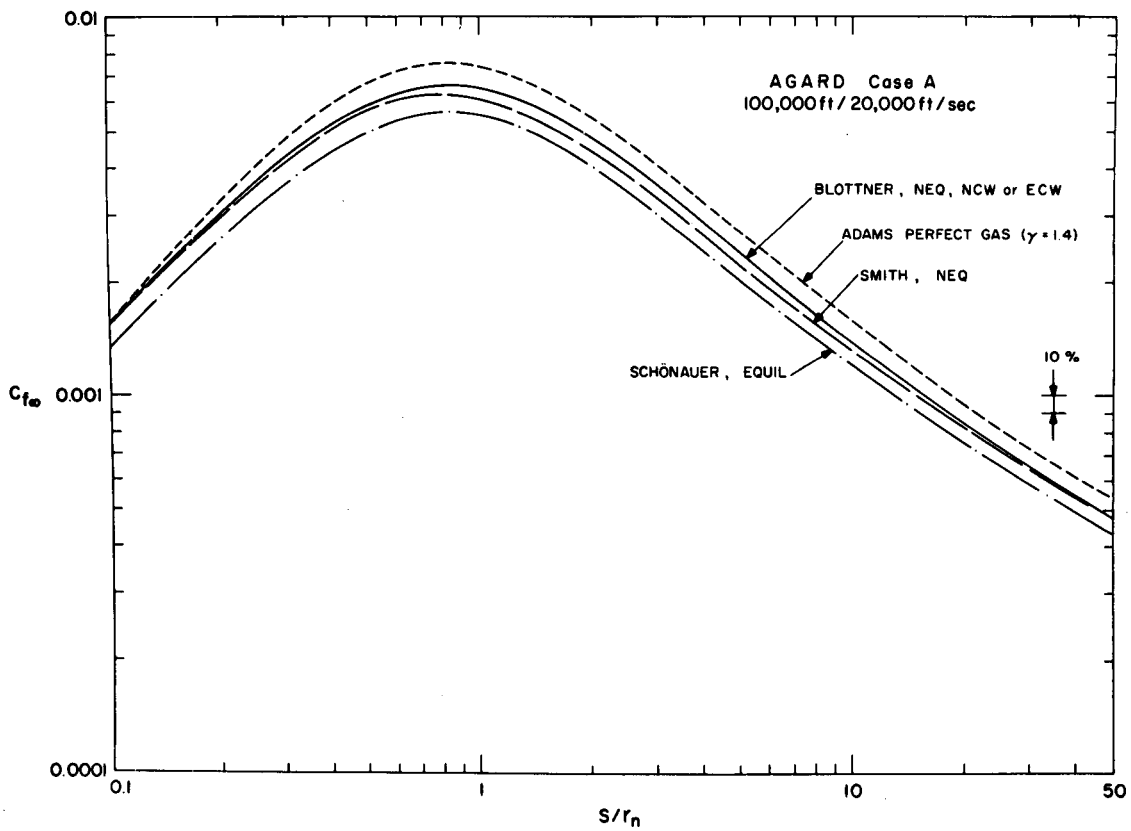

Fig.3 Skin-friction distribution for Case A

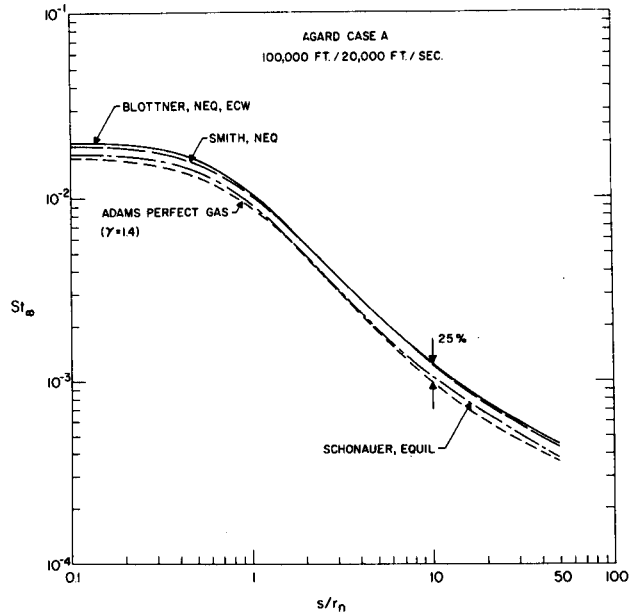

Fig.4 Heat-transfer distribution for Case A

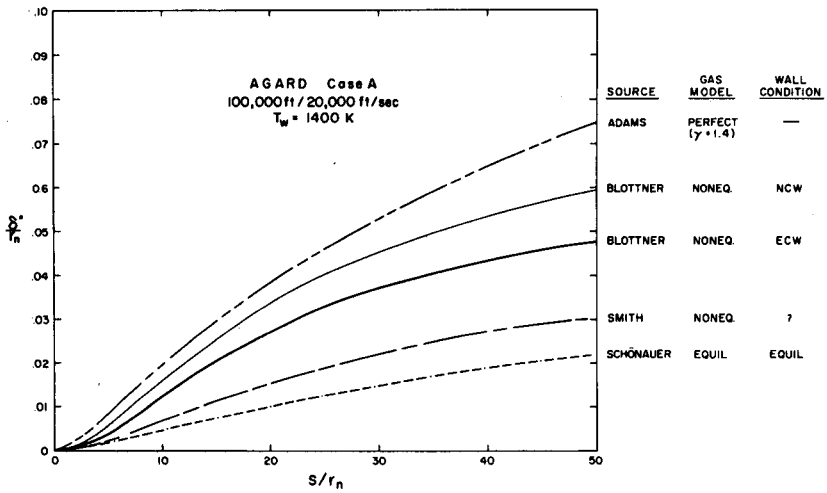

Fig.5 Boundary-layer displacement-thickness distribution for Case A

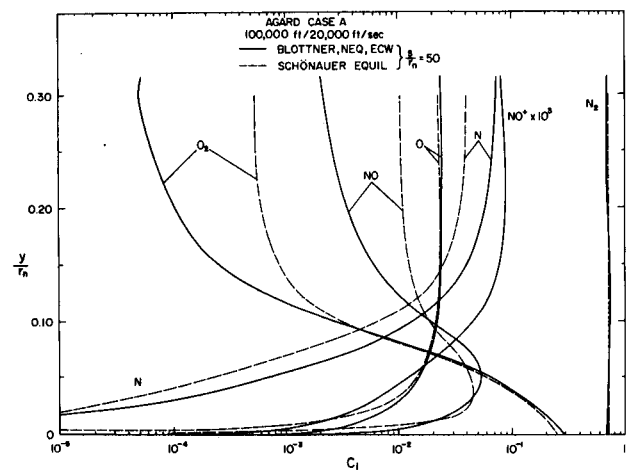

Fig.6 Species distribution for Case A ($s/r_n = 50$)

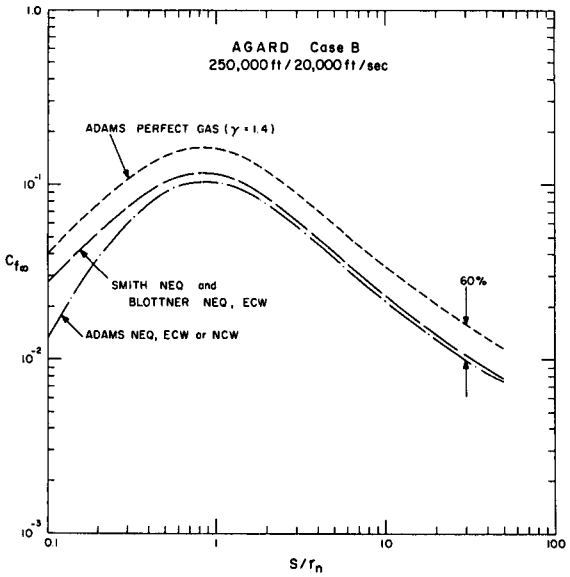

Fig.7 Skin-friction distribution for Case B

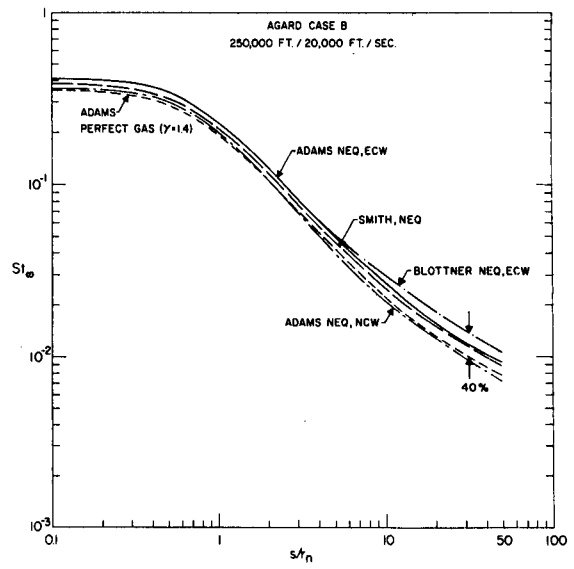

Fig.8 Heat-transfer distribution for Case B

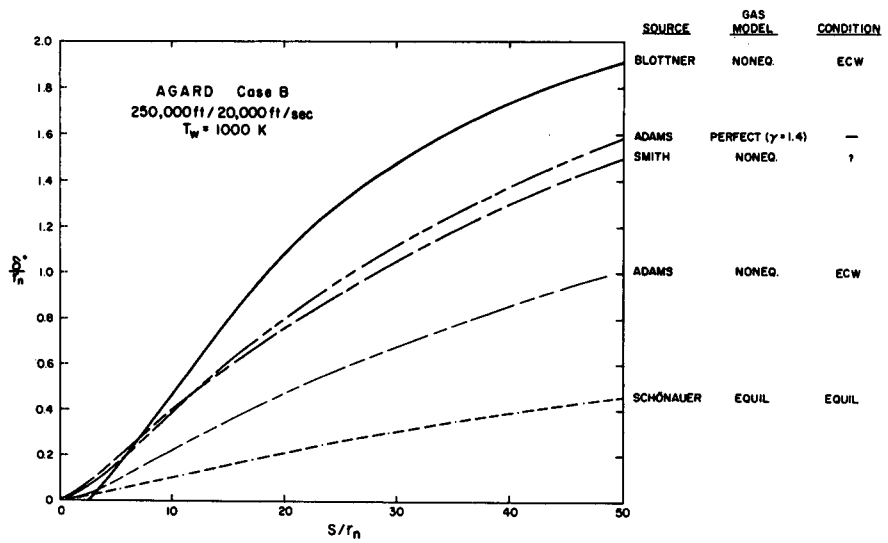

Fig.9 Boundary-layer displacement-thickness distribution for Case B

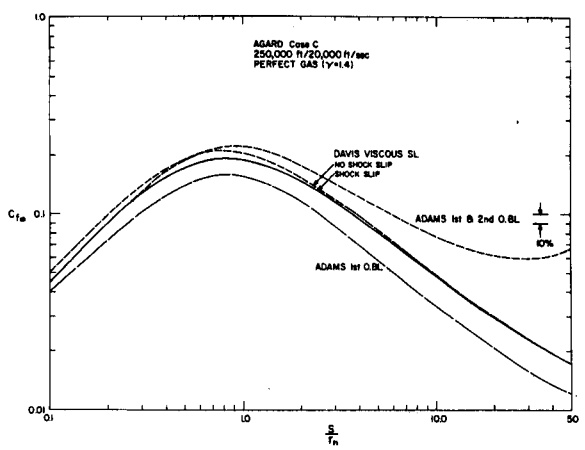

Fig.10 Skin-friction distribution for Case C

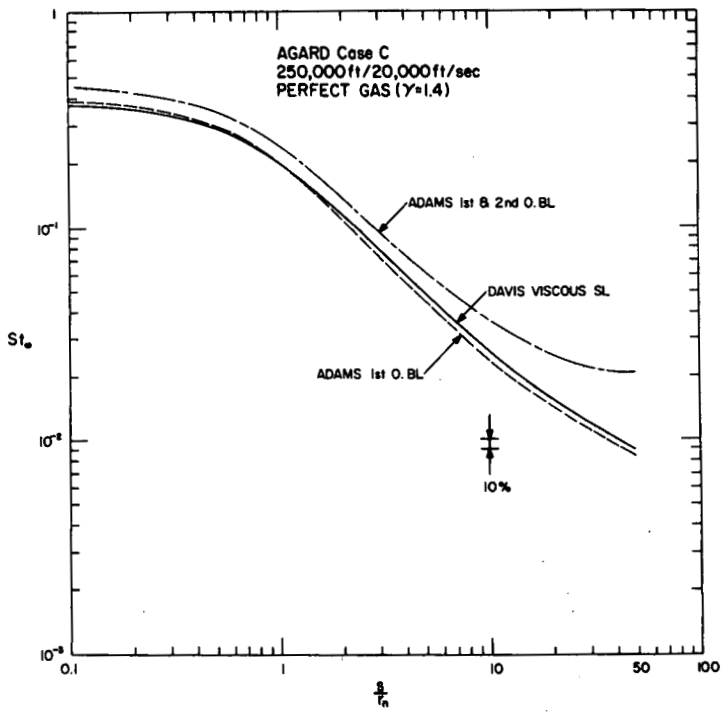

Fig.11 Heat-transfer distribution for Case C

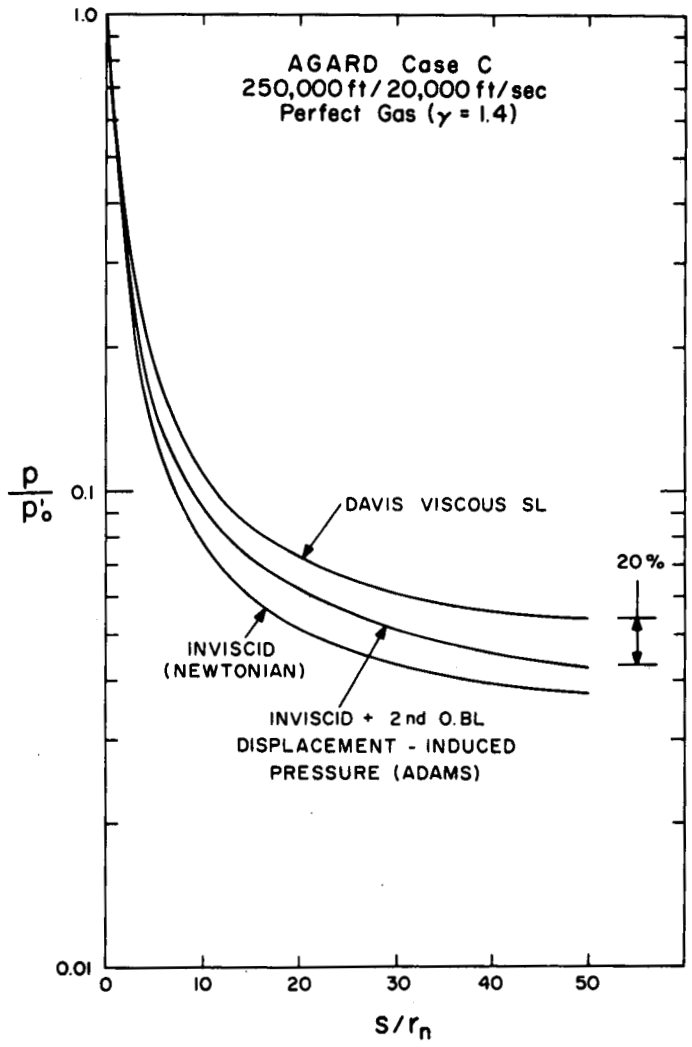

Fig.12 Surface pressure distribution for Case C

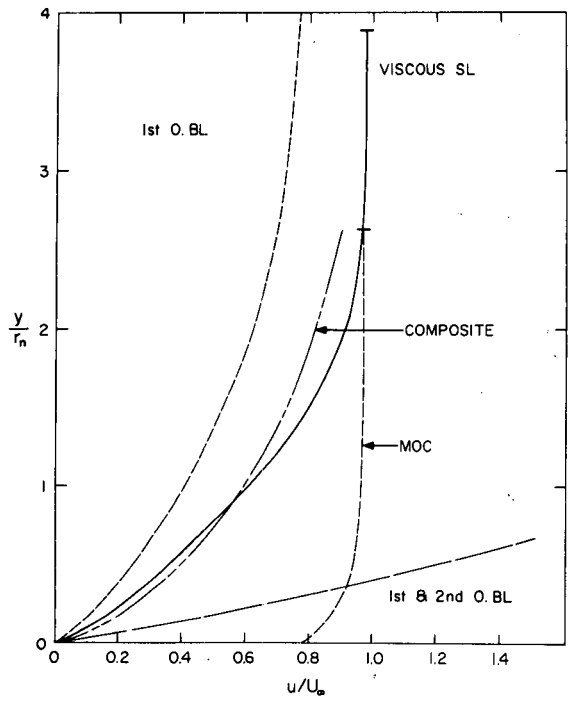

Fig.13(a) Shock layer velocity profile for Case C ($s/r_n = 50$)

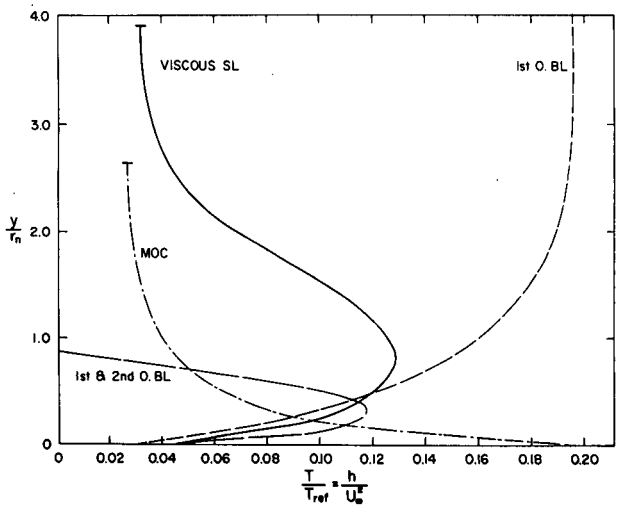

Fig.13(b) Shock layer temperature profile for Case C ($s/r_n = 50$)

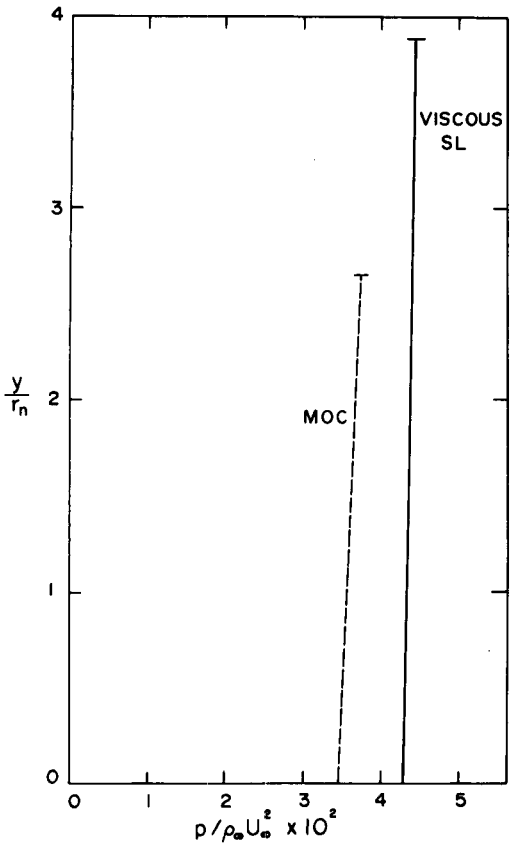

Fig.13(c) Shock layer static pressure profile for Case C ($s/r_n = 50$)

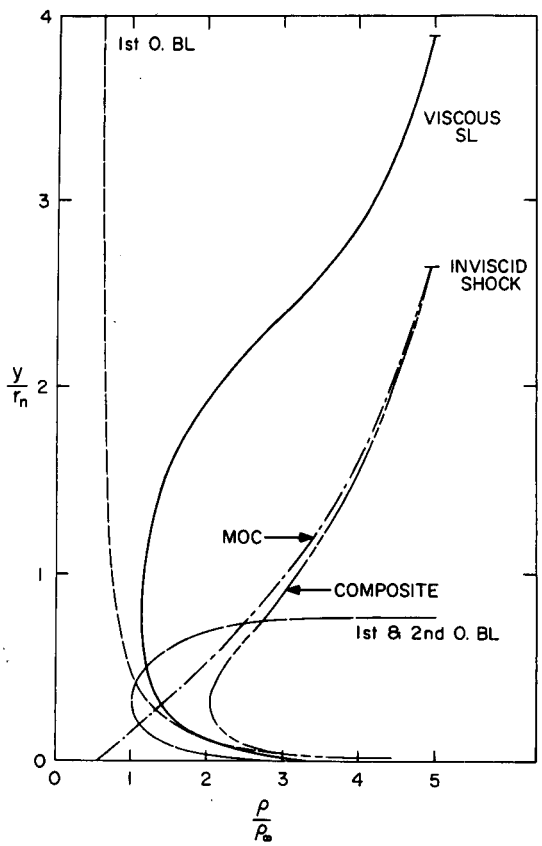

Fig.13(d) Shock layer density profile for Case C ($s/r_n = 50$)

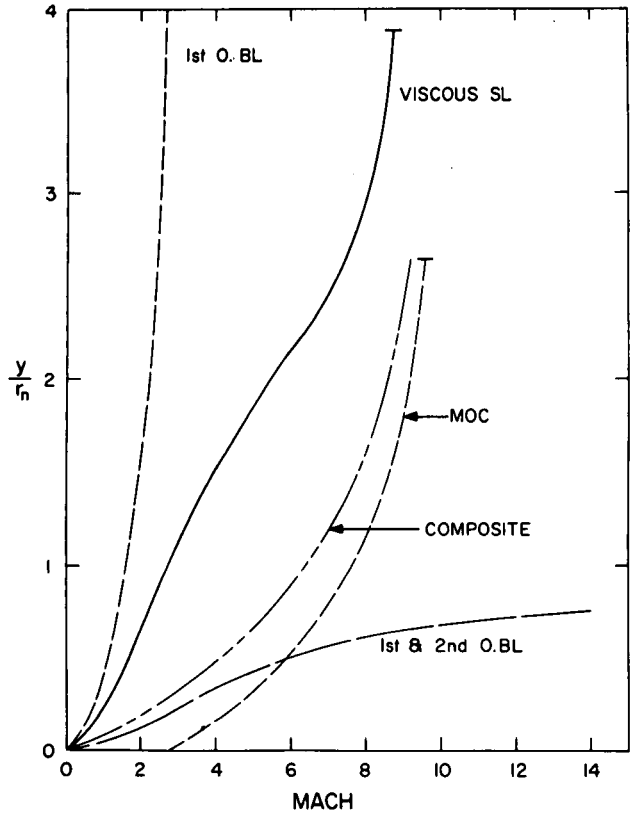

Fig.13(e) Shock layer Mach number profile for Case C ($s/r_n = 50$)

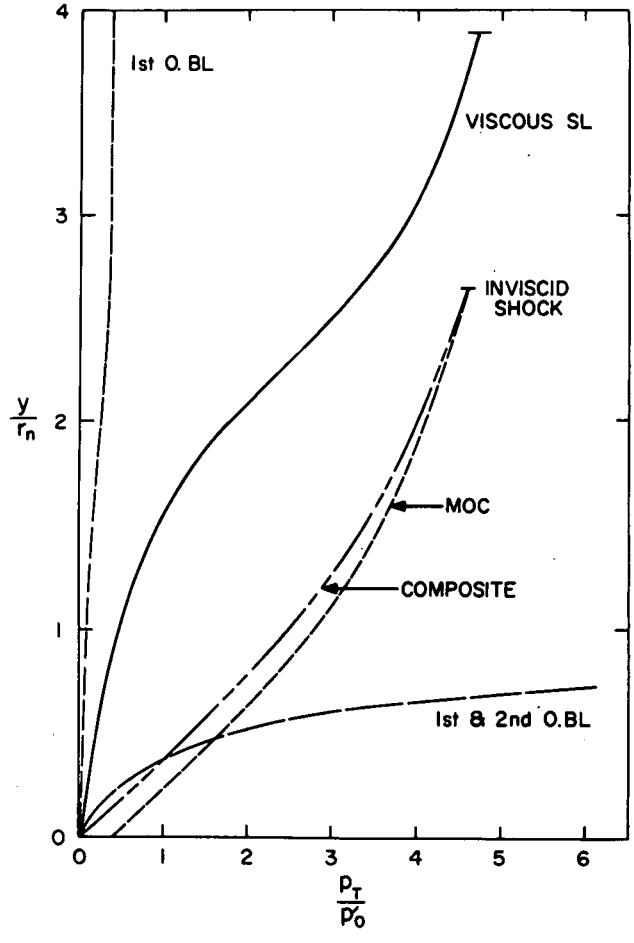

Fig.13(f) Shock layer total (pitot) pressure profile for Case C ($s/r_n = 50$)

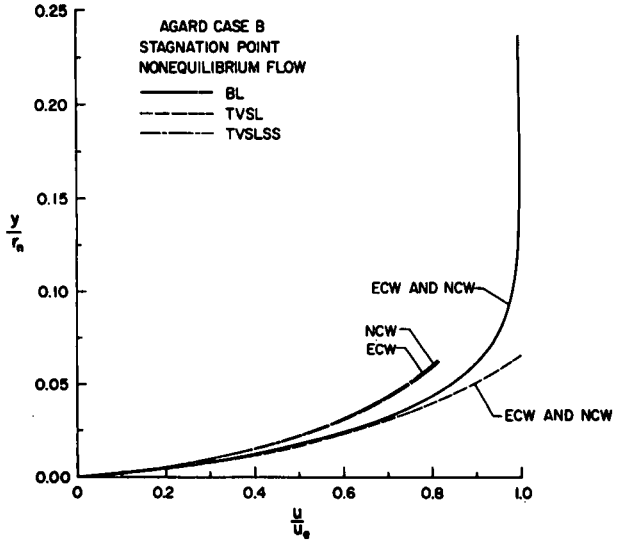

Fig.14(a) Stagnation point velocity profiles for Case B (after Adams)

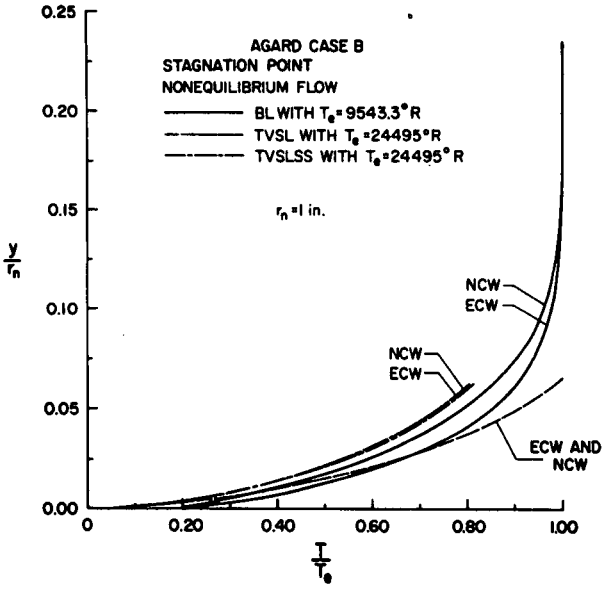

Fig.14(b) Stagnation point temperature profiles for Case B (after Adams)

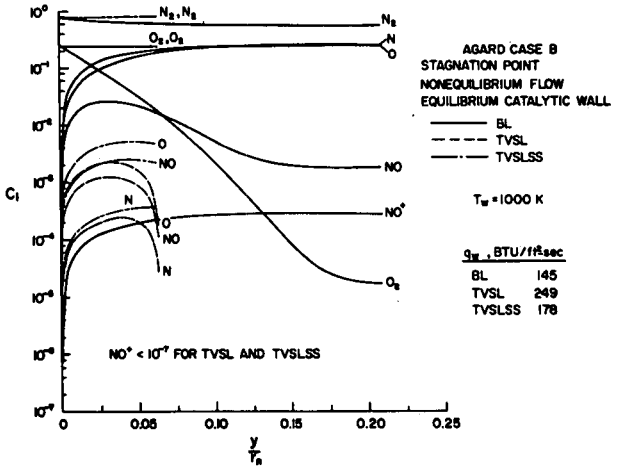

Fig.14(c) Stagnation point species profiles for Case B (after Adams)

AGARDograph No. 147 North Atlantic Treaty Organization, Advisory Group for Aerospace Research and Development NONREACTING AND CHEMICALLY REACTING VISCOUS FLOWS OVER A HYPERBOLOID AT HYPERSONIC CONDITION Edited by Clark H. Lewis Published September 1970 170 pages Results of various numerical methods for calculating viscous flows for a specific set of conditions are presented and compared. The body chosen for the numerical experiments was a 10 degree half-angle hyperboloid at two altitude-velocity conditions and one perfect gas condition. P.T.O.	532.516:533.6.011.55: 533.6.011.8	AGARDograph No. 147 North Atlantic Treaty Organization, Advisory Group for Aerospace Research and Development NONREACTING AND CHEMICALLY REACTING VISCOUS FLOWS OVER A HYPERBOLOID AT HYPERSONIC CONDITION Edited by Clark H. Lewis Published September 1970 170 pages Results of various numerical methods for calculating viscous flows for a specific set of conditions are presented and compared. The body chosen for the numerical experiments was a 10 degree half-angle hyperboloid at two altitude-velocity conditions and one perfect gas condition. P.T.O.	532.516:533.6.011.55: 533.6.011.8
AGARDograph No. 147 North Atlantic Treaty Organization, Advisory Group for Aerospace Research and Development NONREACTING AND CHEMICALLY REACTING VISCOUS FLOWS OVER A HYPERBOLOID AT HYPERSONIC CONDITION Edited by Clark H. Lewis Published September 1970 170 pages Results of various numerical methods for calculating viscous flows for a specific set of conditions are presented and compared. The body chosen for the numerical experiments was a 10 degree half-angle hyperboloid at two altitude-velocity conditions and one perfect gas condition. P.T.O.	532.516:533.6.011.55: 533.6.011.8	AGARDograph No. 147 North Atlantic Treaty Organization, Advisory Group for Aerospace Research and Development NONREACTING AND CHEMICALLY REACTING VISCOUS FLOWS OVER A HYPERBOLOID AT HYPERSONIC CONDITION Edited by Clark H. Lewis Published September 1970 170 pages Results of various numerical methods for calculating viscous flows for a specific set of conditions are presented and compared. The body chosen for the numerical experiments was a 10 degree half-angle hyperboloid at two altitude-velocity conditions and one perfect gas condition. P.T.O.	532.516:533.6.011.55: 533.6.011.8

Wall skin friction and heat transfer coefficients are computed, velocity, temperature, species etc. profiles across the viscous layer at various locations along the body are provided.

Preliminary results of the contributions were presented and discussed at the AGARD Seminar on "Numerical Methods of Viscous Flows", Teddington, England, September 1967. (Reference AGARD Conference Proceedings No.60 published May 1970).

Wall skin friction and heat transfer coefficients are computed, velocity, temperature, species etc. profiles across the viscous layer at various locations along the body are provided.

Preliminary results of the contributions were presented and discussed at the AGARD Seminar on "Numerical Methods of Viscous Flows", Teddington, England, September 1967. (Reference AGARD Conference Proceedings No.60 published May 1970).

Wall skin friction and heat transfer coefficients are computed, velocity, temperature, species etc. profiles across the viscous layer at various locations along the body are provided.

Preliminary results of the contributions were presented and discussed at the AGARD Seminar on "Numerical Methods of Viscous Flows", Teddington, England, September 1967. (Reference AGARD Conference Proceedings No.60 published May 1970).

Wall skin friction and heat transfer coefficients are computed, velocity, temperature, species etc. profiles across the viscous layer at various locations along the body are provided.

Preliminary results of the contributions were presented and discussed at the AGARD Seminar on "Numerical Methods of Viscous Flows", Teddington, England, September 1967. (Reference AGARD Conference Proceedings No.60 published May 1970).

AGARDograph No. 147 North Atlantic Treaty Organization, Advisory Group for Aerospace Research and Development NONREACTING AND CHEMICALLY REACTING VISCOUS FLOWS OVER A HYPERBOLOID AT HYPERSONIC CONDITION Edited by Clark H. Lewis Published September 1970 170 pages Results of various numerical methods for calculating viscous flows for a specific set of conditions are presented and compared. The body chosen for the numerical experiments was a 10 degree half-angle hyperboloid at two altitude-velocity conditions and one perfect gas condition. P.T.O.	532.516:533.6.011.55: 533.6.011.8	AGARDograph No. 147 North Atlantic Treaty Organization, Advisory Group for Aerospace Research and Development NONREACTING AND CHEMICALLY REACTING VISCOUS FLOWS OVER A HYPERBOLOID AT HYPERSONIC CONDITION Edited by Clark H. Lewis Published September 1970 170 pages Results of various numerical methods for calculating viscous flows for a specific set of conditions are presented and compared. The body chosen for the numerical experiments was a 10 degree half-angle hyperboloid at two altitude-velocity conditions and one perfect gas condition. P.T.O.	532.516:533.6.011.55: 533.6.011.8
AGARDograph No. 147 North Atlantic Treaty Organization, Advisory Group for Aerospace Research and Development NONREACTING AND CHEMICALLY REACTING VISCOUS FLOWS OVER A HYPERBOLOID AT HYPERSONIC CONDITION Edited by Clark H. Lewis Published September 1970 170 pages Results of various numerical methods for calculating viscous flows for a specific set of conditions are presented and compared. The body chosen for the numerical experiments was a 10 degree half-angle hyperboloid at two altitude-velocity conditions and one perfect gas condition. P.T.O.	532.516:533.6.011.55: 533.6.011.8	AGARDograph No. 147 North Atlantic Treaty Organization, Advisory Group for Aerospace Research and Development NONREACTING AND CHEMICALLY REACTING VISCOUS FLOWS OVER A HYPERBOLOID AT HYPERSONIC CONDITION Edited by Clark H. Lewis Published September 1970 170 pages Results of various numerical methods for calculating viscous flows for a specific set of conditions are presented and compared. The body chosen for the numerical experiments was a 10 degree half-angle hyperboloid at two altitude-velocity conditions and one perfect gas condition. P.T.O.	532.516:533.6.011.55: 533.6.011.8

Wall skin friction and heat transfer coefficients are computed, velocity, temperature, species etc. profiles across the viscous layer at various locations along the body are provided.

Preliminary results of the contributions were presented and discussed at the AGARD Seminar on "Numerical Methods of Viscous Flows", Teddington, England, September 1967. (Reference AGARD Conference Proceedings No.60 published May 1970).

Wall skin friction and heat transfer coefficients are computed, velocity, temperature, species etc. profiles across the viscous layer at various locations along the body are provided.

Preliminary results of the contributions were presented and discussed at the AGARD Seminar on "Numerical Methods of Viscous Flows", Teddington, England, September 1967. (Reference AGARD Conference Proceedings No.60 published May 1970).

Wall skin friction and heat transfer coefficients are computed, velocity, temperature, species etc. profiles across the viscous layer at various locations along the body are provided.

Preliminary results of the contributions were presented and discussed at the AGARD Seminar on "Numerical Methods of Viscous Flows", Teddington, England, September 1967. (Reference AGARD Conference Proceedings No.60 published May 1970).

Wall skin friction and heat transfer coefficients are computed, velocity, temperature, species etc. profiles across the viscous layer at various locations along the body are provided.

Preliminary results of the contributions were presented and discussed at the AGARD Seminar on "Numerical Methods of Viscous Flows", Teddington, England, September 1967. (Reference AGARD Conference Proceedings No.60 published May 1970).